



**Thermosensitive Display of Carbohydrate
Ligands on Microgel Scaffolds to facilitate
switchable Bioadhesion**

Inaugural-Dissertation

to obtain the academic degree
Doctor rerum naturalium (Dr. rer. nat.)
of the Faculty of Mathematics and Natural Sciences
of Heinrich-Heine-University Düsseldorf

submitted by

Tanja Janine Paul

from Haan

Düsseldorf, Oktober 2020

From the Institute of Organic Chemistry and Macromolecular Chemistry at the Heinrich-Heine-University Düsseldorf

Published by permission of the

Faculty of Mathematics and Natural Sciences at

Heinrich-Heine-University Düsseldorf

Supervisor: Jun. Prof. Dr. Stephan Schmidt

Co-supervisor: Prof. Dr. Christoph Janiak

Date of the oral examination : 11.12.2020

This thesis was accomplished in the period between October 2016 and March 2020 in the Institute of Organic Chemistry and Macromolecular Chemistry at the Heinrich Heine University in Düsseldorf, in the group of Colloidal Bioadhesion under supervision of Jun. Prof. Dr. Stephan Schmidt.

Declaration of authorship

I, Tanja Janine Paul, hereby declare that the thesis submitted is my own work without making use of impermissible aids, considering the “Rules of the Principles of Safeguarding Good Scientific Practice at Heinrich-Heine-University Düsseldorf”. All direct or indirect sources used are acknowledged in the bibliography as references. I further declare that I have not submitted this or a similar thesis at any other examination board in order to obtain a degree.

Düsseldorf, 20.10.2020

Tanja Janine Paul

“Nothing in life is to be feared, it is only to be understood. Now is the time to understand more, so that we may fear less.”
Marie Curie

Table of Contents

| | |
|--|------|
| Abstract | XI |
| List of publications | XV |
| Publications included in this thesis | XV |
| Publications not included in this thesis | XVI |
| Oral and poster presentations | XVII |
| 1. General Introduction | 1 |
| 1.1 The sweet nature of carbohydrates | 1 |
| 1.2 Lectins – The sugar communicators | 3 |
| 1.3 α -D-mannopyranoside binding lectins | 4 |
| 1.3.1 Concanavalin A | 4 |
| 1.3.2 FimH | 5 |
| 1.4 Multivalency | 7 |
| 1.5 Glycomimetics | 10 |
| 1.5.1 Glycopolymers | 11 |
| 1.5.2 Stimuli-responsive polymers | 13 |
| 1.5.3 Microgels: Structure and responsivity | 15 |
| 1.6 Microgel analysis | 18 |
| 1.6.1 Dynamic light scattering | 19 |
| 1.6.2 Atomic force microscopy | 19 |
| 1.7 Methods to determine and characterize carbohydrate–lectin interactions | 21 |
| 1.7.1 Inhibition studies | 21 |

Table of Contents

| | |
|---|-----|
| 2. Aims and Outline | 25 |
| 3. Conclusion and Perspectives | 27 |
| 4. Publications | 33 |
| 4.1 Thermosensitive Display of Carbohydrate Ligands on Microgels for Switchable Binding of Proteins and Bacteria | 33 |
| 4.2. Temperature switchable glycopolymers and their conformation-dependent binding to receptor targets..... | 61 |
| 4.3. Temperature-controlled adhesion to carbohydrate functionalized microgel coatings: an <i>E. coli</i> and lectin binding study | 117 |
| 5. References | 173 |
| 6 Appendix | 189 |
| 6.1 List of abbreviations | 189 |
| 6.1.1 General abbreviations | 189 |
| 6.1.2 Carbohydrate abbreviations | 190 |
| 6.1.3 Chemical abbreviations | 190 |
| 6.1.4 Units, parameters and symbols..... | 192 |
| 6.2 List of Figures | 194 |
| 7. Acknowledgements | 197 |

Abstract

Interactions between carbohydrates and lectins at the surface of cells control numerous biological processes such as fertilization, cell-cell communication, signaling, and bacterial as well as viral infections. The interactions of lectins and carbohydrates are usually weak, thus multivalency is a hallmark of carbohydrate-binding, which is of key importance to increase the affinity and specificity and to control downstream biological functions. These multivalent effects on the cell surface are highly complex and not completely understood. A valuable strategy to decipher these mechanisms are well-controlled glycomimetic structures and studying their interaction with biological targets. These glycomimetics represent simplified analogues of the complex oligosaccharide structures found on the cell surface, e.g. by only presenting the terminal carbohydrate unit on the polymer scaffold. Glycomimetic polymer scaffolds can have various shapes like linear or branched polymers, 2D polymer arrays or microgels. Furthermore, polymer scaffolds allow the control over the elastic modulus and the hydrophobicity of the overall structure, which will, in turn, affect the interaction and adhesion properties to cells. Using so-called responsive polymers, these parameters can be controlled by remotely “switching” the temperature, pH or other parameters. Importantly, the multivalent presentation of carbohydrate ligands on polymer scaffolds and thus the specific adhesion cells could be controlled by such switchable scaffolds as well. This thesis thus aims at synthesizing thermoresponsive glycopolymer mimetics and investigating their binding properties upon temperature stimulus.

In the first part of this thesis, thermoresponsive microgels based on poly(*N*-isopropylacrylamide) (P(NIPAM)) are functionalized with carbohydrate ligands. By varying the glycomonomer concentration, it is possible to synthesize a set of microgels with different carbohydrate densities in a single reaction step below 1 mol%. The microgels show a decrease in the lower critical solution temperature (LCST) and an increase in size when the carbohydrate concentration increases. These microgels are able to undergo a 10-fold change in volume when crossing the LCST, which allows for a drastic change in the ligand density on the surface of the microgels. To test this effect, binding studies towards the lectin Concanavalin A (ConA) are carried out indicating that the binding affinity is increased with temperature and the collapse of the microgels. Additionally, binding studies with *Escherichia coli* (*E.coli*) showed stronger specific binding when the temperature is raised above the LCST. Further studies with fluorescence microscopy and shorter incubation times showed that it is possible to catch and release *E. coli* upon temperature switch (**Figure 1a**).

In the second part of this thesis, carbohydrate-bearing thermoresponsive polymers are synthesized via a two-step approach. In the first step, a poly(active ester) is synthesized. In the second step, amine-functionalized carbohydrates and isopropylamine are grafted onto the polymer. Using this technique, a set of ten glyco-functionalized thermoresponsive polymers is produced, and the effect of different carbohydrate linkers, as well as the ratio of the carbohydrate to the thermoresponsive *N*-isopropylacrylamide (NIPAM) units, is investigated. In the binding studies, the polymers serve as temperature-dependent adhesion inhibitors for ConA and *E. coli* and a change in the adhesion inhibition can be observed in dependence of the carbohydrate concentration within the polymer. Interestingly, for polymers with low amounts of carbohydrate (below 2 mol%), the binding affinity can be switched by temperature stimulus, and the inhibition of ConA decreases with elevated temperature while the inhibition of *E. coli* is enhanced. The coil-to-globule transition of the polymers leads to a different accessibility of the ligands and causing a different inhibition towards the different sized receptors (see **Figure 1b**).

Based on the encouraging results of the first parts, selected carbohydrate-functionalized microgels are used to prepare thin films on solid surfaces (see **Figure 1c**). An inhibition and direct binding assay are carried out, and it is found out that ConA binding is time-dependent, where for short incubation times (30 min) the binding above the LCST is favored and at long incubation times (24 h) the binding towards the swollen microgel surface is stronger due to diffusion of the receptor into the microgel network. The ability of the surfaces to bind bacteria is tested with *E. coli*. As seen before, contradicting results compared to ConA binding are obtained. For an incubation time of 30 min, no differences in binding above or below the LCST can be observed, while for 24 h the affinity towards the collapsed microgel surface is enhanced. Overall, these results show, that diffusion times and the size of the receptor are parameters that lead to diverging binding affinities above or below the LCST of the glycopolymer scaffolds.

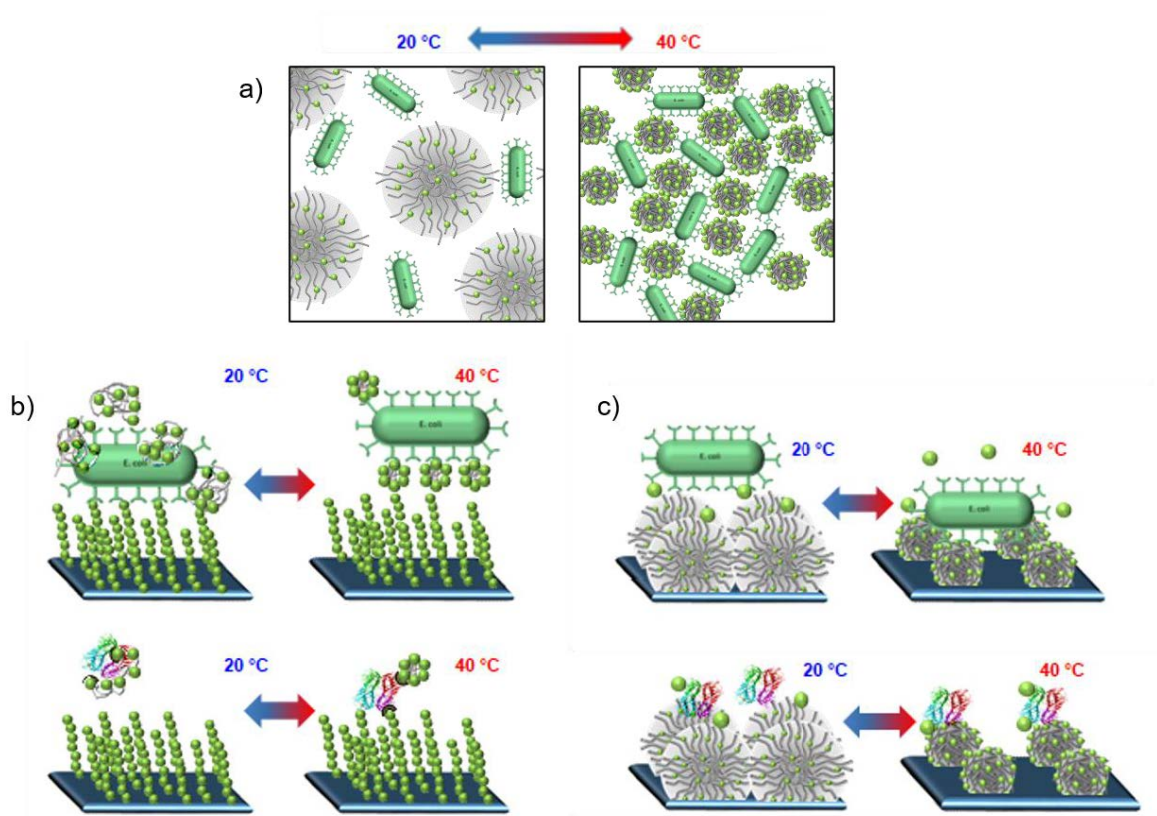


Figure 1. Schematic presentation of the different assays conducted in this thesis. In the first part (a.) the temperature-dependent binding of carbohydrate bearing microgels towards *E. coli* is shown. By raising the temperature above the LCST (40 °C), the binding of bacteria is enhanced, and more aggregates are formed. In the second part (b.) a schematic representation of the temperature-dependent adhesion inhibition assays is given. Green fluorescent protein (GFP) expressing *E. coli* or fluorescein isothiocyanate-ConA (FITC-ConA) adhere to a mannan coated surface. By the addition of glycopolymers the adhesion of the receptor towards the surface is inhibited. In the third part (c.) glyco-functionalized microgels are coated onto surfaces, and the adhesion of GFP-expressing *E. coli* and FITC-ConA is readout at temperatures below and above the LCST.

To summarize, in this thesis, the effects of ligand density on different thermoresponsive scaffolds as well as their temperature-dependent binding towards different sized receptors in solution and on surfaces are demonstrated. The results shed new light on contradicting results in the literature on the specific binding of glycopolymer scaffolds above or below the LCST. New insights are provided, not only in carbohydrate-lectin based interactions but also for the development of catch and release devices for pathogens.

List of publications

Publications included in this thesis

1. **Tanja J. Paul**, Sophie Rübél, Marco Hildebrandt, Alexander K. Strzelczyk, Carina Spormann, Thisbe K. Lindhorst, Stephan Schmidt

Thermosensitive Display of Carbohydrate Ligands on Microgels for Switchable Binding of Proteins and Bacteria

ACS Applied Materials and Interfaces, **2019**, 11 (30), 26674-26683.

2. **Tanja J. Paul**[#], Alexander K. Strzelczyk[#], Melina Feldhof, Stephan Schmidt

Temperature switchable glycopolymers and their conformation-dependent binding to receptor targets

Biomacromolecules **2020**, 21, 7, 2913–2921.

[#]equal contributions

3. **Tanja J. Paul**, Alexander K. Strzelczyk, Stephan Schmidt

Temperature-controlled adhesion to carbohydrate functionalized microgel coatings: an *E. coli* and lectin binding study

In preparation

Publications not included in this thesis

1. Stephan Schmidt, **Tanja J. Paul**, Alexander K. Strzelczyk

Interactive polymer gels as biomimetic sensors for carbohydrate interactions and capture-release devices for pathogens

Macromolecular Chemistry and Physics, **2019**, 22, 1900323.

2. Alexander K. Strzelczyk, **Tanja J. Paul**, Stephan Schmidt

Quantifying thermo-switchable carbohydrate mediated interactions via soft colloidal probe adhesion studies

Macromolecular Bioscience, **2020**, 2000186.

3. Lukas Fischer, Ricarda C. Steffens, **Tanja J. Paul**, Laura Hartmann

Catechol-functionalized sequence-defined glycomacromolecules as covalent inhibitors of bacterial adhesion

Polymer Chemistry, **2020**, DOI: 10.1039/d0py00975j.

4. Dimitri Wilms, Fabian Schröer, **Tanja J. Paul**, Stephan Schmidt

Switchable adhesion of *E. coli* to thermosensitive carbohydrate presenting microgel layers: a single cell force spectroscopy study

Langmuir, **2020**, accepted.

Oral and poster presentations

1. **Tanja J. Paul**, Sophie Rübél, Fawad Jacobi, Stephan Schmidt

Specific Adhesion of Pathogens on Glycocalyx Mimetic Hydrogels

International Conference on Adhesion in Aqueous Media: From Biology to Synthetic Materials, AAM2019, September 09-12, **2019**, Dresden.

2. **Tanja J. Paul**, Sophie Rübél, Carina Spormann, Thisbe K. Lindhorst, Stephan Schmidt,

Synthesis and characterization of biomimetic thermoresponsive microgels and their ability to bind proteins and bacteria in solution and on surfaces

15th Zsigmondy Colloquium, Juli 10-12, **2019**, Dresden.

3. **Tanja J. Paul**, Fawad Jacobi, Hanqing Wang, Carina Spormann, Thisbe K. Lindhorst, Stephan Schmidt

Specific adhesion of pathogens on glycocalyx mimetic hydrogels

Nanolithography of Biointerfaces Faraday Discussion, Juli 3-5, **2019**, London.

4. **Tanja J. Paul**, Pauline Watermann, Sophie Rübél, Stephan Schmidt

Temperature-enhanced adhesion of bacteria and proteins to bioligand presenting microgel surfaces

American Chemical Society, National Meeting & Exposition: Nanoscience, Nanotechnology & Beyond, August 19-23, **2018**, Boston, MA, USA.

5. Tanja J. Paul, Pauline Watermann, Sophie Rübél, Stephan Schmidt

Microgel Surfaces for Temperature-Enhanced Adhesion of Proteins and Bacteria

14th Zsigmondy Colloquium, April 09-11, **2018**, Mainz.

1. General Introduction

1.1 The sweet nature of carbohydrates

Carbohydrates, or simply sugars, are well-known for their role in nutrition and the mechanical support of tissue, but their decisive functions in more intricate processes such as cell adhesion and recognition were underestimated for quite a long time. The research of sugars started with Emil Fischer in 1891, when he was able to solve the spatial shape of three monosaccharides.^[1] These monosaccharides are chiral polyhydroxyalkanal or polyhydroxyalkanone consisting of three to nine carbon atoms, which can be aligned in a ring or a chain.^[2] By combining a wide array of these monosaccharide building blocks complex oligo- and polysaccharides can be built.^[3] Moreover, these structures can be combined through various chemical linkages enabling complex architectures, e.g. linear or branched (see **Figure 2**).^[4]

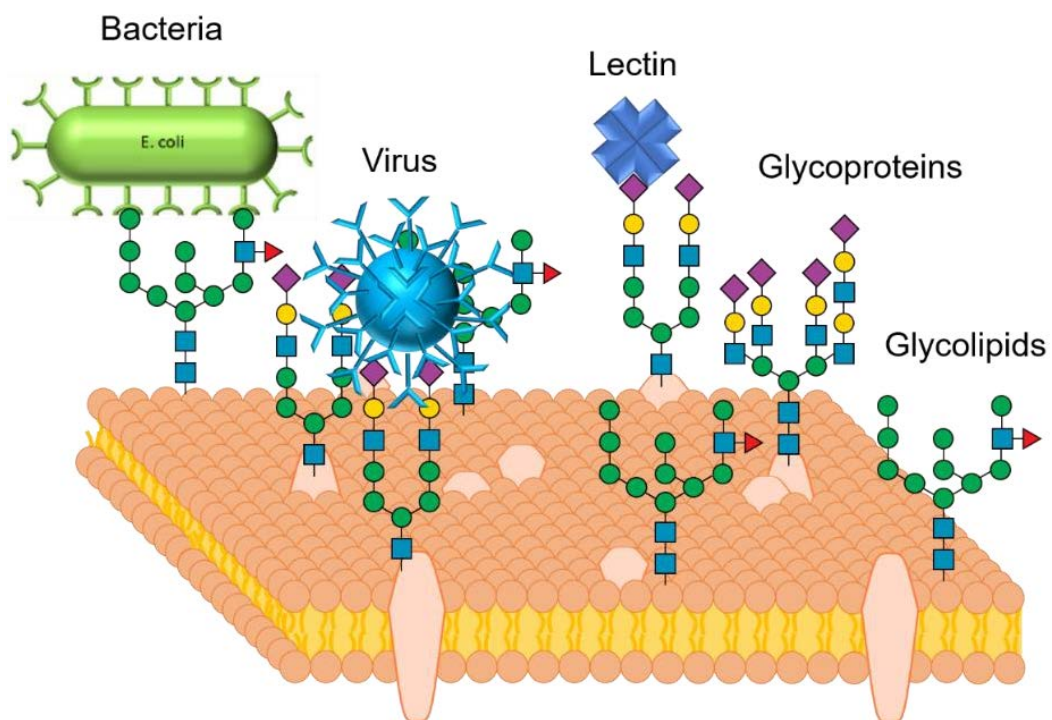


Figure 2. Schematic representation of the cell surface. The lipid double layer with membrane proteins is shown. On top of some lipids and membrane proteins, oligosaccharides are attached and, therefore, form glycolipids or glycoproteins. This dense layer of carbohydrates is called glycocalyx, and it is shown how different receptors interact with these carbohydrates. Examples for receptors that interact with the glycocalyx are bacteria, viruses, and lectins. Glycans adapted from [5].

Though this structural diversity carbohydrates represent one of the three classes of biomacromolecules in the body besides proteins and nucleotides. It was found that carbohydrates are not only an energy source and structural elements but also are involved in important biological processes on the cellular level such as signalling, cell-cell communication, bacterial or viral infection, and fertilization.^[6-8] Carbohydrates, mostly oligo- and polysaccharides, that are involved in these processes are typically attached to lipids and proteins and form glycoconjugates.^[9] These different types of glycoconjugates are found at the surface of cells and form a dense layer, the so-called glycocalyx (see **Figure 2**).^[10]

The thickness of this carbohydrate layer can be up to 100 nm, and the composition of the sugars, especially the terminal sugars is characteristic for each cell type and its stage of development.^[11] In **Figure 3**, the most common terminal monosaccharides that are found at the glycocalyx are shown. It can be seen that α -D-sialic acid, α -L-fucose and β -D-galactose make up nearly three-quarters of the terminal saccharides.^[12] The main role of these carbohydrates is to act as recognition markers for e.g., bacteria, cells, or viruses. For example, α -D-sialic acid is known to bind to the hemagglutinin receptors of the influenza viruses or pseudomonas aeruginosa starts the infection and colonialization with binding to α -L-fucose and β -D-galactose.^[13,14,15]

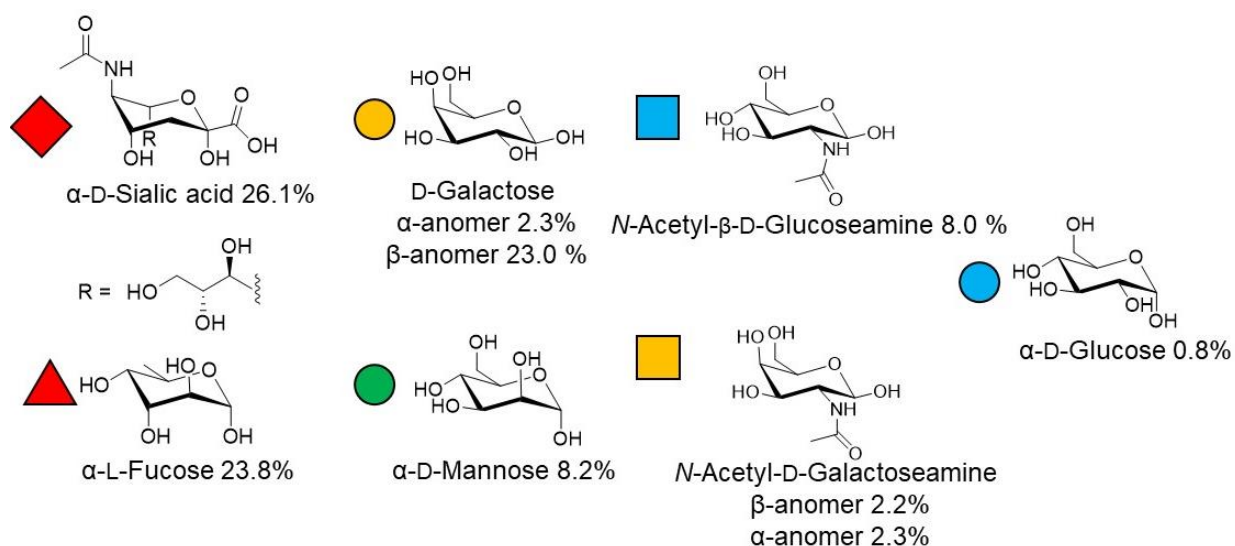


Figure 3. Chemical structures of the terminal monosaccharides found at the glycocalyx. Their appearance frequency was determined by Seeberger *et al.*^[12] Also shown is the schematic representation of the carbohydrates by the colored symbols.

As can be seen in **Figure 3**, the structural diversity of monosaccharides is high and gets even higher when two or more of them are combined. Only at one monosaccharide, five different linkage positions of the second sugar are possible, while there are 100 different structures for trisaccharides.^[16] This high complexity of the carbohydrate chemistry and the structural diversity of oligosaccharides leads to problems in understanding the biological role of carbohydrates. But by looking at the natural processes, e.g. the receptors that bind to the glycocalyx, we can gain an insight into the complex language of carbohydrates. Specific proteins, which bind to sugars are called lectins.

1.2 Lectins – The sugar communicators

Proteins that specifically interact via non-covalent bonds with carbohydrates and which are not enzymes or antibodies are called lectins.^[17-19] The term lectin was first used by Boyd *et al.* in 1954 and originates from the Latin word *legere*, which means to choose.^[20-21] But the discovery of lectins started about one century before in 1853 when Charcot and later Lyden found crystals in the sputum of asthma patients that were later on identified as Galectin-10.^[16] One of the most significant achievements in glycobiology was the isolation of Concanavalin A (ConA) by Sumner in 1919 out of the Jack Bean (*Canavalia ensiformis*). Afterwards, it was shown that ConA is able to agglutinate not only with erythrocytes but to distinguish between malignant cells and healthy cells.^[22-23] With this knowledge, the importance of lectins was recognized, and in 1972, the amino acid sequence and the 3D-structure of ConA were solved.^[24-25] In general, lectins can be found in every organism and can be categorized into plant-, viral-, bacterial- and animal lectins and further into different lectin types. These different lectin types can be, for example, C-type and I-type lectins, which are mainly located in the membrane of cells or M-type and L-type, which are situated in the endoplasmatic reticulum.^[26] Besides their location in organisms, these lectin types can be divided through their function and classification. For example, C-type lectins require Ca^{2+} -ions for their structural function and carbohydrate-binding, whereas I-type lectins must contain an immunoglobulin-like fold.^[4, 27-29] Nevertheless, all lectins exhibit a domain that binds to the referring mono- or oligosaccharide, which are called carbohydrate recognition domains (CRDs).^[30] These CRDs bind specifically to one terminal carbohydrate type.

As mentioned, not only single lectins play an important role in glycobiology, but also their multivalent presentation on organisms, which interact with multiple sugars at the glycocalyx. For example, bacteria have developed a “sweet tooth” using lectins to adhere to carbohydrates on the cell surface of a host’s tissue. This bacterial adhesion can be advantageous when it appears in an appropriate place for the host, or disadvantageous at

a different area of the body. For example, *Escherichia coli* (*E. coli*) adhesion in the intestinal tract of the human body has positive effects for the host, but it can also cause infections when *E. coli* is spread into the urinary tract.^[7, 31]

Of special interest for this thesis are lectins that bind to α -D-mannose units. α -D-mannose is the fourth most common terminal sugar that can be found on the glycocalyx and as model lectins such as ConA bind to this carbohydrate, it is particularly well suited for the experiments in this thesis.^[12]

1.3 α -D-mannopyranoside binding lectins

1.3.1 Concanavalin A

One of the most important model lectins that bind to α -D-mannopyranoside (Man) is the plant lectin Concanavalin A (ConA). It is isolated from the jack beans (*Canavalia ensiformis*) and was the first lectin of which the primary, as well as the quaternary structure, were known.^[24, 32] Like most plant lectins, ConA belongs to the legume family, and as calcium ions are needed to bind to carbohydrates, it is a C-type lectin.^[33] At neutral pH, ConA attains a homotetrameric structure, which consists of four identical subunits with one carbohydrate recognition domain (CRD) each and a minimum distance of 7.2 nm between them (see **Figure 4**).^[34] Under acidic conditions (pH < 6) dimers of two of these subunits are formed. The CRDs of the subunits are equal and bind as mentioned to Man as well as α -D-glucopyranoside (Glc). Even though being able to bind the two different carbohydrates Man and Glc, ConA is unable to bind either to α -D- or β -D-galactopyranoside (Gal). The structural differences of the carbohydrates at the carbon atoms C3-C6 control whether hydrogen bonds with the CRD can be formed or not. In the case of Gal at the C4 position, the hydrogen bond is not formed, and therefore, no recognition is possible.^[35] As a result, Gal is used as a non-binding control in binding or inhibition assays.^[36]

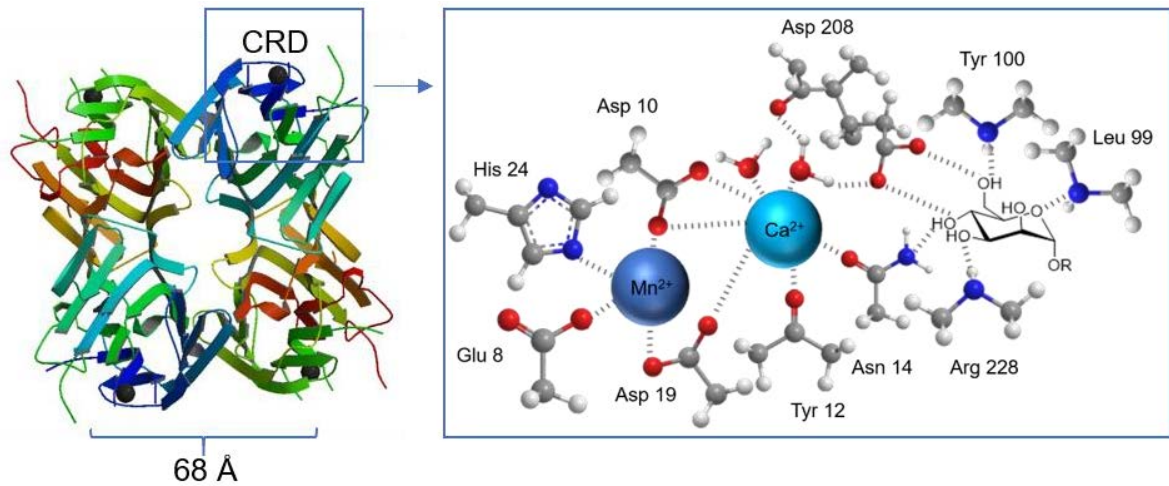


Figure 4. Schematic presentation of the quaternary structure of ConA with a marker on the proteins CRD (left) (Protein Database code: 1jbc). Additionally, the amino acids and metal ions (Mn^{2+} and Ca^{2+}) are shown with their spatial arrangement during a binding event with α -D-mannopyranoside terminally bound on a scaffold R (right). Adapted from [37].

1.3.2 FimH

In 1908 it was assumed for the first time that bacteria could adhere to cells after it had been reported that *Escherichia coli* (*E. coli*) can agglutinate animal cells.^[38] *E. coli* have so-called fimbriae or pili attached to their surface that are responsible for the adhesion to cell surfaces.^[39] This adhesion is mediated via carbohydrate-lectin interactions between the adhesin FimH located on the tip of those pili and Man moieties on the cell surface. This step of bacterial adhesion is the initial step in biofilm formation and colonization, leading to infections.^[40] Urinary tract infections (UTI) are initiated by *E. coli* and are mainly treated with antibiotics.^[41] Due to the development of resistances against antibiotics, it is of major interest to find new ways of treating those infections and infections of any kind.^[42-43] One way to treat *E. coli* infections is by inhibiting the initial step: the adhesion to cells.^[44-45] Therefore, it is important to understand the mechanism that takes place and the protagonist of the adhesion processes: the adhesin FimH. Adhesins are proteins on the surface of cells enabling the attachment to biological surfaces with high selectivity via recognizing molecular motifs.^[46-47] FimH selectively recognizes and binds Man (see **Figure 5**) and, therefore, can be additionally classified as lectin.^[48] In contrast to most lectins, FimH is a monovalent lectin able to bind only one mannose moiety as it has been determined in the X-ray structure of the protein.^[49]

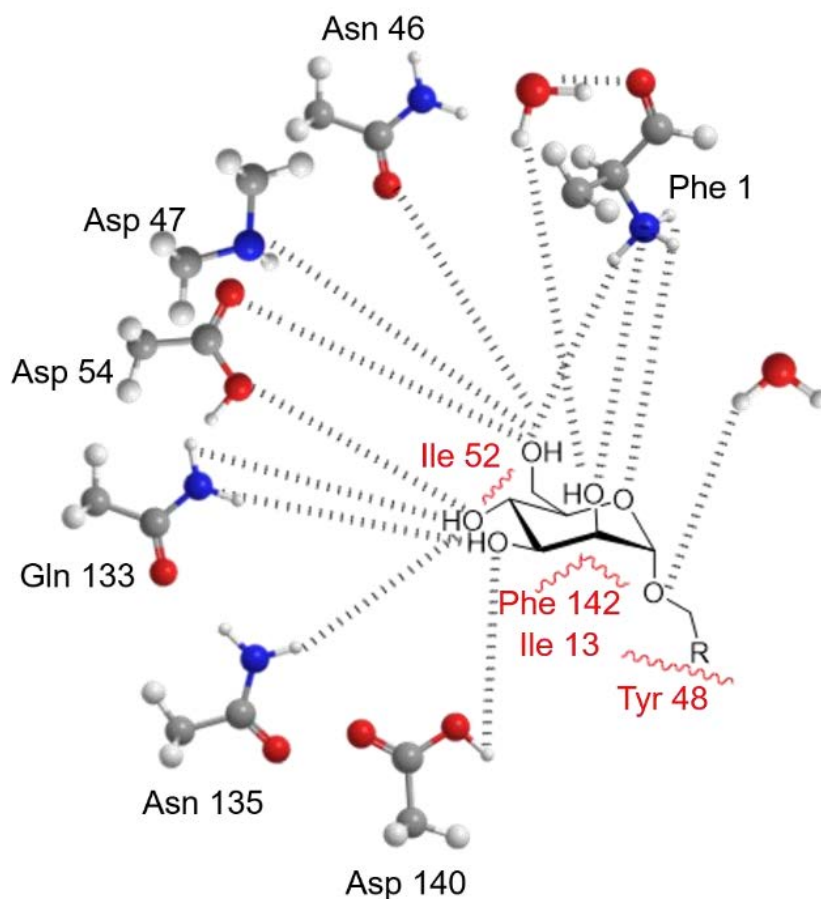


Figure 5. Schematic presentation of the CRD of FimH. Amino acids responsible for the development of hydrogen bonds (grey lines) to Man are shown, as well as hydrophobic interactions between the CRD and Man (red waves). Adapted from [50]

For the development of inhibitors for lectin or bacteria adhesion, it is important to understand the underlying adhesion mechanisms taking place between ligands and receptors. Here, it is essential to know that the interactions between carbohydrate and lectin leading to binding are secondary, non-covalent interactions such as hydrogen bonds and van der Waals forces. Carbohydrate-lectin interactions also work after the lock-key principle, meaning that the recognition is depending on the structural properties of the recognition unit of the lectin and the structure of the carbohydrate ligand. Therefore, a small change in the ligand structure, such as a different position of a single hydroxyl group or the change of a linker, can change the ability of a lectin to recognize and bind a carbohydrate.^[51] As a single carbohydrate-lectin binding is weak and to overcome this problem both, ligand and receptor, are presented in high numbers to interact simultaneously. This effect leads to a stronger binding and is called multivalency. When comparing both lectins ConA and FimH, a major difference is the number of carbohydrate recognition domains presented on the lectin.

Due to its tetrameric structure, ConA is able to bind up to four mannose units, meaning it is able to show multivalent behavior on an nm scale.^[34] However, FimH can only bind one Man unit and is, therefore, presented on bacteria in a multivalent fashion to increase the binding on a μm scale.^[52]

1.4 Multivalency

As the interactions between carbohydrates and lectins are weak, multivalency plays a very important role in adhesion processes on the cell surface. As mentioned above, by increasing the number of ligand-receptor binding pairs, the overall strength of interactions increases.^[53-58] This effect is also present in non-specific interactions and has already been taken advantage of for inventions such as Velcro.^[59] On cell surfaces, the increased number of ligand-receptor pairs increases not only the binding strength, but also the number of bound states. If adhesion processes would only be mediated through single ligand-receptor interactions, there are only two possible states: bound and unbound. But as association and dissociation of a single ligand-receptor pair show low affinity constants between 10^3 and 10^6 M^{-1} ligands need to be presented in a larger number to enhance overall avidity.^[54] By increasing the number of ligands on the same scaffold, the number of bound states in comparison to the unbound state increases. Consequently, a linear increase in binding partners leads to a non-linear increase in bound states (see **Figure 6**).

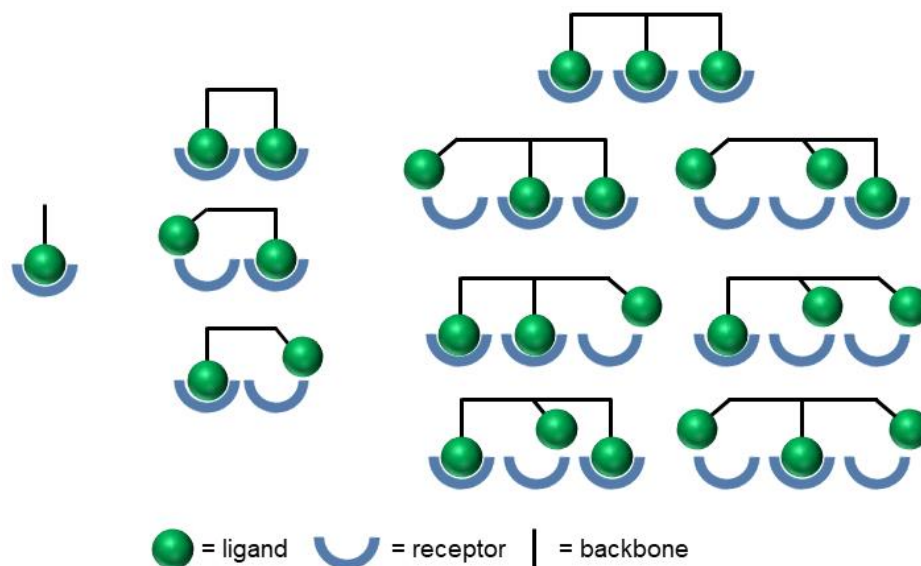


Figure 6. Schematic presentation of increasing binding by multivalent presentation of ligands and receptors. A linear increase in the number in binding partners starting at a single pair (left) going to two (middle) and up to three (right) and their non-linear increase in bound states from one to seven are shown.

When a scaffold presents more than one ligand, it enables additional effects that influence the binding energies. Four different effects can be distinguished (see **Figure 7**): 1) statistical rebinding, 2) chelate effect, 3) clustering and 4) sterical shielding.

1) Statistical rebinding: As mentioned above, ligand-receptor interactions depend on the association and dissociation of the binding partners. Carbohydrate-lectin interactions bind and rebind very fast due to their weak non-covalent interactions. Therefore, having an unbound ligand in proximity to a bound ligand increases the binding due to a fast replacement of the bound ligand by the unbound one.^[60]

2) Chelate effect: The chelate effect occurs when two or more ligands presented on the same scaffold bind to the same receptor at the same time. After the first binding event takes place, subsequent binding events are favored due to entropic requirements of the first binding event.^[61-62] Chelate binding is highly influenced by the flexibility and size of the scaffold, as well as the spacing of binding sites of the receptor, but using an appropriate structure can lead to up to a million times higher binding affinity compared to the monovalent ligand.^[63-64]

3) Clustering: Clustering is the binding of multivalent presented ligands towards more than one receptor. This means that the multivalent ligand acts as a bridging molecule or crosslinker between receptors and can lead to clusters of receptors and ligands up to agglomerates and precipitates depending on the concentrations of both molecules.^[65]

4) Sterical shielding: Ligands that are bound to a receptor can be shielded by the scaffold's backbone, which is called sterical shielding. This prevents other ligands from interacting with the receptors binding pocket and, therefore, a displacement of the receptor-bound ligand by a competing ligand presenting molecule. This effect has been determined as a stabilizing effect for the ligand-receptor complex and, therefore, is important for the design of molecules used for receptor binding.^[66]

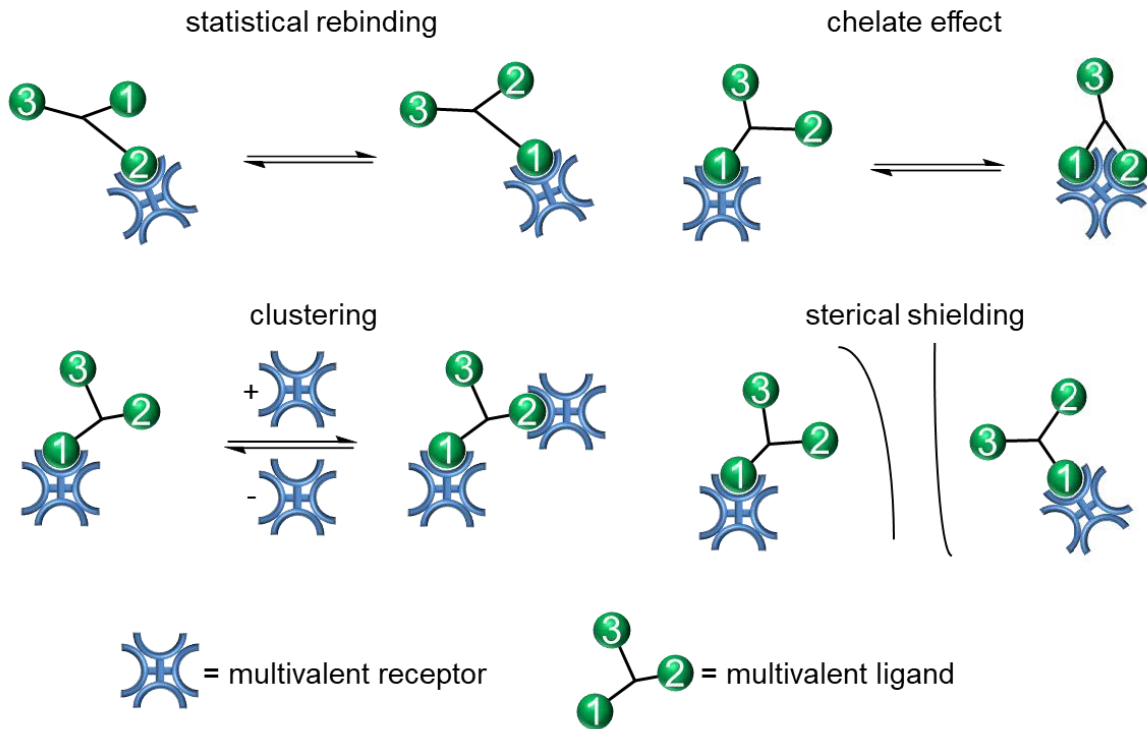


Figure 7. Schematic presentation of the effects occurring by a multivalent presentation of ligands and receptors. Statistical rebinding is shown (top, left), where the bound ligand 2 is replaced by ligand 1 due to their proximity. The chelate effect (top, right) shows the binding of two ligands, presented on the same scaffold, towards the same receptor. Clustering (bottom, left) is the binding of more than one receptor to the ligands presented on a scaffold. Sterical shielding (bottom, right) is the repulsion between the backbones and unbound ligands of two glyco-molecules preventing the displacement of the bound ligands by an unbound one from the other glyco-molecule.

1.5 Glycomimetics

The glycocalyx is made of oligo- and polysaccharides bound to lipids and proteins on the cell surface. Due to the high complexity of those molecules and high numbers of carbohydrates it is, as of yet, impossible to synthesize those highly complex and partially branched carbohydrate structures.^[67] One approach to mimic the glycocalyx is to simplify those complex structures on an artificial backbone, e.g. via glycopolymers or particles such as metal nanoparticles or polymeric microgels.^[68] To target a certain lectin and control a biological function, usually, only the terminal carbohydrates need to be considered.^[69] Depending on the used carbohydrates for the synthesis of a glycomimetic it can be distinguished between homo- and heterovalent glycomimetics, whereas homovalent structures only present one type of carbohydrate and heterovalent present two or more.^[70-72] Here, it has to be noted that a glycomimetic presenting a disaccharide, e.g. lactose (beta-Gal-Glu), is a homovalent structure that binds via the Gal units in case of lactose.

Different architectures of scaffolds for the presentation of carbohydrates are suitable for further applications. The architectures used for the multivalent presentation of ligands go from oligomers and linear polymers to dendrimers and polymeric microgels to metallic nanoparticles (see **Figure 8**).^[72-76]

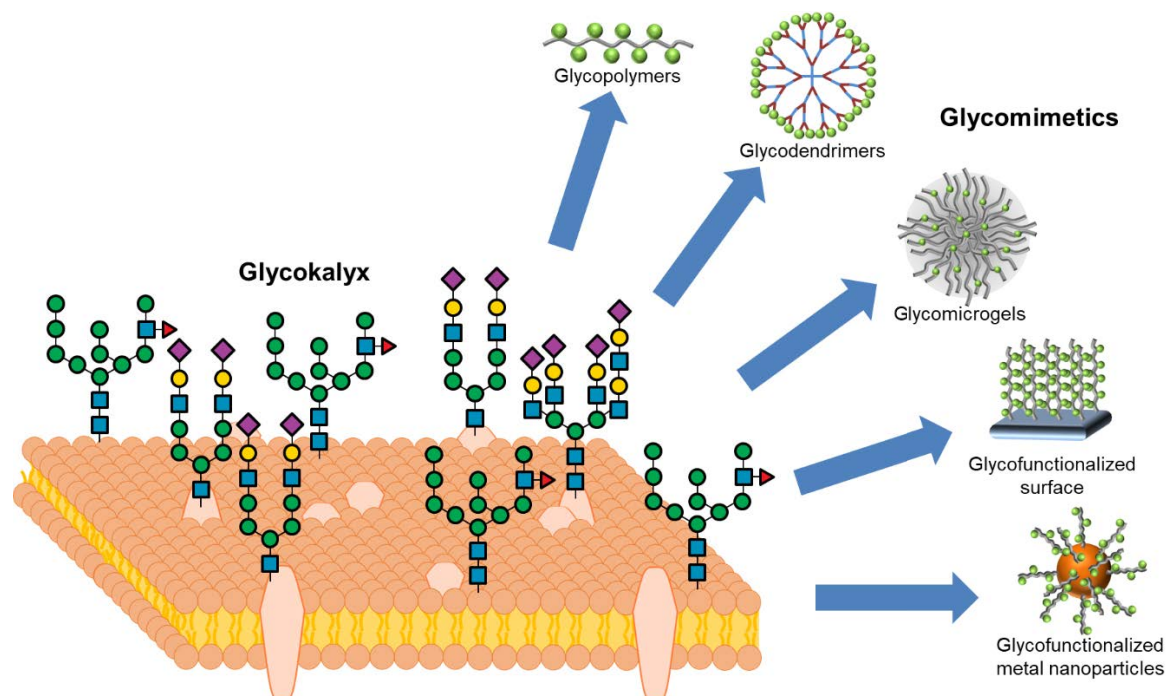


Figure 8. Schematic presentation of the glycocalyx (left) and scaffolds used as a glycomimetic (right). The glycomimetics vary from glycopolymers and -dendrimers, to glycomicrogels and glycofunctionalized surfaces as well as nanoparticles (top to bottom). Glycans adapted from [5].

Due to the incorporation of carbohydrate ligands into these architectures the prefix “glyco” is used, in accordance with the glycocalyx, as for example in glycopolymer.^[77] These mimetics can be used for the investigation of the interaction mechanisms between receptors and ligands as well as for diagnostics and different types of therapeutics.^[78-80] Glycomimetics can be used as therapeutics in many different ways such as inhibitors for the adhesion of bacteria or viruses and, therefore, as an anti-inflammatory agent.^[81-82] Moreover, they show properties to be used as a targeted drug-delivery system. Additionally, using polymeric backbones as a scaffold for the presentation of carbohydrate ligands gives the possibility of incorporating additional properties to the glycomimetic.^[83] By using, for example, stimuli-responsive polymers and functionalize them with carbohydrates, additional characteristics can be included. Incorporating these stimuli responses into the backbone gives a higher level of control over the interactions that take place between the carbohydrate ligands and the lectin receptors.^[84]

1.5.1 Glycopolymers

One important class of glycomimetics are the glycopolymers. These are synthetic polymers with carbohydrate ligands incorporated into the side chain, at the terminal position, or both.^[85-86] These types of polymers are suitable for different biomedical applications because the abilities of these glycomimetics can even exceed the binding properties of the glycocalyx.^[87] Therefore, they can be found in different fields of research, such as biosensors, drug delivery, inhibition, and drugs.^[88-92] The synthesis of glycopolymers is mainly based on radical polymerization techniques. Controlled radical polymerization techniques such as atom transfer radical polymerization (ATRP) and reversible addition-fragmentation polymerization (RAFT) are suitable for the synthesis of glycopolymers and give additional control over the dispersity of the polymer chains, but also free radical polymerization (FRP) is utilized.^[91, 93-94] Moreover, different ways for the incorporation of carbohydrates into the polymer are suitable. In general, it can be distinguished between two approaches: 1) (co-) polymerization of carbohydrate bearing monomers or glycomonomers (see **Figure 9**, top), and 2) post-functionalization (see **Figure 9**, bottom). For the first approach, a carbohydrate monomer with a polymerizable unit needs to be synthesized. During the intense research on polymer-based glycomimetics, different methods have been established for the synthesis of glycomonomers, which are often based on (meth-)acrylate and (meth-)acrylamide as the polymerizable unit.^[95-96] Using these monomers during the polymerization, it is possible to synthesize homopolymers presenting a high density of carbohydrate ligands. These polymers have such a high density of carbohydrates that they cause negative effects overruling the benefits of multivalency.^[97] Therefore, a comonomer

can be included to decrease the carbohydrate density. This approach has the advantage that, when choosing a suitable comonomer, the polymer architecture can be controlled, but in the worst case, no polymer can be synthesized because a copolymerization of both monomers is not possible.^[98] To overcome these difficulties during the polymerization, the post-functionalization approach can be used. Here, a polymer precursor is synthesized bearing reactive groups such as carboxylic acids, chlorides, anhydrides or active esters and are later on functionalized to construct a glycopolymer.^[99-101] Using the post-functionalization approach enables the synthesis of copolymers that could not be synthesized by using the corresponding monomers, and a fast synthesis of a library of glycopolymers with different ligand densities or different carbohydrate ligands is possible.^[77] Both of these approaches can be used to incorporate additional properties into the glycopolymer. One class of polymers has especially caught the attention for the combination with glycopolymers: stimuli-responsive polymers.

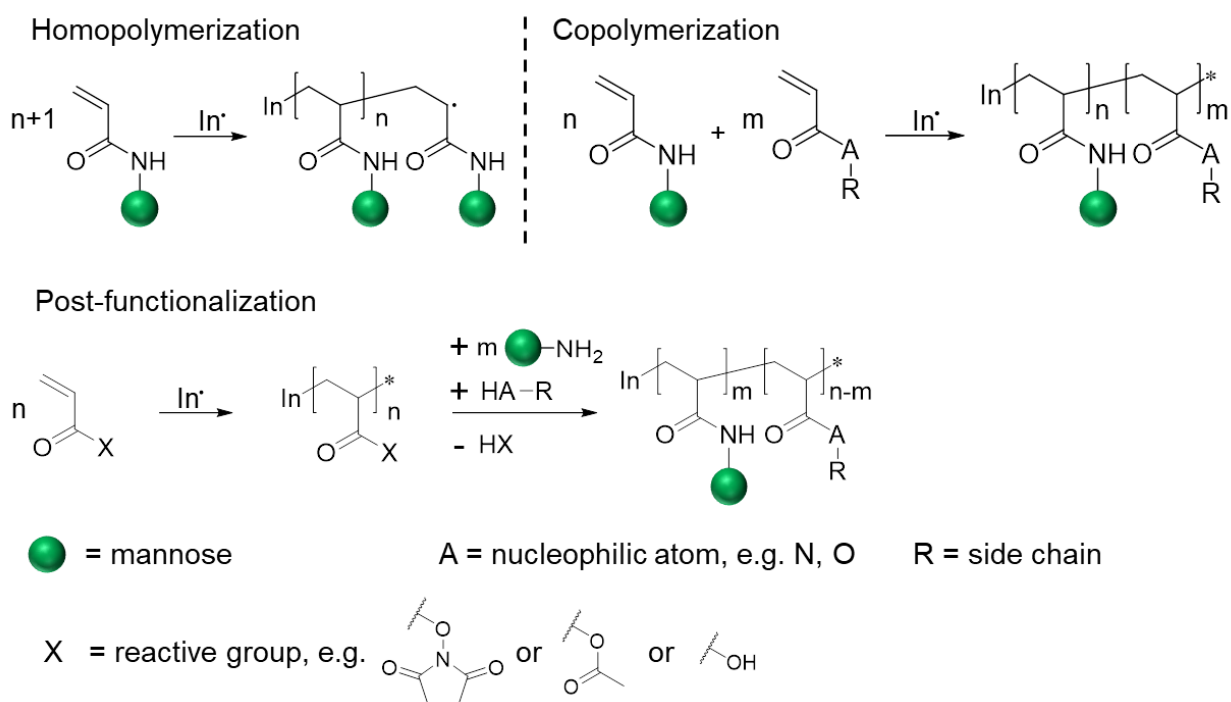


Figure 9. Scheme of different approaches for the synthesis of glycopolymers. The homopolymerization of glycomonomers can be used to synthesize glycopolymers with high carbohydrate densities (top, left). Using a second monomer during the synthesis gives copolymers with variable carbohydrate densities and switchable polymer properties (top, right). For the post-functionalization approach, a homopolymer with a reactive side group (e.g. active ester, anhydride or acid) is synthesized. In a second step, it is functionalized with carbohydrates and a nucleophile to synthesize a glycopolymer with different properties and carbohydrate densities (bottom).

1.5.2 Stimuli-responsive polymers

Stimuli-responsive polymers are a special class of macromolecules that respond to small changes in their environment by changing their properties such as shape, physical or chemical properties.^[102-103] These external stimuli can be a change in pH, light, ionic strength or temperature and, therefore, are called, in accordance with their stimulus, for example, pH- or thermoresponsive.^[84,104-106] Due to their response to different stimuli, those polymers are of great interest for different applications in biotechnology and medicine.^[107] Imaginable applications range from biosensing and biomimetics to controlled drug-delivery.^[108-109] One of the most-investigated stimuli is temperature due to the consideration of being convenient for many of the named applications.^[110] There are two different groups of thermoresponsive polymers. The first group shows an Upper Critical Solution Temperature (UCST) and dissolves easier at elevated temperatures. The second group of thermoresponsive polymers exhibits a so-called Lower Critical solution Temperature (LCST), which shows the exact opposite behavior, meaning that those polymers precipitate at elevated temperatures. Most LCST-polymers show this behavior in a polar solvent like water. Therefore, each thermoresponsive LCST polymer is composed of a hydrophilic and a hydrophobic part. On the one hand, a hydrophilic part is important to build strong intermolecular interactions such as hydrogen bonds to the solvent molecules below the LCST. On the other hand, a hydrophobic part is important to build hydrophobic intramolecular interactions above the LCST. By increasing the temperature, the intermolecular interactions between polymer and solvent are weakened, and the intramolecular interactions of the hydrophobic polymer parts increase. When exceeding the LCST, the polymer collapses from a hydrophilic swollen polymer coil into a hydrophobic polymer globule.^[111] The so-called coil-to-globule transition is only possible by releasing the water. This release leads to an increase in entropy and, due to the collapse into a hydrophobic globule, the polymer chains precipitate. Well-known polymers that show LCST behavior are poly(*N*-isopropylacrylamide) (PNIPAM), poly(oligoethylene glycol methacrylates) and poly(*N*-vinylcaprolactam).^[112-115] These polymers are of special interest because their LCST is in the range of the human body temperature.

1.5.2.1 Thermoresponsive polymer PNIPAM

One of the most-studied thermoresponsive polymers is poly(*N*-isopropylacrylamide) (PNIPAM).^[116] The interest in PNIPAM is partially based on its sharp coil-to-globule transition at 32 °C.^[117] The LCST of PNIPAM can be modified, as for every thermoresponsive polymer, by the incorporation of comonomers to higher or lower values depending on the used comonomer. Important for the variation of the LCST is the comonomer's hydrophilicity. Using a monomer with higher hydrophilicity, than the *N*-isopropylacrylamide (NIPAM) monomer, increases the LCST due to stronger hydrogen bonding with the solvent molecules, whereas a more hydrophobic monomer leads to a decrease in LCST. But if the amount of NIPAM is too low, the polymer loses its thermoresponsiveness.^[118-120] Additionally, not only the LCST can be modified but by using for example methacrylic acid as a hydrophilic comonomer an additional response, here a pH response can be incorporated into the polymer making it a duo responsive polymer.^[121] The combination of two stimuli responses opens up additional possibilities as well as the incorporation of a comonomer or end group functionalization.

The end groups of PNIPAM can be used to graft the polymer chains onto different scaffolds. One scaffold that can be used is, for example, a lectin or a protein that specifically binds to a ligand such as streptavidin.^[122] By grafting onto such a scaffold, it is possible to control the specific binding of streptavidin and its ligand biotin by temperature stimulus.^[123] Furthermore, it is possible to synthesize hybrid materials using nanoparticles or silica surfaces as a scaffold.^[124] Hybrid materials offer the possibility to take advantage of additional properties. By using metal nanoparticles such as gold, a light response can be used to heat up the sample leading to a collapse of the grafted PNIPAM chains. Moreover, properties that only metal particles provide can be incorporated in such hybrid materials when using, for example, Fe₃O₄ particles showing a response to a magnetic field.^[125-126]

In this thesis, it is of special interest to combine thermoresponsive polymers with carbohydrates, vary their architecture, as well as their ligand density, and to see how the polymer conformation influences binding towards receptors. As described in section 1.5.1, two different approaches can be applied to integrate carbohydrate ligands into the polymer. By using a carbohydrate bearing comonomer during the polymerization step or using a comonomer with a reactive group that can be used to graft a carbohydrate in a second step is also suitable for the synthesis of many different thermoresponsive glycomimetics.^[127-130] Besides linear polymers also carbohydrate functionalized microgels, which are based on an LCST-polymer, such as PNIPAM, are of high interest.^[131-132]

1.5.3 Microgels: Structure and responsivity

Microgels are three dimensional crosslinked macromolecules that form colloidal dispersions and are swollen in a good solvent.^[133-134] But the expression “microgel” is often equated with many different terms such as hydrogel, microsphere, nanogel or macrogel.^[135] The term hydrogel is defined over the solvent used, whereas microgels, as well as macrogels and nanogels, are additionally defined over their size.^[136] Therefore, microgels are a sub-class of hydrogels. Due to the use of hydrogels in this thesis that meet the requirements of microgels, the terms “hydrogels” and “microgels” are used equally. Two different types of microgels can be distinguished based on their type of crosslinking: physically and chemically crosslinked microgels (see **Figure 10**).^[137-138] The linkage of physically crosslinked microgels comes from non-covalent interactions such as hydrogen bonding or ionic interactions. One well-known physically crosslinked microgel is based on alginate. Adding alginate solution into a solution of divalent ions such as calcium ions (Ca^{2+}) hydrogels are formed due to interactions between the ions and the guluronic acid units of the alginate.^[139] However, these physically crosslinked microgels are not mechanically stable, as their properties change over time when the ions diffuse into the surrounding medium.^[140] Chemically crosslinked hydrogels are linked via covalent bonds during synthesis and, therefore, they have no reversible linkage and show higher stability.^[141] To synthesize chemically crosslinked microgels, a crosslinker is needed. These crosslinking molecules present two or more polymerizable units as for example, methylene bisacrylamide (MBA).

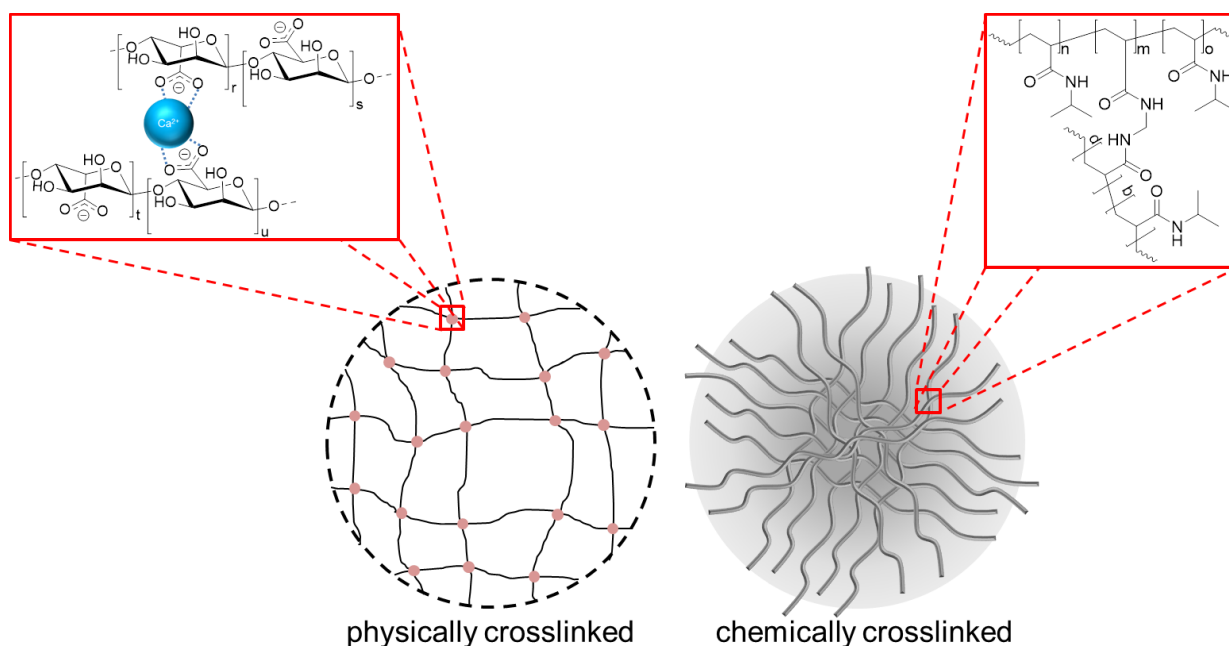


Figure 10. Schematic presentation of different types of crosslinking. Physically crosslinked microgels, here exemplary based on alginate, have crosslinks via non-covalent electrostatic interactions between Ca^{2+} ions and the carboxylate groups of the alginate (left). Chemical crosslinked microgels, here exemplary based on PNIPAM, have PNIPAM chains connected via covalent bonds formed with the crosslinker MBA (right).

Hydrogels offer a wide range of possible applications. Depending on the polymer, which builds the gel, the type of crosslinking and the combination with additional materials such as nanoparticles, they can be used for tissue engineering, controlled-release of molecules (drug-delivery), biosensors and as biomaterials. ^[142-145] Due to the high uptake of water, hydrogels show similar viscoelastic properties as human tissue and, therefore, are good scaffolds to be used as biomimetics. ^[146-147]

1.5.3.1 Thermoresponsive microgels

By combining the three-dimensional microgel architecture with thermoresponsive polymers, thermoresponsive microgels can be synthesized.^[148] PNIPAM is the most used polymer for the synthesis of thermoresponsive microgels, which are usually synthesized via precipitation polymerization. The general synthesis of PNIPAM microgels, and the use of different comonomers, was established by Pelton *et al.* and the resulting particles became popular as drug delivery or tissue engineering systems.^[149] As mentioned in section 1.5.2.1, comonomers can be used during the synthesis to add additional responses such as pH or to functionalize the polymers and microgels, respectively, with additional side chains. For the synthesis of PNIPAM-based microgels, besides NIPAM and a possible comonomer such as methacrylic acid (MAA) or 2-aminoethyl methacrylate hydrochloride (AMEA) a crosslinker such as MBA and a radical initiator, e.g. ammonium persulfate (APS), are needed.^[150-152] A surfactant is not necessary for the synthesis of PNIPAM-based microgels but can be added to stabilize the particle growth during the polymerization.^[153] Throughout the synthesis, the thermoresponsive behavior of PNIPAM is used to synthesize narrowly dispersed microgels. By using the initiation temperature of around 70 °C as reaction temperature, the formed polymers collapse, nuclei are formed and grow until a critical size is reached.^[154-155] To achieve really monodisperse or narrow dispersed microgels, the time frame of the nuclei growth has to be longer than the time frame of nuclei formation. By using thermoresponsive microgels, it is possible to control the elastic properties as well as the water uptake, by the amount of crosslinker used and via temperature change.^[156] Here, the same effects take place as in linear polymer chains. The temperature increase reduces intermolecular interactions and increases intramolecular interactions leading to a release of water that was incorporated into the polymeric network.^[157]

Thermoresponsive microgels are, as well, suitable scaffolds for biomaterials.^[158] By incorporating carbohydrate ligands during the synthesis, they can be used as glycocalyx mimetics.^[159] Due to the importance of carbohydrate-lectin interactions in many different infection processes (see section 1.1) they can possibly be used to prevent adhesion of bacteria or viruses to cells by inhibiting ligand-receptor interactions. Additionally, due to the thermoresponsiveness, the adhesion of receptors can be switched, which makes them suitable for catch-and-release devices.^[160]

Grafting those microgels onto surfaces may be interesting for different applications. As Schmidt *et al.* found out, who coated surfaces with P(NIPAM) microgels, that cell adhesion processes strongly depend on the surface hydrophobicity and the elastic modulus, it is not only important to mimic the carbohydrates on the surface but further to mimic the elastic properties of the cell itself.^[161] Consequently, it is an aim to create carbohydrate functionalized microgels to enable a switchability of the elastic modulus, as well as the ligand density presented on the microgel's surface. Being able to specifically bind cells and bacteria upon temperature-stimulus to those microgel coated surfaces, makes them potentially useful as switchable cell culture dishes or to remove bacteria from wastewater.

1.6 Microgel analysis

Since microgels represent very complex structures and are usually in the nanometer size range, special analytical techniques are required to characterize these structures. The analytical techniques can be distinguished in methods that analyze the properties of microgels in solution and on surfaces. In solution, the stability of microgel dispersions is of great interest for further applications. Therefore, the ζ -potential can be measured to get a deeper insight into the surface charge and the electrostatic stabilization, preventing microgels from aggregation. Additionally, the particle size is of great interest and, for stimuli-responsive microgels, swelling properties in dependence of the stimulus.^[162] To analyze those characteristics, dynamic light scattering (DLS) is a very suitable method. Moreover, analyzing thermoresponsive microgels, DLS is suitable to additionally determine the particles LCST.^[163]

To analyze microgels, bound onto surfaces, different techniques can be applied. A prominent example is atomic force spectroscopy (AFM), which can be used to determine the elastic modulus of surface grafted microgels and the changes that occur upon temperature shifts.^[164-165] Additionally, AFM can be utilized to determine the packing of microgels, grafted onto the surface. Another method that can be used to define the thickness of microgel-layers at surfaces in dependence of the temperature is ellipsometry.^[166]

1.6.1 Dynamic light scattering

Dynamic light scattering, or photon correlation spectroscopy, is a method to determine different parameters of suspended particles.^[167] As microgels in solution scatter light, the scattered light waves of many particles can interfere with each other, leading to fluctuations when laser light is used. By analyzing these fluctuations in dependence of time for spherical particles, two different parameters can be determined: diffusion coefficient D and the hydrodynamic radius R_h . The relation of those parameters is given by the Stokes-Einstein relation as following:

$$D = \frac{k_B T}{6\pi\eta R_h}$$

with k_B as Boltzmann constant, T as temperature, η as viscosity of the solvent.^[168] Moreover, DLS is a suitable method to determine changes in the size of the microgels at different temperatures. By measuring the hydrodynamic radii over a temperature range, it is possible to determine the LCST of a thermoresponsive microgel system.^[169]

1.6.2 Atomic force microscopy

To further analyze the particle properties, atomic force microscopy (AFM) can be used. The AFM method was developed in 1986 by Binnig *et al.* and allows to image the topography of a surface.^[170] Here, the microgels are coated onto a surface, e.g. glass, and washed to remove multilayers and generate a monolayer of microgels. This surface can now be scanned with a cantilever resulting in a height profile of the surface.^[165] These height profiles are generated due to the interactions such as van der Waals forces and repulsive Coulomb forces between the surface and the cantilever. Additionally, in contrast to electron-based microscopy, for example, scanning electron microscopy (SEM), the sample is not damaged. By using these profiles, an image of the surface can be calculated. These profiles give the size of the microgels coated to a surface in a dry state as well as in liquid.^[171] Additionally, the profile and the calculated image show how the microgels are arranged, and the spacing between the single particles on the surface can be determined (see **Figure 11**).^[172] Moreover, besides the determination of the particle size and the surface coating, the AFM technique can be used to measure the elastic modulus (E-modulus) of the particle system. For this technique, a low micrometer-sized silicon dioxide particle is glued on a tipless cantilever and pressed onto the particle leading to a deformation of those. The force-distance curve measured can then be used to calculate the E-modulus using different models.^[173-174]

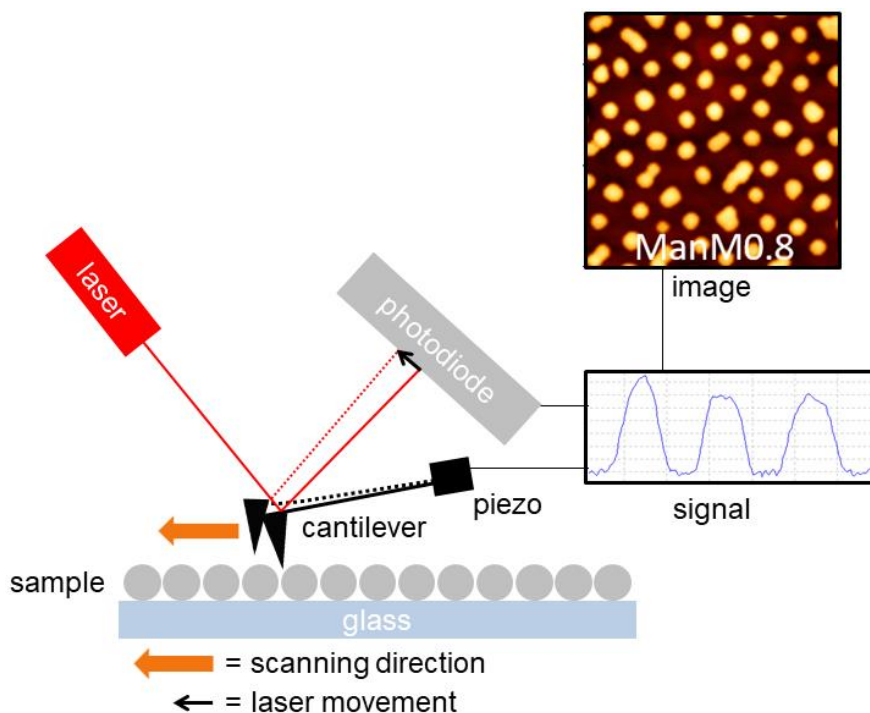


Figure 11. Schematic presentation of atomic force microscopy used for scanning a microgel coated surface. The cantilever moves upon interacting with the microgel surface leading to a laser movement on the photodiode. Those movements are transferred into a height profile of the line scanned. By using height profiles of multiple scanned lines, an image of the microgel coated surface can be calculated.

1.7 Methods to determine and characterize carbohydrate–lectin interactions

As the importance of glycobiology and the interactions at the glycocalyx rose in the scientific audience, a wide array of assays was developed to determine and characterize carbohydrate–lectin interactions. Depending on the setup, the assays can be divided by the presentation of the ligand and the receptor, which can be bound to a surface or be in solution. Further, the assays not only differ in the presentation of the ligand or receptor but also if they are performed in a static or dynamic environment.^[175]

One of the easiest and fastest assays to determine if a ligand binds to the regarding receptor is the turbidity assay.^[176-177] Ligand and receptor are in solution, and since most lectins have multiple carbohydrate recognition domains (CRDs), so-called glycoclusters can be formed when a multivalent carbohydrate ligand is present. The formation of these aggregates then leads to a change in the transmission and, therefore, the turbidity assay is a quick indicator of ligand–receptor interactions. This technique can be utilized to determine the turbidity at varying ratios of ligands and receptors and further on to compare different carbohydrate ligands.^[178-179] Additionally, this technique can be used to analyze the temperature-dependent binding of, for example, ConA to carbohydrate bearing thermoresponsive polymers or microgels.^[119, 180]

1.7.1 Inhibition studies

While turbidity measurements are helpful to observe trends and the change of binding in dependence of the temperature for thermoresponsive glycopolymers and glycomicrogels, however, these studies say little about the potential to inhibit a binding event. To investigate the potency of the referring ligands to inhibit the adhesion of lectins and pathogens towards a cell surface inhibition studies can be performed. A well-known assay for the measurement of inhibition of ligand-receptor interactions is the enzyme-linked immunosorbent assay (ELISA). This assay was first established by Perlmann and Engvall in 1971 and was further developed. In this assay, an antigen or protein is immobilized onto a microtiter plate, and an enzyme-labeled antibody is added.^[181-182] By adding the enzyme's substrate, the binding between antigen and antibody can be detected due to the reaction catalyzed by the enzyme giving a dye that can be detected via fluorescence spectroscopy.^[183-184] Adding an inhibitor for the antibody-protein/antigen interaction, an inhibition potential can be determined by the reduction of the enzyme-catalyzed reaction (see **Figure 12**).^[185]

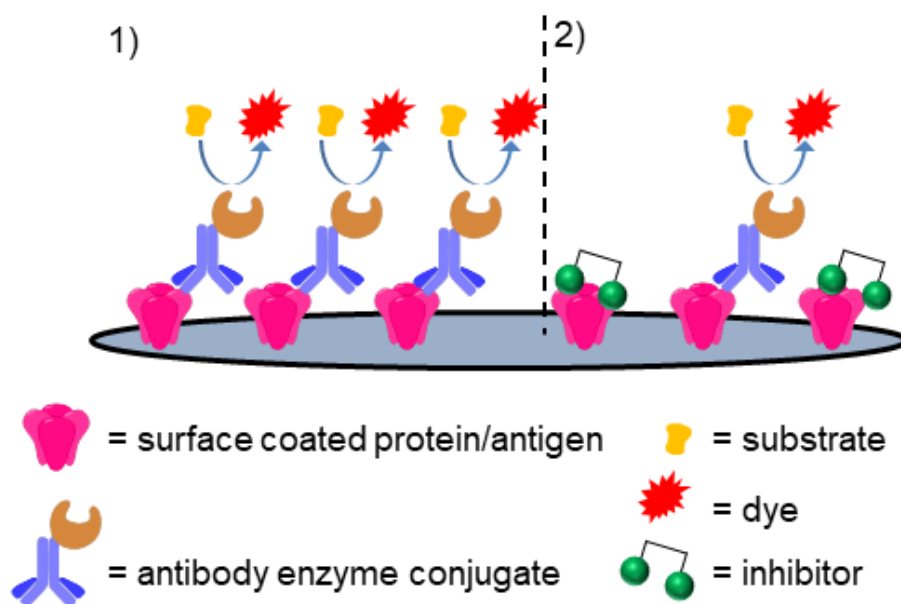


Figure 12. Schematic presentation of an ELISA with and without inhibitor added. The binding of the antibody-enzyme conjugate towards protein/antigen, coated onto the surface, can catalyze a reaction with a substrate giving a dye that can be read out via UV-vis (1). By adding an inhibitor for the binding of the antibody towards the functionalized surface, the enzyme-catalyzed reaction is reduced, and an inhibition potential can be determined (2).

Based on this principle, the inhibition of carbohydrate-lectin or carbohydrate-bacteria interactions can be quantified (see **Figure 13**). Here, the main difference is that the binding of fluorescence labelled lectins or bacteria is inhibited, and no enzyme-catalyzed reaction is used as an indicator for the binding.^[186] Therefore, a microtiter surface is coated with mannan to build a model surface that mimics the glycocalyx.^[187] Mannan is a polysaccharide that belongs to the group of hemicelluloses, containing only mannose and can be extracted via alkaline treatment of plants or yeast.^[188] Next, a lectin, labelled with a fluorescence dye, e.g. ConA or green fluorescent protein (GFP) expressing bacteria and an inhibitor are added. Using a microtiter plate allows the analysis of a series of different inhibitor concentrations in direct comparison to the non-inhibited binding.^[189] An important step before the fluorescence signal is read out is that the inhibited receptor that is hindered from binding to the mannan functionalized surface is washed off.^[190] This measurement is a fast method to analyze different inhibitor concentrations at once and to determine the inhibition potency of the investigated inhibitor. To compare inhibitors with each other, the so-called IC_{50} -value can be used. This value gives the inhibitor concentration, where 50% of the receptor is inhibited.^[191] The IC_{50} -value can be calculated from the slope of the inhibition curve in dependence of the inhibitor concentration by using the Hill plot. Moreover, due to the use of many multivalent inhibitors, the inhibitory potential of a single ligand presented

on a multivalent scaffold can be compared to a monovalent inhibitor to get the relative inhibition potential (RIP) per ligand.

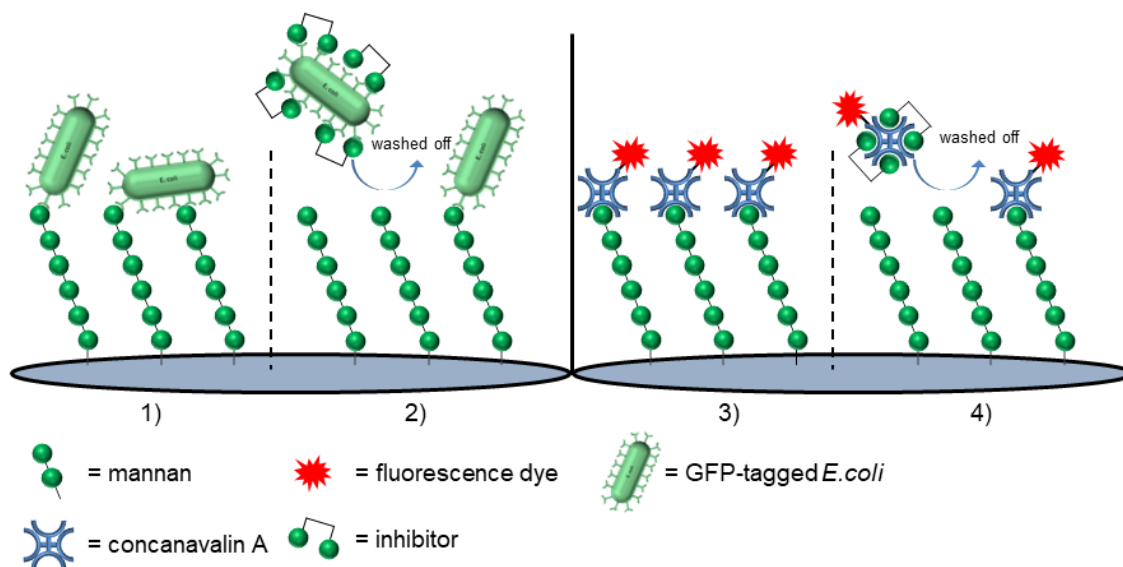


Figure 13. Schemes of adhesion inhibition assays. On the left, GFP-tagged *E. coli* binds to mannan functionalized surfaces, and the number of bound bacteria can be determined via fluorescence readout (1). When an inhibitor is added, the inhibited *E. coli* can be washed off, and the fluorescence intensity during the readout decreases (2). On the right, fluorescence labelled ConA binds to mannan coated microtiter surface. The binding is determined via fluorescence readout (3). Adding an inhibitor that binds to ConA hinders the lectin from binding to the mannan surface and is washed off. Only small amounts of ConA can bind to mannan and, therefore, leads to lower fluorescence intensities (4).

In this work, these inhibition assays were used to investigate the adhesion of ConA as well as *E. coli*. Both receptors are well-known for their binding towards mannose, but they need to be labeled with a fluorescence dye for the readout of the adhered receptor on the surface. Therefore, the *E. coli* strain PKL 1162 was used due to its GFP gene and the possibility to detect the expressed GFP via fluorescence spectroscopy. Additionally, the ConA was labeled with the fluorescence dye fluorescein (FITC). For the inhibition assays, thermoresponsive glycopolymers were used as inhibitors for the investigation of temperature-switchable inhibition of these receptors, as well as thermoresponsive glycomicrogels.

2. Aims and Outline

Carbohydrate-lectin based interactions are known to mediate various important processes at the cell surface such as signaling, fertilization or cell-cell adhesion. Also, in diseased states, such as viral or bacterial infections these interactions play a pivotal role and, therefore, it is of great interest to understand the underlying molecular mechanisms in more detail. Single carbohydrate-lectin interactions are usually weak and show low specificity. Nature overcomes this problem by presenting the ligands in a multivalent fashion and thereby enhance the overall binding. Since the fundamental binding mechanisms of structurally complex natural carbohydrates are hard to decipher, it is an aim to create glycomimetics based on synthetic polymers. With these glycopolymers, it is the aim of this thesis to gain new insights into the different effects that could influence the binding events, such as ligand density, ligand spacing and the scaffold properties.

Furthermore, it is an aim to harness the coil-to-globule transition of responsive polymer scaffolds to control the carbohydrate presentation and thereby carbohydrate binding. The responsive polymer scaffolds used in this work are based on the LCST (lower critical solution temperature) polymer poly(*N*-isopropylacrylamide) (PNIPAM), which has been shown to “switch” cell adhesion on and off through changes in surface hydrophobicity and the elastic modulus.^[161] Here, an aim is to combine the shifts of these “material cues” upon crossing the LCST with the changes in carbohydrate presentation to create materials with tunable specific adhesion to carbohydrate-binding receptors and bacteria.

In the first part of this thesis, carbohydrate functionalized microgels are established and tested for their switchable binding. Via the synthesis of glycomonomers and the copolymerization of these monomers to form crosslinked spherical PNIPAM microgels, the sugar units are incorporated into the polymeric network. Further on, the effects of the carbohydrate density on the microgels' hydrodynamic radii and swelling properties are investigated. The temperature-dependent binding of these glyco-microgels is evaluated in different binding assays towards Concanavalin A (ConA) and type 1-fimbriated *Escherichia coli* (*E. coli*).

In the second part, mannose-functionalized thermoresponsive linear polymers are synthesized via post-functionalization of a poly(active ester) with different carbohydrates. The resulting series of glycopolymers differ in their carbohydrate linker hydrophilicity, length and the amount of sugar units on the polymeric backbone. The coil-to-globule transition of these glycopolymers likely affects the binding affinity of the carbohydrate units, but the

literature showed inconsistent results, i.e. higher and lower affinities have been reported upon phase transition. Therefore, using a series of glycopolymers, the binding towards different receptors (*E. coli* and ConA) is systematically tested in an inhibition-competition assay towards a mannan coated surface.

In the last part of this thesis, thin films composed of the synthesized carbohydrate functionalized microgels are prepared to enable switchable carbohydrate-binding surfaces. The optimal microgel surface coverage for ConA and *E. coli* binding is analyzed via atomic force microscopy and fluorescence readout. The coated surfaces are analyzed towards their temperature-dependent binding properties towards *E. coli* and ConA, and especially different incubation times are tested. Furthermore, the ability to release the bound receptors by washing with buffer below or above the LCST is tested.

3. Conclusion and Perspectives

The synthesis of thermoresponsive carbohydrate-functionalized microgels and polymers and their binding towards different receptors in solution and on surfaces was studied. The following main results were obtained:

- 1) It was confirmed that the binding between carbohydrates and receptors could be controlled via temperature stimulus.
- 2) It was shown that the temperature-induced coil-to-globule transition can lead to an increase or decrease of the binding affinity depending on the accessibility of the carbohydrate units, which in turn depends on the size of the receptor target.
- 3) A full reversibility of carbohydrate mediated interactions to the polymer scaffolds by “switching back” the temperature stimulus was not obtained in most instances. This can be attributed to a large reswelling hysteresis of the polymer scaffolds.

In the first part of this thesis, a set of microgels with varying densities of carbohydrate units was synthesized. Therefore, glycomonomers were synthesized first using the carbohydrates α -D-mannopyranoside (Man) and β -D-galactopyranoside (Gal). These two ligands were used because the tested receptors for the inhibition studies, Concanavalin A (ConA) and *Escherichia coli* (*E. coli*), specifically bind to the Man moiety but are unable to bind Gal and, therefore, the latter was used as non-binding control. First, Man and Gal were functionalized with protecting groups to enable the successful functionalization with hydroxyethyl methacrylamide (HEMAm) in the next step. With the combination of Man and Gal with HEMA, two different glycomonomers *N*-(2-(α -D-mannosepyranosyloxy)ethyl)methacrylamide (ManEMA) and *N*-(2-(β -D-galactopyranosyloxy)ethyl)methacrylamide (GalEMA) were synthesized. These glycomonomers were used to construct microgels with different carbohydrate densities in a single reaction step. By using the radical copolymerization procedure of poly(*N*-isopropylacrylamide) microgels with a bifunctional cross-linker (*N,N'*-methylenebisacrylamide) (MBA), large amounts of the initiator ammonium persulfate (APS), the surfactant sodium dodecyl sulfate (SDS), and varying amounts of the glycomonomers a set of different microgels was synthesized.

The carbohydrate density for the microgels ranged from 0 $\mu\text{mol/g}$ to 67 $\mu\text{mol/g}$, which corresponded a maximum carbohydrate/NIPAM ratio of 0.8%. The dynamic light scattering (DLS) analysis showed that with an increasing amount of carbohydrate ligands, the hydrodynamic radius, as well as the polydispersity index, increased whereas the swelling

ratio was in the same range for all microgels. Moreover, the lower critical solution temperature (LCST) decreased with an increasing Man functionalization degree, which was unexpected due to the hydrophilicity of the glycomonomers that should reduce the tendency for a hydrophobic collapse of the PNIPAM. For the investigation of ConA binding towards the microgels in solution, a Bradford assay was carried out after the incubation of both and filtration of the aggregates below the LCST. The assay showed that with a carbohydrate density of 15 $\mu\text{mol/g}$ only 8% of ConA could be adsorbed on the microgels but having a density of 32 $\mu\text{mol/g}$ almost 90% could be bound. The temperature-dependent binding of ConA was determined via turbidity measurements showing that not only the interactions were specific but also that the reswelling of the microgel system was hindered when ConA was bound to the microgels.

The temperature-dependent binding between microgels and receptors as well as the potential release of receptors upon temperature stimulus was additionally investigated using *E. coli* as a receptor. Therefore, temperature-dependent *E. coli*-microgel aggregation was investigated showing that, in contrast to the binding of ConA, even for the microgels having only 32 $\mu\text{mol/g}$ Man incorporated, a temperature-dependent aggregation could be observed. Only at a high Man content of 67 $\mu\text{mol/g}$, no temperature-dependent binding was observed. Furthermore, an aggregation-filtration assay was carried out to quantify the number of bacteria that are bound onto the microgels. Microgels and bacteria were mixed below and above the LCST, and the effectiveness of capturing bacteria was determined by filtrating the aggregates and quantifying the growth of non-captured bacteria on agar plates. The results show that for all mannose bearing microgels, the temperature increase leads to lower numbers of colonies formed, meaning that at above the LCST the binding between bacteria and microgel is improved. For the microgel sample with 32 $\mu\text{mol/g}$ carbohydrates, nearly all bacteria could be bound during the assay at elevated temperatures. For all these assays, neither galactose bearing microgels nor non-functionalized PNIPAM microgels showed any binding, indicating that the microgel-bacteria binding was due to specific interactions.

Taken together, a straightforward method for the synthesis of carbohydrate-functionalized microgels was achieved, and the binding of ConA and *E. coli* to the microgels in solution proved to be temperature-dependent. All in all, different effects may contribute to the improved binding above the LCST, like reduced steric repulsion and an increase of sugar density on the microgel surface but it was shown that a modest temperature change at around 30 °C enables the control over ligand affinity.

In the second part of this thesis, the binding of linear, non-crosslinked thermoresponsive glycopolymers was investigated in solution. All glycopolymers, synthesized via a two-step approach by a collaboration partner, were composed of PNIPAM and presenting Man or non-binding control Gal units on the polymer backbone with two different linkers. The linkers used for the synthesis were an ethyl linker (EL) as well as a 2-hydroxypropyl linker (HPL) giving a total of ten polymers (eight Man, one Gal, and one unfunctionalized) with a carbohydrate amount of 0% to 97%. Here, the influence of the receptor size of ConA as well as *E. coli* on the temperature-dependent binding strength was investigated. The first analysis of the polymers showed that with an increasing amount of Man the LCST increased up to 40.2 °C for 7% of carbohydrate incorporated and with a higher carbohydrate amount no LCST below 45 °C could be observed and the linkers did not show any influence on the LCST. After the successful characterization of the polymers, first binding studies with ConA were carried out. Here, the different linkers influenced the binding, where the more hydrophobic linker EL showed more stable polymer-lectin complexes via temperature-dependent turbidimetry studies. Overall, the turbidimetry studies confirmed that an increased number of Man units leads to a more persistent clustering with ConA and that the linker affects the cluster formation. Next, these polymers were used as inhibitors for the binding of ConA and *E. coli* towards a mannan coated microtiter surface. For the measurements with *E. coli*, an increased Man functionalization leads to a stronger inhibition of the bacteria adhesion towards the surface. By comparison of ManEL and ManHPL polymers with the same carbohydrate concentration, it can be seen that higher inhibitory potentials were measured for the more hydrophobic linker ManEL. This was attributed to a higher lectin-binding affinity of the hydrophobic linker, which was observed before in the literature.^[190] For polymers with a functionalization degree of 1 to 2%, the inhibition was increased for globular polymer conformations above the LCST. At higher Man concentrations within the polymer the cloud point was above 40 °C, indicating that the coil to globule transition did not take place and, therefore, no differences in the inhibition potential could be observed. The Hill coefficients were determined, and an increase in binding cooperativity could be observed at elevated temperatures for all polymers with less than 5 mol% of Man. This leads to the assumption that the coil-to-globule transition of these polymers increases the adhesion inhibition of *E. coli* towards the mannan surface. The temperature-dependent adhesion inhibition studies with ConA confirmed higher inhibitory potentials for increased carbohydrate densities. However, it could be noted that for the temperature-dependent measurements, the majority of the polymers showed no increase in inhibition when raising the temperature above the LCST. This is explained by the small size of ConA compared to *E. coli*. ConA is a nanometer-sized receptor with a CRD-CRD (carbohydrate recognition domain) distance of a minimum of 7.2 nm (see section 1.3.1).

Below the cloud point, the polymers were swollen, and in a similar size range, thus the polymers were able to bind more than one CRD. When exceeding the LCST, the polymer collapses and shrinks in size only able to bind one CRD even though the hydrophilic ligand is presented in a higher density on the surface of the globules. Taken together, for polymers with low functionalization degrees, a large shift in affinity towards the different receptors was observed. The results from the inhibition studies with ConA and *E. coli* gave first insights that the conformation of the glycopolymers and glycomimetics, in general, is an important factor. Further, first insights into the size-dependence of ligand-receptor interactions, and first explanations of contradictory results of the literature are given.

In the third part of this thesis, it was the aim to study the temperature-dependent carbohydrate binding on surfaces. Therefore, a set of three different microgels, which were synthesized with different carbohydrate densities and different glycomonomers was synthesized to prepare surface coatings. The surface coatings were prepared on polystyrene surfaces, and the conditions were optimized to obtain microgel monolayers. This was confirmed via atomic force microscopy and fluorescence readouts. Next, the binding of ConA to the prepared surfaces was tested via an inhibition assay and direct binding assay for different incubation times of 30 min and 24 h. The inhibition showed that for short incubation times, ConA was more strongly bound above the LCST. For longer incubation times, the ConA binding strength increased. Importantly, given longer incubation time ConA binding was stronger below the LCST suggesting diffusion of ConA into the microgel layer and multivalent binding. On the other hand, when studying the inhibition of *E. coli* adhesion to the microgel surfaces, stronger binding was observed above the LCST at short and long incubation times. This is explained by the inability of *E. coli* to diffuse into the microgel network, i.e. binding is restricted to the surface of the microgel layer. Since the microgel surface attains a smooth structure where the hydrophilic carbohydrates units are likely in contact with the solution phase, the *E. coli* binding is always enhanced when raising the temperature above the LCST. Overall, these experiments showed that by changing the temperature, the affinity of the surfaces can be changed and that this effect can be different when different incubation times are applied.

Overall, the main aim was to shed light into carbohydrate-lectin-based interactions and to see whether it is possible to control the binding affinity towards different receptors by a temperature stimulus. As shown in this thesis, combining specifically interacting carbohydrate scaffolds with thermoresponsive properties can result in quite intricate effects. Nevertheless, this thesis provides first insights into the underlying principles that will allow for a promising platform to create capture and release devices for pathogens and other

carbohydrate-binding species. The discussed effects of parameters such as receptor size, inhibitor size, solution or surface studies and temperature as well as time dependence shed new light on the ongoing contradicting results in the literature.

Based on the results in this thesis, future studies could be performed on glyco-functionalized microgels and polymers. Microgels capable of releasing receptors upon temperature stimulus should be improved in terms of material parameters like the size, the swelling ratio, the positioning of the ligands, the cross-linking density or by including zwitterionic residues into the polymer network. For example, the microgels could be designed in a core-shell structure, where the carbohydrates are located in the core of the microgels and get exposed via the temperature stimulus.

Additionally, it would be interesting to bind, for example, ConA to microgels or nanometer-sized silica-particles, to create a medium-sized receptor (compared to ConA and *E. coli*) for future binding studies. Furthermore, the coupling of other biological ligands to the microgel matrix could be investigated. For example, ligands with a different degree of hydrophobicity, like biotin (hydrophobic) and hyaluronic acid (hydrophilic), could be used. In addition, using glycan mimicking multivalent ligands would offer interesting prospects for further studies.

4. Publications

4.1 Thermosensitive Display of Carbohydrate Ligands on Microgels for Switchable Binding of Proteins and Bacteria

Authors: Tanja J. Paul, Sophie Rübél, Marco Hildebrandt, Alexander K. Strzelczyk, Carina Spormann, Thisbe K. Lindhorst, Stephan Schmidt

Journal: ACS Applied Materials and Interfaces

Issue: **2019**, 11 (30), 26674-26683.

Type of Paper: Full Paper

Impact Factor: 8.758 (2019)

DOI: 10.1021/acsami.9b08537.

Own Contribution (first author):

Collaborative design of the synthetic strategy, synthesis of glycomonomers and microgels. Characterization of the microgels via DLS, ATR-FTIR and zeta-potential measurements. Determination of the carbohydrate density via phenol sulfuric acid method. Performance of binding studies towards Concanavalin A via turbidimetry and Bradford assay. Establishment and performance of aggregation studies, fluorescence microscopy and aggregation filtration assay with *E. coli*. Interpretation of data and writing of the first manuscript draft followed by collaborative finalization of the manuscript.

Reprinted with permission from Tanja J. Paul, Sophie Rübél, Marco Hildebrandt, Alexander K. Strzelczyk, Carina Spormann, Thisbe K. Lindhorst, Stephan Schmidt, Thermosensitive Display of Carbohydrate Ligands on Microgels for Switchable Binding of Proteins and Bacteria, *ACS Applied Materials and Interfaces* **2019**, 11 (30), 26674-26683.

Copyright © 2020 American Chemical Society.

Thermosensitive Display of Carbohydrate Ligands on Microgels for Switchable Binding of Proteins and Bacteria

Tanja J. Paul,[†] Sophie Rübel,[†] Marco Hildebrandt,[†] Alexander K. Strzelczyk,[†] Carina Spormann,[‡] Thisbe K. Lindhorst,[‡] and Stephan Schmidt^{*,†}

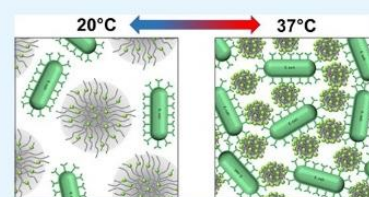
[†]Institute of Organic and Macromolecular Chemistry, Heinrich-Heine-University Düsseldorf, Universitätsstraße 1, 40225 Düsseldorf, Germany

[‡]Otto Diels Institute of Organic Chemistry, Christiana Albertina University of Kiel, Otto-Hahn-Platz 3/4, 24098 Kiel, Germany

Supporting Information

ABSTRACT: The synthesis of carbohydrate-functionalized thermosensitive poly(*N*-isopropylacrylamide) microgels and their ability to bind carbohydrate-binding pathogens upon temperature switch are reported. It is found that the microgels' binding affinity is increased above their lower critical solution temperature (LCST), enabling thermo-triggerable capture of pathogens. Here, a series of microgels with comparatively low mannose functionalization degrees below 1 mol % is achieved by a single polymerization step. Upon increase in mannose density, the microgel size increases, and the LCST decreases to 26 °C. Clustering with concanavalin A indicated that binding affinity is enhanced by a higher mannose content and by raising the temperature above the LCST. Binding studies with *Escherichia coli* confirm stronger specific interactions above the LCST and formation of mechanically stable aggregates enabling efficient separation of *E. coli* by filtration. For small incubation times above the LCST, the microgels' potential to release pathogens again below the LCST is confirmed also. Compared to existing switchable scaffolds, microgels nearly entirely composed of a thermosensitive material undergo a large change in volume, which allows them to drastically vary the density of ligands to switch between capture and release. This straightforward yet novel approach is likely compatible with a broad range of bioactive ligands. Therefore, thermosensitive microgels represent a promising platform for the specific capture or release of cells or pathogens.

KEYWORDS: responsive material, temperature stimulus, LCST, PNIPAM, glycocalyx, lectin, multivalent binding



1. INTRODUCTION

Multifunctional micro- and nanoparticles that can recognize chemical moieties and capture or release specific compounds are particularly relevant in biomedical research, for example, in sensing, targeting, or drug administration.^{1,2} With the discovery of responsive polymer networks, the release of drugs and the activity of targeting moieties of the particles could be controlled by various physical stimuli, for example, temperature, light, pH, or ionic strength.³ A particular relevant class of responsive particle systems are thermosensitive microgels composed of polymers with an LCST in the physiological temperature range. Such microgels are typically composed of poly(*N*-isopropylacrylamide) (PNIPAM), poly(*N*-vinylcaprolactam), or poly(oligo ethylene glycol acrylates).⁴ Due to entropic reasons, raising the temperature above the LCST eliminates the hydration layer at the polymer backbone, and the network forms polymer–polymer contacts instead. This triggers the transition from a highly hydrated and swollen state to a hydrophobic state where the microgel network collapses. The microgels then become hydrophobic,⁵ the elastic modulus⁶ increases, and the surface roughness and steric repulsion^{7–9} decrease. The thermoresponsive control over hydrophobicity, steric repulsion, and elastic modulus of microgels has been frequently used to construct surfaces for triggerable bioadhesion. These materials take advantage of the

fact that the adhesion of cells strongly depends on surface hydrophobicity and elastic modulus.^{10–12} An exceptionally successful application of thermosensitive microgels is the generation of switchable cell culture surfaces.^{5,13,14} Above the LCST, these systems allow for cell adhesion and cultivation, whereas release of cells below the LCST can be triggered for further processing. Another class of thermoresponsive materials capable of triggerable bioadhesion are polymer brushes.^{15–17} Compared to microgels, such polymer brushes offer higher structural precision but require significantly increased synthetic effort and are considered less robust.

It should be noted that microgels or polymer brushes composed of thermoresponsive polymers are not selective regarding the type of cells or bacteria that are adhered or released by an external stimulus. In this regard, carbohydrates could prove useful to induce selective binding in thermoresponsive polymers since they control nearly all adhesive processes on the cellular level.¹⁸ Such specifically interacting carbohydrates are particularly interesting for capturing clinically relevant bacteria or viruses that express carbohydrate receptors at their surface.^{19–21} Therefore, several groups

Received: May 16, 2019

Accepted: July 8, 2019

Published: July 8, 2019

described thermoresponsive polymers presenting the corresponding carbohydrate ligands to control the binding of receptors or bacteria.^{22–27} As of yet, these systems are typically based on polymer brushes grafted on nanoparticles or 2D surfaces. To be able to switch adhesive interactions via a temperature stimulus, the carbohydrate ligands are either presented or buried in a polymer brush, which requires a high degree of structural control and a significant synthetic effort. For example, Gibson et al. established long PNIPAM brushes on gold nanoparticles incorporating shorter carbohydrate-bearing chains that would be exposed predominantly above the LCST when the PNIPAM chains are collapsed.²⁵

In this work, we present a microgel-based approach to the thermosensitive display of carbohydrate ligands to control bacterial adhesion. Compared to polymer brushes, microgels offer a straightforward synthesis and incorporation of carbohydrate ligands by copolymerization. In addition, microgels may exhibit increased robustness (no surface chemistry) compared to the highly optimized brush systems reported before. However, the simple one-step synthesis of microgels offers little control of the ligand position in the network, which may render it difficult to switch the ligands in an activated or deactivated state upon a temperature stimulus. Nevertheless, thermosensitive presentation of carbohydrates in microgels should be achieved by increased ligand density upon microgel collapse above the LCST (Figure 1). In addition, it could be

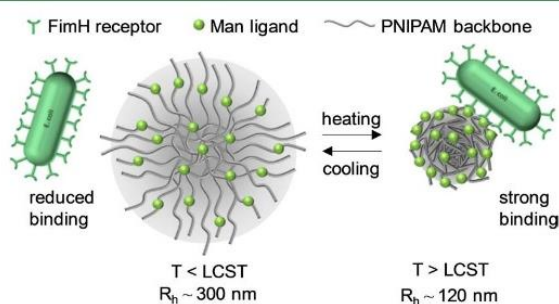


Figure 1. Schematic illustration of carbohydrate-functionalized PNIPAM microgels and the proposed change of bacteria binding upon varying the temperature below (left) and above (right) the LCST. Above the LCST, the microgels become hydrophobic, and the hydrodynamic radius (R_h) decreases by a factor of 2–3. This potentially leads to surface enrichment and an overall increase in carbohydrate density, amplifying specific binding to carbohydrate receptors.

expected that hydrophilic moieties such as carbohydrates tend to enrich at the surface above the LCST since the PNIPAM segments become hydrophobic, minimizing contact to the aqueous phase.²⁸ Such an increase in carbohydrate density and surface presentation might enable multivalent binding to receptor units, also called the “cluster glycoside effect”,^{29–31} facilitating strong binding to pathogens. The release of pathogens from microgels below the LCST could be expected owing to the lower carbohydrate ligand density and repulsive steric interactions of the swollen polymer network. The aim of this work is to show the feasibility of temperature-controlled presentation of carbohydrate ligands in microgels and to apply this concept for the triggered capture of bacteria. Therefore, we synthesize α -D-mannopyranoside (Man)- and β -D-galactopyranoside (Gal)-functionalized microgels at varying degrees of functionalization and then study temperature-dependent binding to a Man-specific carbohydrate receptor (concanavalin

A (ConA)) as well as to *Escherichia coli* as a Man-binding model pathogen. The binding assays are conducted by colorimetry, fluorescence microscopy, aggregation/filtration, and turbidimetry, which allowed us to confirm thermally controllable adhesion of bacteria and proteins on microgels.

2. EXPERIMENTAL SECTION

2.1. Materials. *N*-Isopropylacrylamide (NIPAM) (99%), *N,N'*-methylenebisacrylamide (MBA) (99%), ethanol ($\geq 99.8\%$), acetic acid (99.8–100%), (3-glycidyloxypropyl)-trimethoxysilane ($>98\%$), *p*-toluic acid (98%), phosphate-buffered saline (PBS) tablets, sodium methoxide ($\geq 97.5\%$), Amberlite IR 120 (hydrogen form), acetic anhydride (99.5%), concanavalin A from *Canavalia ensiformis* (type IV), rhodamine B isothiocyanate mixed isomers (RBITC), manganese chloride (99%), sulfuric acid (95–98%), ammonium persulfate (APS) (98%), and LB broth (Miller, powder microbial growth medium) were all purchased from Sigma-Aldrich. Sodium dodecyl sulfate (SDS) ($\geq 99\%$), tetrahydrofuran (99.8%), ethyl acetate (99.5%), and dimethyl sulfoxide ($\geq 99.9\%$) were purchased from Acros Organics. Sodium chloride (99.98%), phenol (99%), acetonitrile (HPLC gradient grade) ($\geq 99.9\%$), magnesium sulfate (laboratory reagent grade), and chloroform (99.9%) were purchased from Fisher Scientific.

2.2. Microgel Synthesis. The polymerization was carried out in a 100 mL three-necked flask fitted with a condenser. In 75 mL of ultrapure water, 0.7 g of *N*-isopropylacrylamide (NIPAM, 6.19 mmol), 0.05 g of *N,N'*-methylenebisacrylamide (MBA, 0.324 mmol), and 0.025 g (0.087 mmol) of sodium dodecyl sulfate (SDS) were added. Additionally, the deprotected glycomonomer was added (Supporting Information S1). The used amounts of the different glycomonomers were 180 mg (0.618 mmol), 85 mg (0.309 mmol), and 18 mg (0.062 mmol) for the Man-containing microgels (Supporting Information S2). The solution was stirred at 350 rpm with a magnetic stir bar and heated to 70 °C under a nitrogen purge for at least 40 min to remove dissolved oxygen. Next, the initiator ammonium persulfate (0.2 g; 0.9 mmol) was dissolved in 5 mL of ultrapure water and added to the reaction solution afterward to start the polymerization. During the reaction, the solution was continuously purged with nitrogen and stirred with 350 rpm. The reaction was stopped after 55 min by cooling with an ice bath. After filtration by glass wool, the reactants were removed by repeated centrifugation at 10,000g and washing with water.

2.3. Colorimetric Assays. The phenol sulfuric acid method was used to quantify the number of glycomonomers that were included into the polymeric network. First, a calibration curve was established using previously reported procedures.^{32–34} A stock solution of 320 μ M methyl α -D-mannopyranoside (MeMan) and dilution series of 20, 40, 80, and 160 μ M in water were prepared. To 125 μ L of each solution, 125 μ L of a 5 wt % phenol solution in ultrapure water was given and thoroughly mixed, followed by rapid addition of 625 μ L of concentrated sulfuric acid and incubation for 30 min at ambient temperature. The absorbance intensity was measured at 490 nm via UV–Vis spectroscopy. For the measurements of the microgel samples, mixtures of 125 μ L of a 0.5 wt % microgel dispersion and 125 μ L of a 5 wt % phenol solution in ultrapure water were prepared. Afterward, 625 μ L of concentrated sulfuric acid was added rapidly and incubated for 30 min at ambient temperature. Cooled solutions were centrifuged at 10,000g for 20 min, followed by analysis of the supernatant.

To quantify ConA binding to microgels, the Bradford assay employing a dye solution of Coomassie brilliant blue G-250 was used. The dye solution according to Selinger and Zor³⁵ was composed of 0.02% Coomassie brilliant blue G-250, 5% aluminum sulfate hydrate (18), 5 vol % ethanol, and 10 vol % orthophosphoric acid. All measurements were carried out on nontreated Corning 96-well clear flat-bottom polystyrene microplates (Sigma-Aldrich, Steinheim, Germany). First, a ConA stock solution in lectin binding buffer (LBB) (0.25 mg mL⁻¹), a dilution series (down to 5 μ g mL⁻¹), and a calibration curve (Supporting Information S3) was established. For all

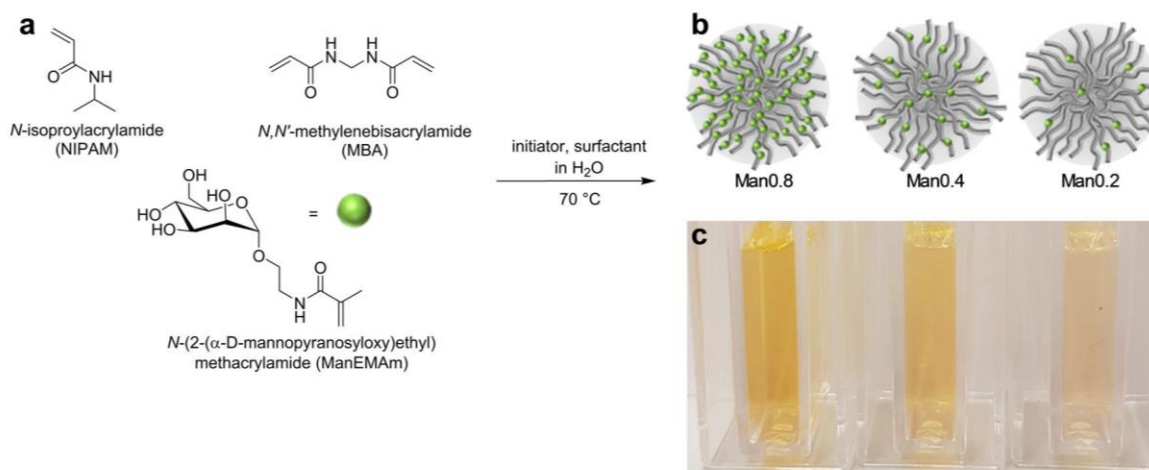


Figure 2. (a) Chemical structures of monomers for the microgel synthesis and (b) resulting microgels with different ligand densities: Man0.2, Man0.4, and Man0.8. (c) Pictures of colorimetric phenol sulfuric acid assay indicating different carbohydrate concentrations within the microgels.

Table 1. Microgel Preparation Recipes and Carbohydrate Concentration of the Microgels As Determined by Phenol Sulfuric Acid Method^a

| microgel sample | NIPAM (mmol) | ManEMAm (mmol) | GalEMAm (mmol) | reaction ratio of carbohydrate/NIPAM (%) | carbohydrate density ($\mu\text{mol g}^{-1}$) | carbohydrate/NIPAM ratio in microgel (%) |
|-----------------|--------------|----------------|----------------|--|---|--|
| Man0.8 | 6.2 | 0.618 | 0 | 10 | 67 ± 5 | 0.8 |
| Man0.4 | 6.2 | 0.309 | 0 | 5 | 32 ± 3 | 0.4 |
| Man0.2 | 6.2 | 0.062 | 0 | 1 | 15 ± 2 | 0.2 |
| Gal0.2 | 6.2 | 0 | 0.062 | 1 | 12 ± 2 | 0.15 |
| NIPAM | 6.2 | 0 | 0 | 0 | 0 | 0 |

^aFor the microgel synthesis, the concentration of surfactant (SDS), cross-linker (MBA), and initiator (APS) were, respectively, 87, 0.324, and 0.876 mmol in all cases.

Bradford assays, the absorption at 450 and 590 nm was determined 5 min after adding the dye solution, and then the absorbance ratio at 590 and 450 nm was calculated. For microgel samples, a dispersion in LBB buffer (0.5 mg mL^{-1}) was prepared. Next, $200 \mu\text{L}$ of the microgel solution was mixed with $200 \mu\text{L}$ of the ConA stock solution followed by shaking (200 rpm) at ambient temperature for 90 min. Afterward, the samples were filtrated by syringe filters ($0.2 \mu\text{m}$ in pore size, Supor Membrane, Pall Corporation) to separate the microgel from nonbound ConA. Nonbound ConA was quantified by adding $50 \mu\text{L}$ of the filtrate and $200 \mu\text{L}$ of the dye solution to a well and determining the absorption at 450 and 590 nm.

2.4. Dynamic Light Scattering. Measurements were performed using a Malvern HPPS 3.3 instrument (Malvern Panalytical, Kassel, Germany) equipped with a 633 nm He/Ne laser with the detector set in backscattering configuration (171°). Microgel samples (0.05 wt %) in 1 cm polystyrene cuvettes were analyzed in a temperature range of 20 to 40°C with a temperature increment of 2°C and a 10 min equilibration time lag between the temperature steps. For evaluation of the autocorrelation functions, the decay constant and first cumulant were determined by exponential fits, and the hydrodynamic radii were calculated by the Stokes–Einstein relation. For comparison, selected microgel samples were analyzed on a Nicomp 3000 setup (Particle Sizing Systems, FL, USA) at a scattering angle of 90° , showing good agreement with hydrodynamic radii determined in the backscattering setup.

2.5. Atomic Force Microscopy (AFM). AFM of dried microgel films was conducted on a JPK NanoWizard 2 (JPK Instruments AG, Berlin, Germany) using cantilevers with a nominal spring constant of 300 N/m (HQ-XSC11, MikroMash, Bulgaria) in tapping mode.

2.6. Turbidimetry. Turbidity measurements were performed on a Tepper turbidity photometer. The instrument contains a 630–690 nm laser with an intensity of 1 mW. For the measurements with a high microgel concentration, $200 \mu\text{L}$ of a microgel solution (LBB, 5 mg mL^{-1}) was diluted in 1.8 mL of LBB in a QS quartz cuvette (Hellma Analytics, Müllheim, Germany). Afterward, 0.5 mL of the

ConA solution (LBB, 1 mg mL^{-1}) was slowly added. The final particle concentration was 0.4 mg mL^{-1} , and the final protein concentration was 0.2 mg mL^{-1} . During the measurements, a temperature ramp of $1^\circ\text{C}/\text{min}$ between 20 and 37°C and then 37 and 20°C was run. For the measurements with a lower microgel concentration, $20 \mu\text{L}$ of a microgel solution (LBB, 5 mg mL^{-1}) was diluted in 1.980 mL of LBB followed by addition of 0.5 mL of the protein solution (LBB, 1 mg mL^{-1}). The final particle concentration was 0.04 mg mL^{-1} , and the final protein concentration was 0.2 mg mL^{-1} .

2.7. Bacteria–Microgel Aggregation Study. Aggregation studies were carried out according to previously described protocols.³⁶ First, 5 mg mL^{-1} of each microgel sample and 2 mg mL^{-1} *E. coli* (PKL1162)^{36,37} in ultrapure water were prepared (Supporting Information S4). In a glass vial, $100 \mu\text{L}$ of the microgel sample was combined with $900 \mu\text{L}$ of *E. coli* dispersion and incubated at 20 or 37°C overnight. Aggregation in the vials was documented by photography. Specific binding was tested by adding MeMan to a final concentration of 10 mM in the vials and vortexing. For testing of the removal of aggregates by filtration, the samples were filtered with a syringe filter ($5 \mu\text{m}$). Care was taken to incubate the syringe filters at the same temperature as the samples. The remaining filtrate was diluted with ultrapure water at a ratio of 1:1000. Next, $100 \mu\text{L}$ of the filtrate was spread on agar plates and incubated overnight at 37°C followed by counting of the colony-forming units (CFU). For each sample, this procedure was done three times (in triplicate).

2.8. Fluorescence Microscopy. The green fluorescent protein (GFP)-expressing *E. coli* (PKL1162) was imaged on an inverted microscope (Olympus IX73, Japan) equipped with an Olympus 60 \times NA 1.35 oil-immersion objective (Olympus, Japan), and a CMOS camera (DMK 33UX174L, The Imaging Source, Germany) was used for imaging of the bacteria. To control the temperature on the microscope, a Petri dish heater (JPK Instruments AG, Germany) was used. Images of the bacteria–microgel dispersions at final concentrations of $100 \mu\text{L}$ of a 0.5 wt % solution of Man0.2 in PBS and $900 \mu\text{L}$ of the *E. coli* solution in PBS (2 mg mL^{-1} , $\text{OD}_{600} = 0.4$)

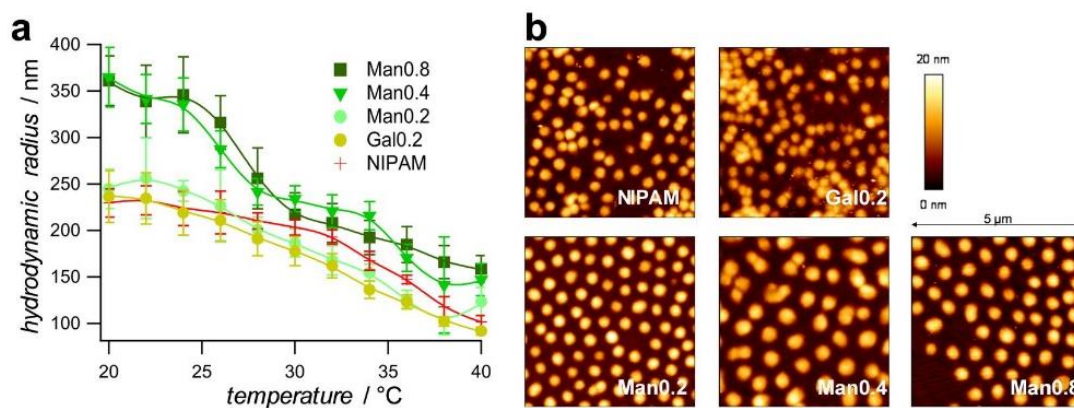


Figure 3. (a) Hydrodynamic radius versus temperature profiles for the carbohydrate-functionalized microgels (Man0.8, Man0.4, Man0.2, and Gal0.2) and unfunctionalized microgels (NIPAM) as a reference. The error bars represent the microgels' polydispersity. (b) AFM images of the microgels (image size, $5 \times 5 \mu\text{m}$; size scale, 20 nm for all images)

were taken immediately after mixing at 20 °C, then after heating to 37 °C and incubation for 30 min, and finally after switching off the heater and cooling back to 20 °C and equilibrating for another 30 min.

3. RESULTS AND DISCUSSION

3.1. Synthesis of Carbohydrate-Functionalized Microgels with Different Ligand Densities. The synthesis of microgels is based on copolymerization of NIPAM in the presence of Man- and Gal-functionalized methacrylamide monomers in a single reaction step. Radical copolymerization procedure of PNIPAM microgels with methacrylamide comonomers and a bifunctional cross-linker (*N,N'*-methylenebisacrylamide) is well established.^{4,38} Here, microgels were prepared using comparatively low amounts of surfactant and a large amount of APS initiator to achieve microgels in the desired size range of 400–500 nm. To construct microgels with varying carbohydrate densities, the carbohydrate monomers *N*-(2-(α -D-mannosepyranosyloxy)ethyl)methacrylamide (ManEMAm) and *N*-(2-(β -D-galactopyranosyloxy)ethyl)methacrylamide (GalEMAm) were used (Figure 2 and Supporting Information S1). The density of carbohydrate ligands in the microgels was varied by using different concentrations of ManEMAm or GalEMAm monomers in the microgel reaction mixture (Table 1). Three microgel samples with different amounts of Man were prepared (Man0.2, Man0.4, and Man0.8). The number in the sample name signifies the percentage of Man with respect to NIPAM repeat units. Microgels without carbohydrate ligands (NIPAM) and microgels with β -D-galactose (Gal0.2) were synthesized for later use as negative controls. The ratio of carbohydrate monomers incorporated into the microgels was quantified by a phenol sulfuric acid assay, giving a colorimetric readout for the monosaccharides. For all microgel samples, the molar ratio between carbohydrate repeat units and NIPAM was less than 1%, which is rather low when compared to the molar ratio in the reaction mixture (1, 5, and 10% in relation to NIPAM for Man0.2, Man0.4, and Man0.8, respectively). We suspect that the carbohydrate monomers are included into the microgels at significantly lower rates as compared to NIPAM. This could be rationalized as ManEMAm and GalEMAm are methacrylamides exhibiting slower polymerization kinetics compared to acrylamides such as NIPAM. Nevertheless, depending on the amount of carbohydrate monomer used during synthesis, different degrees of functionalization could be achieved (Table 1).

3.2. Size Distribution and Temperature-Dependent Swelling of Microgels. Dynamic light scattering (DLS) measurements in water and AFM images of microgels in a dry state showed that, with increasing ManEMAm concentration, the microgel hydrodynamic radii (R_h) were increased (Figure 3). Similar observations were made with other hydrophilic comonomers,³⁹ which may swell the microgel precursor droplets, thus reducing the cross-linking efficiency during the reaction. In addition, the DLS polydispersity index increased when raising the concentration of ManEMAm in the reaction mixture. This could be attributed to reduced stabilization of microgel precursor droplets through the anionic surfactant in the reaction mixture in the case of adding more hydrophilic comonomers. Nevertheless, except for the highest comonomer concentration (Man0.8), all microgel samples were near-monodisperse (Table 2). Regarding temperature-dependent

Table 2. Hydrodynamic Radii (R_h), PDI, and Swelling Degree from DLS Measurements

| microgel sample | R_h at 20 °C (nm) | PDI (DLS) | swelling ratio ($R_{h,20^\circ\text{C}}/R_{h,40^\circ\text{C}}$) |
|-----------------|---------------------|-----------|--|
| Man0.8 | 361 ± 27 | 0.33 | 2.3 |
| Man0.4 | 365 ± 16 | 0.16 | 2.5 |
| Man0.2 | 244 ± 21 | 0.14 | 2.1 |
| Gal0.2 | 236 ± 20 | 0.09 | 2.6 |
| PNIPAM | 229 ± 7 | 0.006 | 2.3 |

deswelling, all microgels showed a comparatively broad phase transition temperature range with swelling ratios of about 2.3. The broad phase transition is likely due to relatively high cross-linker concentrations (5%) and anionic sulfate groups in the microgel, owing to a comparatively large initiator concentration during the reaction. Interestingly, the LCST decreased when increasing the Man concentration within the microgel. This is unusual since hydrophilic monomers should reduce the tendency for hydrophobic collapse of the NIPAM network, as has been seen with charged³⁹ or neutral⁴⁰ hydrophilic comonomers. Moreover, the swelling curve for Man0.4 suggests two transitions at 26 and 35 °C. Although Man comonomers were only incorporated at a low concentration in the PNIPAM network, these effects suggest that the carbohydrate ligands strongly affect polymer–polymer or polymer–solvent interactions. Furthermore, we suspect that, due to the different reactivity of ManEMAm and NIPAM, carbohydrate units are unevenly distributed and could be

expected to be enriched on the microgel surface. This could then also influence the LCST behavior, as has been shown for the high localization of functional monomers in microgels³⁹ and will be explored for the carbohydrates in future studies in more detail.

3.3. Binding of ConA to Carbohydrate-Functionalized Microgels. For all protein binding studies, the Man-specific lectin ConA was used as a well-established model for investigating carbohydrate interactions. At physiological pH, ConA attains a homotetrameric structure with four binding sites at a minimum spacing of 7.2 nm.⁴¹ Activated by Mn^{2+} or Ca^{2+} , ConA specifically binds Man and glucose.^{42–45} To detect the amount of bound ConA to the microgels, the Bradford Coomassie brilliant blue assay was used for quantification of protein in the solution.^{35,46,47} After incubating the microgels in the ConA solution and then separating the microgels from the solution by filtration, unbound ConA remaining in the filtrate was quantified (Figure 4).

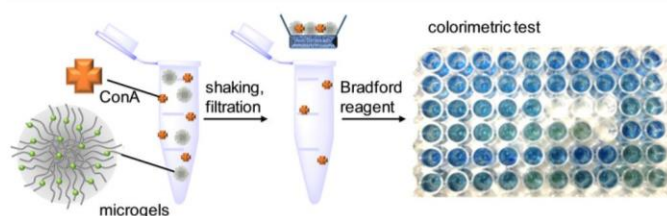


Figure 4. Procedure of the Bradford Assay for microgels. First, microgels and ConA were mixed in the solution, incubated, and shaken at 25 °C temperature for 90 min. Next, the solution was filtered through syringe filters to remove the microgel from the solution. Afterward, Coomassie brilliant blue solution was given to the filtered solutions to detect the remaining ConA via absorption measurements.

As expected, the higher the amount of Man units in the microgel, the higher the amount of bound protein (Figure 5).

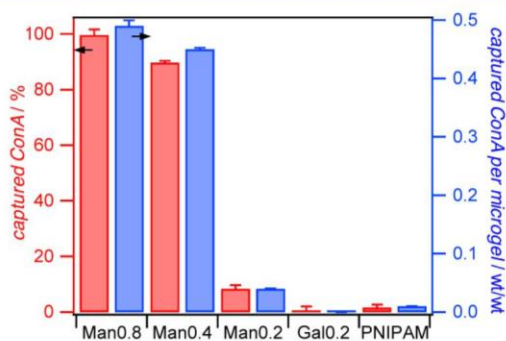


Figure 5. Relative amount of ConA bound to 100 μg of microgels at 25 °C. The amount of ConA in microgel dispersion was fixed to 50 μg (455 pmol of tetrameric ConA). The concentrations were 125 $\mu\text{g mL}^{-1}$ ConA and 50 $\mu\text{g mL}^{-1}$ microgels. The absolute quantities of microgel-bound ConA are shown in Supporting Information S5.

Man0.2 was only able to adsorb 8% of ConA, although the total amount of Man units in the microgels exceeds the amount of ConA in the solution by a factor of 3. This suggests that a significant number of Man in the microgel is inaccessible to ConA. Alternatively, the binding of ligands in Man0.2 gels is too weak to permanently bind to ConA because Man0.4 with a Man density only twice as high as Man0.2 was able to bind almost 90% of ConA. This order-of-magnitude increase in

affinity could be explained by favorable multivalent binding modes at a certain threshold of Man density in the microgels.^{48,49} The microgel sample Man0.8 captured 100% of ConA in the solution with the number of Man units exceeding the amount of ConA by a factor of 15. Overall, loading of the microgels with ConA appears to be quite high; up to 50% of the microgel mass was ConA after incubation.

To confirm that ConA binding to microgels was specific, unfunctionalized microgels without carbohydrate moieties (NIPAM) and Gal-functionalized microgels (Gal) were examined. Both NIPAM and Gal microgels showed no ConA binding. Taken together, we could show that only Man-containing microgels bind ConA specifically at ambient temperature. The strong increase in ConA binding with a higher degree of Man functionalization suggests that changing the Man density by a temperature stimulus might be suitable to switch between low and high ConA affinity.

3.4. Temperature-Dependent Binding of ConA. Next, we studied the effect of temperature-induced changes for specific binding of microgels to ConA. In this case, ConA quantification by Bradford assay proved to be difficult since temperature control is particularly challenging in the filtration step. An alternative readout for protein binding is aggregation. Since ConA has four binding sites, multiple ConA receptors can form large aggregates with polymeric carbohydrate ligands, which is termed glycoclustering. DLS proved to be unreliable for the temperature-dependent affinity assays due to the formation of highly polydisperse aggregates. Therefore, turbidimetry is often used to study glycoclustering.^{37,50} In turbidimetry, aggregation can be studied in real time due to the increase in light scattering intensity by the sixth power of aggregate size. To study the temperature dependence of ConA binding, the temperature was varied between 20 and 37 °C at a rate of 1 K min^{-1} . To ensure cluster formation, the amount of (monomeric) ConA was set to 19 nmol, roughly matching the quantity of presented carbohydrate units in the measurement cell, that is, 32 and 15 nmol for Man0.4 and Man0.2, respectively. The sample Man0.8 showed granular-sized aggregates and fast sedimentation under these conditions; therefore, this sample was excluded from further experiments.

Not surprisingly, all microgel systems showed an increase in turbidity with temperature (Figure 6). In the absence of ConA, microgels show a slight increase in turbidity with temperature also (Supporting Information S6), which is mainly due to an increase in the microgel refractive index above the LCST. In the presence of ConA, the turbidity increase with temperature is significantly stronger for all microgel systems, except for Gal0.2. A sharp increase in turbidity at around 34 °C for pure PNIPAM microgels was observed, which appeared to be less steep at increased Man concentration in the microgels. Here, the increase in turbidity starts at lower temperatures for the Man-bearing microgels compared to PNIPAM microgels. This could be explained by the LCST shift to a lower temperature in the case of Man-functionalized microgels and by glycoclustering owing to ConA binding. The strong aggregation behavior of NIPAM microgels in the presence of ConA might question the role of specific carbohydrate binding in cluster formation. However, Gal0.2 showed no cluster formation above the LCST. The difference in cluster formation of NIPAM and Gal0.2 microgels indicates that introducing small amounts of nonbinding hydrophilic galactose units into the microgels significantly suppressed nonspecific binding. Consequently, for Man microgels with a higher concentration of hydrophilic

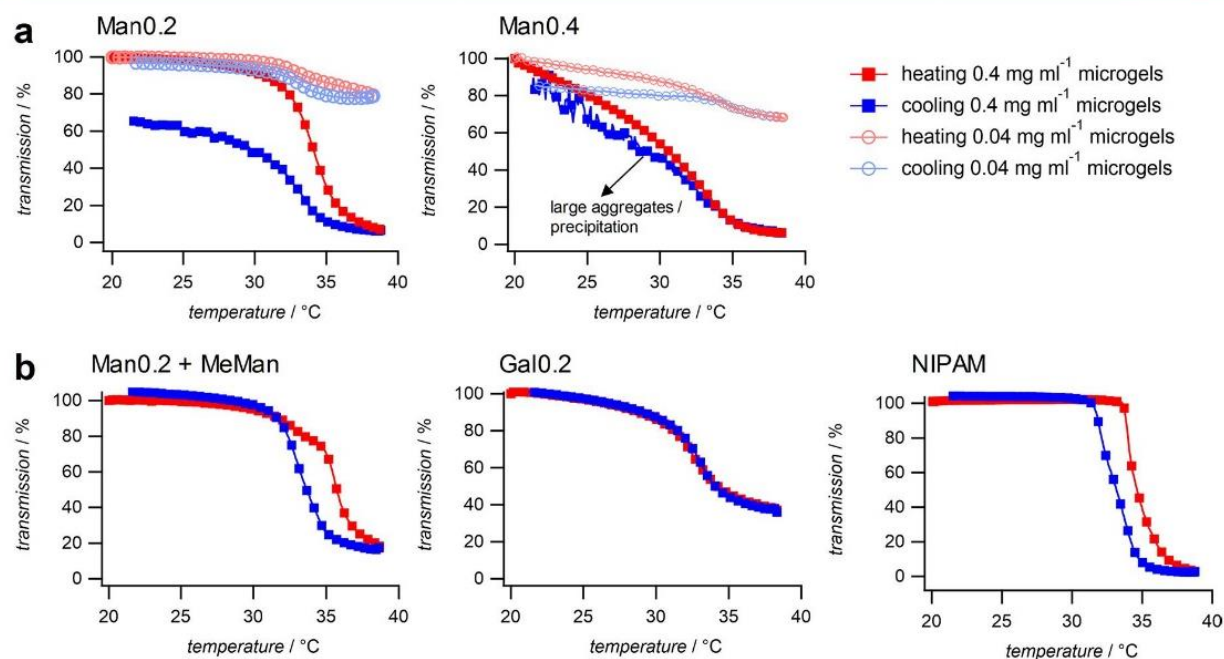


Figure 6. Turbidity under heating (red) and cooling (blue) at 1 K min^{-1} of microgel samples in the presence of 0.2 mg mL^{-1} (1.75 nmol) ConA. All microgel systems show increasing turbidity above the LCST. (a) Man-bearing microgels at 0.4 mg mL^{-1} (solid squares) and 0.04 mg mL^{-1} (empty circles). Man0.2 shows delayed aggregate dissolution at elevated concentration; Man0.4 forms very large aggregates at a high concentration above the LCST, obstructing turbidimetry (Supporting Information S6). Swelling hysteresis is visible at a low concentration. (b) Negative control samples. Upon cooling, the presence of α -D-mannopyranoside leads to rapid dissolution of Man0.2 aggregates. Gal0.2 aggregates show reduced turbidity upon heating and hysteresis. Pure PNIPAM aggregates rapidly dissolve upon cooling.

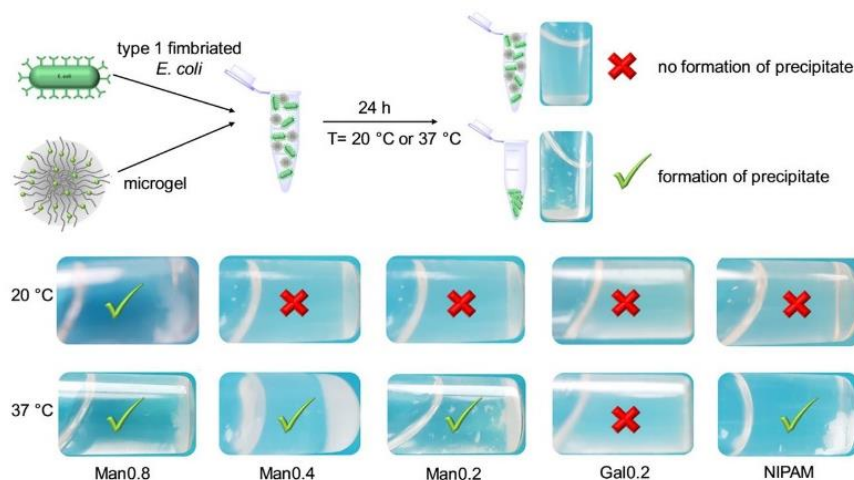


Figure 7. At the top, a schematic overview of the aggregation studies is presented. Pictures of the experiments are shown at 20 and 37 °C. Green check marks indicate a formation of aggregates, and red crosses indicate dispersed bacteria.

sugar units, strong clustering above the LCST is likely explained by specific binding with ConA. Importantly, by again lowering the temperature below the LCST, the turbidity of Man0.2 microgels did not immediately return to the original value. This suggests that aggregation of Man0.2 was stronger when compared to NIPAM microgels where only a small hysteresis between heating and cooling cycles was observed. For Man0.4, the heating/cooling hysteresis appears to vanish completely. Upon visual inspection above the LCST, Man0.4 microgels formed large stable aggregates that could not be analyzed properly with turbidimetry (Supporting Information S7). When reducing the Man0.4 microgel concentration 10 times, turbidimetry could be conducted, and the curves showed similar heating–cooling hysteresis compared to Man0.2 (Figure 6a).

In the case of NIPAM microgels, it could be argued that, above the LCST, the hydrophobicity of microgels leads to nonspecific aggregation in the presence of ConA. The aggregation of PNIPAM microgels with proteins above the LCST is well established.^{51,52} Below the LCST, the hydrophobic interactions between these microgels and ConA are reduced, and steric repulsion of the fuzzy microgel surface is increased; hence, the aggregates dissolve quickly. This did not occur when cooling down the Man-decorated microgels, where specific interactions between ConA and carbohydrates may take place. The ConA–Man interactions hinder reswelling of the microgels, thereby reducing steric repulsion between microgels; hence, the aggregates remained rather large below the LCST. Similar reduction of microgel reswelling due to the presence of macromolecules interacting with the microgel

network has been termed the “corset effect” and is often observed for core–shell microgel systems.⁵³ To confirm the presence of specific ConA–Man interactions, methyl α -D-mannopyranoside (MeMan) was added prior to incubation of microgels and ConA. MeMan acts as monovalent inhibitor by blocking ConA binding sites, thus reducing interactions with Man-functionalized microgels. Indeed, this resulted in faster reswelling of Man0.2 upon cooling (Figure 6b). Overall, the turbidity measurements showed that specific interactions between ConA and Man-presenting microgels are increased above the LCST, which appears to be reversible by cooling down below the LCST. This provides a first indication that the presentation of hydrophilic ligands is enhanced above the microgels' LCST.

3.5. Aggregation Studies with *E. coli*. The results of the turbidity measurements indicated that specific binding of Man-presenting PNIPAM microgels could be controlled by a temperature stimulus. Therefore, we then tested the microgels' ability to capture carbohydrate-binding pathogens in a temperature-dependent fashion. Type 1-fimbriated *E. coli* (PKL1162) presenting the Man-specific receptor FimH³⁷ was used for these studies. To unambiguously compare bacteria binding between the samples, the dispersed microgels were added to the bacterial suspension, and aggregate formation was documented visually (Figure 7). At 20 °C, aggregate formation was only observed for Man0.8; all other samples were in a dispersed state. All samples that were incubated at 37 °C show aggregate formation, except for Gal0.2, confirming low nonspecific binding above the LCST. Man0.2 and Man0.4 microgels as well as NIPAM microgels formed cloudy aggregates above the LCST. As described above, in the case of pure NIPAM microgels, the increased hydrophobicity may lead to nonspecific interaction and aggregation with bacteria. To differentiate between specific and nonspecific interactions, we tested the mechanical stability of the aggregates in the presence and absence of the inhibitor MeMan. In the absence of an inhibitor, aggregates with Man0.8 microgels were still present after cooling and vortexing; that is, the aggregates were mechanically stable at room temperature. The surprising stability of aggregates when cooled down below the LCST could be caused by interdigitation of bacterial fimbria into the microgel network given the long incubation time at 37 °C. When adding MeMan, aggregates slowly dissolved even without agitation, indicating specific interactions between *E. coli* and Man-presenting microgels (Figure 8b). Furthermore, aggregates of NIPAM and bacteria readily resuspended at 37 °C by

vortexing (Figure 8a). Resuspension by mechanical agitation was not possible in the case of any Man-presenting microgels above the LCST, indicating strong specific interactions to *E. coli*. This confirms that the binding between Man-presenting microgels and *E. coli* was mainly due to specific interactions. Importantly, as indicated by Man0.2 and Man0.4 aggregation exclusively occurs above the LCST, thus these specific interactions were shown to be strongly dependent on temperature.

Next, we studied the ability of the microgels to capture bacteria from a solution as a function of temperature. We observed that Man-presenting microgels result in mechanically stable aggregates above the LCST that could be suitable for filtration to separate carbohydrate-binding bacteria or cells. To test such a procedure, microgel and *E. coli* dispersions were mixed and incubated overnight at either 20 or 37 °C. The samples were then filtered with a syringe filter with a pore size of 5 μ m, allowing nonbound bacteria to pass into the filtrate while keeping large bacteria/microgel clusters in the filter. Next, the filtrates were spread on an agar plate and incubated overnight to then quantify the bacteria in the filtrate by the number of colony-forming units (CFU). Man-decorated microgels overall showed reduced CFU from the filtrate, correlating with the concentration of Man units in the microgel (Figure 9). The number of colonies was further reduced when incubating above the LCST. This overall confirmed that *E. coli* formed mechanically strong clusters with Man-bearing microgels that can be readily removed by filtration. Pure PNIPAM or Gal-functionalized microgels did not result in efficient bacteria capture regardless of temperature. This confirmed that the nonspecifically bound bacteria/PNIPAM microgel clusters were not stable under the shear forces during syringe filtration.

As argued above, crossing the LCST may result in an increase in microgel ligand density and surface presentation, which then leads to stronger binding of *E. coli*. This implies that, in the opposite direction, that is, when swelling the microgels by cooling down, the bacteria could be released from the aggregates. However, the aggregation experiments (Figure 7) showed that the bacteria–microgel aggregates incubated above the LCST overnight did not readily dissolve when cooled down to room temperature. To study this process in more detail, a fluorescence microscope was used to image aggregates of the GFP-expressing bacteria and microgels upon heating and cooling (Figure 10). *E. coli* and Man0.2 microgels were shown to form aggregates above the LCST already after a short incubation time of 30 min. Upon cooling down below the LCST, the size and number of aggregates were reduced, indicating that the release of bacteria from microgels is possible for a limited incubation time above the LCST. We therefore suspect that the prolonged incubation above the LCST during aggregation studies results in entanglements between the polymer network and bacterial fimbriae, which might hinder redispersion of the aggregates. To improve the release of bacteria from microgel aggregates, several parameters such as cross-linking density and positioning of the Man ligands in the microgel could be tuned. In addition, monolayer coatings of PNIPAM microgels might reduce interpenetration of bacterial structures with the polymer network for improved release below the LCST, as has been observed with cells.^{5,13,14}

4. CONCLUSIONS

Taken together, a straightforward single-step copolymerization procedure of NIPAM with methacrylamide-bearing carbohy-

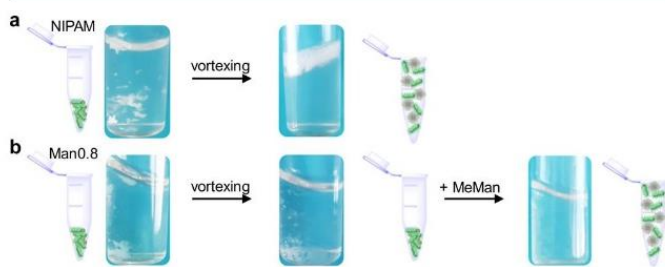


Figure 8. *E. coli* microgel aggregate resuspension by vortexing. (a) Aggregates with pure NIPAM microgels can be readily resuspended at 25 °C, whereas (b) aggregates with Man0.8 microgels could not be resuspended at 25 °C by mechanical agitation alone, only when adding α -D-mannopyranoside as an inhibitor.

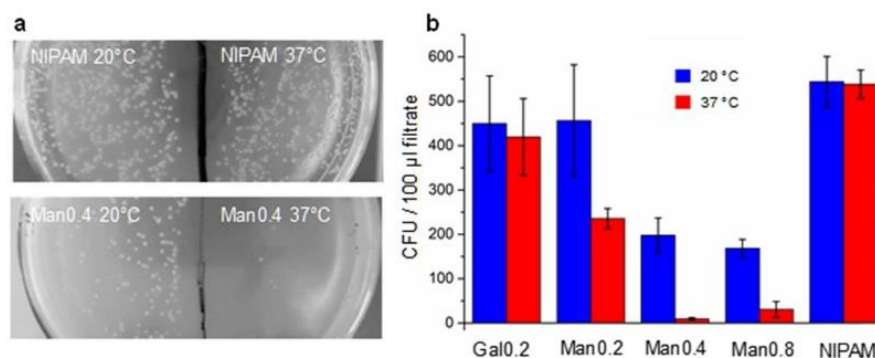


Figure 9. Aggregation-filtration experiment indicates a reduced presence of bacteria in filtrates from suspensions treated with Man-decorated microgels and increased temperature. (a) Image of the culture plate with the filtrates after overnight incubation. (b) Extracted CFU number from the culture plate images for the different microgel systems. The graph presents average values and standard deviations (error bars) obtained from three Petri dishes for each sample (for statistics, see Supporting Information S8).

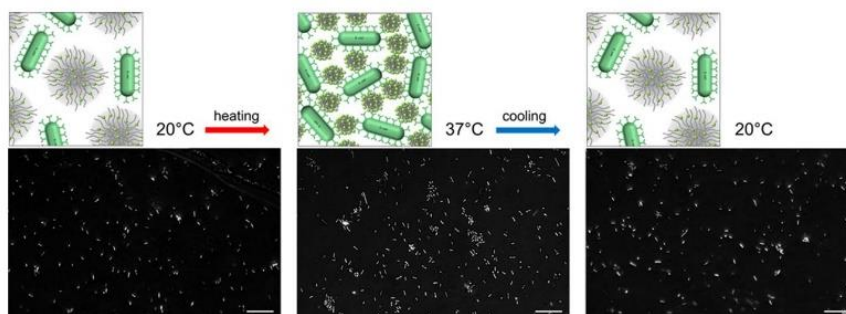


Figure 10. Top: Schematic illustration of bacteria cluster formation in the presence of microgels above the LCST and release of bacterial below LCST. Bottom: Fluorescence microscopy images of a dispersion of Man0.2 and *E. coli* before heating (left), after heating to 37 °C and 30 min incubation (middle), and after cooling down to 20 °C and incubating for 30 min (right). Scale bars, 10 µm.

drates was used to prepare microgels at varying degrees of Man density and nonbinding Gal moieties. Although the overall efficiency of carbohydrate insertion was below 1%, all assays showed that the Man-functionalized microgels specifically bind to ConA and type 1-fimbriated *E. coli*. The temperature-dependent swelling of the microgels showed a shift of the LCST to a lower temperature for carbohydrate-functionalized microgels, while the overall swelling degree remained unaffected. Binding to ConA and *E. coli* proved to be temperature-dependent, where microgels with Man densities of 0.2 to 0.4% showed no clustering with ConA or *E. coli* below the LCST but showed mechanically stable clusters above the LCST. Improved binding above the LCST might be attributed to reduced steric repulsion,^{5,54} smoothing of the microgel surface, and enhanced accessibility of Man groups. Similar mechanisms have been proposed previously to explain the affinity increase of ligand-functionalized polymer brushes above the LCST.^{22–26} Compared to polymer brushes, microgels additionally exhibit a strong increase in ligand density above the LCST since their volume decreases by an order of magnitude.²⁸ Hence, the density of ligands is drastically varied, promoting a large difference in affinity below and above the LCST. The variation of ligand density affects the affinity due to sheer statistical reasons,⁵⁵ which was used here for the first time to enable stimulus control over ligand affinity. The control of affinity by simple density variations should be applicable to a large range of biomolecular moieties in the switchable polymer network. Considering their straightforward synthesis and well-established applications in surface coatings, thermosensitive microgels represent a

promising platform for the capture and release of specific pathogens or cells.

■ ASSOCIATED CONTENT

📄 Supporting Information

The Supporting Information is available free of charge on the ACS Publications website at DOI: 10.1021/acsami.9b08537.

Details on carbohydrate monomer synthesis and chemical analysis, microgel synthesis, Bradford assay, bacteria cultivation and media, turbidity measurements, and instrumentation (PDF)

■ AUTHOR INFORMATION

Corresponding Author

*E-mail: stephan.schmidt@hhu.de.

ORCID

Thisbe K. Lindhorst: 0000-0001-6788-4224

Stephan Schmidt: 0000-0002-4357-304X

Notes

The authors declare no competing financial interest.

■ ACKNOWLEDGMENTS

The authors acknowledge funding by the German Research foundation (DFG) in the project SCHM 2748/5-1.

■ REFERENCES

- (1) Wicki, A.; Witzigmann, D.; Balasubramanian, V.; Huwyler, J. Nanomedicine in cancer therapy: Challenges, opportunities, and clinical applications. *J. Controlled Release* **2015**, *200*, 138–157.

- (2) Lim, E.-K.; Kim, T.; Paik, S.; Haam, S.; Huh, Y.-M.; Lee, K. Nanomaterials for Theranostics: Recent Advances and Future Challenges. *Chem. Rev.* **2015**, *115*, 327–394.
- (3) Stuart, M. A. C.; Huck, W. T. S.; Genzer, J.; Müller, M.; Ober, C.; Stamm, M.; Sukhorukov, G. B.; Szleifer, I.; Tsukruk, V. V.; Urban, M.; Winnik, F.; Zauscher, S.; Luzinov, I.; Minko, S. Emerging applications of stimuli-responsive polymer materials. *Nat. Mater.* **2010**, *9*, 101–113.
- (4) Pich, A.; Richtering, W. Microgels by Precipitation Polymerization: Synthesis, Characterization, and Functionalization. In *Chemical Design of Responsive Microgels*; Pich, A.; Richtering, W., Eds.; Springer-Verlag Berlin: Berlin, 2010; Vol. 234, pp 1–37.
- (5) Schmidt, S.; Zeiser, M.; Hellweg, T.; Duschl, C.; Fery, A.; Möhwald, H. Adhesion and Mechanical Properties of PNIPAM Microgel Films and Their Potential Use as Switchable Cell Culture Substrates. *Adv. Funct. Mater.* **2010**, *20*, 3235–3243.
- (6) Burmistrova, A.; Richter, M.; Uzum, C.; Klitzing, R. V. Effect of cross-linker density of P(NIPAM-co-AAc) microgels at solid surfaces on the swelling/shrinking behaviour and the Young's modulus. *Colloid Polym. Sci.* **2011**, *289*, 613–624.
- (7) Bergmann, S.; Wrede, O.; Huser, T.; Hellweg, T. Super-resolution optical microscopy resolves network morphology of smart colloidal microgels. *Phys. Chem. Chem. Phys.* **2018**, *20*, 5074–5083.
- (8) Gawlitza, K.; Radulescu, A.; von Klitzing, R.; Wellert, S. On the structure of biocompatible, thermoresponsive poly(ethylene glycol) microgels. *Polymer* **2014**, *55*, 6717–6724.
- (9) Keidel, R.; Ghavami, A.; Lugo, D. M.; Lotze, G.; Virtanen, O.; Beumers, P.; Pedersen, J. S.; Bardow, A.; Winkler, R. G.; Richtering, W. Time-resolved structural evolution during the collapse of responsive hydrogels: The microgel-to-particle transition. *Sci. Adv.* **2018**, *4*, eaao7086.
- (10) Folkman, J.; Moscona, A. Role of cell shape in growth control. *Nature* **1978**, *273*, 345–349.
- (11) Pelham, R. J.; Wang, Y.-I. Cell locomotion and focal adhesions are regulated by substrate flexibility. *Proc. Natl. Acad. Sci.* **1997**, *94*, 13661–13665.
- (12) Keskin, D.; Mergel, O.; Van der Mei, H. C.; Busscher, H. J.; van Rijn, P. Inhibiting Bacterial Adhesion by Mechanically Modulated Microgel Coatings. *Biomacromolecules* **2019**, *20*, 243–253.
- (13) Uhlig, K.; Wegener, T.; Hertle, Y.; Bookhold, J.; Jaeger, M.; Hellweg, T.; Fery, A.; Duschl, C. Thermoresponsive Microgel Coatings as Versatile Functional Compounds for Novel Cell Manipulation Tools. *Polymers* **2018**, *10*, 656.
- (14) Uhlig, K.; Wegener, T.; He, J.; Zeiser, M.; Bookhold, J.; Dewald, I.; Godino, N.; Jaeger, M.; Hellweg, T.; Fery, A.; Duschl, C. Patterned Thermoresponsive Microgel Coatings for Noninvasive Processing of Adherent Cells. *Biomacromolecules* **2016**, *17*, 1110–1116.
- (15) Kessel, S.; Schmidt, S.; Müller, R.; Wischerhoff, E.; Laschewsky, A.; Lutz, J. F.; Uhlig, K.; Lankenau, A.; Duschl, C.; Fery, A. Thermoresponsive PEG-Based Polymer Layers: Surface Characterization with AFM Force Measurements. *Langmuir* **2010**, *26* (5), 3462–3467.
- (16) Nagase, K.; Kobayashi, J.; Okano, T. Temperature-responsive intelligent interfaces for biomolecular separation and cell sheet engineering. *J. R. Soc., Interfaces* **2009**, *6*, S293–S309.
- (17) de las Heras Alarcón, C.; Farhan, T.; Osborne, V. L.; Huck, W. T.; Alexander, C. Bioadhesion at micro-patterned stimuli-responsive polymer brushes. *J. Mater. Chem.* **2005**, *15*, 2089–2094.
- (18) Lee, Y. C.; Lee, R. T. Carbohydrate-Protein Interactions: Basis of Glycobiology. *Acc. Chem. Res.* **1995**, *28*, 321–327.
- (19) Ernst, B.; Magnani, J. L. From carbohydrate leads to glycomimetic drugs. *Nat. Rev. Drug Discovery* **2009**, *8*, 661–677.
- (20) Schauer, R. Sialic acids as regulators of molecular and cellular interactions. *Curr. Opin. Struct. Biol.* **2009**, *19*, 507–514.
- (21) Sharon, N. Carbohydrates as future anti-adhesion drugs for infectious diseases. *Biochim. Biophys. Acta, Gen. Subj.* **2006**, *1760*, 527–537.
- (22) Wang, Y.; Kotsuchibashi, Y.; Liu, Y.; Narain, R. Study of Bacterial Adhesion on Biomimetic Temperature Responsive Glycopolymer Surfaces. *ACS Appl. Mater. Interfaces* **2015**, *7*, 1652–1661.
- (23) Dalier, F.; Eghiaian, F.; Scheuring, S.; Marie, E.; Tribet, C. Temperature-Switchable Control of Ligand Display on Adlayers of Mixed Poly(lysine)-g-(PEO) and Poly(lysine)-g-(ligand-modified poly-N-isopropylacrylamide). *Biomacromolecules* **2016**, *17*, 1727–1736.
- (24) Vasani, R. B.; Janardanan, N.; Prieto-Simón, B.; Cifuentes-Rius, A.; Bradley, S. J.; Moore, E.; Kraus, T.; Voelcker, N. H. Microwave Heating of Poly(N-isopropylacrylamide)-Conjugated Gold Nanoparticles for Temperature-Controlled Display of Concanavalin A. *ACS Appl. Mater. Interfaces* **2015**, *7*, 27755–27764.
- (25) Won, S.; Richards, S. J.; Walker, M.; Gibson, M. I. Externally controllable glycan presentation on nanoparticle surfaces to modulate lectin recognition. *Nanoscale Horiz.* **2017**, *2*, 106–109.
- (26) Won, S.; Hindmarsh, S.; Gibson, M. I. Triggerable Multivalent Glyconanoparticles for Probing Carbohydrate-Carbohydrate Interactions. *ACS Macro Lett.* **2018**, *7*, 178–183.
- (27) Pasparakis, G.; Cockayne, A.; Alexander, C. Control of Bacterial Aggregation by Thermoresponsive Glycopolymers. *J. Am. Chem. Soc.* **2007**, *129*, 11014–11015.
- (28) Pelton, R. H.; Pelton, H. M.; Morphesis, A.; Rowell, R. L. Particle sizes and electrophoretic mobilities of poly(N-isopropylacrylamide) latex. *Langmuir* **1989**, *5*, 816–818.
- (29) Lundquist, J. J.; Toone, E. J. The Cluster Glycoside Effect. *Chem. Rev.* **2002**, *102*, 555–578.
- (30) Kiessling, L. L.; Grim, J. C. Glycopolymer probes of signal transduction. *Chem. Soc. Rev.* **2013**, *42*, 4476–4491.
- (31) Miura, Y.; Hoshino, Y.; Seto, H. Glycopolymer Nanobiotechnology. *Chem. Rev.* **2016**, *116*, 1673–1692.
- (32) DuBois, M.; Gilles, K. A.; Hamilton, J. K.; Rebers, P. A.; Smith, F. Colorimetric Method for Determination of Sugars and Related Substances. *Anal. Chem.* **1956**, *28*, 350–356.
- (33) Gerchako, S. M.; Hatcher, P. G. Improved Technique for Analysis of Carbohydrates in Sediments. *Limnol. Oceanogr.* **1972**, *17*, 938–943.
- (34) Boden, S.; Wagner, K.; Karg, M.; Hartmann, L. Presenting Precision Glycomacromolecules on Gold Nanoparticles for Increased Lectin Binding. *Polymer* **2017**, *9*, 716.
- (35) Zor, T.; Selinger, Z. Linearization of the Bradford Protein Assay Increases Its Sensitivity: Theoretical and Experimental Studies. *Anal. Biochem.* **1996**, *236*, 302–308.
- (36) Hartmann, M.; Betz, P.; Sun, Y.; Gorb, S. N.; Lindhorst, T. K.; Krueger, A. Saccharide-Modified Nanodiamond Conjugates for the Efficient Detection and Removal of Pathogenic Bacteria. *Chem. – Eur. J.* **2012**, *18*, 6485–6492.
- (37) Hartmann, M.; Horst, A. K.; Klemm, P.; Lindhorst, T. K. A kit for the investigation of live Escherichia coli cell adhesion to glycosylated surfaces. *Chem. Commun.* **2010**, *46*, 330–332.
- (38) Pelton, R. Temperature-sensitive aqueous microgels. *Adv. Colloid Interface Sci.* **2000**, *85*, 1–33.
- (39) Hoare, T.; Pelton, R. Functional Group Distributions in Carboxylic Acid Containing Poly(N-isopropylacrylamide) Microgels. *Langmuir* **2004**, *20*, 2123–2133.
- (40) Nolan, C. M.; Reyes, C. D.; Debord, J. D.; Garcia, A. J.; Lyon, L. A. Phase transition behavior, protein adsorption, and cell adhesion resistance of poly(ethylene glycol) cross-linked microgel particles. *Biomacromolecules* **2005**, *6*, 2032–2039.
- (41) Wittmann, V.; Pieters, R. J. Bridging lectin binding sites by multivalent carbohydrates. *Chem. Soc. Rev.* **2013**, *42*, 4492–4503.
- (42) Becker, J. W.; Reeke, G. N., Jr.; Cunningham, B. A.; Edelman, G. M. New evidence on the location of the saccharide-binding site of concanavalin A. *Nature* **1976**, *259*, 406.
- (43) Mandal, D. K.; Kishore, N.; Brewer, C. F. Thermodynamics of Lectin-Carbohydrate Interactions. Titration Microcalorimetry Measurements of the Binding of N-Linked Carbohydrates and Ovalbumin to Concanavalin A. *Biochemistry* **2002**, *33*, 1149–1156.

- (44) Bryce, R. A.; Hillier, I. H.; Naismith, J. H. Carbohydrate-protein recognition: molecular dynamics simulations and free energy analysis of oligosaccharide binding to concanavalin A. *Biophys. J.* **2001**, *81*, 1373–1388.
- (45) Dam, T. K.; Brewer, C. F. Thermodynamic Studies of Lectin–Carbohydrate Interactions by Isothermal Titration Calorimetry. *Chem. Rev.* **2002**, *102*, 387–430.
- (46) Bradford, M. M. A rapid and sensitive method for the quantitation of microgram quantities of protein utilizing the principle of protein-dye binding. *Anal. Biochem.* **1976**, *72*, 248–254.
- (47) Ernst, O.; Zor, T. Linearization of the Bradford Protein Assay. *J. Visualized Exp.* **2010**, *38*, 1918.
- (48) Jacobi, F.; Camaleño de la Calle, A.; Boden, S.; Grafmüller, A.; Hartmann, L.; Schmidt, S. Multivalent Binding of Precision Glycooligomers on Soft Glycocalyx Mimicking Hydrogels. *Biomacromolecules* **2018**, *19*, 3479–3488.
- (49) Vetri, V.; Carrotta, R.; Picone, P.; Di Carlo, M.; Militello, V. Concanavalin A aggregation and toxicity on cell cultures. *Biochim. Biophys. Acta, Proteins Proteomics* **2010**, *1804*, 173–183.
- (50) Singh, A. V.; Vyas, V.; Patil, R.; Sharma, V.; Scopelliti, P. E.; Bongiorno, G.; Podesta, A.; Lenardi, C.; Gade, W. N.; Milani, P. Quantitative characterization of the influence of the nanoscale morphology of nanostructured surfaces on bacterial adhesion and biofilm formation. *PLoS One* **2011**, *6*, No. e25029.
- (51) Huo, D.; Li, Y.; Qian, Q.; Kobayashi, T. Temperature–pH sensitivity of bovine serum albumin protein-microgels based on cross-linked poly(N-isopropylacrylamide-co-acrylic acid). *Colloids Surf., B* **2006**, *50*, 36–42.
- (52) Guan, Y.; Zhang, Y. PNIPAM microgels for biomedical applications: from dispersed particles to 3D assemblies. *Soft Matter* **2011**, *7*, 6375–6384.
- (53) Berndt, I.; Pedersen, J. S.; Richtering, W. Temperature-Sensitive Core–Shell Microgel Particles with Dense Shell. *Angew. Chem., Int. Ed.* **2006**, *45*, 1737–1741.
- (54) Woodward, N. C.; Snowden, M. J.; Chowdhry, B. Z.; Jenkins, P.; Larson, I. Measurement of the Interaction Forces between Poly(N-isopropylacrylamide–acrylic acid) Microgel and Silica Surfaces by Colloid Probe Microscopy. *Langmuir* **2002**, *18*, 2089–2095.
- (55) Mammen, M.; Choi, S.-K.; Whitesides, G. M. Polyvalent interactions in biological systems: implications for design and use of multivalent ligands and inhibitors. *Angew. Chem. Int. Ed.* **1998**, *37*, 2754–2794.

Supporting Information

Thermosensitive display of carbohydrate ligands on microgels for switchable binding of proteins and bacteria

*Tanja J. Paul¹, Sophie Rübel¹, Marco Hildebrandt¹, Alexander K. Strzelczyk¹, Carina Spormann², Thisbe K. Lindhorst² and Stephan Schmidt¹**

¹Institute of Organic and Macromolecular Chemistry, Heinrich-Heine-University Düsseldorf, Universitätsstraße 1, 40225 Düsseldorf, Germany

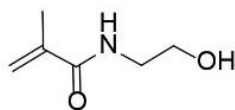
²Otto Diels Institute of Organic Chemistry, Christiana Albertina University of Kiel, Otto-Hahn-Platz 3/4, 24098 Kiel, Germany

Email: Stephan Schmidt – stephan.schmidt@hhu.de

* Corresponding author

S1 Glycomonomer synthesis

Synthesis of N-(2-hydroxyethyl)-2-methacrylamide (HEMAm)



Scheme S1a (HEMAm)

N-(2-hydroxyethyl)-2-methacrylamide was synthesized according to a protocol published by Parry et al.¹ Briefly, ethanolamine (8 mL, 132 mmol) was dissolved in anhydrous dry chloroform (100 mL) and cooled with an ice bath to 0 °C. Then a solution of methacryloyl chloride (6.4 mL, 67 mmol) and chloroform (75 mL) were slowly added, followed by stirring for 2 h at 0 °C. The formed solid was filtered off and the remaining chloroform was removed in vacuo. Next, the crude product was again dissolved in 250 mL chloroform and stirred over basic alumina for 15 h. On the next day the basic alumina was filtered off and the remaining solvent was removed under reduced pressure to give a pale-yellow oil. The product was purified by column chromatography (ethyl acetate/*n*-hexane 1:1). The overall yield of the synthesis was 80% (6.92 g).

¹H-NMR (600 MHz, CDCl₃): δ 6.41 (s, 1H, -NH), 5.73 (t, ³*J*_{HH} = 1.0 Hz, 1H, -C=CH₂ E to -CH₃), 5.37 – 5.33 (m, 1H, -C=CH₂ Z to -CH₃), 3.75 (dd, ³*J*_{HH} = 5.5, 4.5 Hz, 2H, -NHCH₂CH₂), 3.50 – 3.46 (m, 2H, -NH-CH₂-CH₂), 2.57 (s, 1H, -OH), 1.97 – 1.95 (m, 3H, -CH₃).

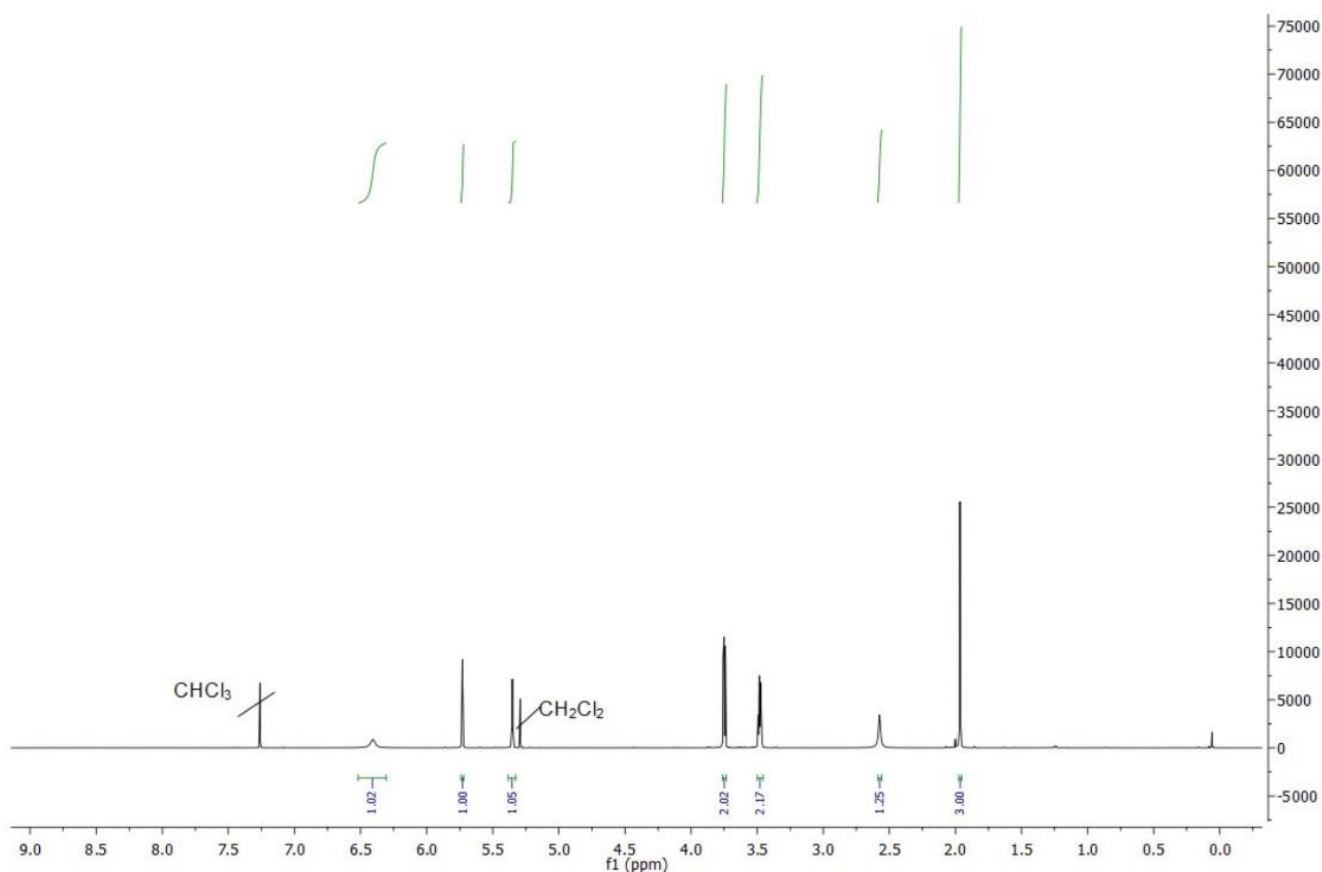
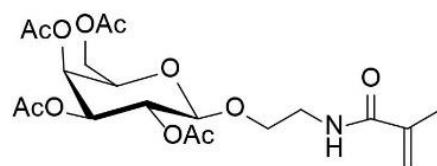


Figure S1a. ¹H-NMR (600 MHz, CDCl₃) HEMAm.

2'-acrylamidoethyl-2,3,4,6-tetra-O-acetyl-β-d-galactopyranoside



Scheme S1b *2,3,4,6-tetra-O-acetyl-β-d-galactopyranoside*

The synthesis was adapted from Gibson et al.². In a 1000 mL round bottom flask 1,2,3,4,6-Penta-O-acetyl-β-D-galactopyranoside (20.6 g, 52.8 mmol) and *N*-(2-hydroxyethyl)-2-methacrylamide (6.2 g, 48.2 mmol) were dissolved in dichloromethane (500 mL). Followed the solution was cooled to 0 °C and additionally purged with nitrogen for at least 15 min. After that slowly boron trifluoride diethyl etherate (35 mL, 276.2 mmol) was added to the solution. After the addition of boron trifluoride diethyl etherate was completed the reaction solution was

allowed to reach room temperature. After 48 h stirring at ambient temperature organic layer was washed with ice water, two times with saturated sodium hydrogen carbonate solution, distilled water and brine. The solution was dried with MgSO₄, filtered and the remaining dichloromethane was removed under reduced pressure. The crude colorless gummy was additionally purified by column chromatography (ethyl acetate/n-hexane 1:1). The overall yield of the colorless gum was 25% (5.54 g).

¹H NMR (600 MHz, CDCl₃): δ 6.23 (s, 1H, NH), 5.70 – 5.66 (m, 1H, -C=CH₂), 5.38 – 5.35 (m, 1H, -C=CH₂), 5.33 – 5.30 (m, 1H, H4), 5.16 (dd, ³J_{H4H2} = 10.5, 7.9 Hz, 1H, H2), 4.99 (dd, ³J_{H4H3} = 10.5, 3.4 Hz, 1H, H3), 4.46 (d, ³J_{H1H2} = 7.9 Hz, 1H, H-1), 4.12 – 4.09 (m, 2H, H6), 3.92 – 3.85 (m, 2H, -OCH₂CH₂NH), 3.74 – 3.68 (m, 1H, H5), 3.60 – 3.51 (m, 1H, -OCH₂CH₂NH), 3.48 – 3.40 (m, 1H, -OCH₂CH₂NH), 2.12 (s, 3H, -COCH₃), 2.02 – 2.01 (m, 6H, -COCH₃), 1.96 (s, 3H, -COCH₃), 1.94 (s, 3H, -CH₃).

¹³C NMR (600 MHz, CDCl₃): δ 170.43 (1C, -COCH₃), 170.21 (1C, -COCH₃), 170.12 (1C, -COCH₃), 169.65 (1C, -COCH₃), 168.38 (1C, -CONH), 139.98 (1C, COC(CH₃)CH₂), 119.72 (1C, COC(CH₃)CH₂), 101.37 (1C, C1), 70.89 (1C, C2), 70.82 (1C, C3), 68.99 (1C, C4), 68.90 (1C, C5), 67.06 (1C, -OCH₂CH₂), 61.38 (1C, C6), 39.39 (1C, NHCH₂CH₂), 20.86 (1C, -COCH₃), 20.72 (1C, -COCH₃), 20.71 (1C, -COCH₃), 20.63 (1C, -COCH₃), 14.27 (1C, -CH₃).

MS for C₂₀H₂₉NO₁₁ (ESI) *m/z* [M+ H⁺]⁺ calc. 460.17; found 460.20, [M+Na⁺]⁺ calc.: 482.16; found 482.27.

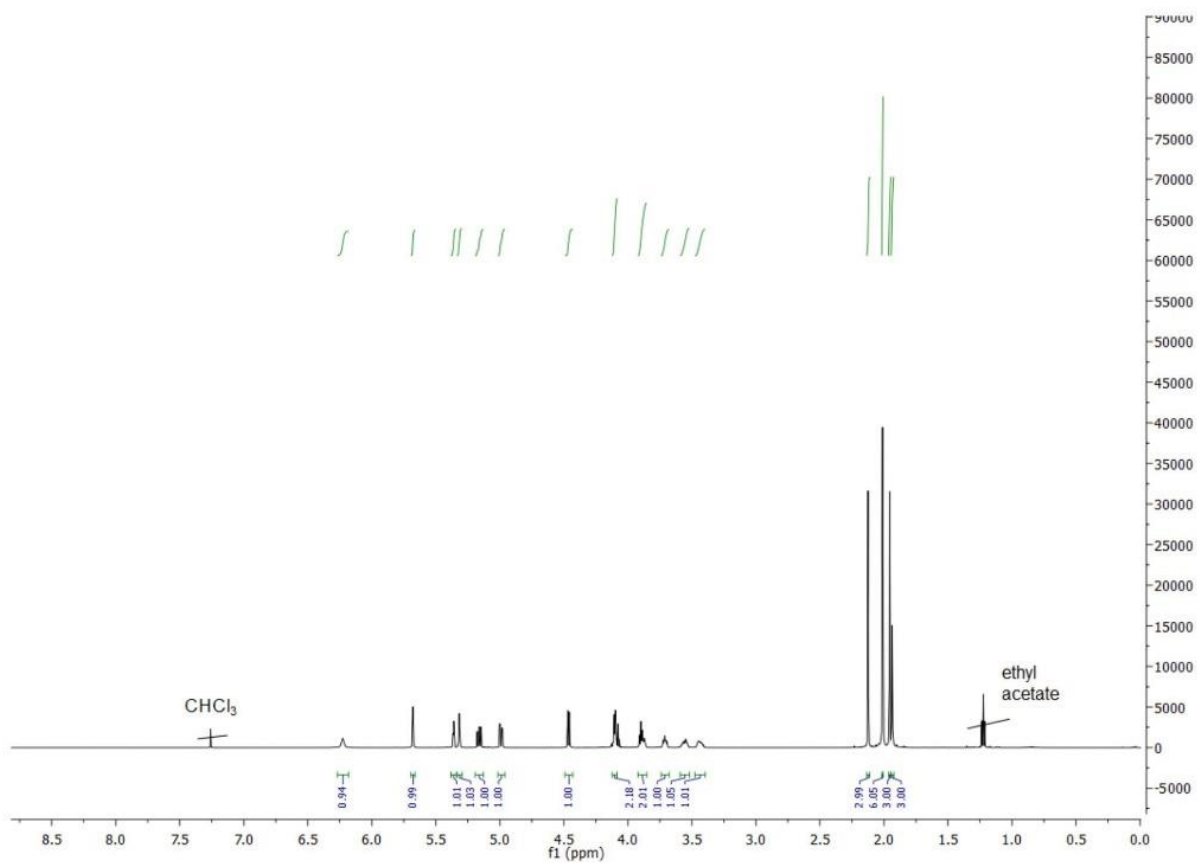


Figure S1b. ^1H NMR (600 MHz, CDCl_3) AcGalEMAm.

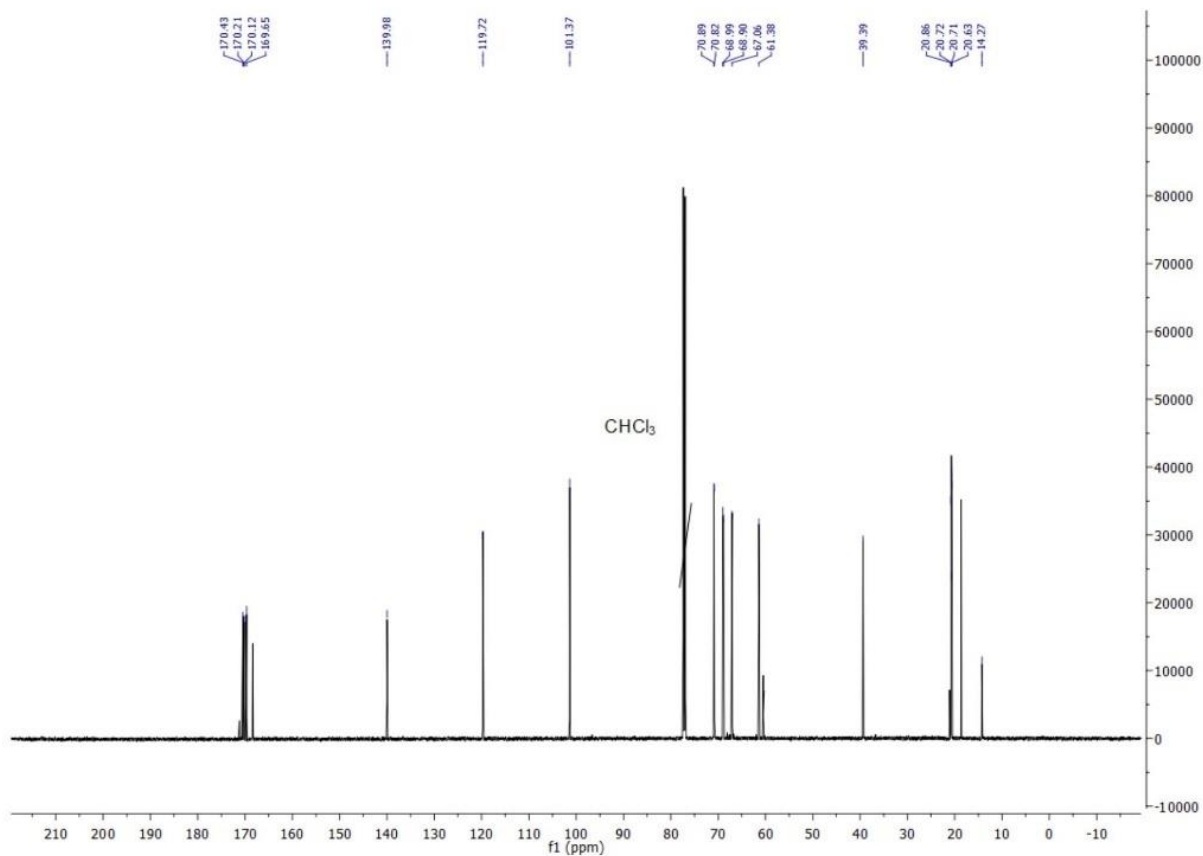
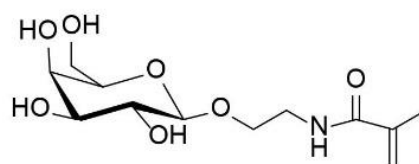


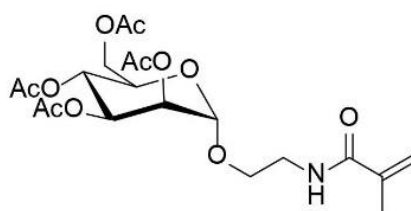
Figure S1c. ^{13}C -NMR (600 MHz, CDCl_3) of AcGalEMAm.

For polymerizations in water the glycomonomer had to be deprotected. Therefore, 0.5 g of the glycomonomer was given into 6.5 mL of a 0.3 M sodium methanolate solution in methanol and shaken for at least 2 h. The monomer formed a precipitate and was separated. The solid was washed with methanol 3 times. Afterwards, the remaining solid was dried *in vacuo*. The overall yield of the deprotection and the resulting white solid was 90 % (0.27 g).



Scheme S1c ManEMAm (deprotected)

2'-acrylamidoethyl-2,3,4,6-tetra-O-acetyl- α -D-mannopyranoside (AcManEMAm)



Scheme S1d AcManEMAm

The synthesis was adapted from Gibson et al.² In a 1000 mL round bottom flask 1,2,3,4,6-Penta-O-acetyl- α -D-mannopyranoside (20.6 g, 52.8 mmol) and *N*-(2-hydroxyethyl)-2-methacrylamide (6.2 g, 48.2 mmol) were dissolved in dichloromethane (500 mL). Followed the solution was cooled to 0 °C and additionally purged with nitrogen for at least 15 min. After that slowly boron trifluoride diethyl etherate (35 mL, 276.2 mmol) was added to the solution. After the addition of boron trifluoride diethyl etherate was completed the reaction solution was allowed to reach room temperature. After 48 h stirring at ambient temperature organic layer was washed with ice water, two times with saturated sodium hydrogen carbonate solution, distilled water and brine. The solution was dried with MgSO₄, filtered and the remaining

dichloromethane was removed under reduced pressure. The crude colorless gum was additionally purified by column chromatography (ethyl acetate/n-hexane 1:1). The overall yield of the colorless gum was 21% (4.65 g).

^1H NMR (600 MHz, CDCl_3) δ 6.29 (s, 1H, NH), 5.69 – 5.67 (m, 1H, $-\text{C}=\text{CH}_2$) 5.38 – 5.35(m, 1H, $-\text{C}=\text{CH}_2$), 5.34 – 5.31 (m, 1H, H2), 5.29 (dd, $^3J_{\text{HH}} = 10.1, 3.4$ Hz, 1H, H3), 5.25 – 5.20 (m, 2H, H4), 4.80 (d, $^3J_{\text{HH}} = 1.8$ Hz, 1H, H1), 4.21 (dd, $^3J_{\text{HH}} = 12.2, 5.7$ Hz, 1H, H6), 4.08 – 4.05 (m, 2H, 1H, H6'), 3.95 – 3.90 (m, 1H, H5), 3.82 – 3.77 (m, 1H, $-\text{OCH}_2\text{CH}_2$), 3.63 – 3.52 (m, 2H, $-\text{OCH}_2\text{CH}_2$, $-\text{OCH}_2\text{CH}_2\text{NH}$), 3.51 – 3.44 (m, 1H, $-\text{OCH}_2\text{CH}_2\text{NH}$), 2.12 (s, 3H, $-\text{COCH}_3$), 2.06 (s, 3H, $-\text{COCH}_3$), 2.01(s, 3H, $-\text{COCH}_3$), 1.96 (s, 3H, $-\text{COCH}_3$), 1.94 (s, 3H, $-\text{CH}_3$).

^{13}C NMR (600 MHz, CDCl_3) δ 170.66(1C, $-\text{COCH}_3$), 170.11 (1C, $-\text{COCH}_3$), 170.05 (1C, $-\text{COCH}_3$), 169.70 (1C, $-\text{COCH}_3$), 168.51 (1C, $-\text{CONH}$), 139.84 (1C, $\text{COC}(\text{CH}_3)\text{CH}_2$), 119.93 (1C, $\text{COC}(\text{CH}_3)\text{CH}_2$), 97.69 (1C, C1), 69.42 (1C, C2), 69.06 (1C, C3), 68.87 (1C, C4), 67.32 (1C, C5), 66.15 (1C, $-\text{OCH}_2\text{CH}_2$), 62.52 (1C, C6), 39.29 (1C, NHCH_2CH_2), 21.10 (1C, $-\text{COCH}_3$), 20.92 (1C, $-\text{COCH}_3$), 20.76 (1C, $-\text{COCH}_3$), 18.68 (1C, $-\text{COCH}_3$), 14.25 (1C, $-\text{CH}_3$).

MS for $\text{C}_{20}\text{H}_{29}\text{NO}_{11}$ (ESI) m/z $[\text{M} + \text{H}]^+$ calc. 460.17; found 460.22, $[\text{M} + \text{Na}]^+$ calc.: 482.16; found 482.22.

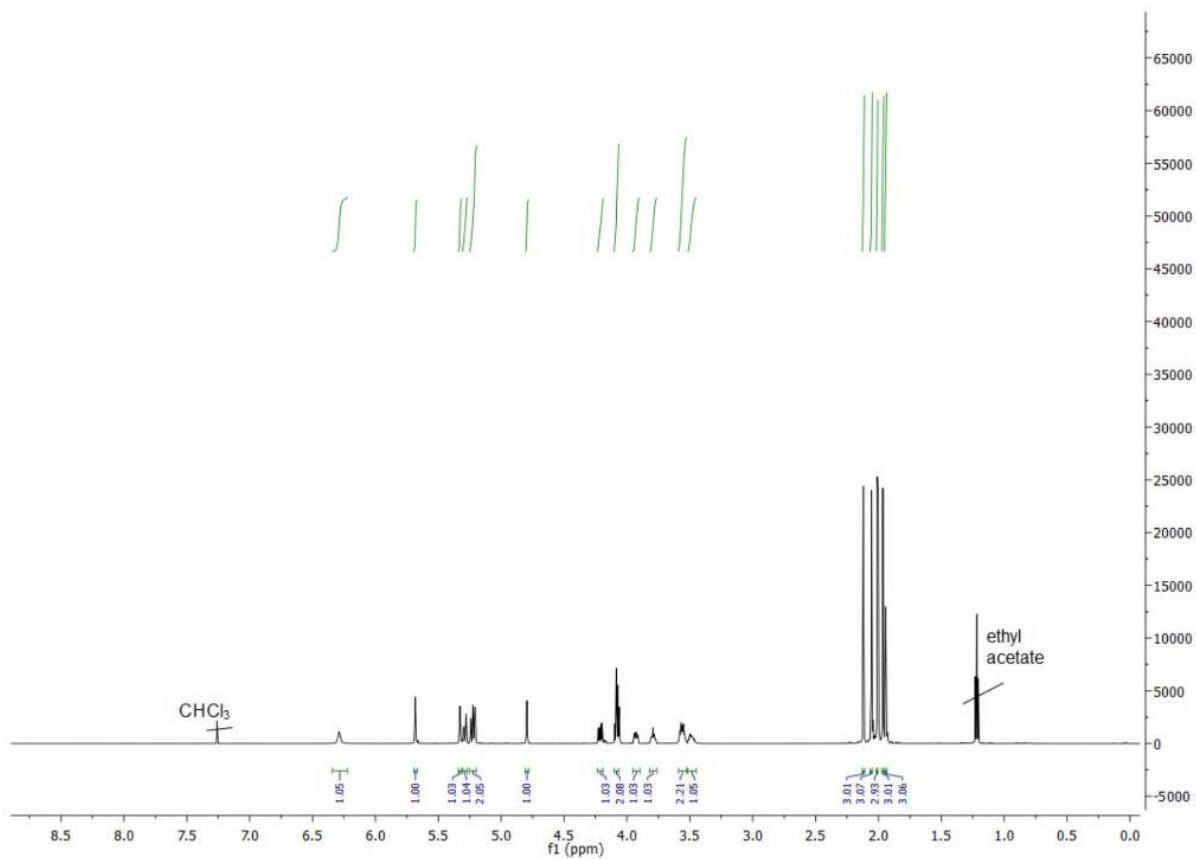


Figure S1d. $^1\text{H-NMR}$ (600 MHz, CDCl_3) AcManEMAm.

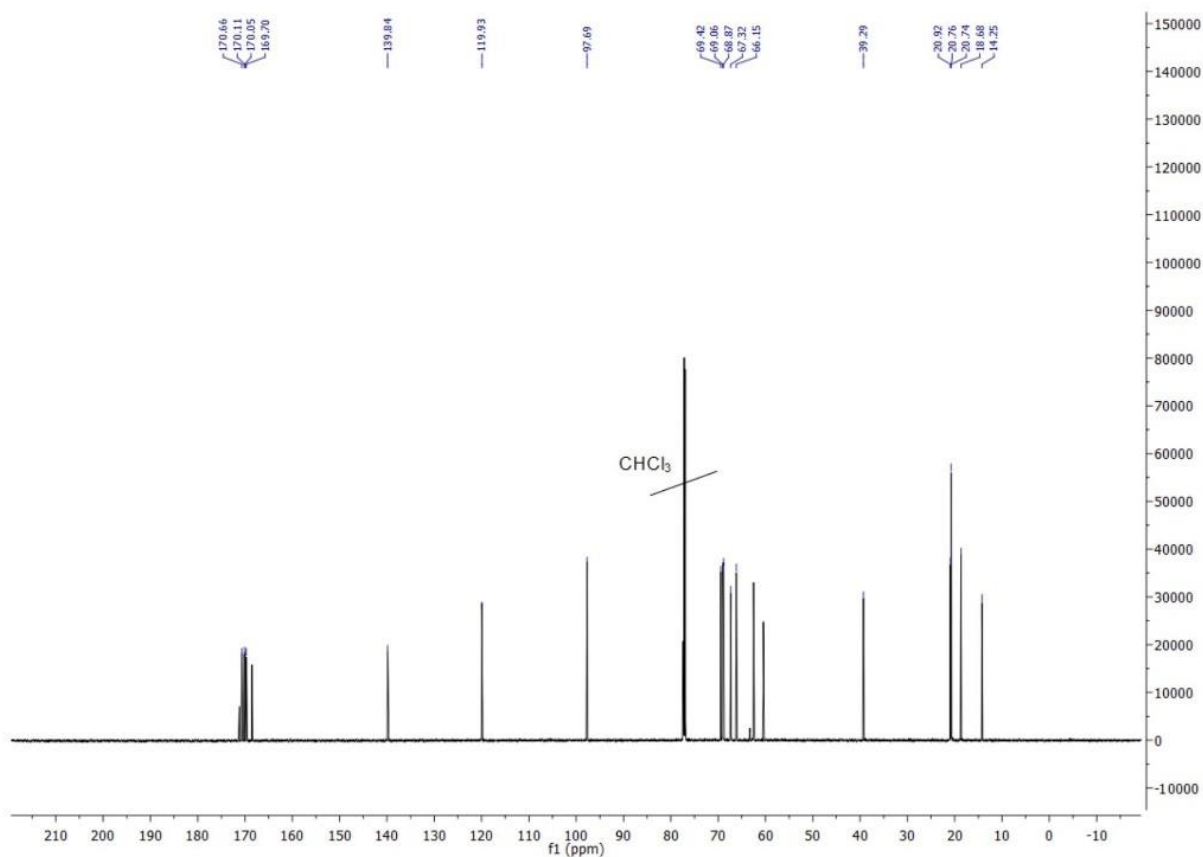


Figure S1e. ^{13}C -NMR (600 MHz, CDCl_3) AcManEMAm.

^1H NMR (600 MHz, D_2O): δ 5.73 – 5.66 (m, 1H, $-\text{C}=\text{CH}_2$), 5.47 – 5.45 (m, 1H, $-\text{C}=\text{CH}_2$), 4.87 (d, $^3J_{\text{HH}} = 1.7$ Hz, 1H, H1), 3.93 (dd, $^3J_{\text{HH}} = 3.5, 1.7$ Hz, 1H, H2), 3.85 (dd, $^3J_{\text{HH}} = 12.2, 2.2$ Hz, 1H, H6), 3.83 – 3.80 (m, 1H, H3), 3.78 (dd, $^3J_{\text{HH}} = 9.5, 3.4$ Hz, 1H, H4), 3.74 (dd, $^3J_{\text{HH}} = 12.2, 5.9$ Hz, 1H, H6'), 3.71 – 3.62 (m, 2H, $-\text{OCH}_2\text{CH}_2\text{NH}$), 3.61 – 3.57 (m, 1H, H5), 3.56 – 3.51 (m, 1H, $-\text{OCH}_2\text{CH}_2\text{NH}$), 3.49 – 3.44 (m, 1H, $-\text{OCH}_2\text{CH}_2\text{NH}$), 1.93 (s, 3H, $-\text{CH}_3$).

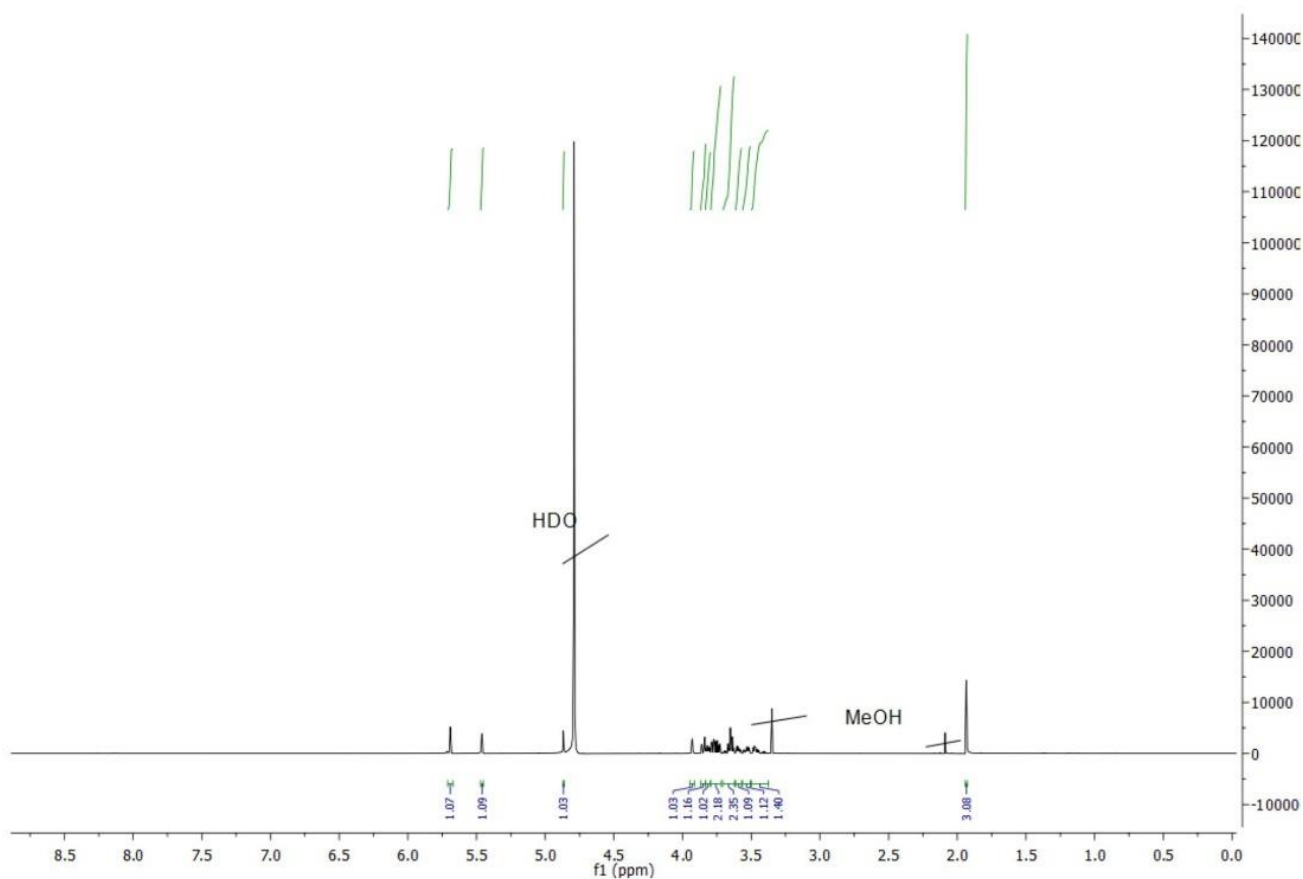


Figure S1f. $^1\text{H-NMR}$ (600 MHz, D_2O) ManEMAm.

S2 Microgel synthesis, composition of the reaction mixtures overview

Table S1. Used chemicals for the synthesis of the different microgel samples.

| Microgel sample | NIPAM | MBA | Sugar/Glycomonomer | SDS | APS |
|-----------------|------------------|------------------|---------------------|-----------------|----------------------|
| Man0.8 | 0.7 g (6.2 mmol) | 50 mg (324 nmol) | 180 mg (0.618 mmol) | 25 mg (87 nmol) | 200 mg 0.876 mmol |
| Man0.4 | 0.7 g (6.2 mmol) | 50 mg (324 nmol) | 85 mg (0.309 mmol) | 25 mg (87 nmol) | 200 mg 0.876 mmol |
| Man0.2 | 0.7 g (6.2 mmol) | 50 mg (324 nmol) | 18 mg (0.062 mmol) | 25 mg (87 nmol) | 200 mg 0.876 mmol |
| Gal0.15 | 0.7 g (6.2 mmol) | 50 mg (324 nmol) | 18 mg (0.062 mmol) | 25 mg (87 nmol) | 200 mg 0.876 mmol |

| | | | | | |
|---------------|------------------|------------------|---|-----------------|---------------------|
| PNIPAM | 0.7 g (6.2 mmol) | 50 mg (324 nmol) | - | 25 mg (87 nmol) | 200 mg (0.876 mmol) |
|---------------|------------------|------------------|---|-----------------|---------------------|

S3 Bradford assay calibration curve

For the calibration curve the amount of ConA was varied between 1 and 20 μg per well. The absorption ratio at 590 nm and 450 nm was determined 5 min after the dye solution was added.

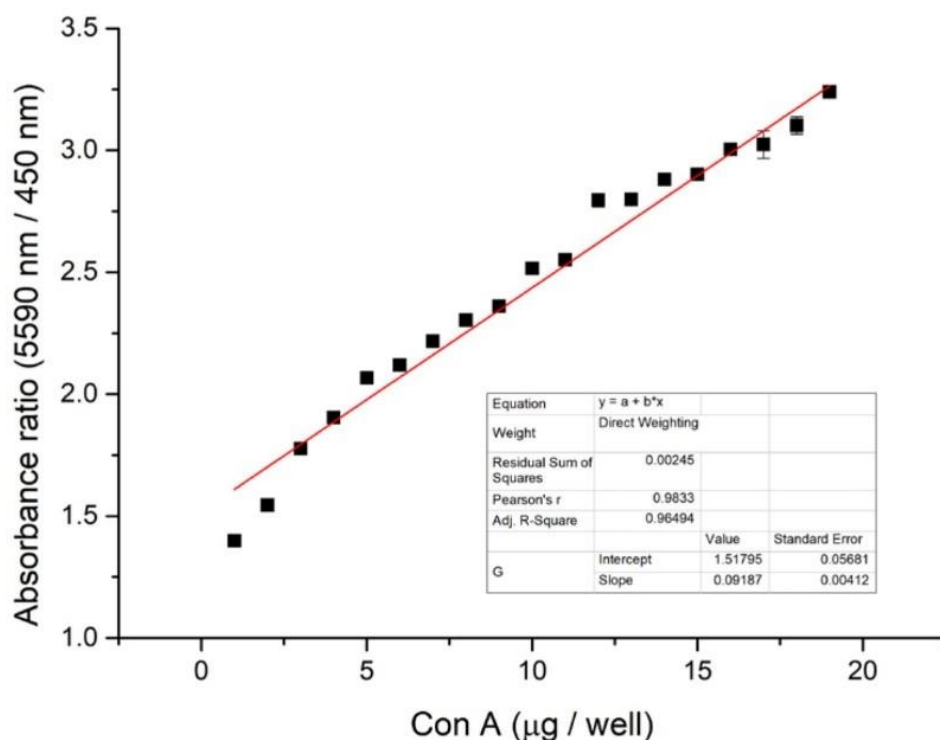


Figure S3. Bradford assay calibration curve

S4 Bacteria cultivation, buffer and media

E. coli PKL 1162 were grown in LB medium (PKL 1162) overnight in a sterilized test tube, which was covered with aluminum foil at 37 °C. The tubes were shaken with a speed of 140 rpm to guarantee a constant mixing of the solution.

LB-medium (PKL1162)

12.5 g of LB Broth (Miller) (powder microbial growth medium) were dissolved in 500 mL ultrapure water. The powder contains tryptone (5.0 g), sodium chloride (5.0 g) and yeast extract

(2.5 g). Afterwards the solution was sterilized for 30 min at 121 °C and cooled to room temperature. 50.0 mg of ampicillin and 25.0 mg of chloramphenicol were added.

Agar plates (PKL1162)

12.5 g of LB Broth (Miller) (powder microbial growth medium) were dissolved in 500 mL ultrapure water. The powder contains tryptone (5.0 g), sodium chloride (5.0 g), yeast extract (2.5 g) and 6.0 g agar agar were added. Afterwards the solution was sterilized for 30 min at 121 °C and cooled to 50 – 60 °C. Then 50.0 mg of ampicillin and 25.0 mg of chloramphenicol were added and the petri dishes were coated with the medium and cooled to room temperature.

PBS buffer

Five tablets of phosphate buffered saline were dissolved in 1 L of ultrapure water. The final concentrations of the buffer were 0.01 M phosphate buffer, 0.0027 M potassium chloride and 0.137 M sodium chloride. The pH was checked with a potentiometer and set to 7.4.

LBB buffer

Lectin binding buffer (LBB) was used for all measurements with Concanavalin A. Lectin binding buffer contains 10 mM HEPES ((4-(2-hydroxyethyl)-1-piperazineethanesulfonic acid) as buffering agent, which was adjusted to a pH of 7.4 with 1 M NaOH. Thereafter, calcium chloride (1 mM), manganese chloride (1 mM) and sodium chloride (50 mM) were dissolved in the solution. To prevent bacterial growth in the buffer, sodium azide was added to a final concentration of 0.05 wt%

S5 absolute quantities of microgel-bound ConA

| Sample | Carbohydrate quantity (nmol) | ConA quantity in filtrate (pmol) | Captured ConA (pmol) | Captured ConA (%) | Captured mass of ConA per microgel (wt/wt) |
|--------|------------------------------|----------------------------------|----------------------|-------------------|--|
| Man0.8 | 6.7 | 2±9 | 453±9 | 99.6±2.0 | 0.49 |
| Man0.4 | 3.2 | 47±2 | 408±2 | 89.7±0.6 | 0.45 |
| Man0.2 | 1.5 | 419±5 | 36±5 | 8.3±1.3 | 0.04 |
| Gal0.2 | 1.2 | 455±5 | 0.0±5 | 0.0±2.0 | 0 |

| | | | | | |
|--------|---|-------|------|---------|------|
| PNIPAM | 0 | 445±5 | 10±5 | 1.6±1.0 | 0.01 |
|--------|---|-------|------|---------|------|

S6 Turbidity measurements on microgels in absence of ConA

Additionally, measurements without concanavalin A were carried out to check whether all detected effects are related to the interaction of microgel and protein. Therefore, 200 μ L of the microgel stock solution was diluted with 2.3 mL LBB for the measurements with a higher microgel concentration.

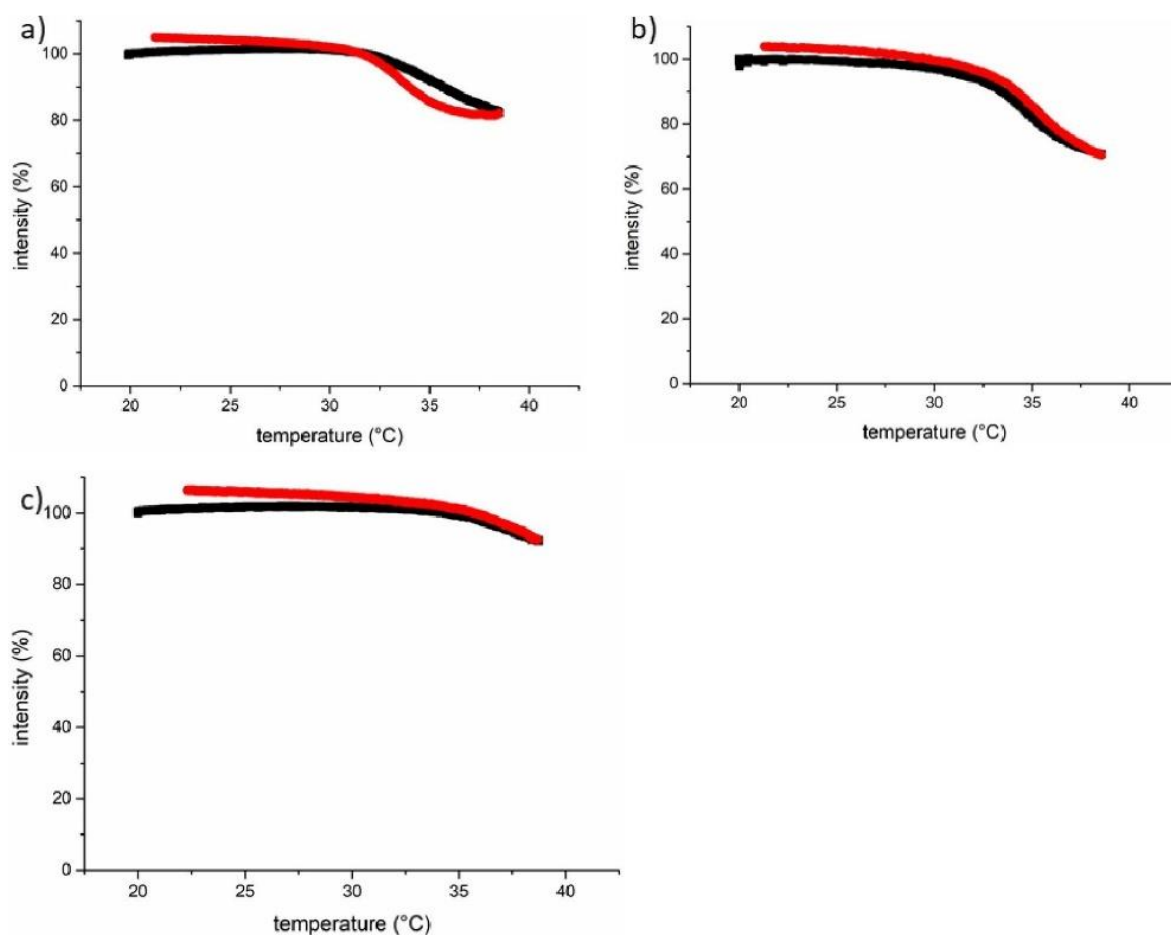


Figure S4. Turbidity measurements with a microgel concentration of 0.04 mg/mL without ConA in LBB. a) Man0.2 b) Man0.4 c) Man0.8. Black lines denote heating cycle. Red line denotes cooling cycle.

S7 Turbidity measurements, granular-sized aggregates

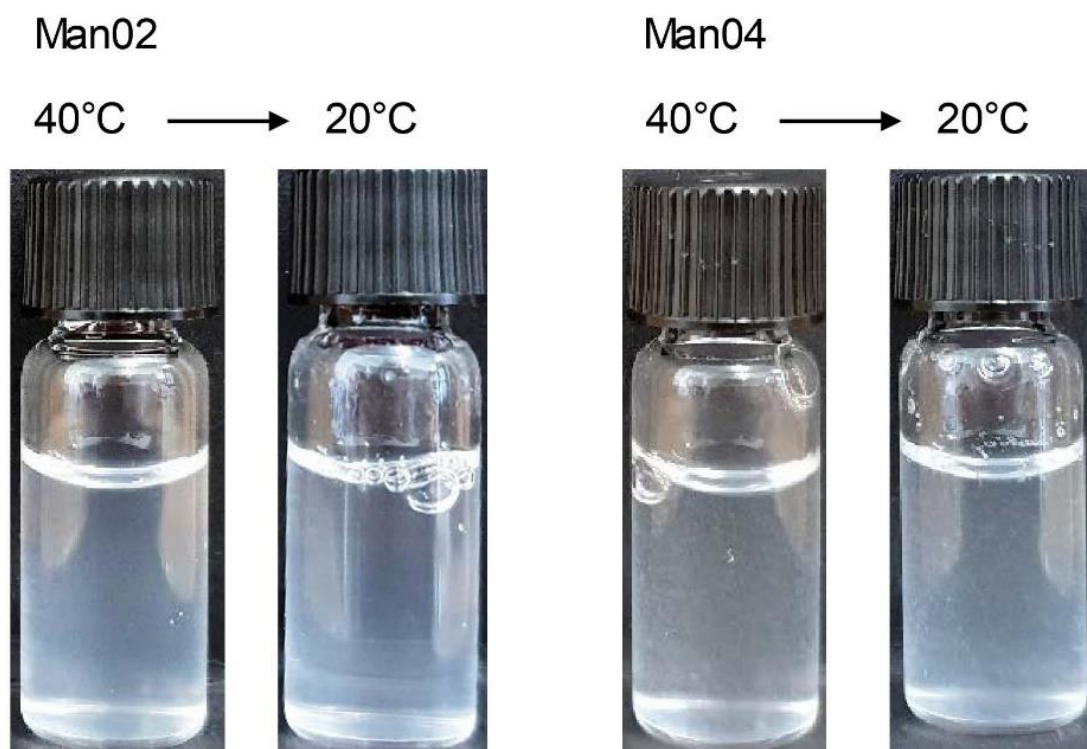


Figure S5. Left: Images of Man0.2 microgels in presence of ConA indicate largely microscopic aggregates suitable for turbidity measurements. Right: Images of Man0.4 in presence of ConA indicate granular sized aggregates that may give rise to artifacts in turbidity measurements

S8 Colony forming units (CFU) data from filtration-cultivation assay

Table S2

| sample | temp. | CFU | | | average | st. Dev |
|--------|-------|---------|---------|---------|---------|---------|
| | | plate 1 | plate 2 | plate 3 | | |
| Gal02 | 20 °C | 338 | 460 | 552 | 450 | 107 |
| | 37 °C | 467 | 472 | 320 | 420 | 86 |
| Man0.8 | 20 °C | 171 | 187 | 147 | 168 | 20 |
| | 37 °C | 51 | 20 | 21 | 31 | 18 |
| Man0.4 | 20 °C | 153 | 216 | 224 | 198 | 39 |
| | 37 °C | 6 | 11 | 11 | 9 | 3 |
| Man0.2 | 20 °C | 585 | 450 | 334 | 456 | 126 |
| | 37 °C | 246 | 251 | 209 | 235 | 23 |
| NIPAM | 20 °C | 576 | 478 | 578 | 544 | 57 |
| | 37 °C | 511 | 530 | 574 | 538 | 32 |

S9 Instrumentation

Nuclear magnetic resonance (NMR) spectroscopy

^1H -NMR and ^{13}C -NMR (600 MHz) were measured on a Bruker AVANCE III 600 (Bremen, Germany). As internal standard chemical shifts were referenced to the residual non-deuterated solvents (CDCl_3 : ^1H 7.26, ^{13}C 77.16, D_2O : ^1H 4.79). All chemical shifts are reported in delta (δ) expressed in parts per million (ppm). The following abbreviations were used to indicate multiplicities: s = singlet, d = doublet, t = triplet, m = multiplet.

Reversed phase high pressure liquid chromatography – mass spectrometry (RP-HPLC-MS)

All RP-HPLC-MS measurements were performed on an Agilent 1260 infinity instrument (Agilent Technologies, Waldbronn, Germany). The instrument is coupled to a variable wavelength detector (VWD) and was set to 214 nm and a 6120 Quadrupole LC/MS containing an Electrospray Ionization source (operating in positive ionization mode in a m/z range of 200 to 2000). A Poroshell 120 EC-C18 1.8 μm (3.0 \times 50 mm, 2.5 μm) RP column was used as HPLC column. The mobile phase A was 95/5 $\text{H}_2\text{O}/\text{MeCN}$ and B 5/95 $\text{H}_2\text{O}/\text{MeCN}$, both containing 0.1 % formic acid. Samples were analyzed with a flow rate of 0.4 mL/min using a linear gradient from 100 % A to 50 % B in a time range of 17 min at 25 °C. Using OpenLab ChemStation software for LC/MS from Agilent Technologies (Waldbronn, Germany) spectral analysis of UV and MS data was performed.

Optical microscopy

For microscope measurements an inverted microscope (Olympus IX73, Japan) equipped with an Olympus 60 x NA 1.35 oil-immersion objective (Olympus, Japan). A CMOS camera (UI-3360CP-M-GL, IDS, Germany) was used for imaging of the surfaces. As a light source a collimated LED (530 nm, Thorlabs, Germany, M530L2-C1) was used. For image acquisition $\mu\text{Manager}$ (v.1.4.16) was used and image analysis was performed with ImageJ.

UV-Vis spectroscopy

On a dual-trace spectrometer Specord® 210 Plus from *Analytik Jena AG* (Jena, Germany) all UV-Vis measurements were performed at 25 °C. Using Win ASPECT PLUS software the instrument was operated. Protein concentration measurements were performed in a cuvette QX quartz cuvette (d = 1 cm, V = 3.5 mL) from Hellma Analytics (Mühlheim, Germany). For calculation of the Con A concentration the absorption from 270-320 nm was measured. Using the Lambert-Beer law the concentration was calculated using the molar extinction coefficient $\epsilon_{280} = 30150 \text{ M}^{-1} \text{ cm}^{-1}$ for tetravalent Con A.

Zeta potential measurements

All Zeta potential measurements were performed at a Zetasizer Nano-Z instrument (Malvern) using a DTS1070 folded capillary cell. To operate the instrument, the Zetasizer software version 7.11 (Malvern) was used. For all measurements a 0.05 wt% microgel dispersion in 5 mM Na₂HPO₄ buffer (pH 7.4) was used. All measurements were carried out at 20 °C. For all microgel samples a zeta potential of -1.0 mV to 0.3 mV was measured. The slightly negative charge can be attributed to the negative charges of the used initiator.

Supporting References

1. Parry, A. L.; Clemson, N. A.; Ellis, J.; Bernhard, S. S. R.; Davis, B. G.; Cameron, N. R., 'Multicopy Multivalent' Glycopolymer-Stabilized Gold Nanoparticles as Potential Synthetic Cancer Vaccines. *Journal of the American Chemical Society* **2013**, *135* (25), 9362-9365.
2. Wilkins, L. E.; Phillips, D. J.; Deller, R. C.; Davies, G.-L.; Gibson, M. I., Synthesis and characterisation of glucose-functional glycopolymers and gold nanoparticles: study of their potential interactions with ovine red blood cells. *Carbohydrate Research* **2015**, *405*, 47-54.

4.2. Temperature switchable glycopolymers and their conformation-dependent binding to receptor targets

Authors: Tanja J. Paul[#], Alexander K. Strzelczyk[#], Melina I. Feldhof, Stephan Schmidt

Journal: *Biomacromolecules*

Issue: **2020**, 21, 7, 2913–2921.

Type of Paper: Full Paper

Impact Factor: 5.680 (2019)

DOI: 10.1021/acs.biomac.0c00676.

Own Contribution (first author, equal contribution)

Collaborative design of the synthetic strategy and synthesis of 2',3'-epoxypropyl-2,3,4,6-tetra-O-acetyl- α -D-mannopyranoside and 2',3'-epoxypropyl-2,3,4,6-tetra-O-acetyl- β -D-galactopyranoside. Synthesis and characterization of 2-azidoethyl-2,3,4,6-tetra-O-acetyl- α -D-mannopyranose. Performance and establishment of temperature-dependent adhesion inhibition assays with *E. coli* and ConA. Interpretation of data and collaborative writing of the manuscript.

Reprinted with permission from Tanja J. Paul, Alexander K. Strzelczyk, Melina I. Feldhof, Stephan Schmidt, Temperature switchable glycopolymers and their conformation-dependent binding to receptor targets, *Biomacromolecules* **2020**, 21, 7, 2913–2921.

Copyright © 2020 American Chemical Society.

Temperature-Switchable Glycopolymers and Their Conformation-Dependent Binding to Receptor Targets

Tanja J. Paul,[#] Alexander K. Strzelczyk,[#] Melina I. Feldhof, and Stephan Schmidt*

Cite This: *Biomacromolecules* 2020, 21, 2913–2921

Read Online

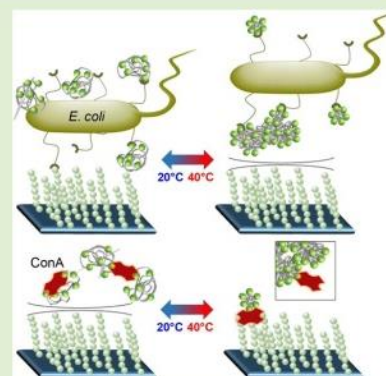
ACCESS |

Metrics & More

Article Recommendations

Supporting Information

ABSTRACT: The temperature-dependent binding of copolymers from poly(*N*-isopropylacrylamide) (PNIPAM) and mannose ligands to *Escherichia coli* and concanavalin A (ConA) is determined. Through polymer analogous reactions using poly(*N*-acryloxysuccinimide) and amine-linked mannose residues with different linkers, glycopolymers are prepared with the variation of the mannose density. Quantitative adhesion inhibition assays show the inhibitory potential of the glycopolymers as a function of the mannose/NIPAM ratio and linker type above and below their lower critical solution temperature (LCST). Intriguingly, opposite temperature effects on the binding to *E. coli* and ConA are observed. While the *E. coli* inhibition is stronger above the LCST, the ConA inhibition is, in overall, weaker at elevated temperatures. When going beyond the LCST, the polymers undergo a coil-to-globule transition, forming microphases with surface-enriched hydrophilic sugar moieties exhibiting increased *E. coli* inhibition through steric shielding. However, the formation of such microphases above the LCST renders a fraction of carbohydrate ligands inaccessible, and the polymers remaining in the solution phase then have coil sizes below the minimum binding site spacing of the ConA receptor, explaining reduced ConA inhibition. Overall, these results suggest that the coil-to-globule transition of glycopolymers may induce lower or higher inhibitory potentials due to the adverse effects of steric shielding and carbohydrate ligand accessibility.



1. INTRODUCTION

Interactions between carbohydrates and proteins at the surface of cells or pathogens control numerous biological processes including infections, fertilization, recognition, or signaling.¹ Lectins, as a class of carbohydrate-binding proteins, decorate the pathogen surface and form complexes with glycans at the cell's glycocalyx, which is a critical step in the development of infectious diseases. The macromolecular glycans involved in these processes interact with the pathogen receptors through multiple weak interactions generating sufficient adhesion across large interfacial areas^{2,3} to drive pathogen invasion and disease progression. The ability to suppress such lectin-glycan mediated adhesion processes by multivalent carbohydrate-presenting inhibitors has been proposed as a strategy to fight infections.^{4–6} Different glycoconjugates have been developed for this purpose, for example, nanogels,⁷ gold nanoparticles,^{8,9} and many more, see recent reviews.^{10–12} To improve the viability of such inhibitors in practice, being able to increase or decrease their affinity toward pathogens by remote stimulus is desired, for example, to first capture pathogens at a high-affinity state of the glycoconjugate and to release the pathogen afterward for diagnosis by switching to a low-affinity state. Remote stimuli could also reduce side effects, for example, by locally restricting bacterial inhibition/capture to the inflamed tissues. For a controlled drug release, many of such remotely switchable and site specific scaffolds are successfully established.¹³ Recent studies also applied this

concept to glyco-conjugated thermoresponsive polymers in order to control the interactions with lectins, bacteria, or viruses via temperature stimulus.^{14–23} The involved polymers have a lower critical solution temperature (LCST) in the physiological temperature range. They form extended coils below the LCST and attain a collapsed globule conformation above the LCST. It was reasonably assumed that the temperature-controlled coil-to-globule transition affects the presentation of carbohydrate ligands as well as the size of the scaffold and thus controls the binding affinity of the glycoconjugate. However, the literature shows diverging results on how temperature changes affect the affinity. One the one hand, affinities toward single lectins or bacteria were shown to decrease above the LCST,^{14–16} whereas other studies showed increasing affinities.^{19–23} For example, using linear copolymers composed of *N*-isopropylacrylamide (NIPAM) and mannose derivatives, Pasparakis et al. showed that binding to *E. coli* and their clustering is preferred below the LCST.¹⁴ Using a similar pair of monomers and additional cross-linkers to form

Received: April 30, 2020

Revised: June 12, 2020

Published: June 16, 2020



microgels, we showed that the binding and clustering of *E. coli* is preferred above the LCST.¹⁹ Other works showed no clear effect of temperature transition on the binding efficiency.^{18,24,25}

This work is aimed at investigating the changes in the temperature-dependent affinity of thermosensitive glycopolymers to understand the diverging findings and interpretations in the literature. It could be argued that carbohydrate units become inaccessible at elevated temperatures when linear LCST polymers attain a globule conformation and aggregate to exhibit reduced affinity. On the other hand, the surface presentation of hydrophilic carbohydrate units of such globules might increase above the LCST when the polymer becomes hydrophobic. In addition, the size ratio between the glycopolymer ligands and their targets are shifted by the coil-to-globule transition, which may affect their inhibitory potential due to steric shielding effects.²⁶ Such steric shielding effects describe the ability of a large inhibitor particle to block the binding between ligands and receptor-decorated surfaces due to the steric screening of binding sites.²⁷ Furthermore, the multivalent binding to receptor sites could be affected because of the change of the polymer coil size when crossing the LCST, for example, when the coil size falls below the minimum binding site of the receptor. Therefore, here, we systematically vary the compositions of linear PNIPAM/mannose copolymers as well as the linkers between mannose units and the polymer backbone. We study their binding via inhibition assays with concanavalin A (ConA) as a well-known mannose-specific lectin with a minimum binding site distance of 7.2 nm²⁸ and *E. coli*, a bacteria binding to mannose via monovalent FimH receptors.²⁹ By choosing these targets with broadly different properties and systematically varying the glycopolymer mannose density and linker type, we aim to elucidate the phase transition effects in glycopolymer binding.

2. EXPERIMENTAL SECTION

2.1. Materials. α -D-mannopyranoside (99%, Acros Organics), β -D-galactose pentaacetate (95%, Fluorochem), acetonitrile ($\geq 99.9\%$, PanReac AppliChem), *p*-toluenesulfonic acid (98%, Alfa Aesar), sodium methanolate (98%, Alfa Aesar), isopropylamine (99 + %, Alfa Aesar), acetic anhydride ($\geq 98\%$, VWR Chemicals), *n*-hexane (99%, VWR Chemicals), ethyl acetate (freshly distilled), sodium bicarbonate (100%, Fisher Chemicals), Amberlite-IR120 (Fisher Chemicals), magnesium sulfate (62–70%, Fisher Chemicals), tetrahydrofuran (99.99%, Fisher Chemicals), chloroform (99.97%, Fisher Chemicals), dimethylsulfoxide (99.99%, Fisher Chemicals), allyl alcohol ($\geq 99\%$, Merck KGaA), trimethylamine ($>99.0\%$, Merck KGaA), acryloyl chloride (96%, Merck KGaA), boron trifluoride diethyl etherate ($\geq 98\%$, TCI), hydrogen (Air Liquide), and *N,N*-dimethylformamide ($\geq 99.8\%$, Biosolve Chemicals). All other chemicals were obtained from Sigma-Aldrich (Germany).

2.2. Synthesis of *N*-Acryloxysuccinimide (NAS). The synthesis of NAS was carried out according to previously published protocols.¹⁶ In 200 mL of chloroform, *N*-Hydroxysuccinimide (14.4 g, 125 mmol) and triethylamine (22 mL, 155 mmol) were dissolved at 0 °C. Then, acryloyl chloride (10 mL, 125 mmol) was added dropwise under stirring at 0 °C for 30 min. The organic phase was washed three times with a saturated sodium bicarbonate solution and dried over sodium sulfate. The volume was then reduced to 1/3 and NAS was precipitated by the addition of *n*-hexane. The supernatant *n*-hexane was removed under reduced pressure. The remaining yellow oil was dissolved in chloroform. This cycle was repeated until the remaining oil was not soluble in chloroform giving a yield of 18.09 g (88%).^{1H}-NMR (300 MHz, CDCl₃) δ 6.74–6.67 (dd, ³J_{HH} = 17.4, 0.8 Hz, 1H, H1), δ 6.38–6.27 (dd, ³J_{HH} = 16.6, 10.3 Hz, 1H, H2), δ 6.20–6.14

(dd, ³J_{HH} = 10.7, 0.8 Hz, 1H, H3), and δ 2.89–2.81 (s, 4H, H4–7) (Supporting Information S1).

2.3. Synthesis of Poly(*N*-Acryloxysuccinimide) (PNAS). NAS (15.3 g, 90 mmol) in 140 mL of *N,N*-dimethylformamide (DMF) was heated to 80 °C and flushed with nitrogen for 15 min. The polymerization was initiated by the addition of 4,4'-Azobis(4-cyanovaleic acid) (255.6 mg, 0.9 mmol) in 10 mL of DMF. After 20 h, the polymer was precipitated in cold tetrahydrofuran, filtered, and dried under vacuum. A brown solid was obtained (yield 12.21 g, 79%, \bar{M}_n = 15,340 Da).^{1H}-NMR (600 MHz, CDCl₃) δ = 12.38–12.14 (s, 1H, H9) 3.28–3.00 (s, 1H, H3), 2.85–2.74 (s, 4H, H4–7), and 2.25–1.90 (s, 2H, H1 + 2) 1.40–1.33 (s, 3H, H8) (Supporting Information S2).

2.4. Synthesis of Glycopolymers. Poly(*N*-acryloxysuccinimide) (1.00 g, 65 μ mol) was dissolved in 10 mL of dimethyl sulfoxide (DMSO) and heated to 40 °C. Depending on the Man/Gal functionalization degree, different amounts of amine-functionalized sugar (Supporting Information S4) were added. After 2 h of the reaction, isopropylamine (1.5 mL, 17.7 mmol) was added to react for additional 2 h. The reaction solution was cooled down and diluted with 35 mL of water and dialyzed for 48 h followed by freeze drying. The Supporting Information shows the ^{1H} NMR analysis (Supporting Information S4) and the size exclusion chromatography (Supporting Information S5) of the polymers.

2.5. Phenol Sulfuric Acid (PSA) Method. To determine the glycopolymer Man/Gal functionalization degree, the PSA method was used.³⁰ At first, a calibration curve was measured using a methyl α -D-mannopyranoside (MeMan) dilution series in water (160, 80, 40, and 20 μ M). To 125 μ L of each MeMan solution, 125 μ L of a 5 wt % phenol solution in water was added and vigorously shaken. Afterward, 625 μ L of concentrated sulfuric acid was added, vigorously shaken, and reacted at 30 °C for 30 min. Next, the absorbance at a wavelength of 490 nm was measured. For analyzing the functionalization degree, 125 μ L of the polymer solution at a known concentration was used (Supporting Information S6).

2.6. Turbidimetry. Turbidity measurements were performed with a Tepper turbidity photometer using a 1 mW laser at 630–690 nm. Solution (2 mL) of 5 mg mL⁻¹ polymer in LBB was poured into a QS quartz cuvette (Hellma Analytics, Müllheim, Germany). After reaching the starting temperature of 20 °C, 0.5 mL of a ConA solution (1 mg mL⁻¹) was added followed by heating and cooling cycles from 20 to 44 °C and back to 20 °C at a temperature rate of 1 °C min⁻¹. To determine the cloud point as an indication for the LCST of the polymers, the measurement was executed without proteins (Supporting Information S9). From the transmission-temperature traces, the onset of the transmission decrease was used to determine the cloud points.

2.7. Mannan Coating. For coating the 96-well plates, mannan from *Saccharomyces cerevisiae* (Sigma-Aldrich) was used. A volume of 120 μ L of mannan solution (1.2 mg mL⁻¹) in carbonate buffer (pH 9.5) was filled into each well. The plates were dried at 37 °C overnight followed by washing with PBST (PBS with 0.5 wt % Tween 20, 3 \times 120 μ L per well).

2.8. GFP-Based Bacterial Adhesion Inhibition Assay. The adhesion assay was carried out according to previously published protocols.²⁹ For blocking nonspecific binding, each well was filled with 120 μ L of 1 wt % polyvinylalcohol (22,000 g/mol) in PBS at 37 °C followed by shaking at 120 rpm for 1 h. Next, the plates were washed three times with 120 μ L of PBST and one time with PBS. Then, a dilution series of the polymers was prepared and added to the well plates. The bacteria suspension (50 μ L) at a concentration of 2 mg mL⁻¹ (OD = 0.4) was added to the wells, and the plates were incubated for 1 h. at 100 rpm at either 20 or 40 °C. Afterward, the plates were washed three times with 120 μ L of PBS and then filled with 100 μ L of PBS per well. Finally, the fluorescence intensity of the adhered *E. coli* was detected at 485 nm/535 nm.

2.9. FITC–ConA Adhesion Inhibition Assay. The mannan-coated surfaces were blocked with a 5 wt % solution of bovine serum albumin in carbonate buffer (pH 9.5) by adding 120 μ L of a BSA solution into each well and shaking at 120 rpm for 1 h at ambient

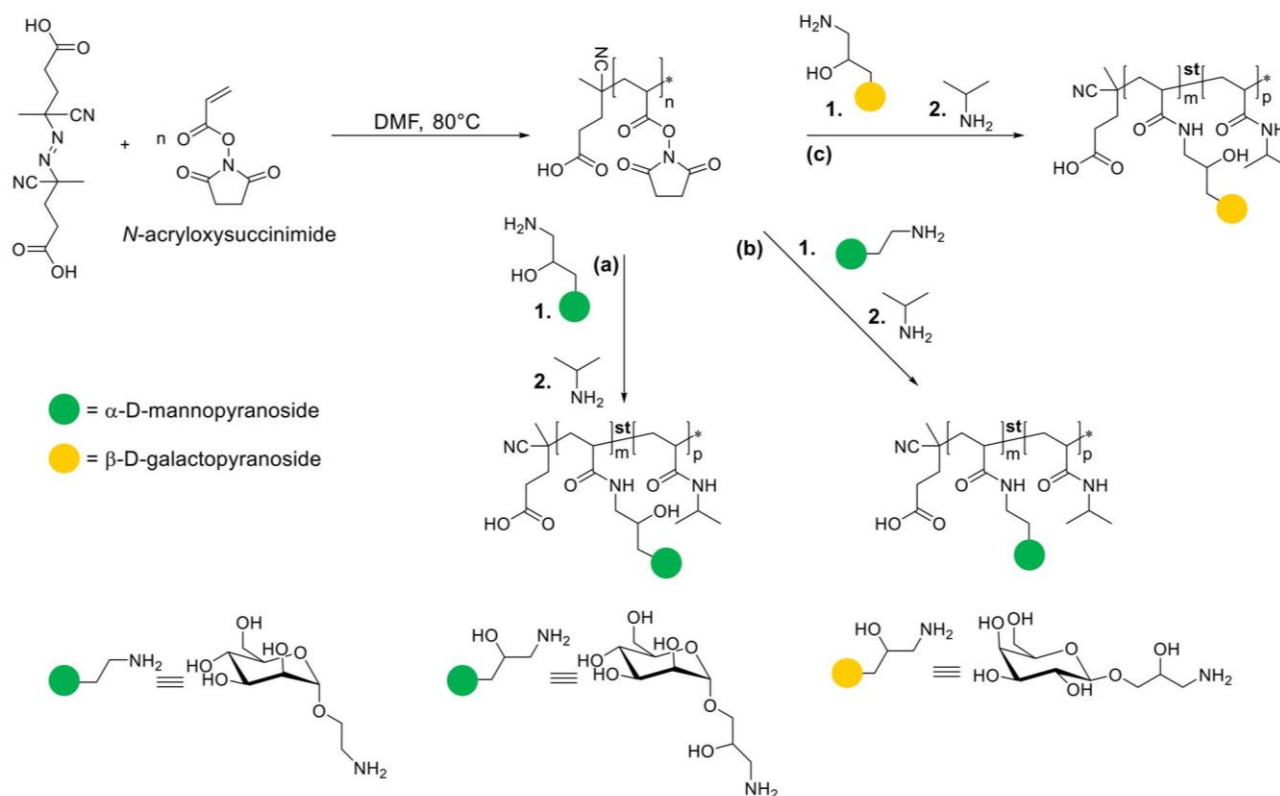


Figure 1. Schematic of the synthesis of active ester and grafting of different sugars. Grafting of (a) **ManHPL**, (b) **ManEL**, and (c) **GalHPL** at different carbohydrate densities on the polymer backbone is followed by the addition of isopropylamine to quench the remaining active esters and to form thermoresponsive NIPAM residues.

temperature. After blocking, the plates were washed three times with 120 μL of PBST and one time with 120 μL of LBB. A dilution series of the polymers was prepared on the mannan-coated, BSA-blocked well plates. A solution of FITC–ConA at a concentration of 0.1 mg mL^{-1} in LBB was prepared. The ConA solution (50 μL) was added to each well, and the plates were incubated for 1 h at 100 rpm either at 20 or at 40 $^{\circ}\text{C}$. After 1 h, the plates were washed three times with 120 μL of LBB and filled with 100 μL of LBB per well. The fluorescence intensity of the adhered FITC–ConA was determined at 485 nm/535 nm.

3. RESULTS AND DISCUSSION

3.1. Synthesis of Thermoresponsive Glycopolymers.

The key objective of this work is to control the sugar density and linker type in thermoresponsive glycopolymers and to test the effect of these parameters on the inhibition of ConA and *E. coli* FimH receptors. Ten different polymers with varying carbohydrate densities and different linkers were prepared. For straightforward variation of the sugar densities and linker type, a polymer analogous reaction was chosen (Figure 1). By postfunctionalization of a poly(active ester), the NIPAM repeating units and the sugar ligands were introduced. First, the succinimide-based poly(active ester) was synthesized according to a previously published protocol.¹⁶ Using free radical polymerization (FRP) with 4,4'-azobis(4-cyanovaleric acid) as the initiator, an active ester polymer poly(*N*-acryloxysuccinimide) (PNAS) was synthesized. As expected from FRP, PNAS exhibited a dispersity of 1.51 and a number average molecular weight (\bar{M}_n) of 15.34 kDa as determined via size exclusion chromatography (SEC) and $^1\text{H-NMR}$. As carbohydrate ligands, varying quantities of 2-aminoethyl- α -D-mannopyranoside (**ManEL**) and 3-amino-2-hydroxypropyl- α -D-mannopyranoside (**ManHPL**) were then reacted with

PNAS. The two carbohydrates have different linkers, where the hydroxypropyl (**HPL**) linker can be considered slightly more hydrophilic due to the added hydroxy group as compared to the ethyl (**EL**) linker. In the second reaction step, isopropylamine was added to quench the remaining active esters and to create thermoresponsive NIPAM repeating units.

The incorporation of carbohydrates into the polymers took place with an efficiency of roughly 50% (Supporting Information S4). Because of the presence of hydroxyl groups, it is possible that a fraction of sugar units was grafted to the polymer backbone via ester groups. However, as evidenced by the absence of ester groups in the IR traces (Supporting Information S7), the esters were likely substituted by isopropylamine groups in the second grafting step under basic conditions. With this synthetic route, five glycopolymers bearing **ManHPL** with carbohydrate functionalization degrees from 1 to 97% and three glycopolymers bearing **ManEL** with carbohydrate functionalization degrees from 1 to 5% were produced. As negative controls, two non-Man-presenting polymers were prepared: pure **PNIPAM** without sugar ligands and a galactose-decorated polymer via grafting of 3-amino-2-hydroxypropyl- β -D-galactopyranoside (**GalHPL**). In Table 1, the synthesized polymers are listed and named by the grafted carbohydrate followed by a number representing the functionalization degree, for example, **ManHPL7** signifies 7% Man units compared to NIPAM. The polymer's carbohydrate functionalization degree was determined using a quantitative colorimetric test for sugars (PSA-test).^{31,32} In addition, the degree of carbohydrate functionalization was confirmed by AT-FTIR. The glycopolymer molecular weights were determined by considering the \bar{M}_n of PNAS as determined by NMR and the degree of carbohydrate functionalization as determined by

Table 1. Glycopolymers Functionalized with Different Quantities of Man and Gal, \bar{M}_n , T_g, Cloud Point, and Carbohydrate Functionalization Degree are Listed^f

| polymer sample | \bar{M}_n [kDa] ^a | T _g [°C] ^b | LCST [°C] ^c | man/gal functionalization degree [$\mu\text{mol g}^{-1}$] ^d |
|----------------|--------------------------------|----------------------------------|------------------------|--|
| PNIPAM | 10.30 | 117 | 32.6 | 0.0 |
| ManHPL1 | 10.48 | 122 | 35.9 | 4.2 ± 0.1 |
| ManHPL2 | 10.65 | 126 | 36.8 | 5.7 ± 0.1 |
| ManHPL7 | 11.53 | 126 | 40.2 | 23 ± 0.1 |
| ManHPL34 | 16.24 | 133 | >45 ^e | 99 ± 0.3 |
| ManHPL97 | 27.24 | 123 | >45 ^e | 298 ± 2.2 |
| ManEL1 | 10.45 | 125 | 35.6 | 3.5 ± 0.1 |
| ManEL2 | 10.59 | 128 | 36.7 | 6.8 ± 0.1 |
| ManEL5 | 11.04 | 129 | 40.8 | 14 ± 0.1 |
| GalHPL3 | 10.83 | 132 | 40.8 | 8.3 ± 0.1 |

^aThe \bar{M}_n of the active ester polymer (PNAS) was determined by ¹H-NMR. ^bDSC measurements. ^cTurbidimetry measurements. ^dPhenol sulfuric acid assay. ^eNo sigmoidal curve, LCST could not be determined. ^fThe polymers are named by the sugar type and the functionalization degree in mol %.

the PSA-test. Size exclusion chromatography confirmed the shifts in \bar{M}_n with varying degrees of functionalization because of the higher molecular weight of the carbohydrates compared to isopropylamine. Also, the glass transition temperature (T_g) increased with a higher carbohydrate content (Supporting Information S8), in agreement with the literature.³³ The cloud point of the polymers, as determined by turbidimetry, increased at higher carbohydrate functionalization, in line with previous studies on carbohydrate-functionalized microgels.¹⁹ For **ManHPL97** and **ManHPL34**, no temperature responsive behavior could be observed owing to a high carbohydrate content.

3.2. Aggregation of ConA with Glycopolymers.

Turbidity measurements were conducted to test the temperature dependent binding of the glycopolymers to ConA. ConA exhibits a homotetrameric structure at neutral pH, with four Man-binding sites and a minimum spacing of 7.2 nm.³⁴ All studies were carried out in lectin-binding buffer (LBB) containing Mn²⁺ and Ca²⁺ to activate the ConA-binding sites.^{35–37} Since ConA exhibits four binding sites, it typically forms clusters with multivalent carbohydrates.^{28,38} The formation of such ConA–glycopolymer clusters can be studied using turbidimetry in real time, due to the increase of light scattering for increased cluster sizes.³⁹

The temperature-dependent cluster formation was tested under a heating/cooling rate of 1 °C min^{−1} between 20 and 44 °C. Without adding ConA, all polymers showed an increase in turbidity above the phase transition temperature as indicated by the cloud point. This can be attributed to the formation of polymer–polymer aggregates (Supporting Information S9a–h). All measurements in the absence of ConA reach the starting turbidity value after cooling back to 20 °C. However, when ConA is added to the measurement cell, the turbidity value does not return to the starting value upon cooling for all Man-bearing polymers (Figure 2). This hysteresis effect can be assigned to ConA–glycopolymer binding and the formation of clusters that dissolve only very slowly below the cloud point. Moreover, this hysteresis effect is stronger for the polymers bearing **ManEL**. This suggests that the more hydrophobic linker leads to slower cluster dissolution. For the non-carbohydrate-bearing polymers **PNIPAm** and **GalHPL3**, the hysteresis effect was not observed (Supporting Information S9). This indicates that the delayed cluster dissolution for Man-bearing polymers is because of the specific binding to ConA. In addition, when inhibiting ConA binding using an excess of MeMan, the hysteresis was significantly reduced confirming specific binding. When the cooling rate was

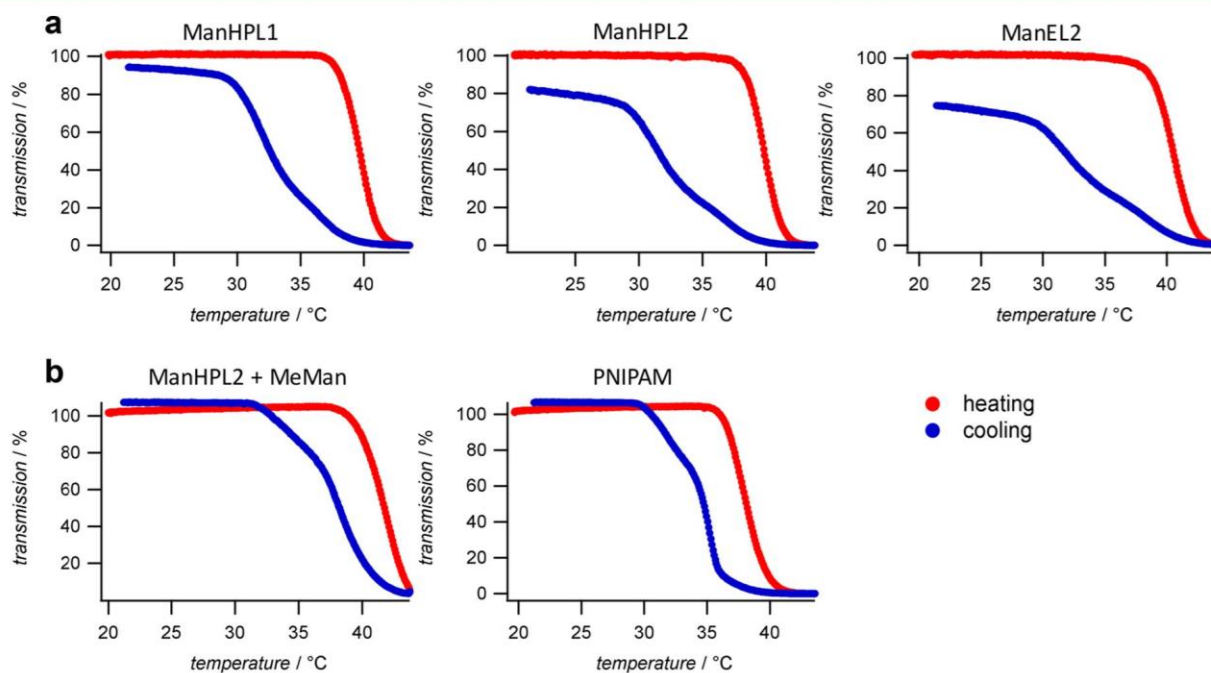


Figure 2. Turbidity under heating (solid red line) and cooling (solid blue line) at 1 °C min^{−1} of glycopolymers samples in the presence of 0.2 mg mL^{−1} of ConA. (a) Three different Man functionalized polymers are shown. **ManEL2** showed a stronger heating/cooling hysteresis compared to **ManHPL2** as indicated by the lower transmission value after cooling. (b) Negative control samples **PNIPAm** and **GalHPL3** showed a reduced hysteresis. The inhibitor MeMan also led to a reduced hysteresis upon cooling.

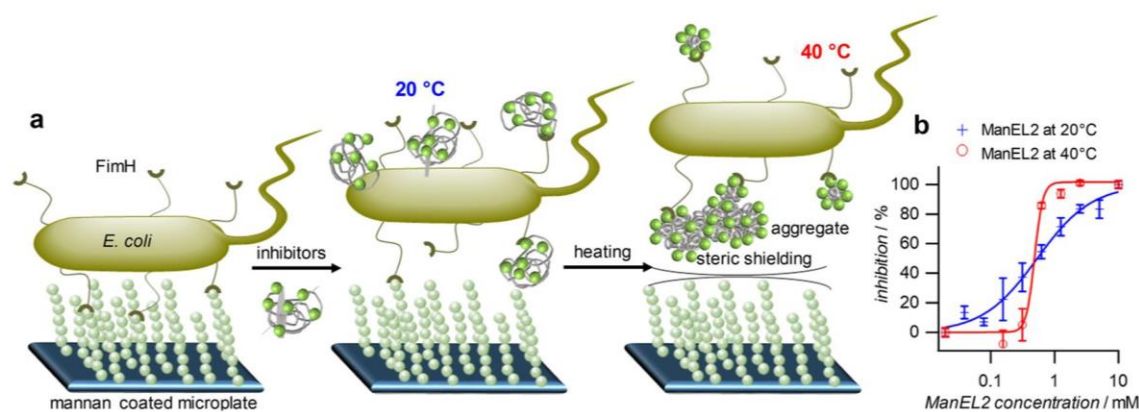


Figure 3. (a) Temperature-dependent inhibition assay of *E. coli* adhesion. GFP-tagged *E. coli* adhere to mannan-coated surfaces. After the addition of the thermoresponsive glycopolymers, the *E. coli* adhesion to the mannan-coated surface is hindered. The glycopolymers form aggregates and show an increased Man surface density above the cloud point. (b) A typical inhibition curve at 20 and 40 °C for **ManEL2**. The full set of inhibition curves is shown in Supporting Information S10.

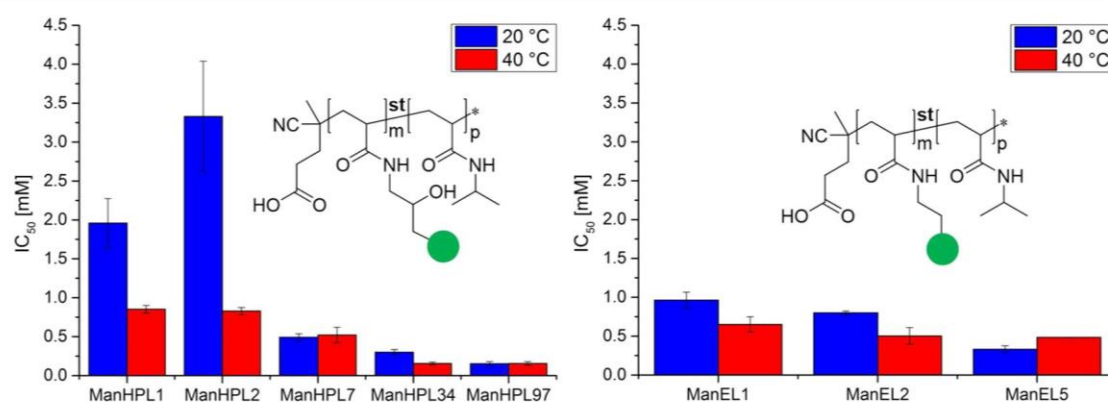


Figure 4. Left: IC_{50} values for the inhibition of *E. coli* adhesion with **ManHPL** glycopolymers at 20 °C (solid blue bars) and 40 °C (solid red bars). Right: IC_{50} values for **ManEL** glycopolymers. The IC_{50} values are related to the polymer concentration. All measurements were performed in triplicate, and averaged values and standard deviations are presented.

reduced to $0.1 \text{ } ^\circ\text{C min}^{-1}$, the starting turbidity value was reached indicating that glycoclusters with Man functionalization degrees up to 2% as tested are not stable below the phase transition temperature but their dissolution is merely delayed (Supporting Information S9k). Overall, these measurements confirm a statistical/additive effect on glycopolymer binding,³⁹ that is, an increased number of Man units leads to larger and more persistent clustering with ConA. Moreover, the linker chemistry affects the cluster dissolution, where the more hydrophilic linker in **ManHPL** leads to faster dissolution than the more hydrophobic linker in **ManEL**.

3.3. Temperature-Dependent Adhesion Inhibition of *E. coli*. The turbidity measurements confirmed the phase behavior of glycopolymers. To understand the phase transition effect on the glycopolymer affinity, a quantitative binding assay is required. Therefore, we carried out adhesion inhibition assays with *E. coli*. These bacteria have evolved hairy adhesive organelles, called pili or fimbriae, allowing the bacteria to adhere to cells via carbohydrate–lectin interactions and cause infections.⁴⁰ One of the best characterized adhesive organelles is the type 1 fimbriae, which comprises various protein subunits and the monovalent α -D-mannopyranoside-binding lectin FimH.^{41,42}

To evaluate the Man-specific adhesion of the GFP-tagged type 1-fimbriated pKL1162 strain, we used a mannan-coated microtiter plate, added the bacteria, incubated/washed with glycopolymers, and then quantified the number of adhered

bacteria using a fluorescent readout (Figure 3). In this manner, glycopolymers compete with the mannan-coated surface for binding to FimH. Therefore, by increasing the concentration of the Man-presenting glycopolymers, a larger inhibition of the bacterial adhesion was achieved as measured by a reduction of the fluorescence signal.²⁹ From the changes in fluorescence intensity as a function of glycopolymer concentration, the inhibitory concentration at half maximum intensity (IC_{50}) was determined. The IC_{50} value represents the concentration of glycopolymers, where 50% of the bacterial adhesion to the surface was inhibited. If the IC_{50} value is low, the inhibitory potency of the glycopolymers is high and vice versa.

At increased Man functionalization, a stronger adhesion inhibition took place (Figure 4). Furthermore, **GalHPL3** showed only a small inhibition effect due to the low affinity to FimH. Comparing **ManEL** and **ManHPL** with the same Man concentration, it can be seen that the IC_{50} values for **ManEL** are lower. This is likely due to a higher lectin-binding affinity of the hydrophobic linker, which was also observed by Lindhorst and co-workers.⁴³ For low Man functionalization degrees of less than 5%, an affinity increase is observed for both **ManEL** and **ManHPL** when heating to 40 °C, where **ManHPL** polymers show a stronger temperature response. At elevated Man content larger than 5%, the cloud point was above 40 °C for all polymers, indicating that coil-to-globule transition and glycopolymer aggregate formation did not take place.

Consequently, no clear temperature dependence on the IC_{50} was observed for these polymers.

A comparison of the Hill coefficients shows the degree of cooperative binding. Cooperative binding is observed when ligand/receptor complex formation between multivalent structures yields a higher binding energy as compared to the sum of energies from single ligand/receptor subunits.²⁷ A Hill coefficient below 1 represents negative cooperativity, and a value higher than 1 stands for a positive cooperativity effect. For all polymers incorporating less than 5 mol % Man, the Hill coefficient increases above the cloud point, which was below 40 °C for these polymers (Table 2). This could be attributed

Table 2. Hill Coefficients from the *E. coli* Adhesion Inhibition Curves

| sample | hill coefficient 20 °C | hill coefficient 40 °C |
|----------|------------------------|------------------------|
| ManHPL1 | 0.5 ± 0.2 | 3.1 ± 0.4 |
| ManHPL2 | 0.4 ± 0.5 | 2.7 ± 0.2 |
| ManHPL7 | 1.1 ± 0.1 | 2.3 ± 0.8 |
| ManHPL34 | 0.6 ± 0.2 | 0.3 ± 1.0 |
| ManHPL97 | 0.4 ± 0.2 | 0.1 ± 1.6 |
| ManEL1 | 1.4 ± 0.2 | 3.3 ± 1.1 |
| ManEL2 | 1.2 ± 0.4 | 4.0 ± 2.7 |
| ManEL5 | 0.1 ± 1.4 | 0.7 ± 0.1 |

to the formation of highly multivalent glycopolymer aggregates, which likely show an increased surface presentation of hydrophilic Man units as these polymers aggregate via hydrophobic polymer–polymer contacts. This results in increased sugar surface densities and explains the increased binding cooperativity and reduced IC_{50} values. Furthermore, the glycopolymer aggregates can block additional areas on the bacteria besides the Man-FimH binding sites, that is, steric shielding by these aggregates amplifies the inhibitory potential. The fraction of glycopolymers not incorporated into aggregates above the cloud point still attained a collapsed coil conformation since their LCST likely exceeded, thus showing improved affinity to FimH due to the increased carbohydrate surface density. For polymers with a larger Man functionalization degree (ManHPL7, ManHPL34, ManHPL97, and ManEL5), the Hill coefficients tend to decrease at elevated temperatures since their cloud point was not reached, that is, a complete coil-to-globule transition and aggregate formation did not take place.

These results overall showed that the coil-to-globule transition of glycopolymers followed by aggregate formation

and steric shielding increased the *E. coli* adhesion inhibition. In particular, polymers with low Man-functionalization degrees showed a large temperature response, most likely due to the high fraction of thermoresponsive repeating units. The inhibitory potential of polymers with hydrophobic linkers (ManEL) did not benefit significantly from the coil-to-globule transition since they exhibit strong inhibition in the coiled state below the LCST. In addition, owing to the linker hydrophobicity, the proposed effect of increased surface presentation of sugars on collapsed coils could be reduced compared to ManHPL.

3.4. Temperature-Dependent Adhesion Inhibition of ConA. We compared *E. coli* inhibition studies to inhibition studies employing ConA as carbohydrate-binding species (Figure 5). The microplates were again coated with mannan and the IC_{50} values were determined by incubating a glycopolymer concentration series in the presence of fluorescein-labeled ConA.

As observed in the *E. coli* assay, increasing the degree of Man functionalization reduced the IC_{50} values (Figure 6). However, the results from the inhibition assay with ConA show two striking differences compared to the *E. coli* assay. First, the majority of compounds now shows increasing IC_{50} values (weaker inhibition) when increasing the temperature above the cloud point. Second, changing the linker type does not affect the IC_{50} values significantly. Regarding the temperature dependence of the IC_{50} values, it should be noted that ConA offers four binding sites with a minimum spacing of 7.2 nm,^{28,34} whereas *E. coli*'s FimH receptor has only a single binding site and is positioned with a larger spacing on the bacteria.⁴⁴ Dynamic light scattering of the glycopolymers showed that their coil size was around 8 nm at 20 °C (Supporting Information S12). Therefore, the glycopolymers may bind to more than just one ConA binding site, whereas this is not possible when binding to FimH. At elevated temperatures where the polymer forms small globules, such multivalent binding to ConA is not possible leading to reduced affinity and increased IC_{50} values. In addition, an extended coil conformation at 20 °C may increase the accessibility of Man units for small receptors in solution phase (ConA), whereas a large fraction of Man units was rendered inaccessible due to aggregate formation above the cloud point temperature. The presence of microscopic aggregates thus effectively reduced the glycopolymer inhibitory potential for ConA but not for *E. coli* as the bacteria are also of microscopic size, that is, their inhibition benefits less from an excess of low-affinity glycopolymers in solution but more from similar-sized high-

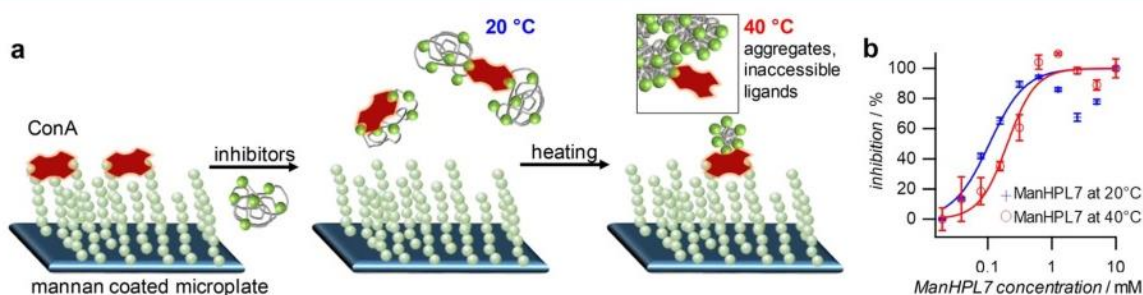


Figure 5. (a) Temperature-dependent inhibition of ConA binding. Below the phase transition temperature, the extended glycopolymer coil can bind to multiple ConA-binding sites resulting in low IC_{50} values, whereas this is not possible in the collapsed state where a large fraction of carbohydrate units is inaccessible due to aggregate formation. (b) A typical inhibition curve at 20 and 40 °C for ManHPL7. The full set of inhibition curves is shown in Supporting Information S11.

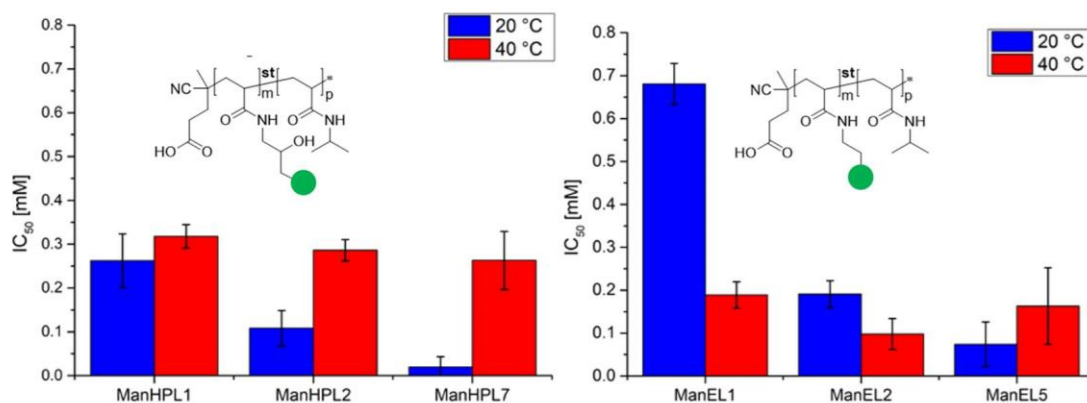


Figure 6. Left: IC_{50} values for the inhibition of ConA with ManHPL glycopolymers at 20 °C (solid blue bars) and 40 °C (solid red bars). Right: IC_{50} values for ManEL glycopolymers. All measurements were performed in triplicate.

affinity aggregates capable of additional steric shielding.²⁶ Therefore, the temperature-induced phase transition upon heating resulted in weaker inhibition of ConA but stronger inhibition of *E. coli*. Nevertheless, the proposed increase in affinity in a compact globule state at elevated temperatures due to an increased surface density of Man units should also be present in case of binding to ConA. Therefore, the thermoresponsive binding of the glycooligomers to ConA is mediated by adverse effects: (1) reduced multivalent binding and lower Man accessibility above the LCST and (2) increased binding due to increased surface density of Man in the globule state. These opposing contributions may explain the less obvious temperature trend for inhibiting ConA as compared to inhibiting *E. coli*. This is also reflected in the comparatively small changes of the Hill coefficients at 20 and 40 °C (Table 3).

Table 3. Hill Coefficients from the ConA Inhibition Curves

| sample | hill coefficient at 20 °C | hill coefficient at 40 °C |
|---------|---------------------------|---------------------------|
| ManHPL1 | 5.2 ± 1.4 | 1.8 ± 0.4 |
| ManHPL2 | 1.8 ± 0.4 | 3.4 ± 1.0 |
| ManHPL7 | 2.0 ± 0.7 | 2.6 ± 1.2 |
| ManEL1 | 1.7 ± 0.9 | 3.6 ± 0.8 |
| ManEL2 | 2.5 ± 0.1 | 2.7 ± 1.1 |
| ManEL5 | 3.4 ± 1.1 | 4.4 ± 0.8 |

The reduced influence of the linker on inhibiting ConA binding when compared to *E. coli* binding could be explained by structural differences of the binding sites. The ConA binding pocket mainly has hydrophobic amino acids favoring hydrophobic linkers but at the binding pocket's entrance hydrophilic amino acids such as asparagine residue are present.^{43,45} These residues may serve as hydrogen bond acceptors for the hydrophilic HPL linker or, alternatively, hydrogen bonding bridged by a hydration shell may increase binding to these residues.⁴⁶ In addition, such hydration layer-mediated hydrogen bonding is generally less favored at increased temperatures,⁴⁷ which reduces the inhibitory potential at elevated temperatures, as observed.

4. CONCLUSIONS

Taken together, the straightforward synthesis of a poly(active ester) followed by grafting of carbohydrates with varying linker hydrophobicity and isopropylamine to induce thermoresponsiveness was carried out. A set of polymers was synthesized

with carbohydrate functionalization degrees between 1 and 97% and tested using inhibition assays with ConA and type 1-fimbriated *E. coli* at 20 and 40 °C. For polymers with low functionalization degrees of 1 to 2% reaching the cloud point at around 40 °C, a large shift in affinity was observed. Importantly, the inhibition of *E. coli* was increased under cloud point conditions, whereas the inhibition of ConA had a tendency to decrease at elevated temperatures although the results are not fully consistent in the case of ConA binding. This confirms the contradicting observations by several groups studying the effect of temperature-induced coil-to-globule transition on glycopolymer-binding affinities. We propose that the enhanced inhibition of *E. coli* binding is driven by an enhanced presentation of carbohydrate units in the collapsed state where the glycopolymers form micrometer-sized high-affinity aggregates capable of steric shielding. ConA binding is reduced above the LCST because of reduced multivalent binding and reduced accessibility of the Man units compared to the extended coil state below the phase transition temperature. This suggests that small receptor targets such as single lectins in the solution phase are bound strongly by nonaggregated multivalent glycopolymers in the extended coil conformation, whereas the inhibition of large targets with surface-anchored receptors having access only to the exterior of polymer coils (bacteria and viruses) benefits from the increased surface density of ligands and steric shielding of polymer aggregates above the phase transition temperature. Overall, these results shed light on the conformation-dependent binding of glycopolymers and provide the blueprint for the design of switchable ligand-presenting polymers for biomedical applications.

■ ASSOCIATED CONTENT

Supporting Information

The Supporting Information is available free of charge at <https://pubs.acs.org/doi/10.1021/acs.biomac.0c00676>.

Chemical analysis, polymer characterization, IC_{50} curves, DLS measurements, turbidity traces, and details on instrumentation, buffers, and media (PDF)

■ AUTHOR INFORMATION

Corresponding Author

Stephan Schmidt – Institute of Organic and Macromolecular Chemistry, Heinrich-Heine-University Düsseldorf, Düsseldorf

40225, Germany; orcid.org/0000-0002-4357-304X;
Email: stephan.schmidt@hhu.de

Authors

Tanja J. Paul – Institute of Organic and Macromolecular Chemistry, Heinrich-Heine-University Düsseldorf, Dusseldorf 40225, Germany

Alexander K. Strzelczyk – Institute of Organic and Macromolecular Chemistry, Heinrich-Heine-University Düsseldorf, Dusseldorf 40225, Germany

Melina I. Feldhof – Institute of Organic and Macromolecular Chemistry, Heinrich-Heine-University Düsseldorf, Dusseldorf 40225, Germany

Complete contact information is available at:

<https://pubs.acs.org/10.1021/acs.biomac.0c00676>

Author Contributions

#T.J.P. and A.K.S. contributed equally to this paper.

Notes

The authors declare no competing financial interest.

ACKNOWLEDGMENTS

The authors thank Maria Breuer for performing the NMR measurements and Stephanie Scheelen for performing the SEC measurements. The authors acknowledge funding from the German Research foundation (DFG) in the project SCHM 2748/5-1.

REFERENCES

- (1) Reitsma, S.; Slaaf, D. W.; Vink, H.; van Zandvoort, M. A.; oude Egbrink, M. G. A. The endothelial glycocalyx: composition, functions, and visualization. *Pflugers Arch.* **2007**, *454*, 345–359.
- (2) Schmidt, S.; Paul, T. J.; Strzelczyk, A. K. Interactive Polymer Gels as Biomimetic Sensors for Carbohydrate Interactions and Capture–Release Devices for Pathogens. *Macromol. Chem. Phys.* **2019**, *220*, 1900323.
- (3) Jacobi, F.; Camaleno de la Calle, A.; Boden, S.; Grafmuller, A.; Hartmann, L.; Schmidt, S. Multivalent Binding of Precision Glycooligomers on Soft Glycocalyx Mimicking Hydrogels. *Biomacromolecules* **2018**, *19*, 3479–3488.
- (4) Ofek, I.; Hasty, D. L.; Sharon, N. Anti-adhesion therapy of bacterial diseases: prospects and problems. *FEMS. Immunol. Med. Microbiol.* **2003**, *38*, 181–191.
- (5) Kiessling, L. L.; Grim, J. C. Glycopolymer probes of signal transduction. *Chem. Soc. Rev.* **2013**, *42*, 4476–4491.
- (6) Hudak, J. E.; Bertozzi, C. R. Glycotherapy: new advances inspire a reemergence of glycans in medicine. *Chem. Biol.* **2014**, *21*, 16–37.
- (7) Steinhilber, D.; Seiffert, S.; Heyman, J. A.; Paulus, F.; Weitz, D. A.; Haag, R. Hyperbranched polyglycerols on the nanometer and micrometer scale. *Biomaterials* **2011**, *32*, 1311–1316.
- (8) Papp, I.; Sieben, C.; Ludwig, K.; Roskamp, M.; Bottcher, C.; Schlecht, S.; Herrmann, A.; Haag, R. Inhibition of influenza virus infection by multivalent sialic-acid-functionalized gold nanoparticles. *Small* **2010**, *6*, 2900–2906.
- (9) Li, M. H.; Choi, S. K.; Leroueil, P. R.; Baker, J. R., Jr. Evaluating binding avidities of populations of heterogeneous multivalent ligand-functionalized nanoparticles. *ACS Nano* **2014**, *8*, S600–S609.
- (10) Bernardi, A.; Jimenez-Barbero, J.; Casnati, A.; De Castro, C.; Darbre, T.; Fieschi, F.; Finne, J.; Funken, H.; Jaeger, K. E.; Lahmann, M.; Lindhorst, T. K.; Marradi, M.; Messner, P.; Molinaro, A.; Murphy, P. V.; Nativi, C.; Oscarson, S.; Penades, S.; Peri, F.; Pieters, R. J.; Renaudet, O.; Reymond, J. L.; Richichi, B.; Rojo, J.; Sansone, F.; Schaffer, C.; Turnbull, W. B.; Velasco-Torrijos, T.; Vidal, S.; Vincent, S.; Wennekes, T.; Zuilhof, H.; Imberty, A. Multivalent glycoconjugates as anti-pathogenic agents. *Chem. Soc. Rev.* **2013**, *42*, 4709–4727.
- (11) Bhatia, S.; Camacho, L. C.; Haag, R. Pathogen Inhibition by Multivalent Ligand Architectures. *J. Am. Chem. Soc.* **2016**, *138*, 8654–8666.
- (12) Muller, C.; Despras, G.; Lindhorst, T. K. Organizing multivalency in carbohydrate recognition. *Chem. Soc. Rev.* **2016**, *45*, 3275–3302.
- (13) Stuart, M. A.; Huck, W. T.; Genzer, J.; Muller, M.; Ober, C.; Stamm, M.; Sukhorukov, G. B.; Szleifer, I.; Tsukruk, V. V.; Urban, M.; Winnik, F.; Zauscher, S.; Luzinov, I.; Minko, S. Emerging applications of stimuli-responsive polymer materials. *Nat. Mater.* **2010**, *9*, 101–113.
- (14) Pasparakis, G.; Cockayne, A.; Alexander, C. Control of bacterial aggregation by thermoresponsive glycopolymers. *J. Am. Chem. Soc.* **2007**, *129*, 11014–11015.
- (15) Mahon, C. S.; Wildsmith, G. C.; Haksar, D.; de Poel, E.; Beekman, J. M.; Pieters, R. J.; Webb, M. E.; Turnbull, W. B. A 'catch-and-release' receptor for the cholera toxin. *Faraday Discuss.* **2019**, *219*, 112–127.
- (16) Dalier, F.; Eghiaian, F.; Scheuring, S.; Marie, E.; Tribet, C. Temperature-Switchable Control of Ligand Display on Adlayers of Mixed Poly(lysine)-g-(PEO) and Poly(lysine)-g-(ligand-modified poly-N-isopropylacrylamide). *Biomacromolecules* **2016**, *17*, 1727–1736.
- (17) Tang, J. S. J.; Rosencrantz, S.; Tepper, L.; Chea, S.; Klopzig, S.; Kruger-Genge, A.; Storsberg, J.; Rosencrantz, R. R. Functional Glyco-Nanogels for Multivalent Interaction with Lectins. *Molecules* **2019**, *24*, 22.
- (18) Siirila, J.; Hietala, S.; Ekholm, F. S.; Tenhu, H. Glucose and Maltose Surface-Functionalized Thermoresponsive Poly(N-Vinyl-caprolactam) Nanogels. *Biomacromolecules* **2020**, *21*, 955–965.
- (19) Paul, T. J.; Rubel, S.; Hildebrandt, M.; Strzelczyk, A. K.; Spormann, C.; Lindhorst, T. K.; Schmidt, S. Thermosensitive Display of Carbohydrate Ligands on Microgels for Switchable Binding of Proteins and Bacteria. *ACS Appl. Mater. Interfaces* **2019**, *11*, 26674–26683.
- (20) Vasani, R. B.; Janardanan, N.; Prieto-Simon, B.; Cifuentes-Rius, A.; Bradley, S. J.; Moore, E.; Kraus, T.; Voelcker, N. H. Microwave Heating of Poly(N-isopropylacrylamide)-Conjugated Gold Nanoparticles for Temperature-Controlled Display of Concanavalin A. *ACS Appl. Mater. Interfaces* **2015**, *7*, 27755–27764.
- (21) Wang, Y.; Kotsuchibashi, Y.; Liu, Y.; Narain, R. Study of bacterial adhesion on biomimetic temperature responsive glycopolymer surfaces. *ACS Appl. Mater. Interfaces* **2015**, *7*, 1652–1661.
- (22) Won, S.; Hindmarsh, S.; Gibson, M. I. Triggerable Multivalent Glyconanoparticles for Probing Carbohydrate-Carbohydrate Interactions. *ACS Macro. Lett.* **2018**, *7*, 178–183.
- (23) Won, S.; Richards, S. J.; Walker, M.; Gibson, M. I. Externally controllable glycan presentation on nanoparticle surfaces to modulate lectin recognition. *Nanoscale Horiz.* **2017**, *2*, 106–109.
- (24) Hoshino, Y.; Nakamoto, M.; Miura, Y. Control of protein-binding kinetics on synthetic polymer nanoparticles by tuning flexibility and inducing conformation changes of polymer chains. *J. Am. Chem. Soc.* **2012**, *134*, 15209–15212.
- (25) Tang, J. S. J.; Rosencrantz, S.; Tepper, L.; Chea, S.; Klöpzig, S.; Krüger-Genge, A.; Storsberg, J.; Rosencrantz, R. R. Functional Glyco-Nanogels for Multivalent Interaction with Lectins. *Molecules* **2019**, *24*, 1865.
- (26) Vonnemann, J.; Liese, S.; Kuehne, C.; Ludwig, K.; Dervede, J.; Bottcher, C.; Netz, R. R.; Haag, R. Size dependence of steric shielding and multivalency effects for globular binding inhibitors. *J. Am. Chem. Soc.* **2015**, *137*, 2572–2579.
- (27) Mammen, M.; Choi, S. K.; Whitesides, G. M. Polyvalent interactions in biological systems: Implications for design and use of multivalent ligands and inhibitors. *Angew. Chem. Int. Ed.* **1998**, *37*, 2755–2794.
- (28) Wittmann, V. Structural investigation of multivalent carbohydrate-protein interactions using synthetic biomolecules. *Curr. Opin. Chem. Biol.* **2013**, *17*, 982–989.

- (29) Hartmann, M.; Horst, A. K.; Klemm, P.; Lindhorst, T. K. A kit for the investigation of live *Escherichia coli* cell adhesion to glycosylated surfaces. *Chem. Commun.* **2010**, *46*, 330–332.
- (30) Gerchakov, S. M.; Hatcher, P. G. Improved Technique for Analysis of Carbohydrates in Sediments. *Limnol. Oceanogr. Lett.* **1972**, *17*, 938–943.
- (31) DuBois, M.; Gilles, K. A.; Hamilton, J. K.; Rebers, P. A.; Smith, F. Colorimetric Method for Determination of Sugars and Related Substances. *Anal. Chem.* **1956**, *28*, 350–356.
- (32) Boden, S.; Wagner, K. G.; Karg, M.; Hartmann, L. Presenting Precision Glycomacromolecules on Gold Nanoparticles for Increased Lectin Binding. *Polymer* **2017**, *9*, 716.
- (33) Bordegé, V.; Muñoz-Bonilla, A.; León, O.; Sánchez-Chaves, M.; Cuervo-Rodríguez, R.; Fernández-García, M. Glycopolymers with glucosamine pendant groups: Copolymerization, physico-chemical and interaction properties. *React. Funct. Polym.* **2011**, *71*, 1–10.
- (34) Wittmann, V.; Pieters, R. J. Bridging lectin binding sites by multivalent carbohydrates. *Chem. Soc. Rev.* **2013**, *42*, 4492–4503.
- (35) Becker, J. W.; Reeke, G. N., Jr.; Cunningham, B. A.; Edelman, G. M. New evidence on the location of the saccharide-binding site of concanavalin A. *Nature* **1976**, *259*, 406–409.
- (36) Bryce, R. A.; Hillier, I. H.; Naismith, J. H. Carbohydrate-protein recognition: molecular dynamics simulations and free energy analysis of oligosaccharide binding to concanavalin A. *Biophys. J.* **2001**, *81*, 1373–1388.
- (37) Dam, T. K.; Brewer, C. F. Thermodynamic studies of lectin-carbohydrate interactions by isothermal titration calorimetry. *Chem. Rev.* **2002**, *102*, 387–430.
- (38) Lundquist, J. J.; Toone, E. J. The cluster glycoside effect. *Chem. Rev.* **2002**, *102*, 555–578.
- (39) Gestwicki, J. E.; Cairo, C. W.; Strong, L. E.; Oetjen, K. A.; Kiessling, L. L. Influencing receptor-ligand binding mechanisms with multivalent ligand architecture. *J. Am. Chem. Soc.* **2002**, *124*, 14922–14933.
- (40) Sperling, O.; Fuchs, A.; Lindhorst, T. K. Evaluation of the carbohydrate recognition domain of the bacterial adhesin FimH: Design, synthesis and binding properties of mannoside ligands. *Org. Biomol. Chem.* **2006**, *4*, 3913–3922.
- (41) Knight, S. D.; Bouckaert, J. Structure, function, and assembly of type 1 fimbriae. *Topics Curr. Chem.* **2009**, *288*, 67–107.
- (42) Cecioni, S.; Imbert, A.; Vidal, S. Glycomimetics versus multivalent glycoconjugates for the design of high affinity lectin ligands. *Chem. Rev.* **2015**, *115*, 525–561.
- (43) Igde, S.; Roblitz, S.; Müller, A.; Kolbe, K.; Boden, S.; Fessele, C.; Lindhorst, T. K.; Weber, M.; Hartmann, L. Linear Precision Glycomacromolecules with Varying Interligand Spacing and Linker Functionalities Binding to Concanavalin A and the Bacterial Lectin FimH. *Macromol. Biosci.* **2017**, *17*, 1700198.
- (44) Mortezaei, N.; Singh, B.; Zakrisson, J.; Bullitt, E.; Andersson, M. Biomechanical and structural features of CS2 fimbriae of enterotoxigenic *Escherichia coli*. *Biophys. J.* **2015**, *109*, 49–56.
- (45) Sanders, D. A.; Moothoo, D. N.; Raftery, J.; Howard, A. J.; Helliwell, J. R.; Naismith, J. H. The 1.2 Å resolution structure of the Con A-dimannose complex. *J. Mol. Biol.* **2001**, *310*, 875–884.
- (46) Loris, R.; Stas, P. P.; Wyns, L. Conserved waters in legume lectin crystal structures. The importance of bound water for the sequence-structure relationship within the legume lectin family. *J. Biol. Chem.* **1994**, *269*, 26722–26733.
- (47) Lemieux, R. U. How Water Provides the Impetus for Molecular Recognition in Aqueous Solution. *Acc. Chem. Res.* **1996**, *29*, 373–380.

Supporting Information

Temperature switchable glycopolymers and their conformation-dependent binding to receptor targets

Tanja J. Paul[†], Alexander K. Strzelczyk[†], Melina I. Feldhof, and Stephan Schmidt^{*}

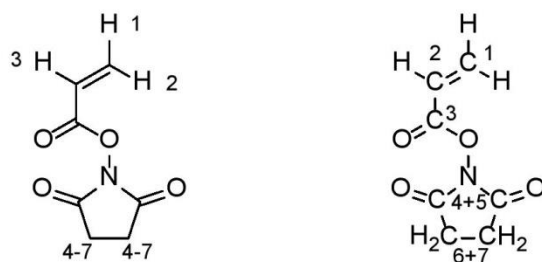
[†]Institute of Organic and Macromolecular Chemistry, Heinrich-Heine-University Düsseldorf, Universitätsstraße 1, 40225 Dusseldorf, Germany,

Email: Stephan Schmidt – stephan.schmidt@hhu.de

Contents

| | |
|--|----|
| S1 Synthesis of <i>N</i> -acryloxysuccinimide..... | 2 |
| S2 Synthesis of polymer precursor poly (<i>N</i> -acryloxysuccinimide) | 3 |
| S3 Synthesis of carbohydrate ligands with different linkers..... | 4 |
| S4 Synthesis of Poly(<i>N</i> -isopropylacrylamide-co- <i>N</i> -(2-hydroxypropyl) α -D-mannopyranoside acrylamide) and Poly(<i>N</i> -isopropylacrylamide-co- <i>N</i> -ethyl α -D-mannopyranoside acrylamide)..... | 13 |
| S5 Size exclusion chromatography | 25 |
| S6 Phenol sulfuric acid method (PSA)..... | 27 |
| S7 ATR-FTIR Spectroscopy | 27 |
| S8 Differential scanning calorimetry (DSC)..... | 30 |
| S9 Turbidimetry studies | 32 |
| S10 Temperature dependent adhesion inhibition of <i>E. coli</i> | 37 |
| S11 Temperature dependent adhesion inhibition of ConA | 41 |
| S12 Dynamic light scattering of the glycopolymers | 44 |
| S13 Instrumentation | 44 |
| S14 Buffer and Media | 46 |

S1 Synthesis of *N*-acryloxysuccinimide



Scheme S1: Structure of monomer *N*-acryloxysuccinimide with numbering of protons (left) and carbons (right).

$^1\text{H-NMR}$ (600 MHz, CDCl_3) δ 6.74 - 6.67 (dd, $^3J_{\text{HH}} = 17.4, 0.8$ Hz, 1H, *H1*), δ 6.38 - 6.27 (dd, $^3J_{\text{HH}} = 16.6, 10.3$ Hz, 1H, *H2*), δ 6.20 - 6.14 (dd, $^3J_{\text{HH}} = 10.7, 0.8$ Hz, 1H, *H3*), δ 2.89 - 2.81 (s, 4H, *H4-7*).

$^{13}\text{C-NMR}$ (600 MHz, CDCl_3) δ 169,17 ($\text{C}_{\text{quart.}}$, 1C, *C3*), δ 161,18 ppm ($\text{C}_{\text{quart.}}$, 2C, *C4+5*), δ 136,33 (CH_2 , 1C, *C1*), δ 123,08 (CH , 1C, *C2*), δ 25,75 (CH_2 , 2C, *C6+7*).

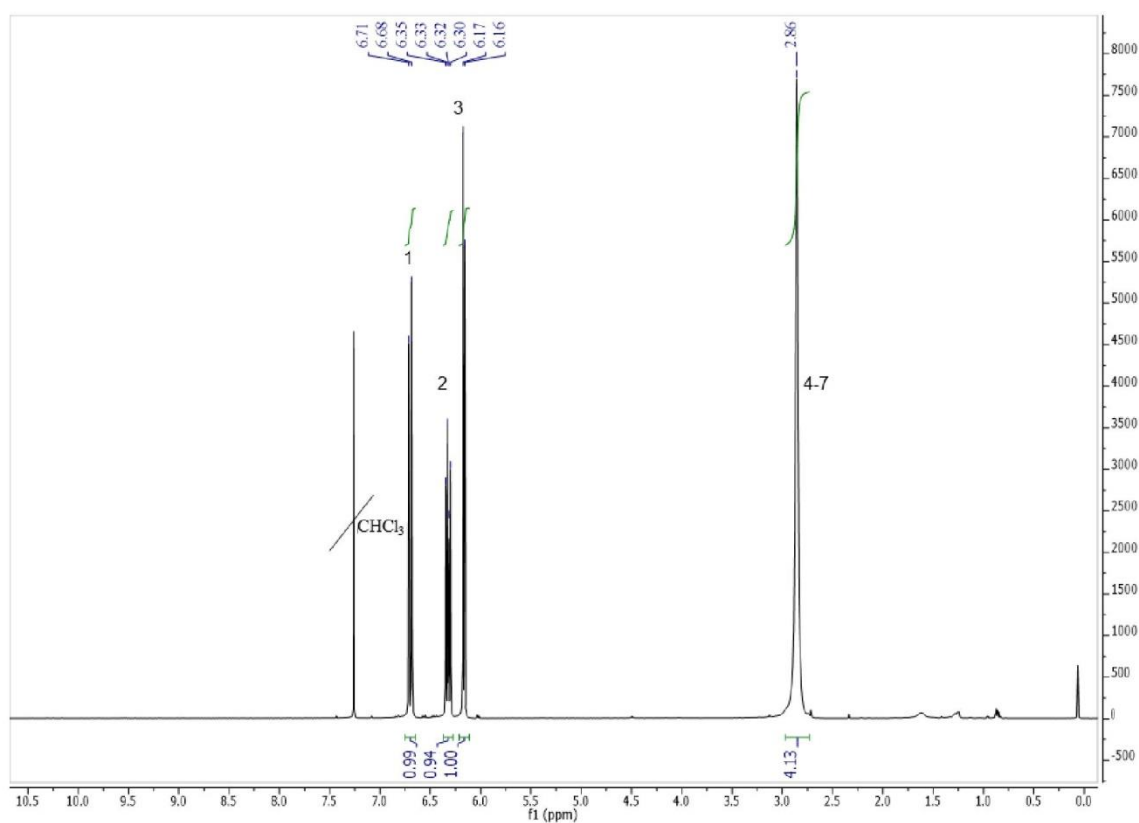


Figure S1a: $^1\text{H-NMR}$ (600 MHz, CDCl_3) of NAS.

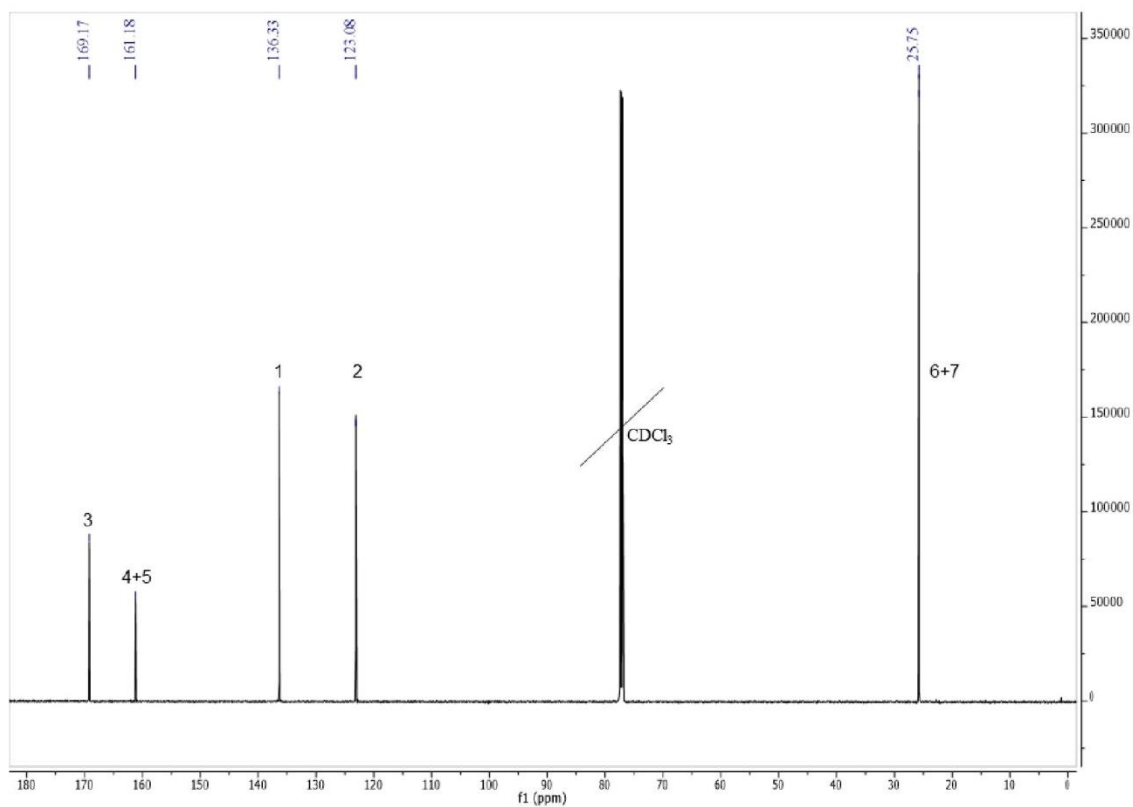
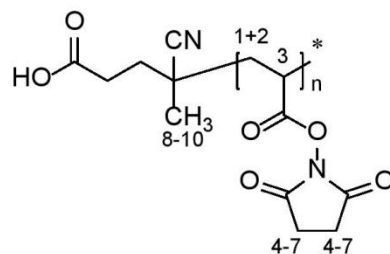


Figure S1b: ^{13}C -NMR (600 MHz, CDCl_3) of NAS.

S2 Synthesis of polymer precursor poly (*N*-acryloxysuccinimide)



Scheme S2: Structure of polymer precursor poly (*N*-acryloxysuccinimide).

^1H -NMR (600 MHz, CDCl_3) δ 3.28 - 3.00 (s, 90H, *H*3), δ 2.85 - 2.74 (s, 360H, *H*4-7), δ 2.25 - 1.90 (s, 180H, *H*1+2) δ 1.40 - 1.33 (s, 3H, *H*8-10).

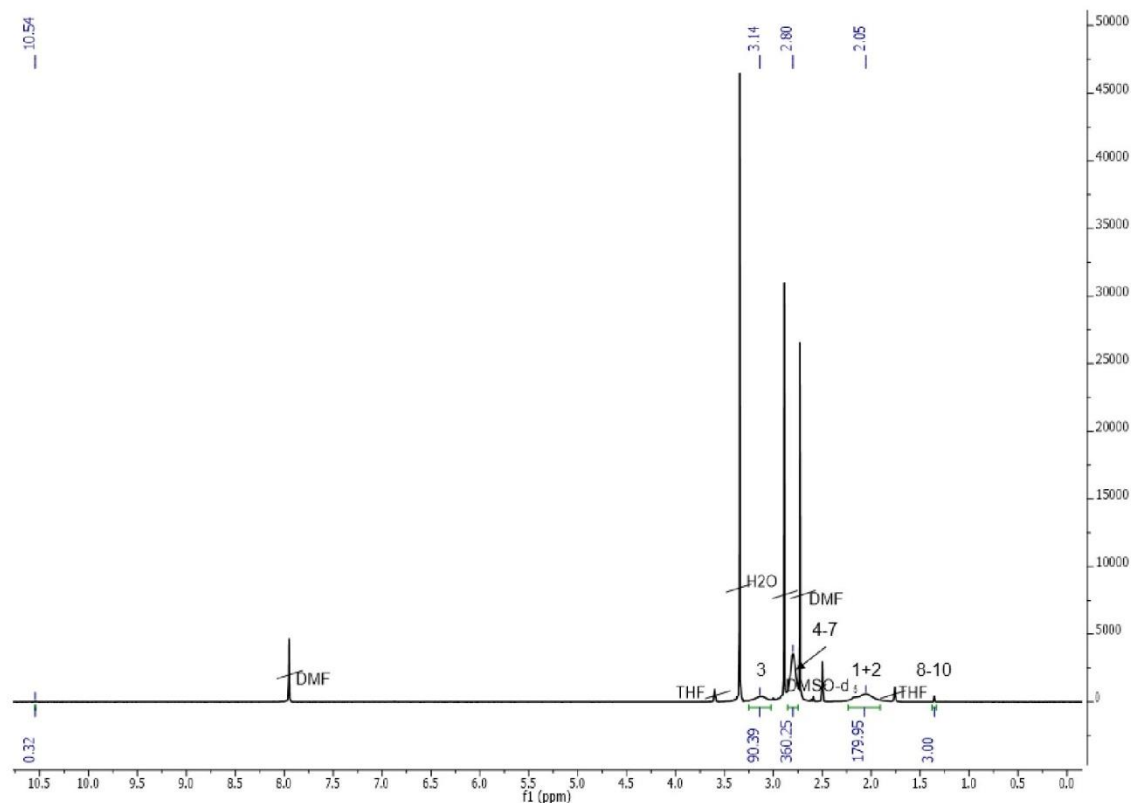
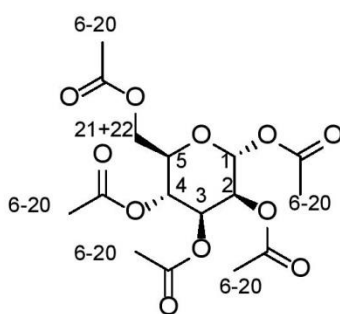


Figure S2: $^1\text{H-NMR}$ (600 MHz, CDCl_3) of PNAS.

S3 Synthesis of carbohydrate ligands with different linkers

Synthesis of 3-amino-2-hydroxypropyl-linker functionalized ligands

Synthesis of 1,2,3,4,6-penta-*O*-acetyl- α -D-mannopyranoside



Scheme S3a: Structure of 1,2,3,4,6-penta-*O*-acetyl- α -D-mannopyranoside.

α -D-mannose (30.0 g, 166.6 mmol) was dissolved in 500 mL acetonitrile at 0 °C. Then *p*-toluenesulfonic acid (3.18 g, 18.5 mmol) was added and the solution was flushed with nitrogen for 20 min and over the next 20 min acetic anhydride (100 mL, 1.1 mole) was added and the solution was stirred at room temperature for 48 h. Afterwards the solvent was removed and the residue was dissolved in 600 mL ethyl acetate and washed with saturated sodium

bicarbonate solution, water and dried over magnesium sulfate. Solvent was removed under reduced pressure and the product was dried under vacuum (yield: 64.2 g, 99%).

$^1\text{H-NMR}$ (600 MHz, CDCl_3) δ 6.11 - 5.83 (dd, $^3J_{\text{HH}} = 67.2, 1.8$ Hz 1H, *H1*), δ 5.50 - 5.09 (m, 3H, *H2-4*), δ 4.34 - 4.24 (m, 1H, *H5*), δ 4.18 - 3.75 (m, 2H, *H21+22*), δ 2.23 - 2.20 (s, 3H, *H6-20*), δ 2.18 - 2.15 (d, $^3J_{\text{HH}} = 2.4$ Hz, 3H, *H6-20*), δ 2.09 - 2.07 (s, 3H, *H6-20*), δ 2.06 - 2.02 (s, 3H, *H6-20*), δ 2.02 - 1.96 (s, 3H, *H6-20*).

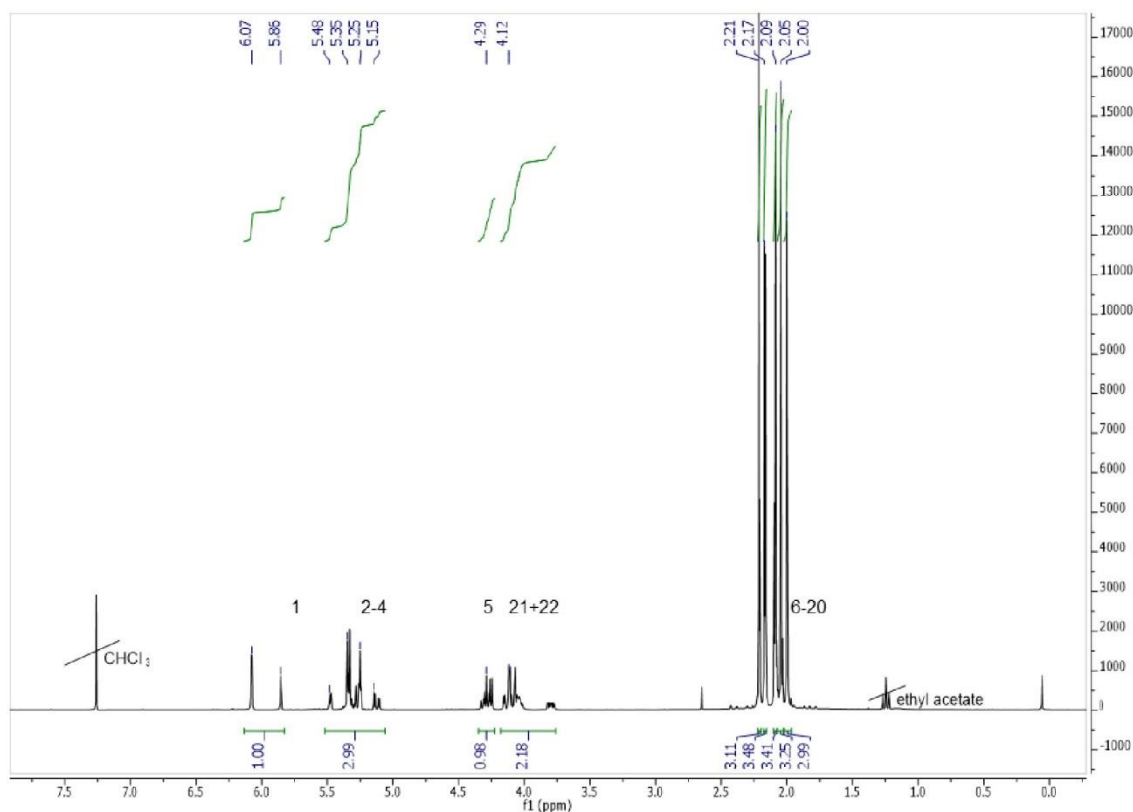


Figure S3a: $^1\text{H-NMR}$ (600 MHz, CDCl_3) 1,2,3,4,6-penta-*O*-acetyl- α -D-mannopyranoside.

Synthesis of allyl-2,3,4,6-tetra-*O*-acetyl- α -D-mannopyranoside and allyl-2,3,4,6-tetra-*O*-acetyl- β -D-galactopyranoside



Scheme S3b: Structures of allyl-2,3,4,6-tetra-*O*-acetyl- α -D-mannopyranoside (left) and allyl-2,3,4,6-tetra-*O*-acetyl- β -D-galactopyranoside (right).

The synthesis was done according to literature.¹ The protected sugar (25.5 g, 65.4 mmol) was dissolved in 410 mL dichloromethane before allyl alcohol (25 mL, 360.9 mmol) was added. After 30 min of flushing with nitrogen at 0 °C boron trifluoride diethyl etherate (250 mL, 1.97 mol) was added dropwise over 15 min and the solution was then stirred for 72 h at room temperature. Afterwards the solution was poured into 1000 mL of ice water. The organic phase was washed with saturated sodium bicarbonate, water and dried over magnesium sulfate. Solvent was removed and product was purified via column chromatography using n-hexane:ethyl acetate (1:1) (yield mannose: 15.99 g, 63%; galactose 17.75 g, 69%).

¹H-NMR allyl-2,3,4,6-tetra-*O*-acetyl- α -D-mannopyranoside: (600 MHz, CDCl₃) δ 5.93 - 5.86 (tdd, ³*J*_{HH} = 11.3, 5.3, 0.9 Hz, 1H, *H*8), δ 5.38 - 5.35 (dd, ³*J*_{HH} = 10.0, 3.5 Hz, 1H, *H*4), δ 5.33 - 5.26 (m, 2H, *H*9+10), δ 5.26 - 5.22 (m, 2H, *H*2+3), δ 4.88 - 4.85 (d, ³*J*_{HH} = 1.7 Hz, 1H, *H*1), δ 4.30 - 4.26 (dd, ³*J*_{HH} = 12.1, 5.3 Hz, 1H, *H*23+24), δ 4.21 - 4.16 (ddt, ³*J*_{HH} = 12.8, 5.3, 1.4 Hz, 1H, *H*5), δ 4.12 - 4.08 (dd, ³*J*_{HH} = 12.3, 2.4 Hz, 1H, *H*23+24), δ 4.05 - 3.99 (m, 2H, *H*6+7), δ 2.17 - 2.14 (s, 3H, *H*11-22), δ 2.12 - 2.09 (s, 3H, *H*11-22), δ 2.05 - 2.03 (s, 3H, *H*11-22), δ 2.00 - 1.97 (s, 3H, *H*11-22).

¹H-NMR allyl-2,3,4,6-tetra-*O*-acetyl- β -D-galactopyranoside (600 MHz, CDCl₃) δ 5.90 - 5.80 (td, ³*J*_{HH} = 11.3, 4.9 Hz, 1H, *H*8), δ 5.48 - 5.40 (dd, ³*J*_{HH} = 3.7, 1.0 Hz, 1H, *H*1), δ 5.39 - 5.32 (m, 1H, *H*3), δ 5.31 - 5.25 (dd, ³*J*_{HH} = 17.2, 1.4 Hz, 1H, *H*2), δ 5.22 - 5.18 (dd, ³*J*_{HH} = 10.4, 1.1 Hz, 1H, *H*5), δ 5.15 - 4.97 (m, 2H, *H*9+10), δ 4.25 - 4.19 (t, ³*J*_{HH} = 6.4 Hz, 1H, *H*4), δ 4.19 - 4.13 (dd, ³*J*_{HH} = 13.0, 5.1 Hz, 1H, *H*23+24), δ 4.13 - 4.03 (m, 2H, *H*6+7), δ 4.03 - 3.96 (dd, ³*J*_{HH} = 13.1, 6.1 Hz, 1H, *H*23+24), δ 2.14 - 2.11 (s, 3H, *H*11-22), δ 2.08 - 2.04 (s, 3H, *H*11-22), δ 2.04 - 2.01 (s, 3H, *H*11-22), δ 1.97 - 1.94 (s, 3H, *H*11-22).

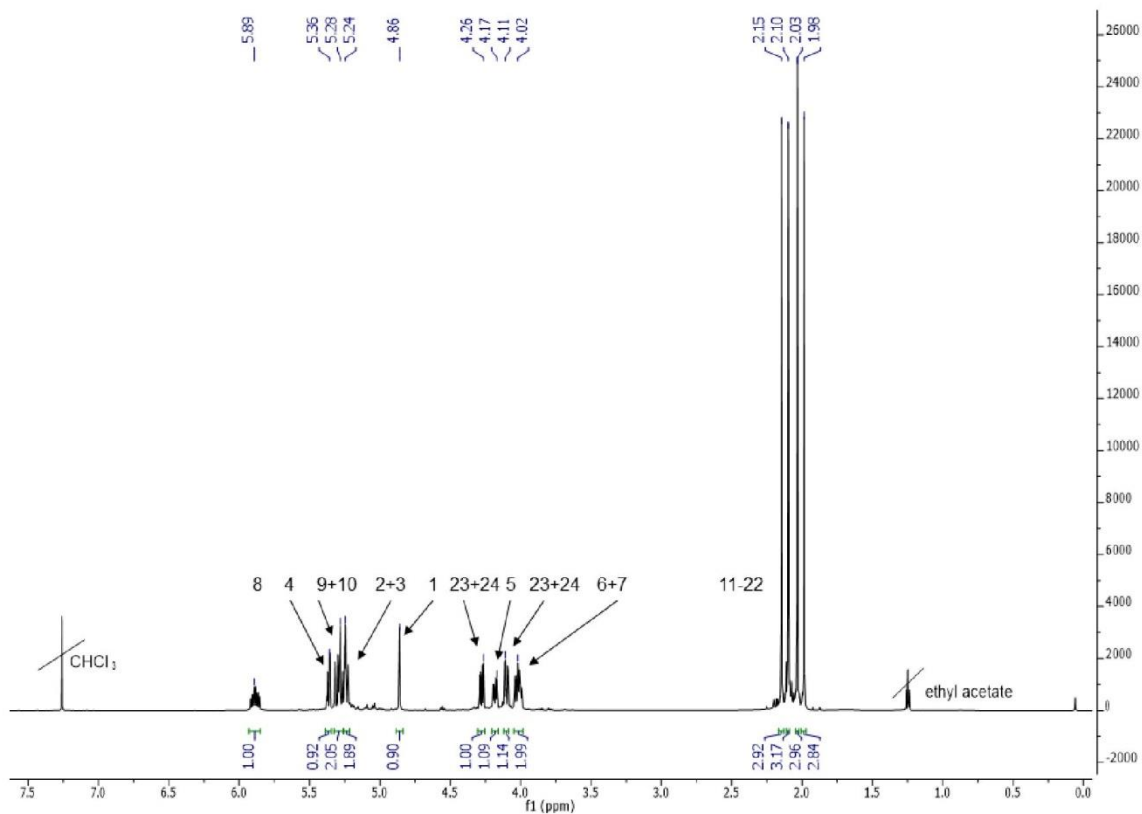


Figure S3b: $^1\text{H-NMR}$ (600 MHz, CDCl_3) allyl-2,3,4,6-tetra-*O*-acetyl- α -D-mannopyranoside.

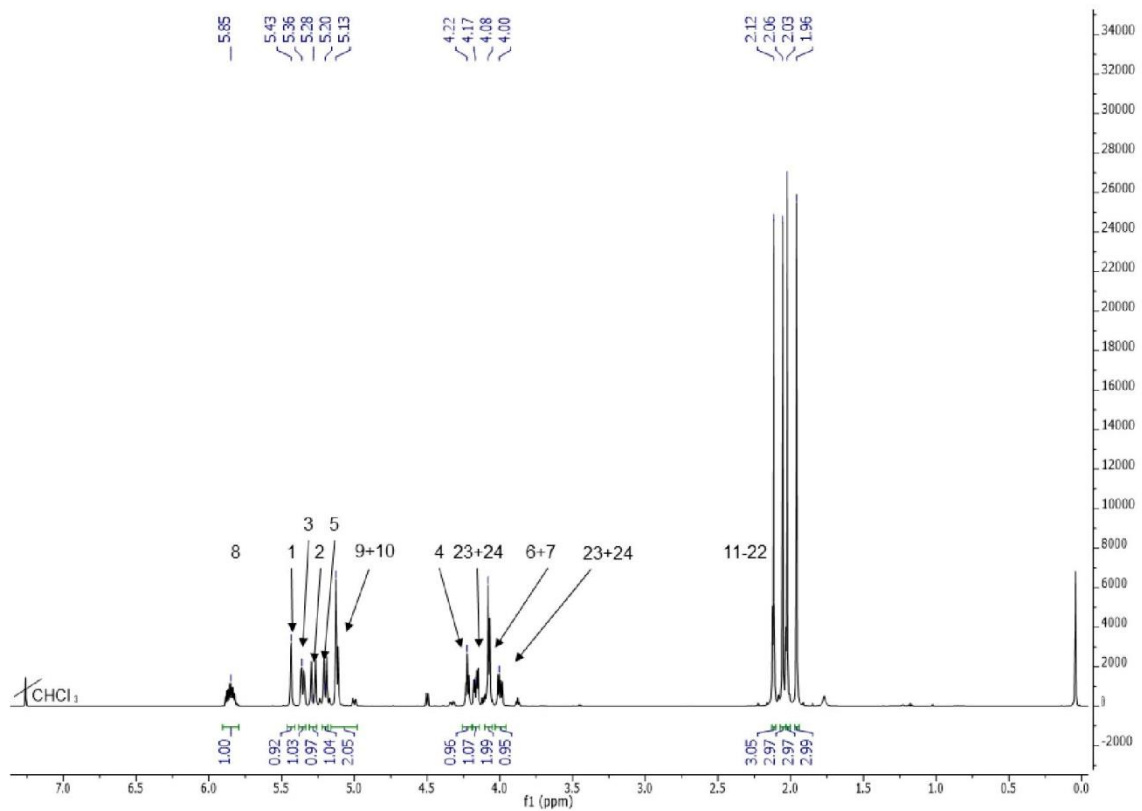
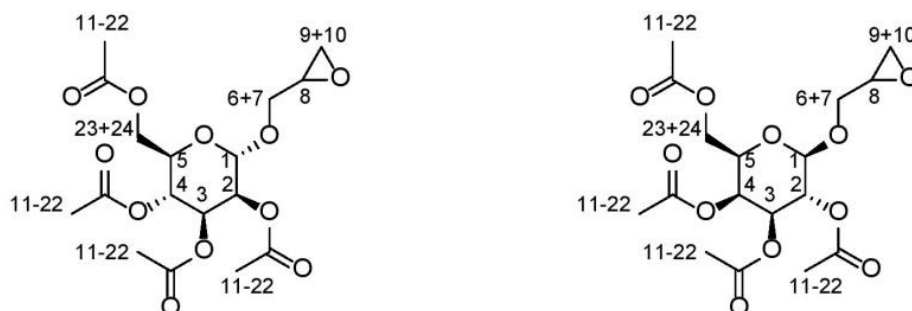


Figure S3c: $^1\text{H-NMR}$ (600 MHz, CDCl_3) allyl-2,3,4,6-tetra-*O*-acetyl- α -D-galactopyranoside.

Synthesis of 2',3'-epoxypropyl-2,3,4,6-tetra-*O*-acetyl- α -D-mannopyranoside and 2',3'-epoxypropyl-2,3,4,6-tetra-*O*-acetyl- β -D-galactopyranoside



Scheme S3c: Structures of 2',3'-epoxypropyl-2,3,4,6-tetra-*O*-acetyl- α -D-mannopyranoside (left) and 2',3'-epoxypropyl-2,3,4,6-tetra-*O*-acetyl- β -D-galactopyranoside (right).

The allyl-functionalized sugar (15.5 g, 40 mmol) was dissolved in 300 mL dichloromethane and flushed with nitrogen. Then *m*-chloroperoxybenzoic acid (14 g, 81.2 mmol) was added and the solution was stirred for 48 h. After that additional *m*-chloroperoxybenzoic acid (4.24 g, 24.2 mmol) was added and stirred for another 24 h. After that 20 ml of dichloromethane was added and washed with saturated sodium bicarbonate before dried with sodium sulfate. Solvent was removed under reduced pressure and product was purified via column chromatography using n-hexane:ethyl acetate (3:2) (yield mannose: 10.1 g, 63%; galactose: 9.86 g, 61%).

$^1\text{H-NMR}$ 2',3'-epoxypropyl-2,3,4,6-tetra-*O*-acetyl- α -D-mannopyranoside (600 MHz, CDCl_3) δ 5.39 - 5.33 (m, 1H, *H*4), δ 5.32 - 5.26 (m, 2H, *H*2+3), δ 4.93 - 4.84 (dd, $^3J_{\text{HH}} = 34.3$, 1.6 Hz, 1H, *H*1), δ 4.30 - 4.26 (m, 1H, *H*5), δ 4.14 - 4.10 (m, 1H, *H*23+24), δ 4.07 - 4.02 (m, 1H, *H*23+24), δ 3.92 - 3.79 (ddd, $^3J_{\text{HH}} = 57.3$, 11.9, 3.0 Hz, 1H, *H*6+7), δ 3.59 - 3.52 (ddd, $^3J_{\text{HH}} = 25.0$, 11.7, 5.6 Hz, 1H, *H*6+7), δ 3.22 - 3.18 (m, 1H, *H*8), δ 2.85 - 2.82 (m, 1H, *H*9+10), δ 2.65 - 2.62 (m, 1H, *H*9+10), δ 2.18 - 2.14 (s, 3H, *H*11-22), δ 2.11 - 2.08 (s, 3H, *H*11-22), δ 2.06 - 2.03 (s, 3H, *H*11-22), δ 2.02 - 1.98 (s, 3H, *H*11-22).

$^1\text{H-NMR}$ 2',3'-epoxypropyl-2,3,4,6-tetra-*O*-acetyl- β -D-galactopyranoside (600 MHz, CDCl_3) δ 5.48 - 5.42 (m, 1H, *H*1), δ 5.39 - 5.33 (m, 1H, *H*3), δ 5.20 - 5.14 (dd, $^3J_{\text{HH}} = 17.2$, 3.7 Hz, 1H, *H*2), δ 5.14 - 5.11 (m, 1H, *H*4), δ 4.30 - 4.25 (ddt, $^3J_{\text{HH}} = 6.7$, 3.3, 1.2 Hz, 1H, *H*5), δ 4.13 - 4.05 (m, 2H, *H*23+24), δ 3.92 - 3.79 (ddd, $^3J_{\text{HH}} = 55.5$, 11.8, 3.0 Hz, 1H, *H*6+7), δ 3.64 - 3.46 (ddd, $^3J_{\text{HH}} = 82.8$, 12.2, 5.4 Hz, 1H, *H*6+7), δ 3.20 - 3.12 (m, 1H, *H*8), δ 2.84 - 2.77 (dd, $^3J_{\text{HH}} = 10.2$, 4.8 Hz, 1H, *H*9+10), δ 2.69 - 2.58 (ddd, $^3J_{\text{HH}} = 46.4$, 5.3, 2.7 Hz, 1H, *H*9+10), δ 2.16 - 2.12 (d, $^3J_{\text{HH}} = 1.8$ Hz, 3H, *H*11-22), δ 2.10 - 2.06 (d, $^3J_{\text{HH}} = 2.9$ Hz, 3H, *H*11-22), δ 2.04 - 2.02 (s, 3H, *H*11-22), δ 2.00 - 1.97 (s, 3H, *H*11-22).

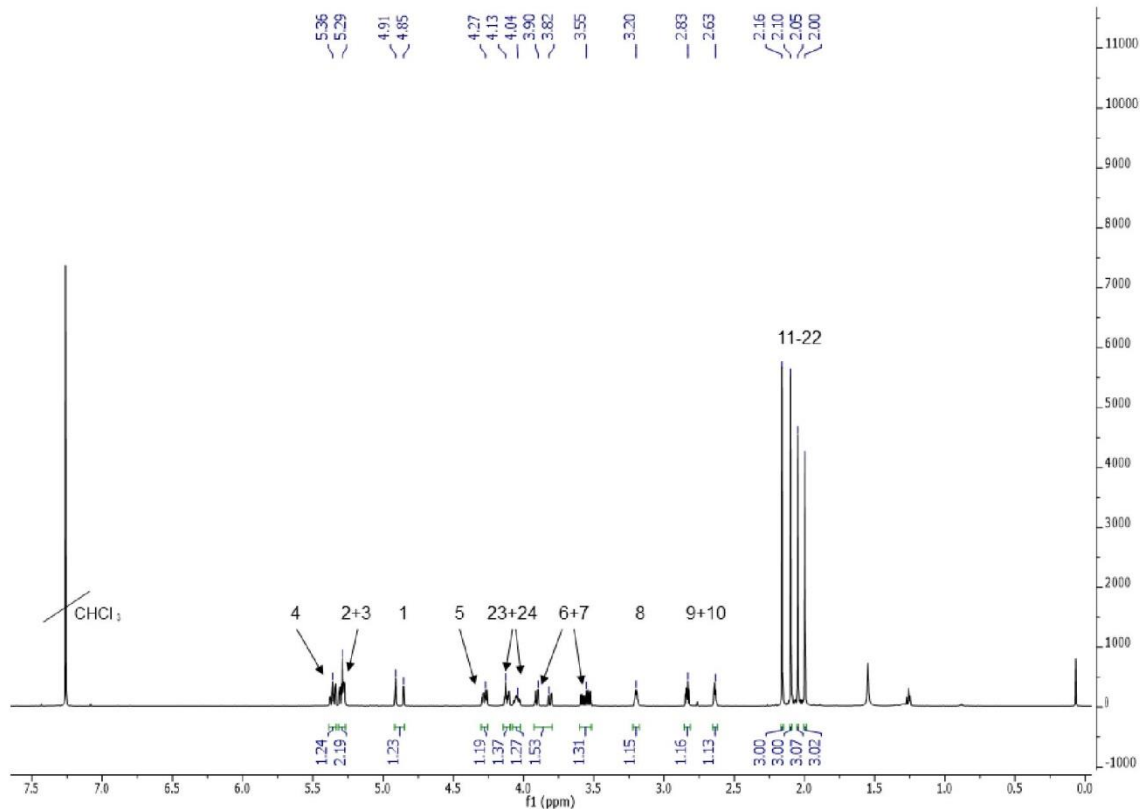


Figure S3d: $^1\text{H-NMR}$ (600 MHz, CDCl_3) 2',3'-epoxypropyl-2,3,4,6-tetra-*O*-acetyl- α -D-mannopyranoside.

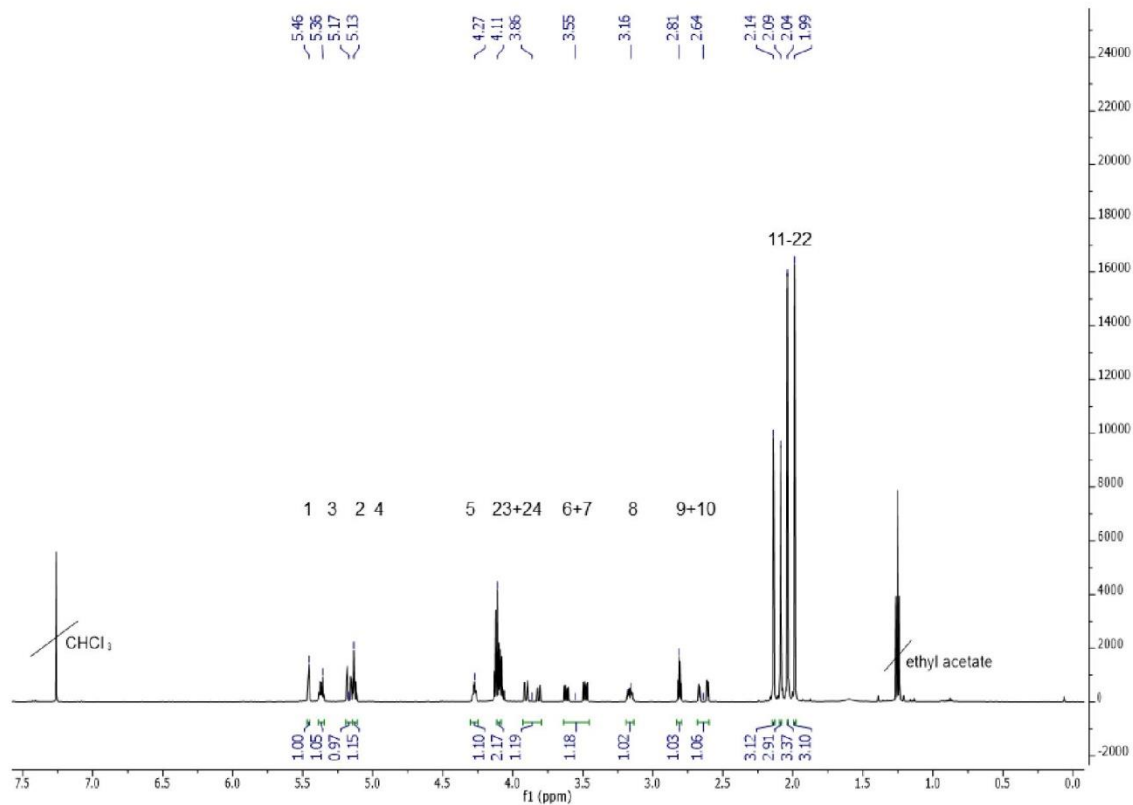
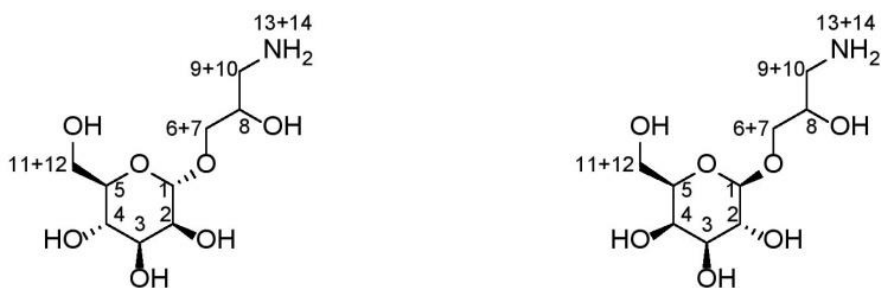


Figure S3d: $^1\text{H-NMR}$ (600 MHz, CDCl_3) 2',3'-epoxypropyl-2,3,4,6-tetra-*O*-acetyl- α -D-galactopyranoside.

Synthesis of 3-amino-2-hydroxypropyl- α -D-mannopyranoside and 3-amino-2-hydroxypropyl- β -D-galactopyranoside



Scheme S3d: 3-amino-2-hydroxypropyl- α -D-mannopyranoside (left) and 3-amino-2-hydroxypropyl- β -D-galactopyranoside (right).

The epoxy-functionalized sugar (9.7 g, 24.2 mmol) was dissolved in 3 mL acetonitrile. After dissolving the sugar ammonia solution (25%, 21 mL) was added and stirred for 72 h. After that the solvent was removed under vacuum and the residue was dissolved in acetone, precipitated in diethyl ether, filtered and dried under vacuum (yield mannose: 5.16 g, 85%; galactose: 3.71 g, 61%).

$^1\text{H-NMR}$ 3-amino-2-hydroxypropyl- α -D-mannopyranoside (600 MHz, CD_3OD) δ 4.80 - 4.76 (s, 1H, $H1$), δ 3.87 - 3.81 (m, 3H, $H8-10$), δ 3.76 - 3.68 (dd, $^3J_{HH} = 12.4, 1.5$ Hz, 3H, $H2+6+7$), δ 3.63 - 3.58 (m, 1H, $H4$), δ 3.56 - 3.51 (m, 1H, $H3$), δ 3.47 - 3.42 (m, 1H, $H5$), δ 2.95 - 2.68 (m, 2H, $H11+12$), δ 1.91 - 1.89 (s, 1H, $H13+14$),

$^1\text{H-NMR}$ 3-amino-2-hydroxypropyl- β -D-galactopyranoside (600 MHz, CD_3OD) δ 4.85 - 4.83 (s, 1H, $H1$), δ 3.84 - 3.65 (m, 8H, $H2-4+6-10$), δ 3.91 - 3.77 (td, $^3J_{HH} = 10.3, 3.4$ Hz 1H, $H5$), δ 2.99 - 2.77 (m, 2H, $H11+12$), δ 1.91 - 1.88 (s, 2H, $H13+14$).

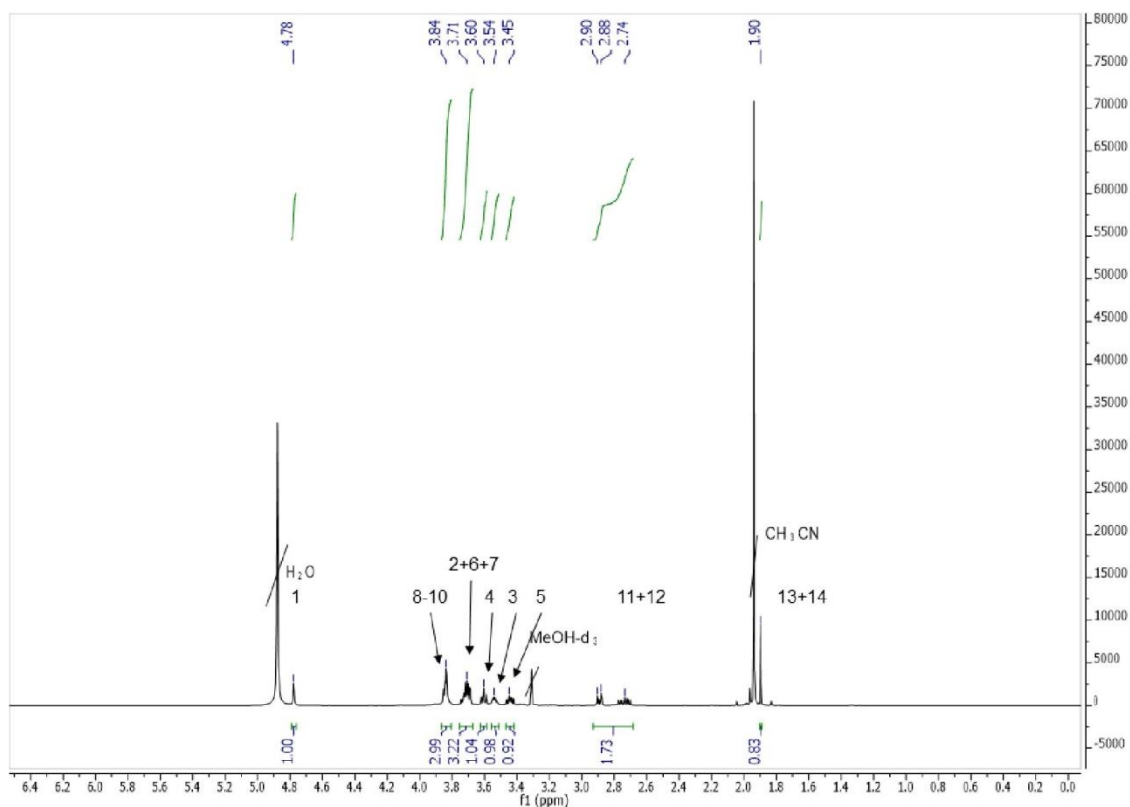


Figure S3e: $^1\text{H-NMR}$ (600 MHz, CD_3OD) 3-amino-2-hydroxypropyl- α -D-mannopyranoside.

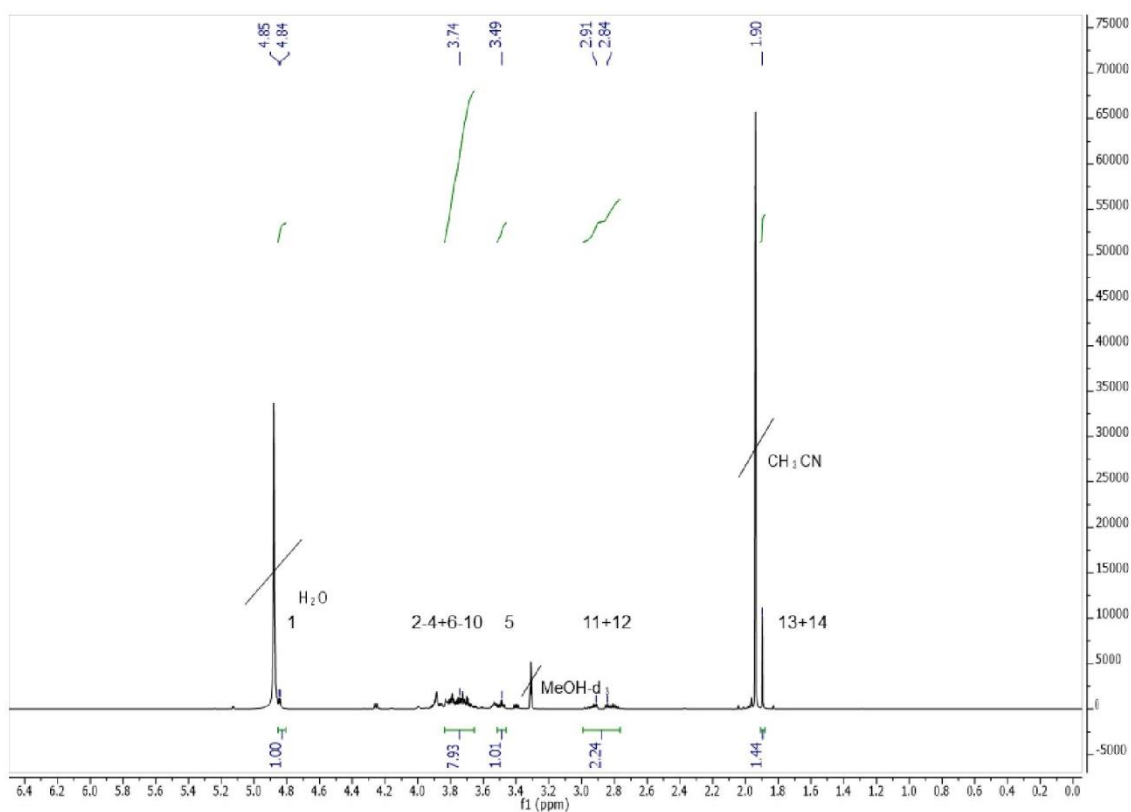
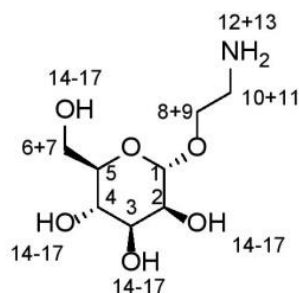


Figure S3f: $^1\text{H-NMR}$ (600 MHz, CD_3OD) 3-amino-2-hydroxypropyl- α -D-galactopyranoside.

Synthesis of ethyl-linker functionalized ligand

Synthesis of 2-aminoethyl- α -D-mannopyranoside

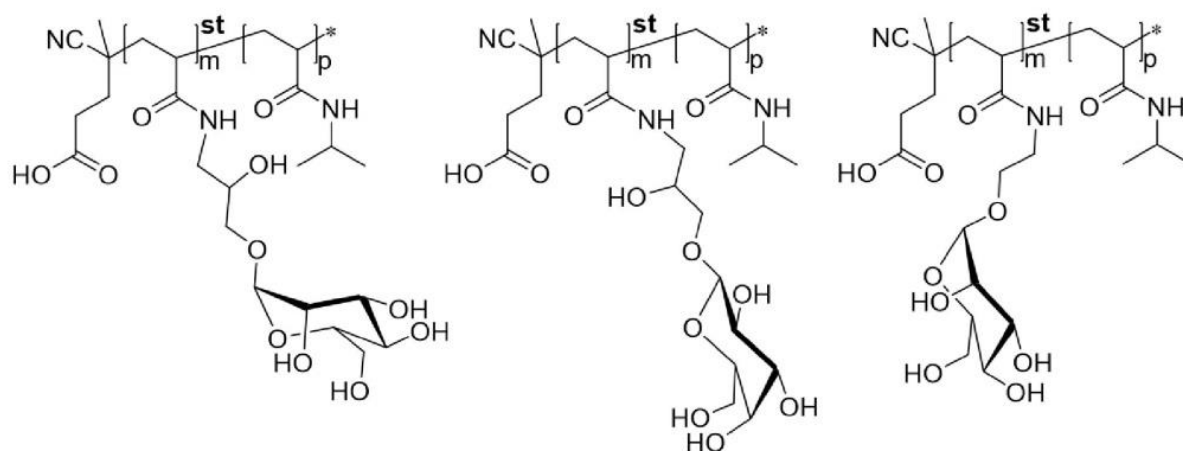


Scheme S3e: 2-aminoethyl- α -D-mannopyranoside.

2-azidoethyl-2,3,4,6-tetra-*O*-acetyl- α -D-mannopyranose was synthesized according to literature.² 0.2 M sodium methoxide in methanol solution (8 mL) was added to 2-azidoethyl-2,3,4,6-tetra-*O*-acetyl α -D-mannopyranose (1.5 g, 3.6 mmol) and shaken for 48 h. Afterwards Amberlite-IR120[®] was added until pH6 was reached. Afterwards, Amberlite-IR120 was filtered off and methanol was added to the filtrate up to a volume of 25 mL. Then palladium on charcoal (10wt%, 106.5 mg, 1 mmol) was added and the solution was flushed three times with hydrogen. The solution was stirred for 24 h under hydrogen atmosphere, filtered and dried under vacuum giving 0.68 g product (yield: 84%).

¹H-NMR (600 MHz, DMSO-*d*₆) δ 4.63 - 4.57 (dd, ³*J*_{HH} = 8.9, 1.4 Hz, 1H, *H*1), δ 3.66 - 3.62 (dd, ³*J*_{HH} = 11.6, 2.1 Hz, 1H, *H*14-16), δ 3.62 - 3.59 (dd ³*J*_{HH} = 3.5, 1.7 Hz, 1H, *H*14+16), δ 3.59 - 3.54 (m, 1H, *H*14-16), δ 3.49 - 3.45 (dd, ³*J*_{HH} = 8.9, 3.4 Hz, 1H, *H*17), δ 3.45 - 2.41 (dd, ³*J*_{HH} = 11.6, 6.1 Hz, 1H, *H*2), δ 3.39 - 3.28 (m, 3H, *H*3-7+12+13), δ 3.17 - 3.16 (s, 4H, *H*3-7+12+13), δ 2.77 - 2.63 (o, ³*J*_{HH} = 6.1 Hz, 2H, *H*8+9), δ 1.85 - 1.78 (s, 2H, *H*10+11).

S4 Synthesis of Poly(*N*-isopropylacrylamide-co-*N*-(2-hydroxypropyl) α -D-mannopyranoside acrylamide) and Poly(*N*-isopropylacrylamide-co-*N*-ethyl α -D-mannopyranoside acrylamide)



Scheme S4a: General structures of Poly(*N*-isopropylacrylamide-co-*N*-(2-hydroxypropyl) α -D-mannopyranoside acrylamide) (left), Poly(*N*-isopropylacrylamide-co-*N*-ethyl α -D-mannopyranoside acrylamide) (right) and Poly(*N*-isopropylacrylamide-co-*N*-(2-hydroxypropyl) α -D-galactopyranoside acrylamide) (middle) polymers.

Table S4a: Amount of sugar added during polymer functionalization and reaction yield after dialysis.

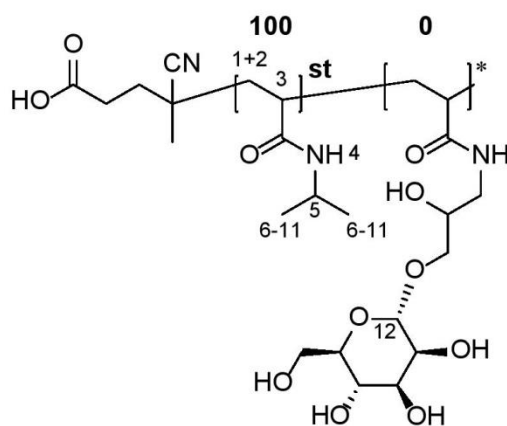
*for **GalHPL3** 3-amino-2-hydroxypropyl- β -D-galactopyranose was used.

| Polymer | Amount of sugar added [mg] | | Yield | |
|----------|---|---|-------|-----|
| | 3-amino-2-hydroxypropyl- α -D-mannopyranose* | 2-aminoethyl- α -D-mannopyranose | [mg] | [%] |
| Man0 | --- | --- | 452 | 67 |
| ManHPL1 | 60 | --- | 438 | 64 |
| ManHPL2 | 120 | --- | 435 | 63 |
| ManHPL7 | 150 | --- | 540 | 74 |
| ManHPL34 | 1600 | --- | 855 | 81 |
| ManHPL97 | 3200 | --- | 1358 | 80 |
| ManEL1 | --- | 26 | 415 | 61 |
| ManEL2 | --- | 53 | 421 | 61 |
| ManEL5 | --- | 132 | 441 | 61 |
| GalHPL3 | 150 | --- | 456 | 63 |

Molecular weight of PNAS was calculated from $^1\text{H-NMR}$ spectroscopy giving a $\bar{M}_n = 15340 \text{ g mol}^{-1}$, divided by the molecular weight of the monomer giving a number of repeating units of 90. The ratio of the anomeric hydrogen integral at the carbohydrate in comparison to the backbone CH-group integral gave similar results to the colorimetric carbohydrate assay (PSA method). The PSA functionalization degrees were used due to higher accuracy of the method. By multiplication of functionalization degrees with number of repeating units and molecular weight of the monomers the molecular weights were calculated.

Table S4b: Functionalization degrees determined by $^1\text{H-NMR}$ -spectroscopy and phenol sulphuric acid (PSA) method and the molecular weight calculated from PSA methods functionalization degree.

| Polymer | Results | | |
|----------|---|------------------------------------|--|
| | Functionalization degree ($^1\text{H-NMR}$) [%] | Functionalization degree (PSA) [%] | Molecular weight (PSA) [g mol^{-1}] |
| Man0 | 0 | 0 | 10300 |
| ManHPL1 | 1.3 | 1.4 | 10480 |
| ManHPL2 | 1.8 | 1.9 | 10650 |
| ManHPL7 | 7.4 | 7.5 | 11525 |
| ManHPL34 | 31.1 | 33.6 | 16240 |
| ManHPL97 | 89.3 | 96.9 | 27770 |
| ManEL1 | 1.3 | 1.1 | 10450 |
| ManEL2 | 2.8 | 2.2 | 10600 |
| ManEL5 | 4.2 | 4.6 | 11040 |
| GalHPL3 | 2.6 | 2.7 | 10825 |



Scheme S4b: Structure of **PNIPAM**. Bold numbers showing functionalization degree.

$^1\text{H-NMR}$ **PNIPAM** (600 MHz, CDCl_3) δ 7.15 - 5.90 (s, 1H, H_4), δ 4.15 - 3.90 (s, 1H, H_5), δ 2.32 - 1.96 (s, 1H, H_3) δ 1.95 - 1.30 (s, 2H, H_{1+2}), δ 1.28 - 0.94 (s, 6H, H_{6-11}).

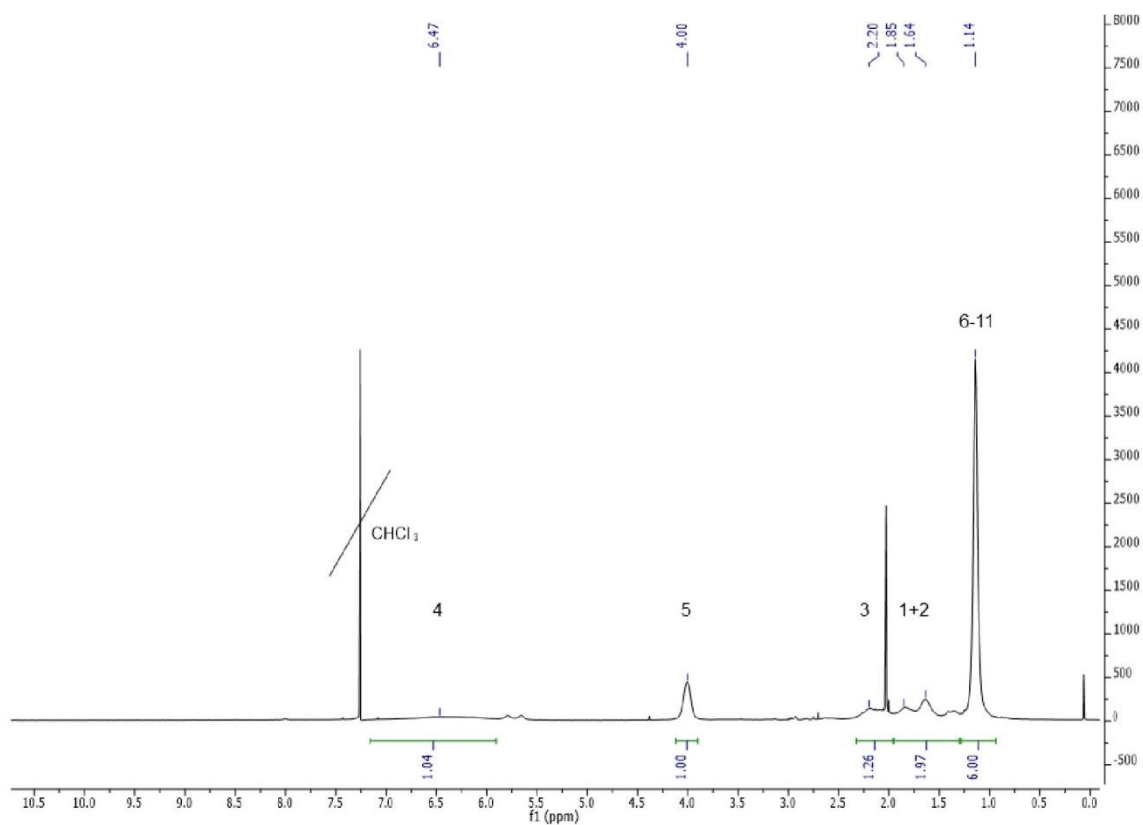
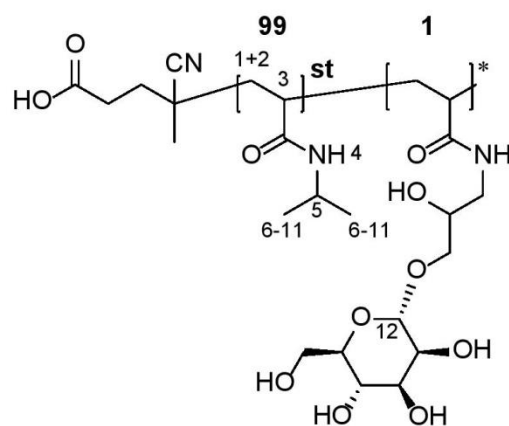


Figure S4a: $^1\text{H-NMR}$ (600 MHz, CDCl_3) of **PNIPAM**.



Scheme S4c: Structure of **ManHPL1**. Bold numbers showing functionalization degree.

$^1\text{H-NMR}$ **ManHPL1** (600 MHz, CDCl_3) δ 7.14 - 6.03 (s, 1H, H_4) δ 4.97 - 4.85 (s, 1H, H_{12}), δ 4.07 - 3.95 (s, 75H, H_5) δ 2.32 - 1.99 (s, 76H, H_3), δ 1.93 - 1.55 (s, 152H, H_{1+2}), δ 1.31 - 0.94 (s, 305H, H_{6-11}).

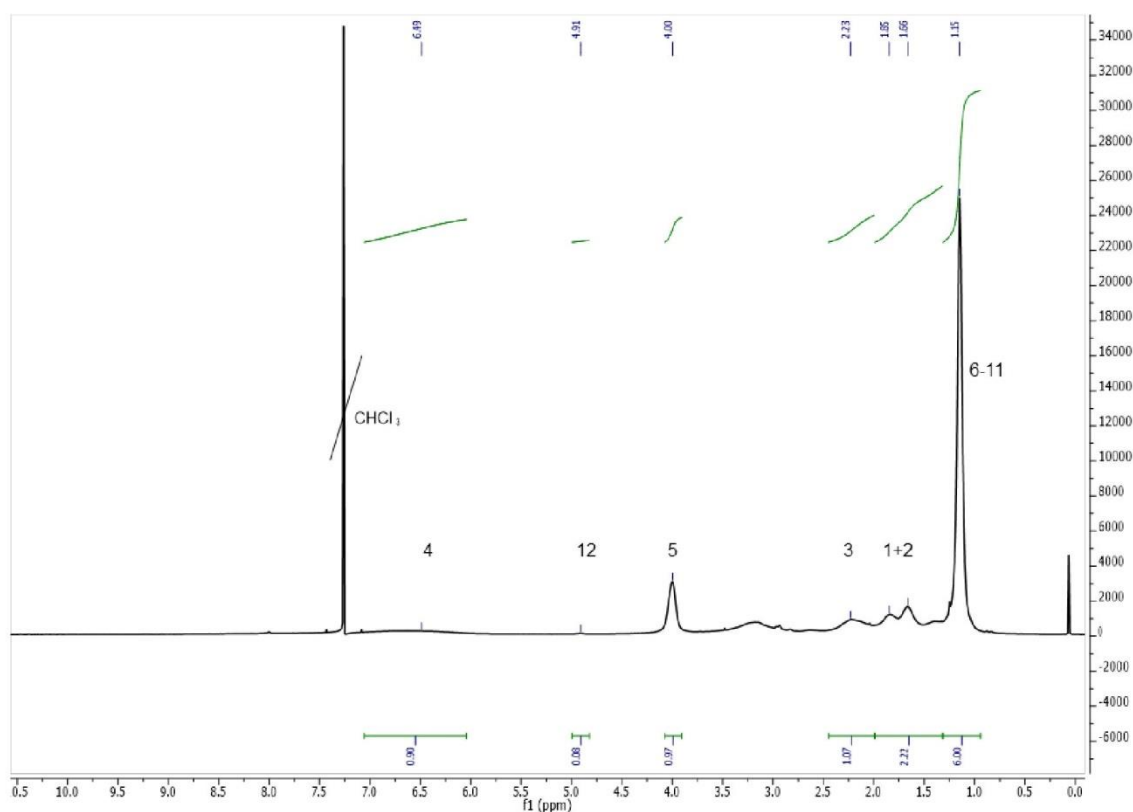
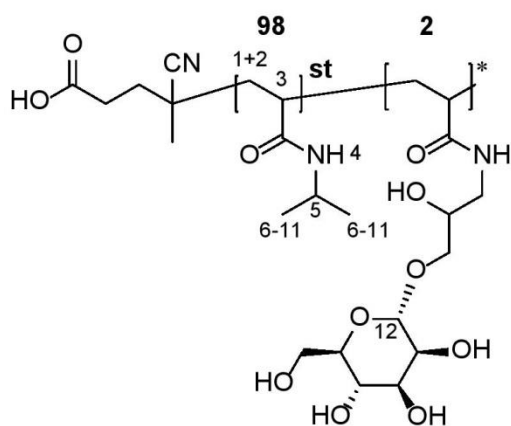


Figure S4b: $^1\text{H-NMR}$ (600 MHz, CDCl_3) of **ManHPL1**.



Scheme S4d: Structure of **ManHPL2**. Bold numbers showing functionalization degree.

$^1\text{H-NMR}$ **ManHPL2** (600 MHz, CDCl_3) δ 7.03 - 5.57 (s, 55H, *H4*), δ 4.92 - 4.86 (s, 1H, *H12*), δ 4.07 - 3.92 (s, 56H, *H5*) δ 2.65 - 1.98 (s, 55H, *H3*), δ 1.95 - 1.25 (s, 111H, *H1+2*), δ 1.19 - 1.03 (s, 334H, *H6-11*).

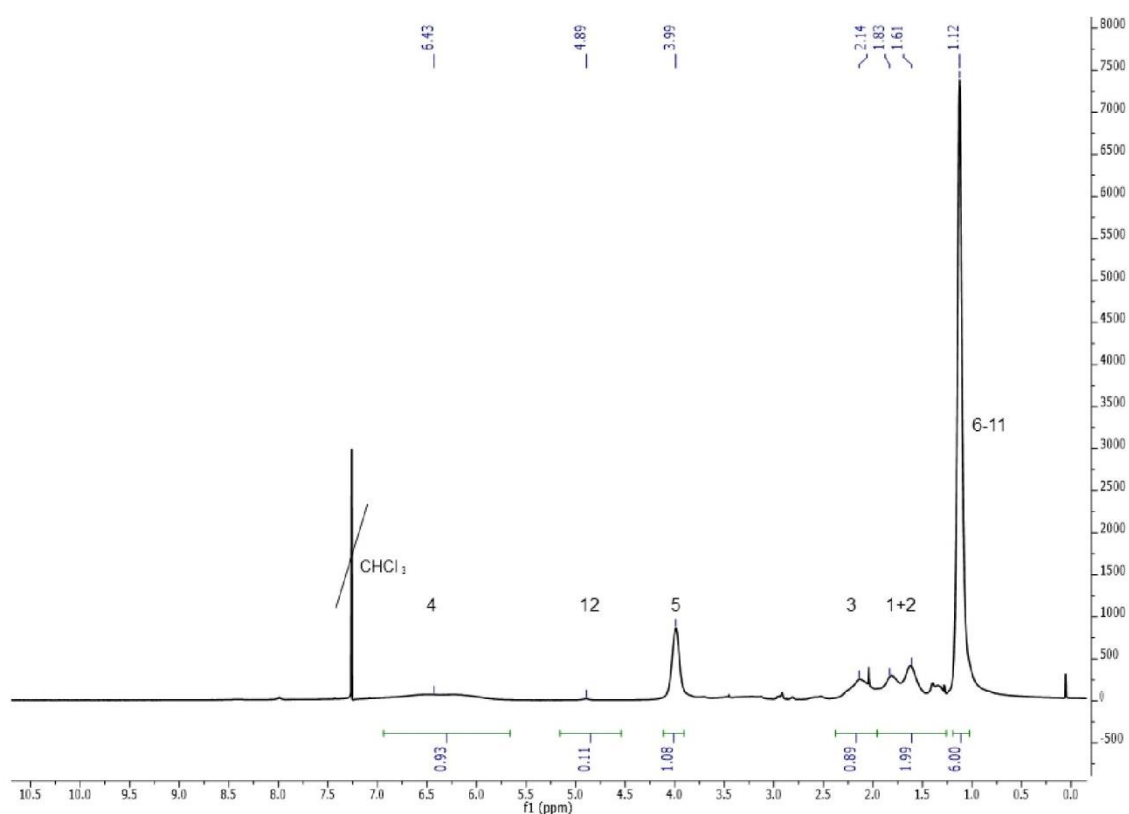
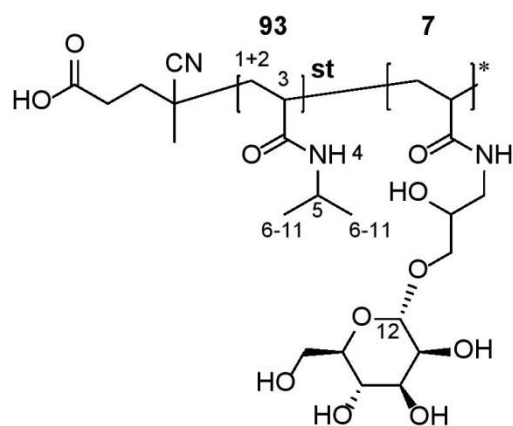


Figure S4c: $^1\text{H-NMR}$ (600 MHz, CDCl_3) of **ManHPL2**.



Scheme S4e: Structure of **ManHPL7**. Bold numbers showing functionalization degree.

$^1\text{H-NMR}$ **ManHPL7** (600 MHz, CDCl_3) δ 6.95 - 5.68 (s, 14H, *H4*), δ 4.95 - 4.83 (s, 1H, *H12*), δ 4.07 - 3.92 (s, 14H, *H5*) δ 2.40 - 1.92 (s, 14H, *H3*), δ 1.91 - 1.25 (s, 28H, *H1+2*), δ 1.17 - 0.98 (s, 84H, *H6-11*).

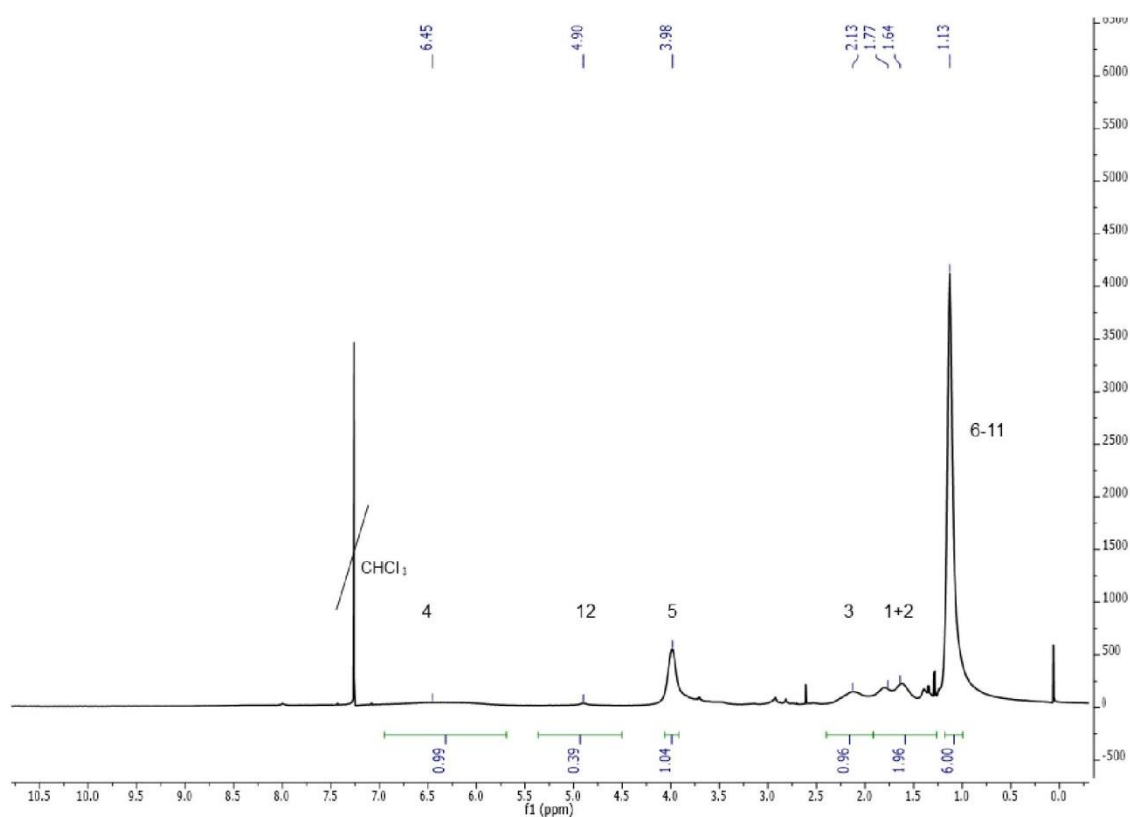
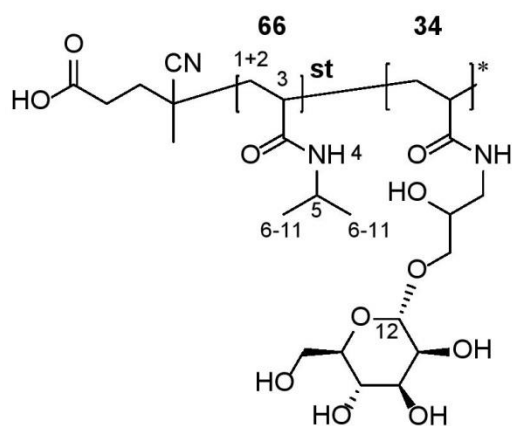


Figure S4d: $^1\text{H-NMR}$ (600 MHz, CDCl_3) of **ManHPL7**.



Scheme S4f: Structure of **ManHPL34**. Bold numbers showing functionalization degree.

$^1\text{H-NMR}$ **ManHPL34** (600 MHz, D_2O) δ 4.91 - 4.88 (s, 1H, H_{12}), δ 2.37 - 1.87 (s, 3H, H_3), δ 1.85 - 1.40 (s, 5H, H_{1+2}) δ 1.25 - 0.80 (s, 6H, H_{6-11}).

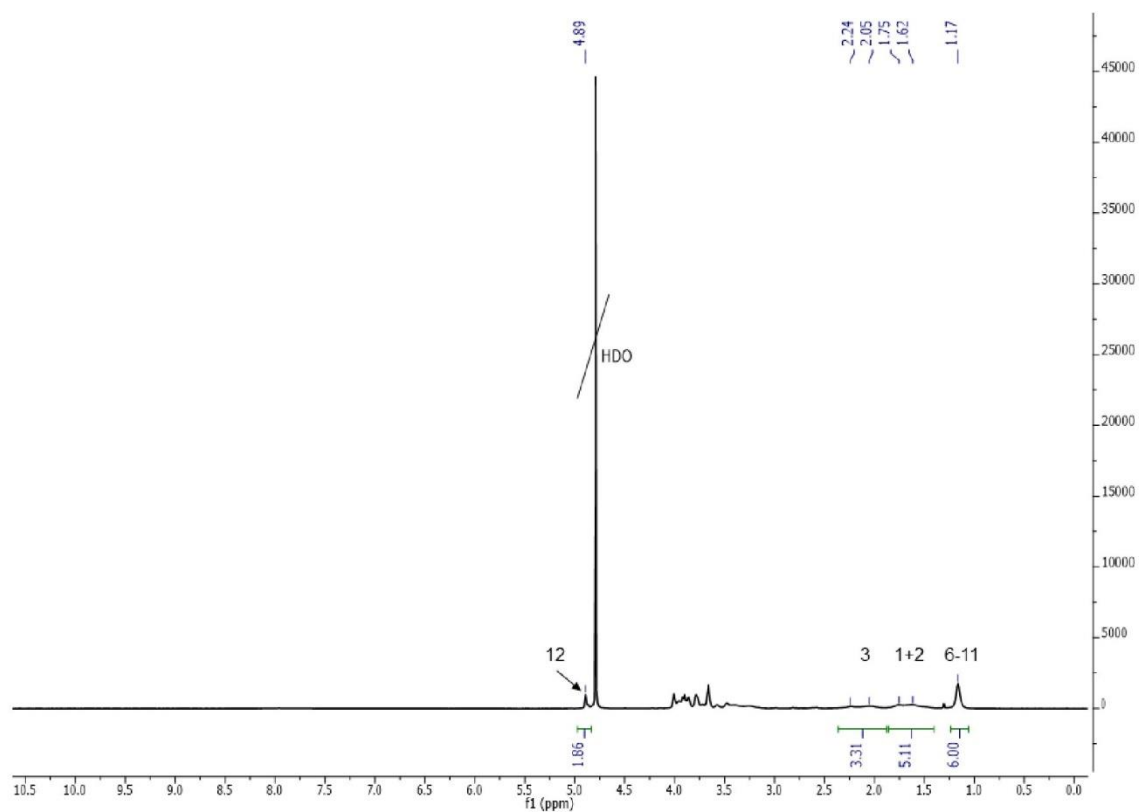
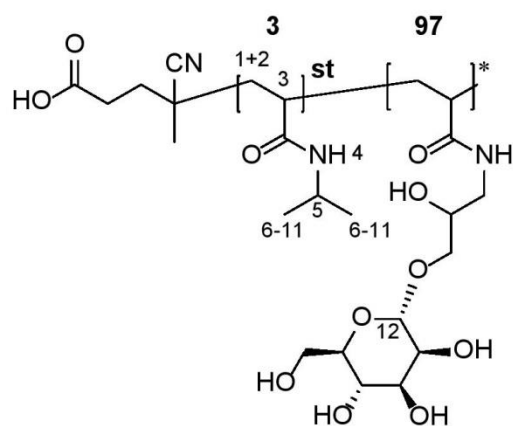


Figure S4e: $^1\text{H-NMR}$ (600 MHz, D_2O) of **ManHPL34**.



Scheme S4g: Structure of **ManHPL97**. Bold numbers showing functionalization degree.

$^1\text{H-NMR}$ **ManHPL97** (600 MHz, D_2O) δ 4.95 - 4.85 (s, 1H, *H12*), δ 2.60 - 1.96 (s, 1.18H, *H3*), δ 1.95 - 1.25 (s, 2.14H, *H1+2*) δ 1.18 - 1.12 (s, 0.12H, *H6-11*).

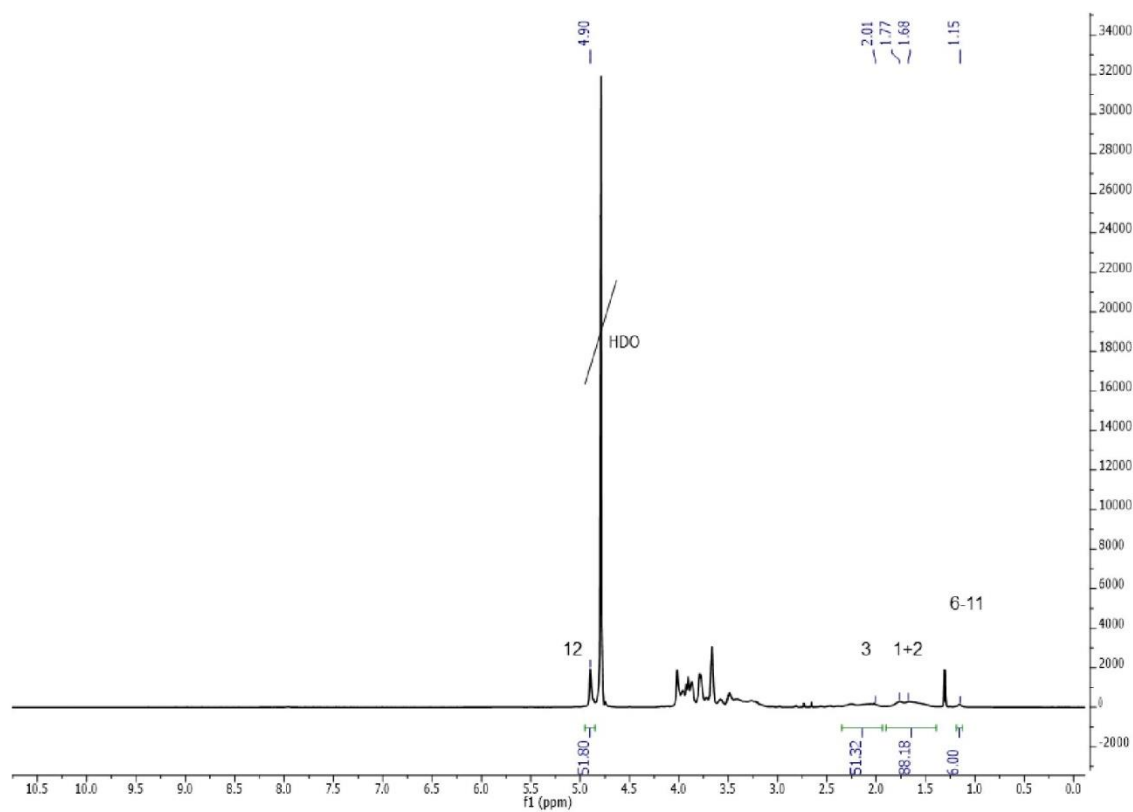
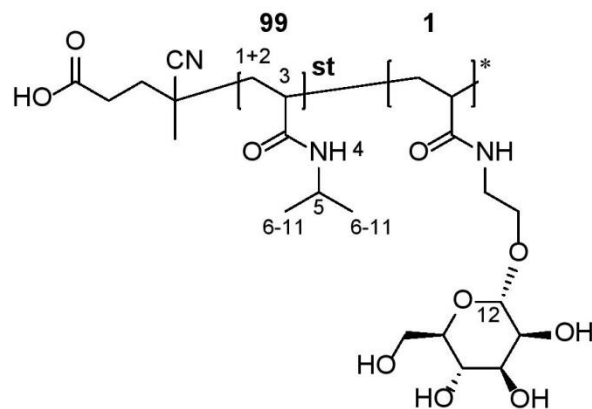


Figure S4f: $^1\text{H-NMR}$ (600 MHz, D_2O) of **ManHPL97**.



Scheme S4h: Structure of **ManEL1**. Bold numbers showing functionalization degree.

$^1\text{H-NMR}$ **ManEL1** (600 MHz, CDCl_3) δ 7.10 - 5.85 (s, 75H, *H4*), δ 4.90 - 4.85 (s, 1H, *H12*), δ 4.07 - 3.91 (s, 77H, *H5*) δ 2.40 - 1.95 (s, 79H, *H3*), δ 1.90 - 1.30 (s, 158H, *H1+2*), δ 1.24 - 0.95 (s, 463H, *H6-11*).

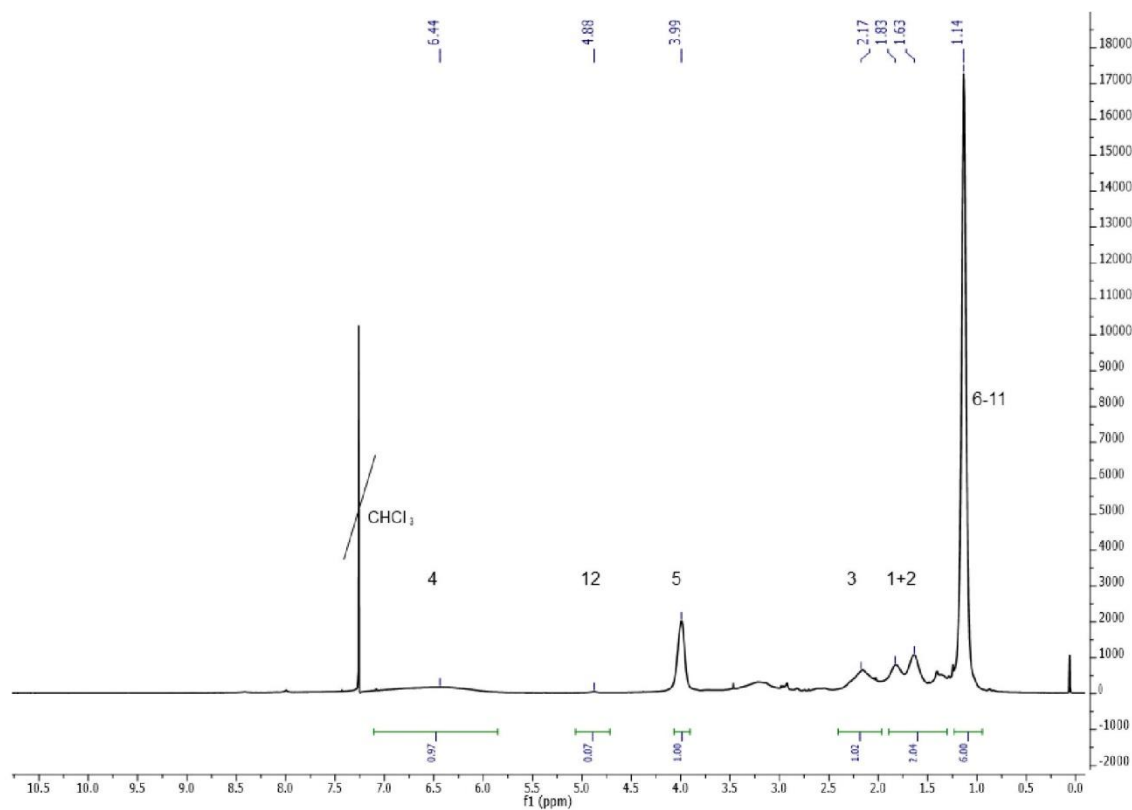
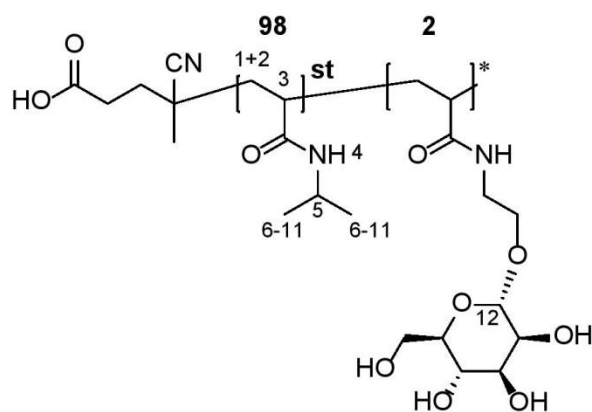


Figure S4g: $^1\text{H-NMR}$ (600 MHz, CDCl_3) of **ManEL1**.



Scheme S4i: Structure of **ManEL2**. Bold numbers showing functionalization degree.

$^1\text{H-NMR}$ **ManEL2** (600 MHz, CDCl_3) δ 7.00 - 6.05 (s, 32H, *H4*), δ 4.91 - 4.87 (s, 1H, *H12*), δ 4.20 - 3.82 (s, 40H, *H5*) δ 2.40 - 1.98 (s, 35H, *H3*), δ 2.00 - 1.31 (s, 72H, *H1+2*), δ 1.30 - 0.75 (s, 203H, *H6-11*).

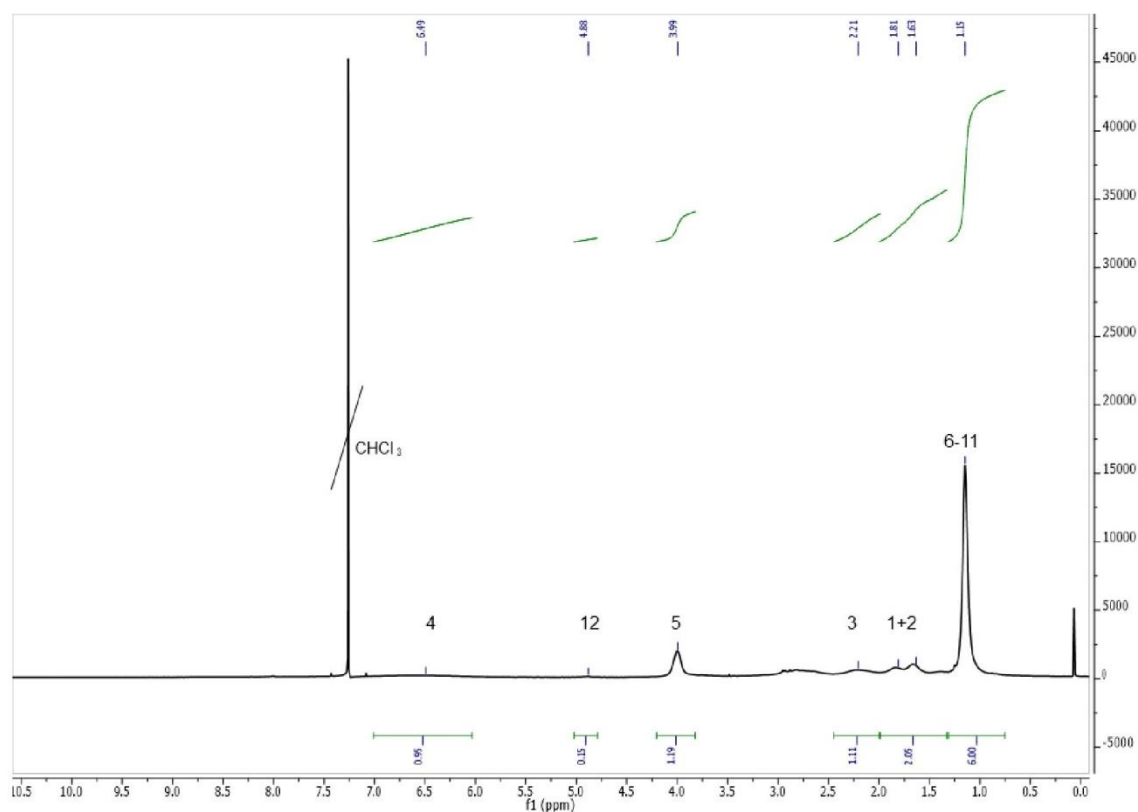
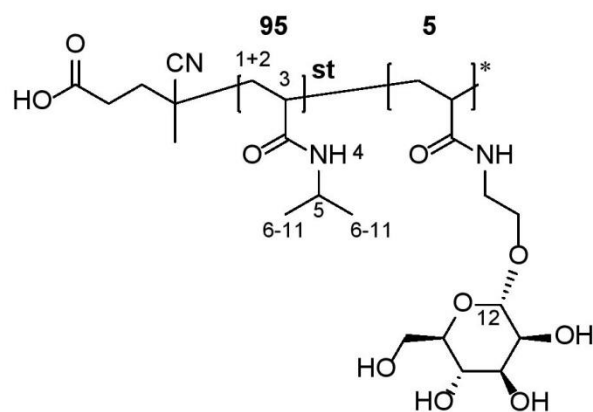


Figure S4h: $^1\text{H-NMR}$ (600 MHz, CDCl_3) of **ManEL2**.



Scheme S4j: Structure of **ManEL5**. Bold numbers showing functionalization degree.

$^1\text{H-NMR}$ **ManEL5** (600 MHz, CDCl_3) δ 6.97 - 5.68 (s, 24H, *H4*), δ 4.90 - 4.84 (s, 1H, *H12*), δ 4.09 - 3.87 (s, 29H, *H5*) δ 2.66 - 1.98 (s, 24H, *H3*), δ 1.95 - 1.25 (s, 48H, *H1+2*), δ 1.20 - 0.96 (s, 149H, *H6-11*).

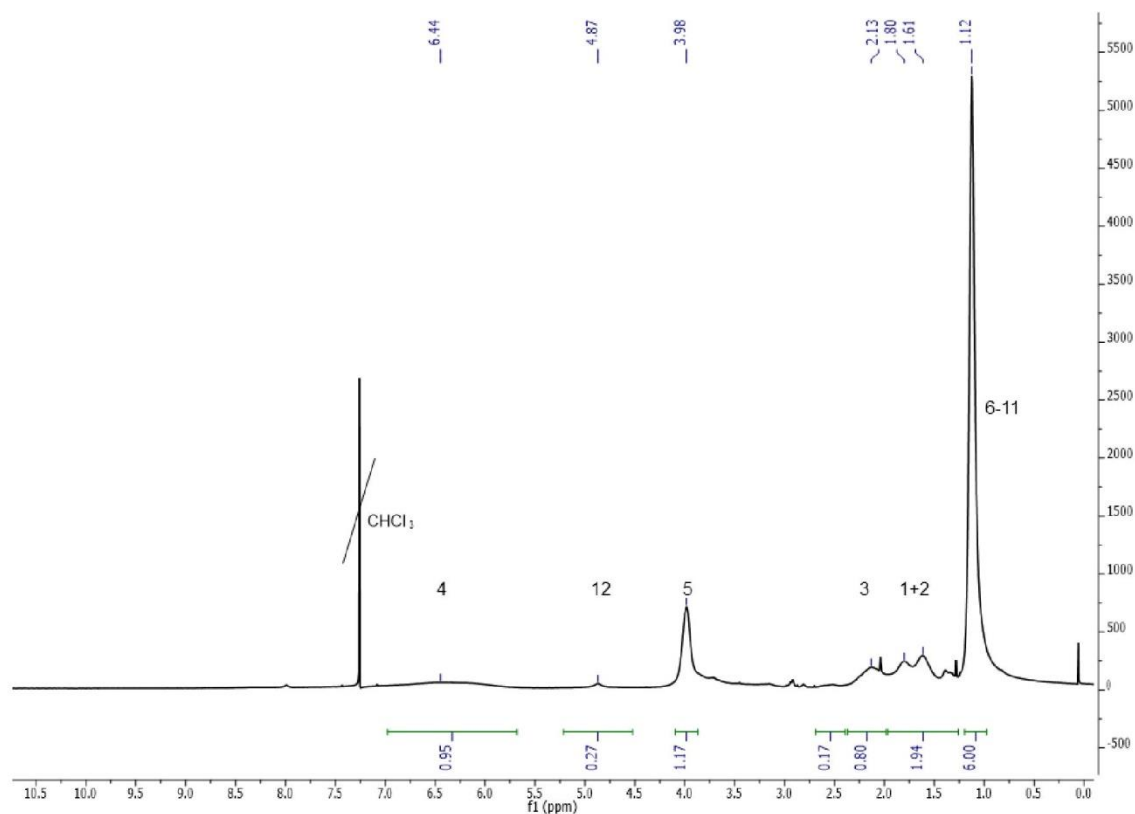
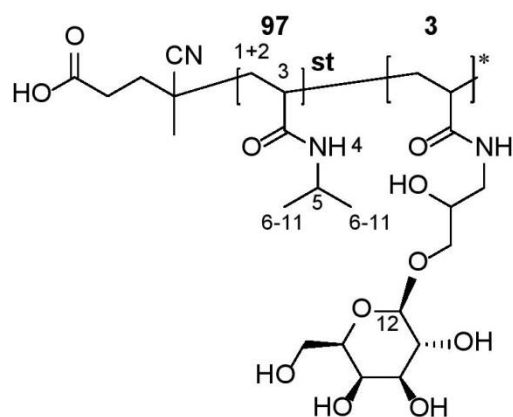


Figure S4i: $^1\text{H-NMR}$ (600 MHz, CDCl_3) of **ManEL5**.



Scheme S4k: Structure of **GalHPL3**. Bold numbers showing functionalization degree.

$^1\text{H-NMR}$ **GalHPL3** (600 MHz, CDCl_3) δ 6.79 - 5.82 (s, 22H, *H4*), δ 4.97 - 4.90 (s, 1H, *H12*), δ 4.06 - 3.90 (s, 31H, *H5*) δ 2.72 - 1.95 (s, 30H, *H3*), δ 1.91 - 1.25 (s, 51H, *H1+2*), δ 1.17 - 1.05 (s, 151H, *H6-11*).

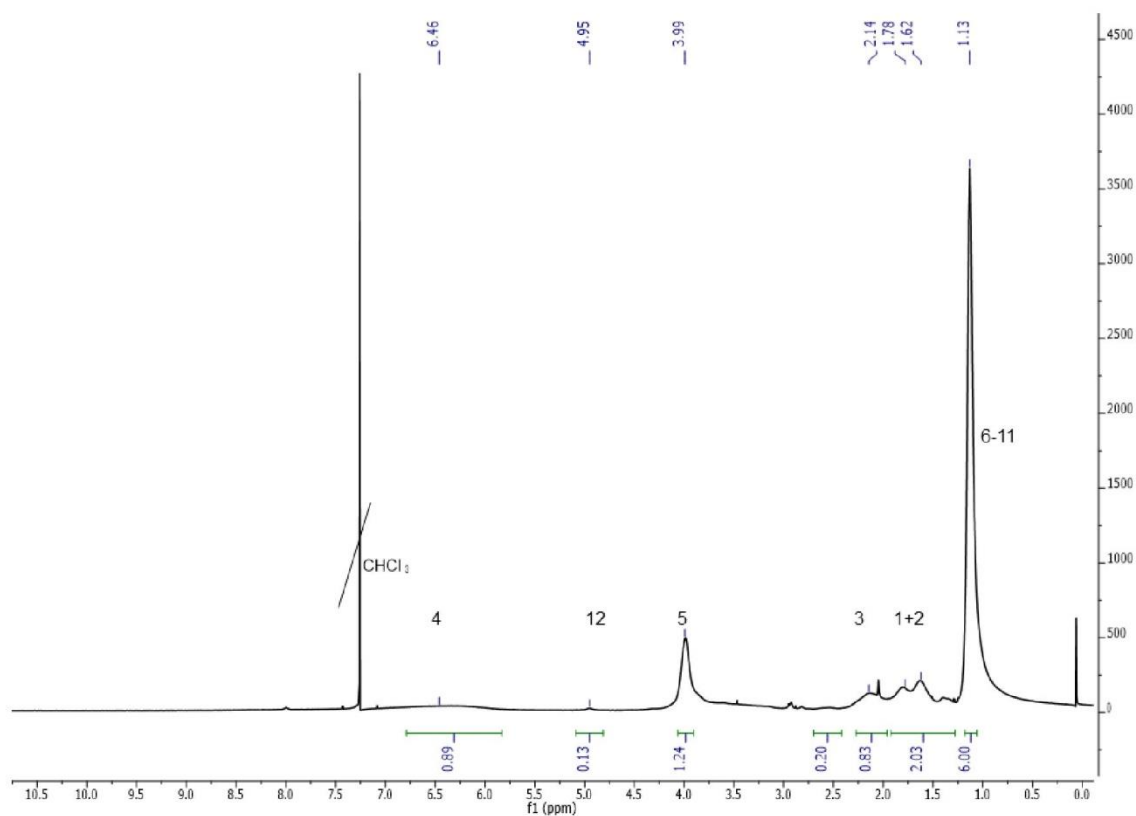


Figure S4j: $^1\text{H-NMR}$ (600 MHz, CDCl_3) of **GalHPL3**.

S5 Size exclusion chromatography

ManHPL34 and **ManHPL97** were insoluble in DMF, therefore, no SEC measurements were executed for these samples. Having only polystyrene standard at hand and without suitable Marc-Houwink parameters, the SEC measurements were done for determination of \bar{M}_w -values and not for molecular weight. These measurements show that carbohydrate ligand does not act as intermolecular bridges between two polymer backbones. The molecular weight was calculated using number of repeating units from PNAS determined via $^1\text{H-NMR}$ spectroscopy and PSA test for determining the amount of incorporated carbohydrate.

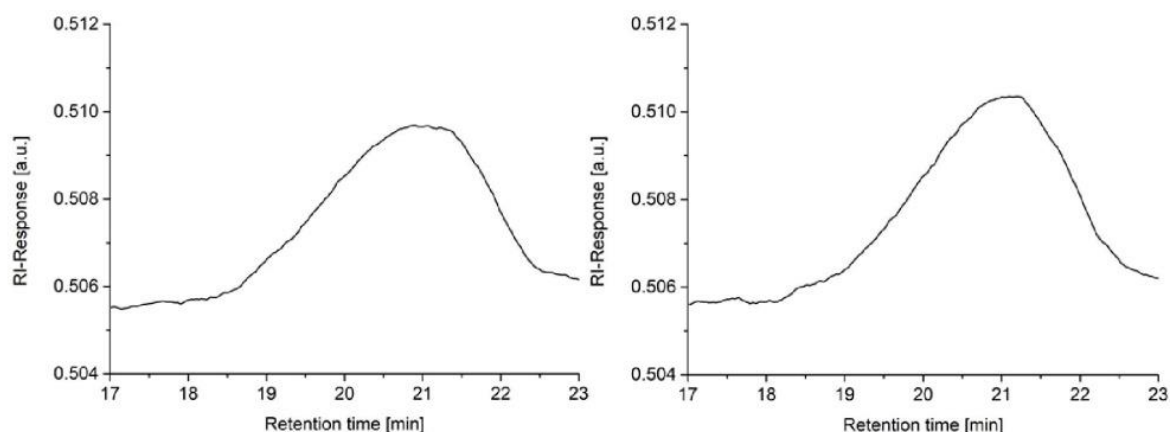


Figure S5a: Size exclusion chromatographies of polymer precursor poly(N-acryloxysuccinimide) (left) and negative control **PNIPAM** (right).

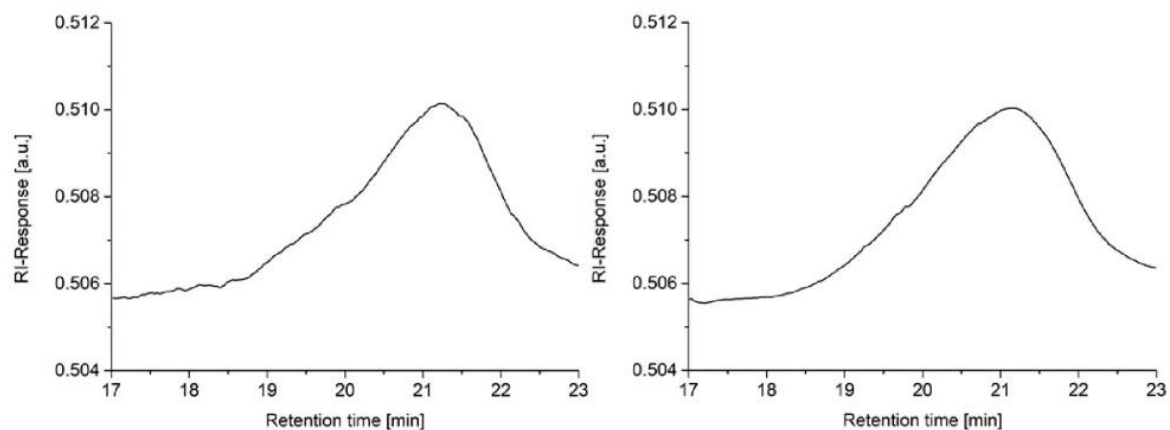


Figure S5b: Size exclusion chromatographies of glycopolymers **ManHPL1** (left) and **ManHPL2** (right).

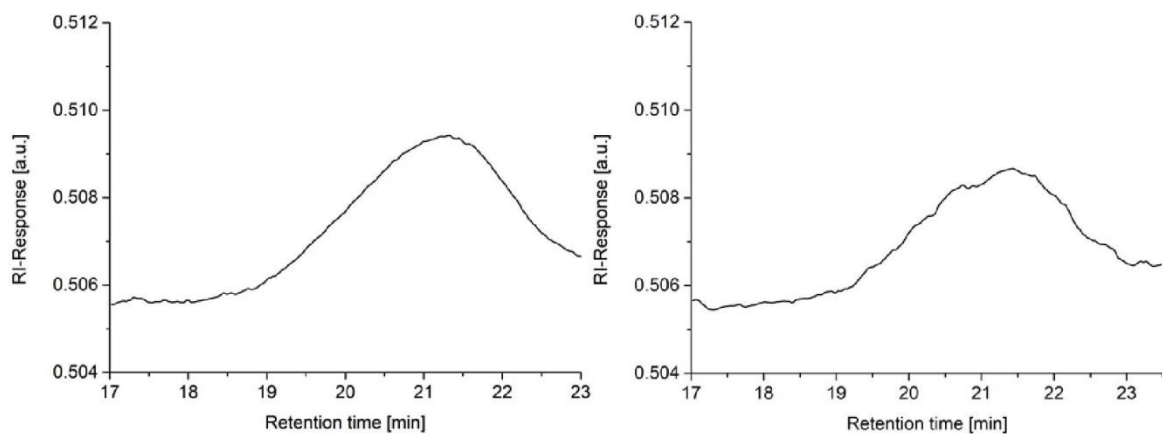


Figure S5c: Size exclusion chromatographies of glycopolymer **ManHPL7** (left) and negative binding control **GalHPL3** (right).

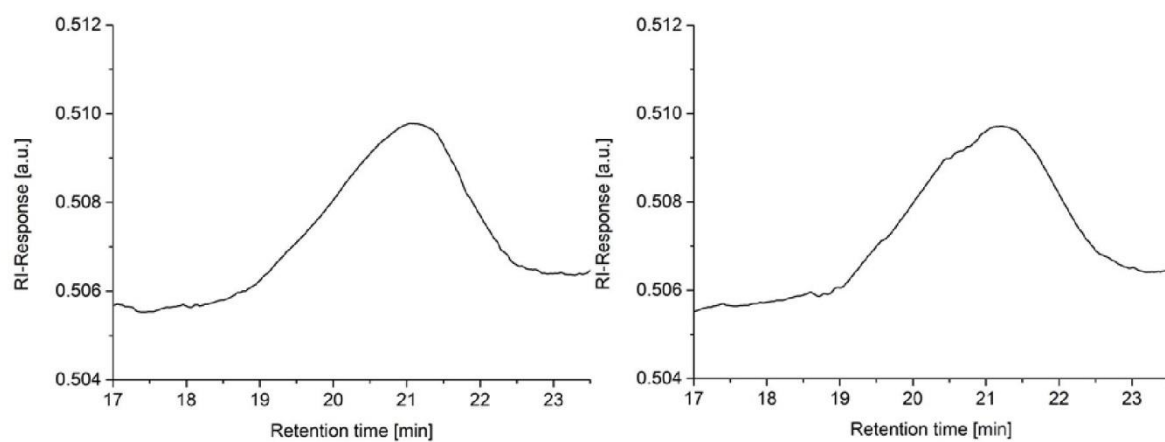


Figure S5d: Size exclusion chromatographies of glycopolymers **ManEL1** (left) and **ManEL2** (right).

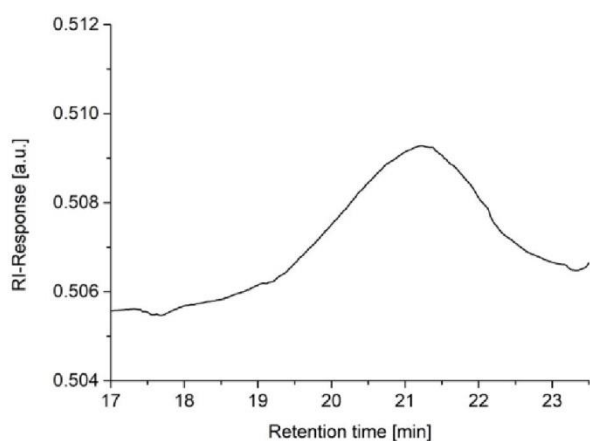


Figure S5e: Size exclusion chromatography of glycopolymer **ManEL5**.

S6 Phenol sulfuric acid method (PSA)

For analysis of the polymer samples to 125 μL of polymer solution with a specific concentration depending on the expected functionalization degree of the polymer (see Table S6) was used. Procedure for polymer sample was the same as for the calibration curve.

Table S6: For sulfuric acid phenol method used concentration of polymer concentration based on the expected functionalization degree.

| Polymer | Amount of polymer used [mg mL^{-1}] |
|----------|--|
| PNIPAM | 5.84 |
| ManHPL1 | 5.83 |
| ManHPL2 | 2.75 |
| ManHPL7 | 0.62 |
| ManHPL34 | 0.22 |
| ManHPL97 | 0.12 |
| ManEL1 | 5.74 |
| ManEL2 | 2.66 |
| ManEL5 | 1.26 |
| GalHPL3 | 2.92 |

S7 ATR-

FTIR

Spectroscopy

To show the successful functionalization of PNAS with isopropyl amine to **PNIPAM** ATR-FTIR measurements were executed. Comparison of both measurements (see **Figure S7a**) show an increase in $\nu(\text{NH})$ and a loss of $\nu(\text{CO-O-R})$ indicating a successful functionalization.

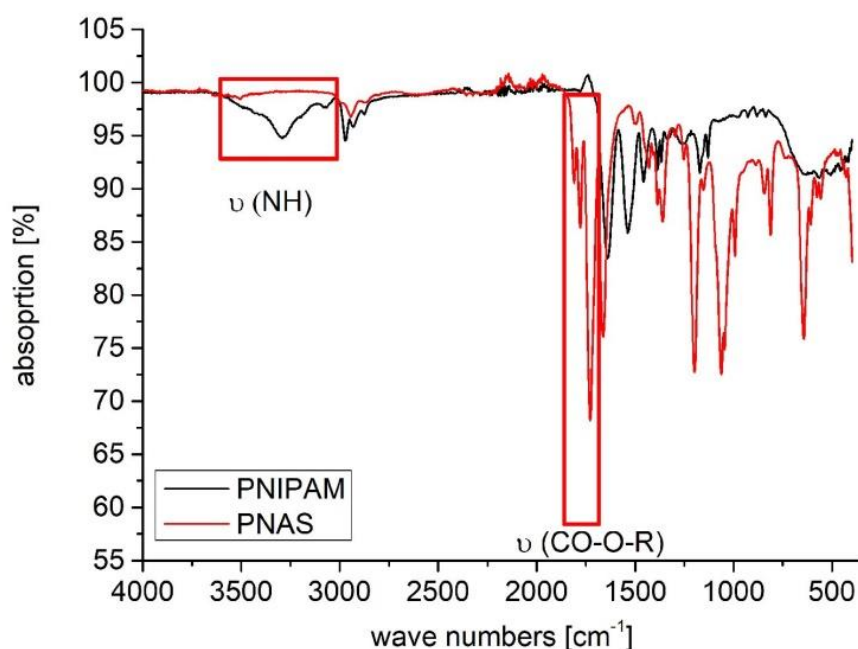


Figure S7a: Comparison of ATR-FTIR measurement of **PNIPAM** and PNAS.

As an indication of the successful functionalization of PNAS with isopropyl amine and carbohydrate ligands ATR-FTIR measurements were executed. Comparison of ATR-FTIR

measurements of **PNIPAM** and **ManHPL** glycopolymers (see **Figure S7b**) show a decrease in amide vibrations and an increase in carbohydrate vibrations.

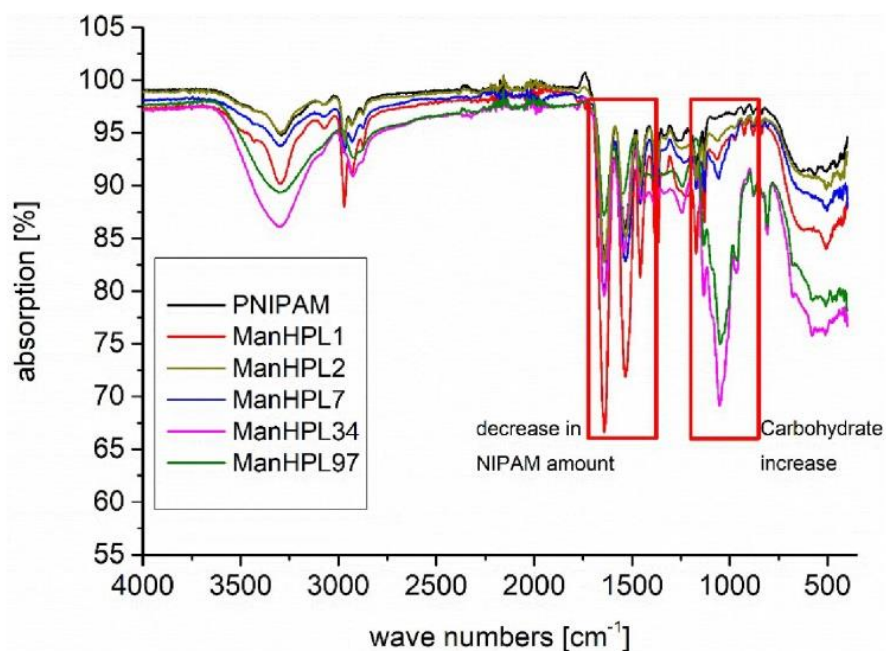


Figure S7b: Comparison of ATR-FTIR measurement of **PNIPAM** and **ManHPL** glycopolymers.

Magnification of wave number range 1250-2000 cm⁻¹ (see **Figure S7c**) show that in the area of expected ester vibration no signal is visible for ManHPL glycopolymers. Therefore, no Carbohydrate unit is linked to the polymer backbone by an ester bond.

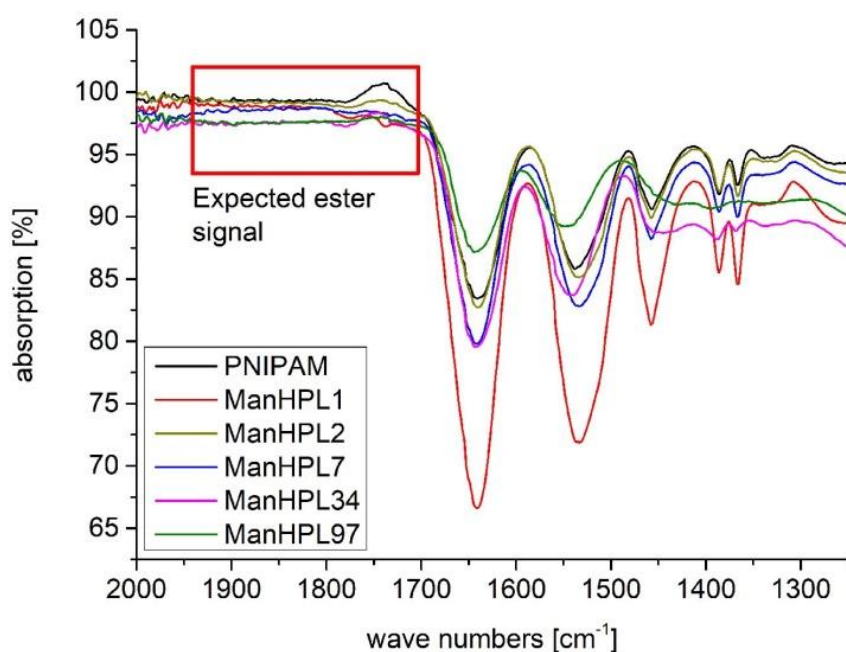


Figure S7c: Magnification of ATR-FTIR measurement of **PNIPAM** and **ManHPL** glycopolymers from wave numbers 1250-2000 cm⁻¹.

Comparison of ManEL glycopolymers (see **Figure S7d**) show and confirm an increase in carbohydrate vibrations at increasing functionalization degree and a decrease in amide vibrations.

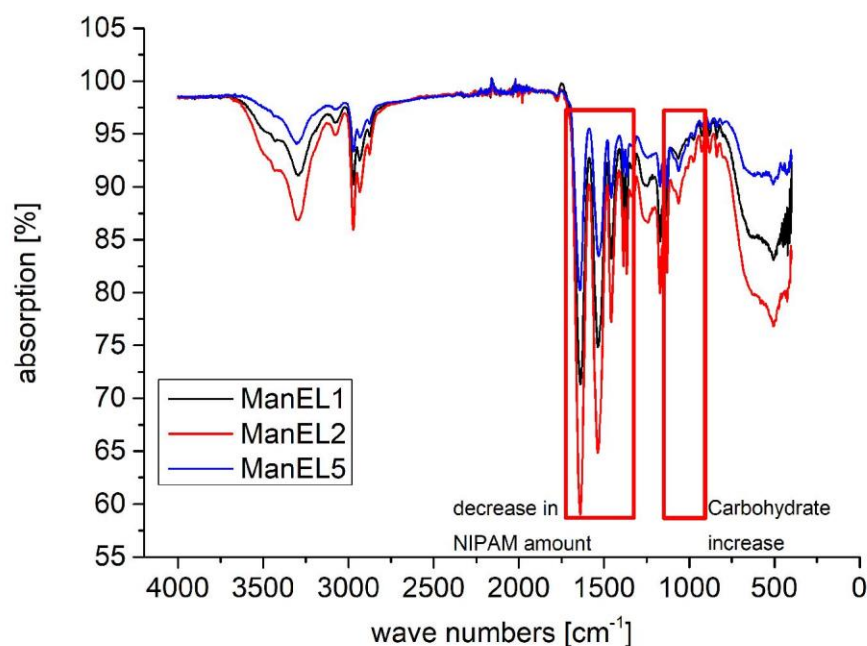


Figure S7d: Comparison of ATR-FTIR measurement of **ManEL** glycopolymers.

Magnification of wave number range 1250-2000 cm⁻¹ (see **Figure S7e**) show that in the area of expected ester vibration no signal is visible for ManEL glycopolymers. Therefore, no Carbohydrate unit is linked to the polymer backbone by an ester bond.

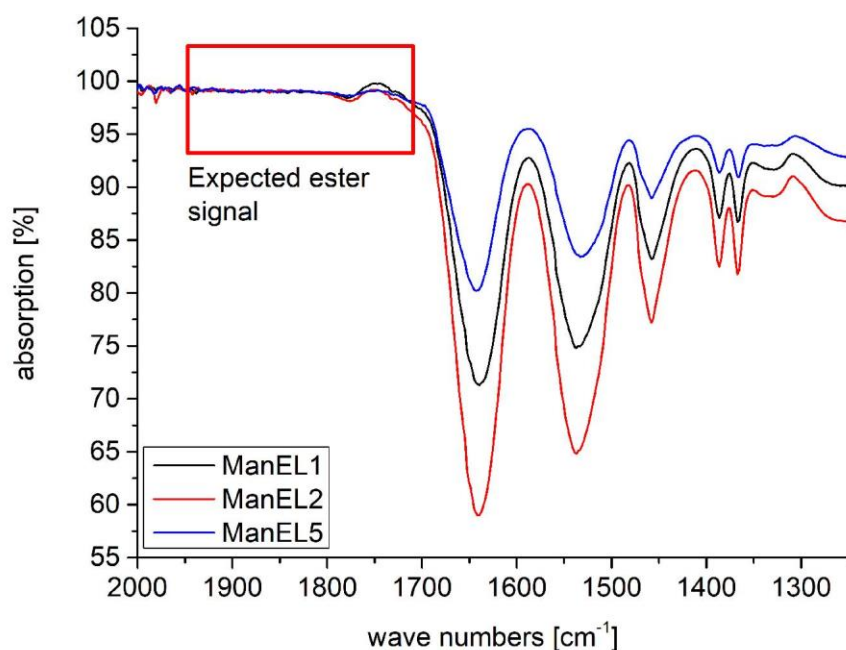


Figure S7e: Magnification of ATR-FTIR measurement of **PNIPAM** and **ManHPL** glycopolymers from wave numbers 1250-2000 cm⁻¹.

S8 Differential scanning calorimetry (DSC)

Below the DSC measurements are shown. Nine heating/cooling segments were done during the measurement. The segments were done as following: Heating segment 1 (black), cooling segment 1 (red), Heating segment 2 (blue), cooling segment 2 (magenta), Heating segment 3 (olive), cooling segment 3 (navy blue), Heating segment 4 (violet), cooling segment 4 (purple), Heating segment 5 (brown). The first heating segment was done to remove solvent leftovers and therefore, the measurements end with a heating segment. T_g was determined by the average values of turning points during the heating segments.

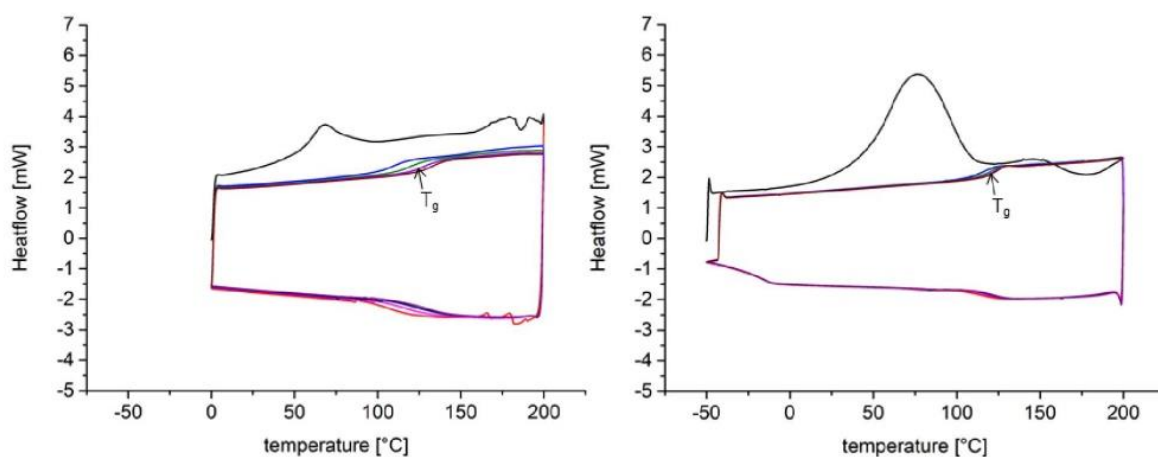


Figure S8a: DSC measurements of polymer precursor PNAS (left) and negative control PNIPAM (right).

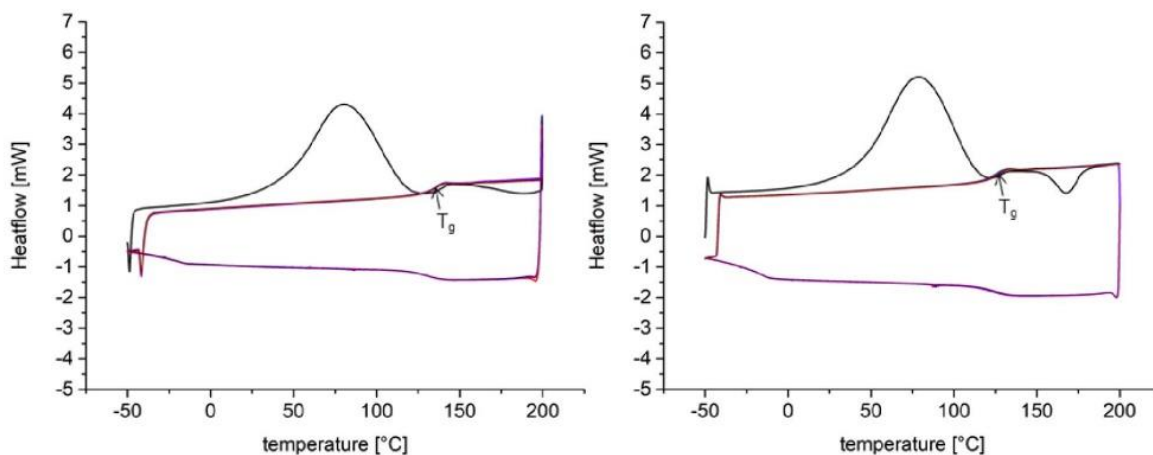


Figure S8b: DSC measurements of non-binding control GalHPL3 (left) and glycopolymer ManHPL1 (right).

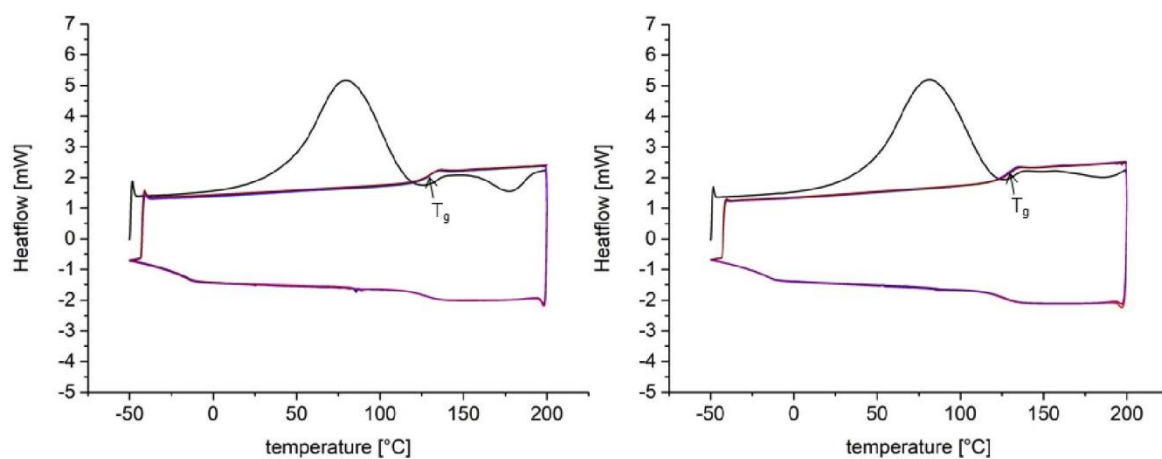


Figure S8c: DSC measurements of glycopolymer **ManHPL2** (left) and glycopolymer **ManHPL7** (right).

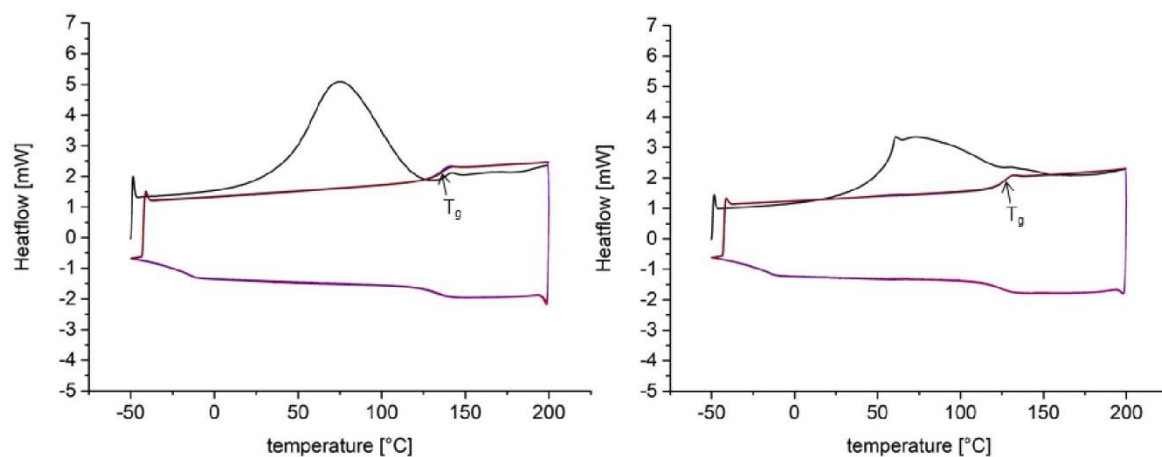


Figure S8d: DSC measurements of glycopolymer **ManHPL34** (left) and glycopolymer **ManHPL97** (right).

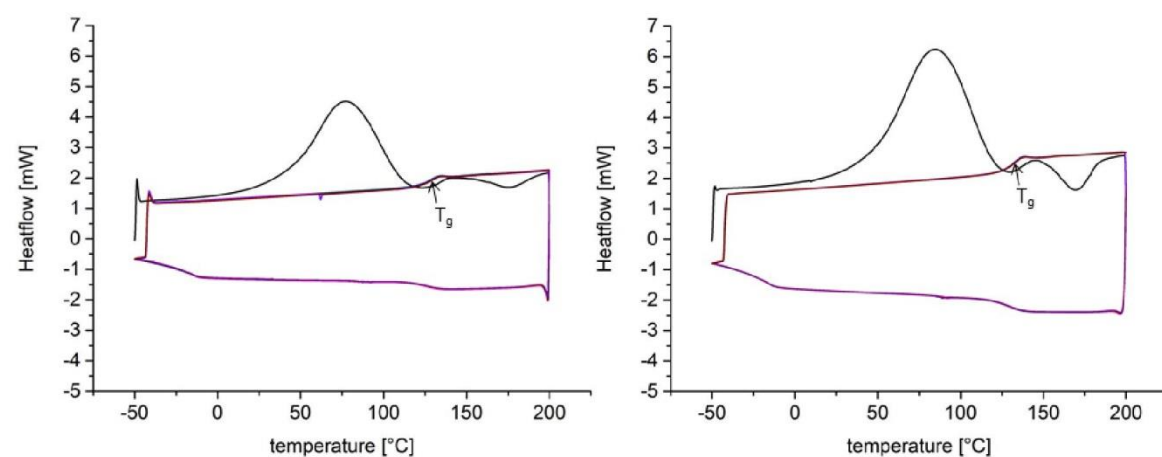


Figure S8e: DSC measurements of glycopolymer **ManEL1** (left) and glycopolymer **ManEL2** (right).

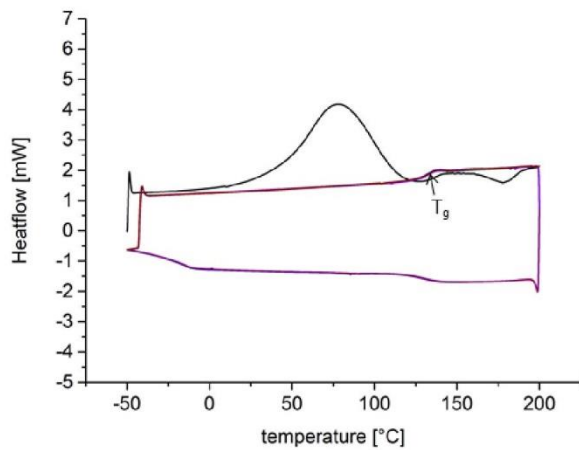


Figure S8f: DSC measurement of glycopolymer **ManEL5**.

S9 Turbidimetry studies

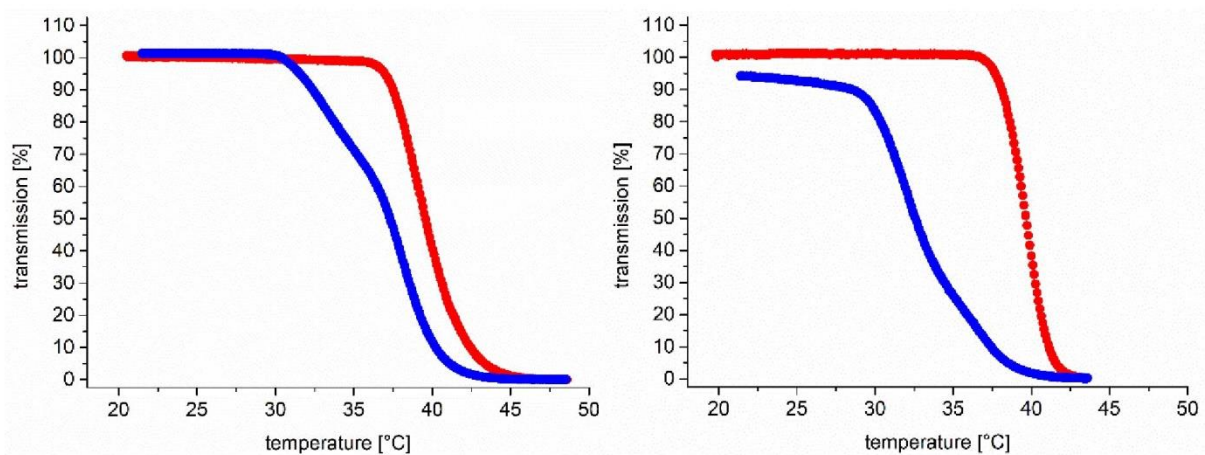


Figure S9a: Turbidity measurements of **ManHPL1** with a polymer concentration of 5 mg mL^{-1} in LBB. left: without ConA, right: with ConA. Red lines denote heating cycle. Blue line denotes cooling cycle.

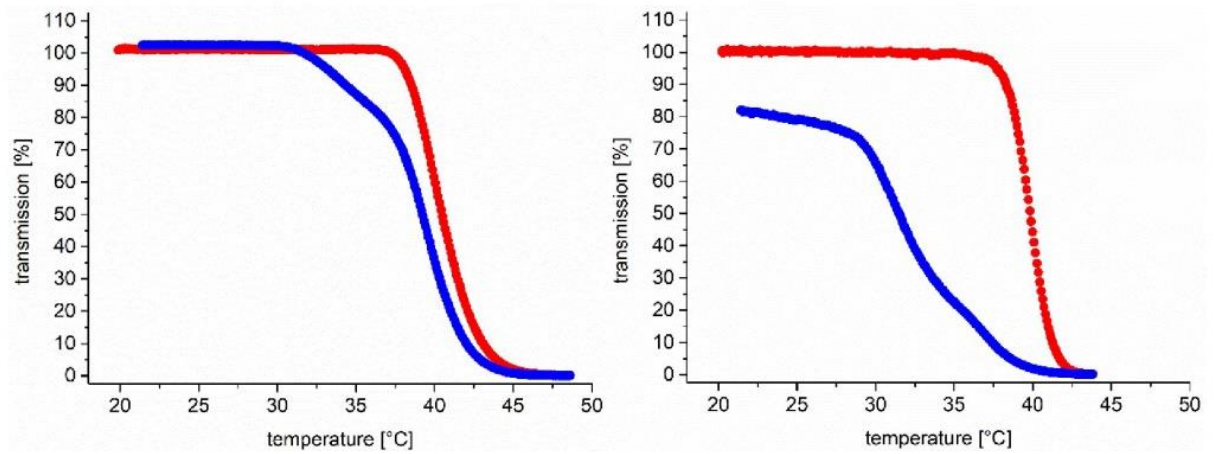


Figure S9b: Turbidity measurement of **ManHPL2** with a polymer concentration of 5 mg mL⁻¹ in LBB, left: without ConA, right: with ConA.

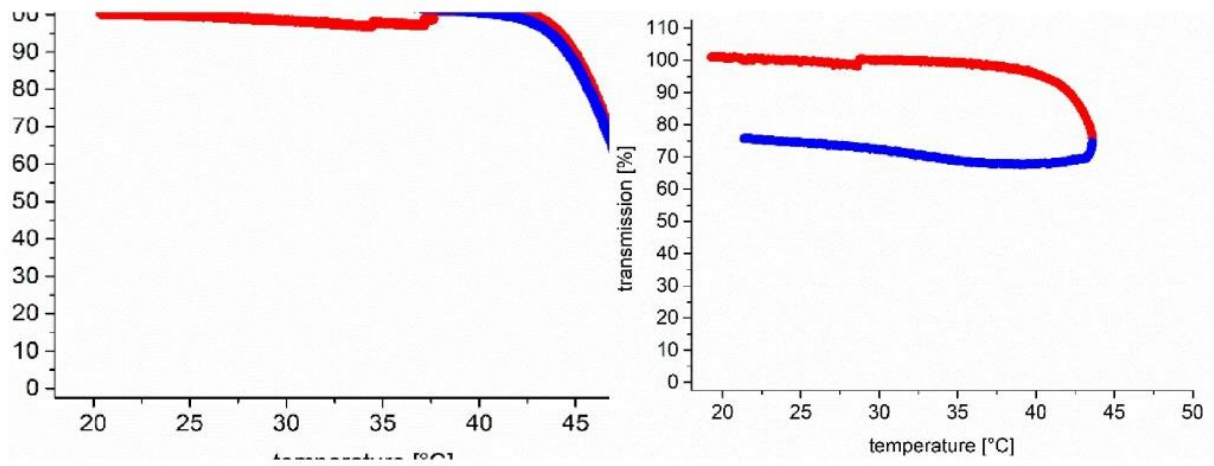


Figure S9c: Turbidity measurements of **ManHPL7** with a polymer concentration of 5 mg mL⁻¹ in LBB, left: without ConA, right: with ConA.

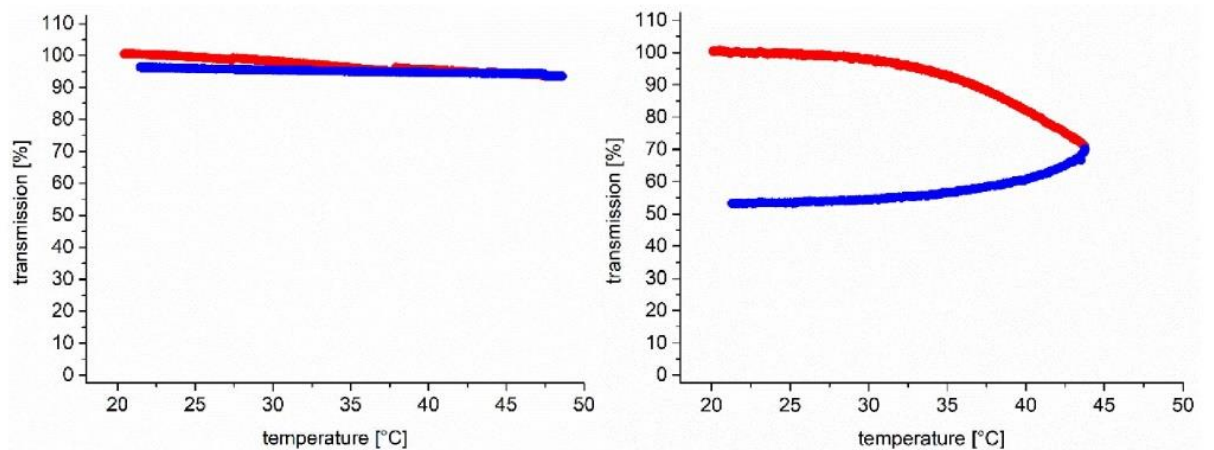


Figure S9d: Turbidity measurements of **ManHPL34** with a polymer concentration of 5 mg mL⁻¹ in LBB, left: without ConA, right: with ConA.

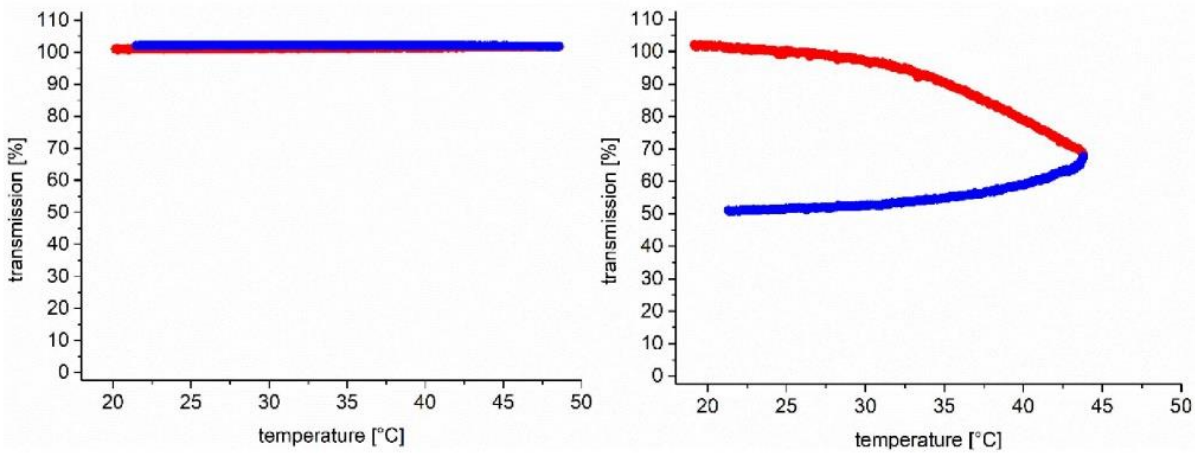


Figure S9e: Turbidity measurements of **ManHPL97** with a polymer concentration of 5 mg mL⁻¹ in LBB, left: without ConA, right: with ConA.

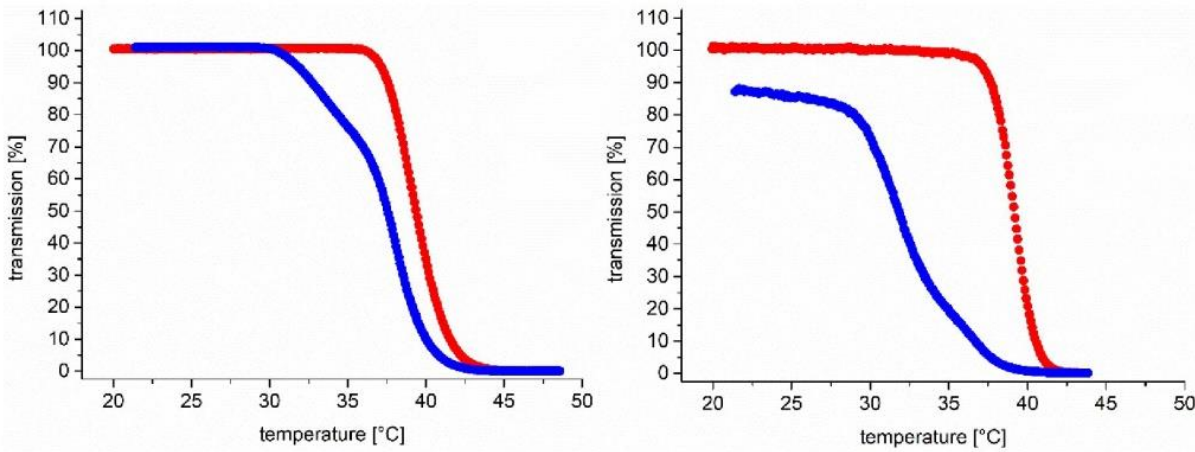


Figure S9f: Turbidity measurements of **ManEL1** with a polymer concentration of 5 mg mL⁻¹ in LBB, left: without ConA, right: with ConA.

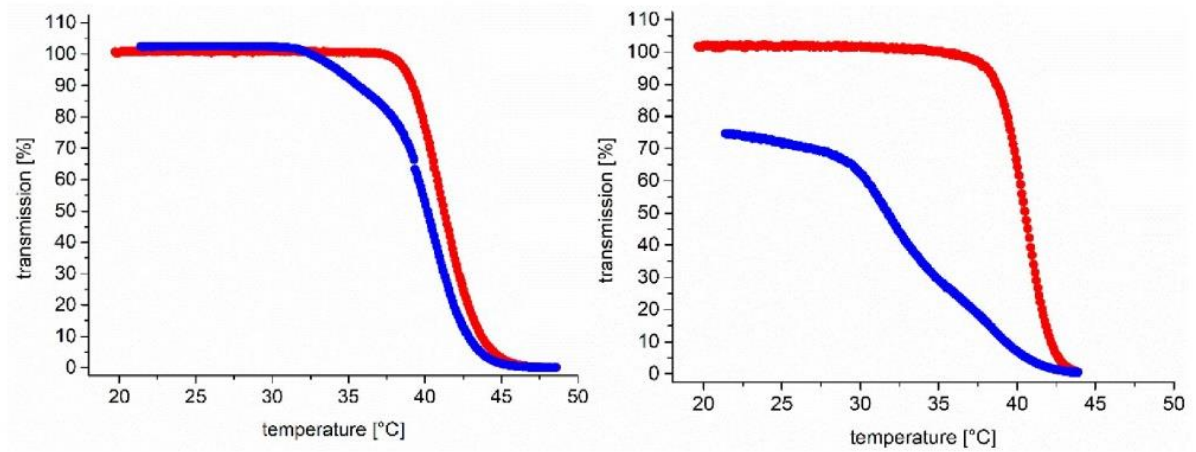


Figure S9g: Turbidity measurement of **ManEL2** with a polymer concentration of 5 mg mL⁻¹ in LBB, left: without ConA, right: with ConA.

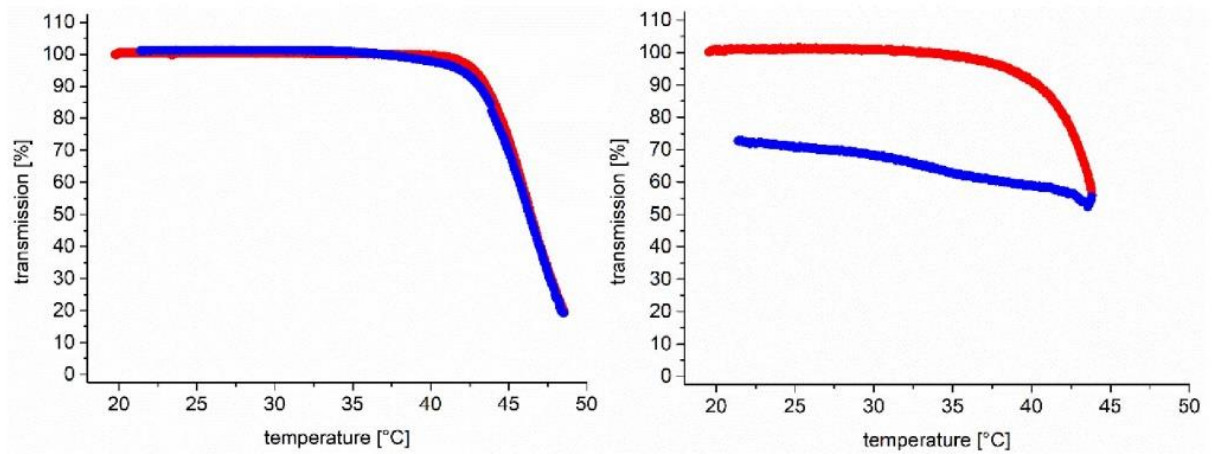


Figure S9h: Turbidity measurement of **ManEL5** with a polymer concentration of 5 mg mL⁻¹ in LBB, left: without ConA, right: with ConA.

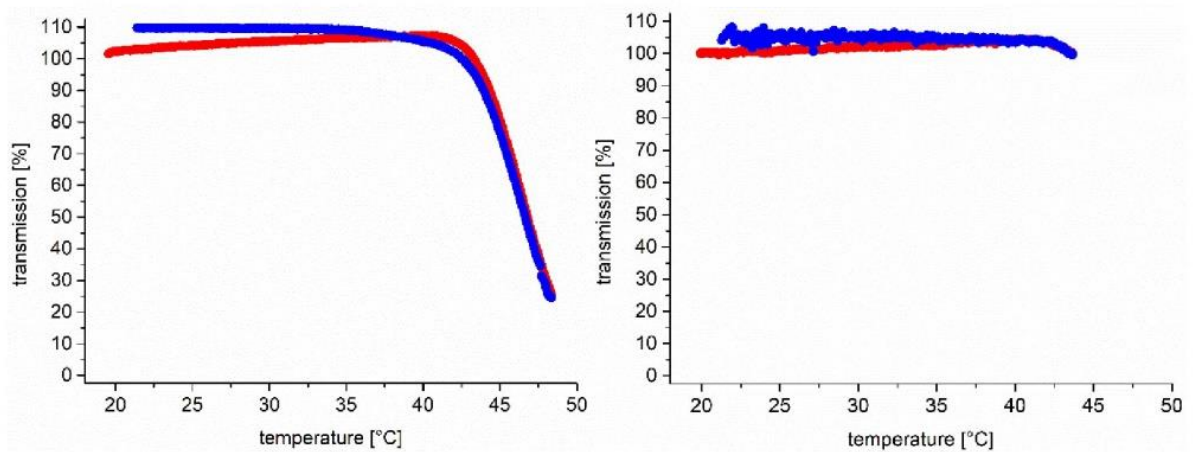


Figure S9i: Turbidity measurements of **GalHPL3** with a polymer concentration of 5 mg mL⁻¹ in LBB, left: without ConA, right: with ConA.

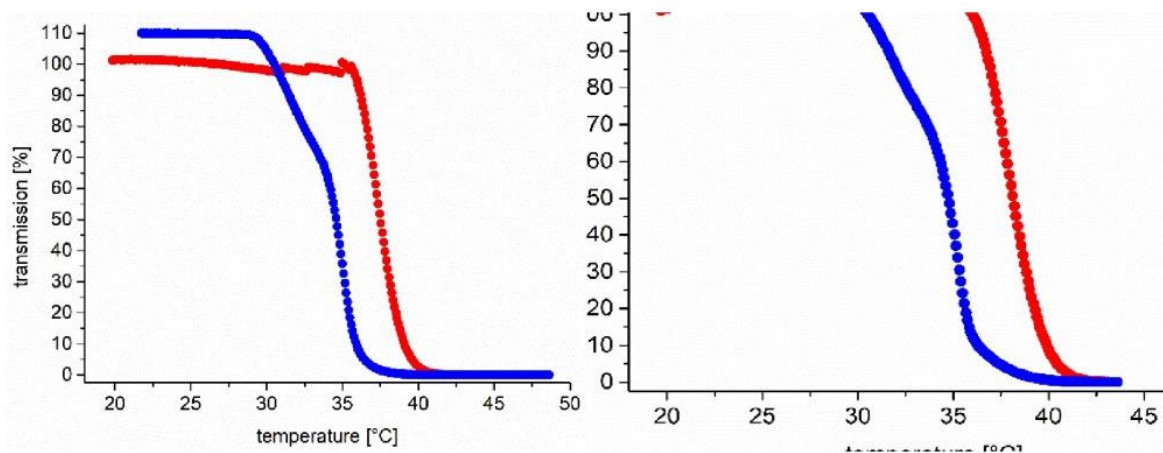


Figure S9j: Turbidity measurements of **PNIPAM** with a polymer concentration of 5 mg mL^{-1} in LBB, left: without ConA, right: with ConA.

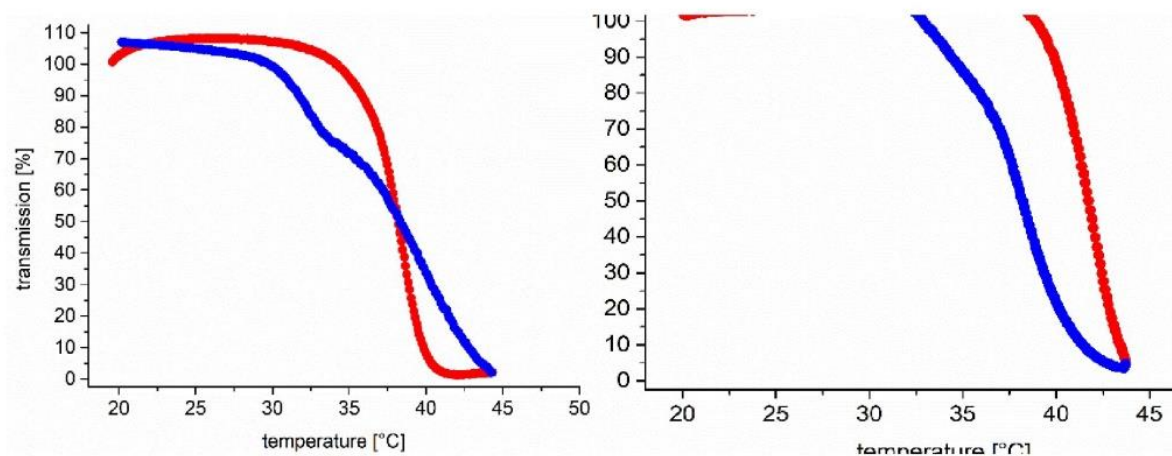


Figure S9k: Turbidity measurement of **ManHPL2** with a polymer concentration of 5 mg mL^{-1} in LBB, left: with ConA at a heating rate of 0.1 °C min^{-1} , right with ConA and 10 mM MeMan .

S10 Temperature dependent adhesion inhibition of *E. coli*

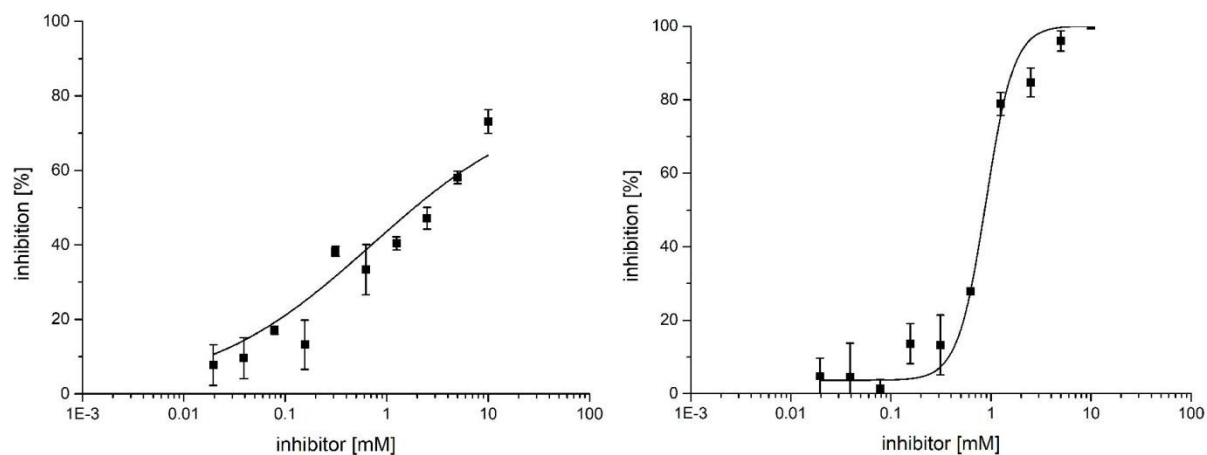


Figure S10a: Representative inhibition curves obtained in testing of **ManHPL1**. The curves result from one experiment and the depicted standard deviations from triplicate determinations on one plate, left: 20 °C, right: 40 °C.

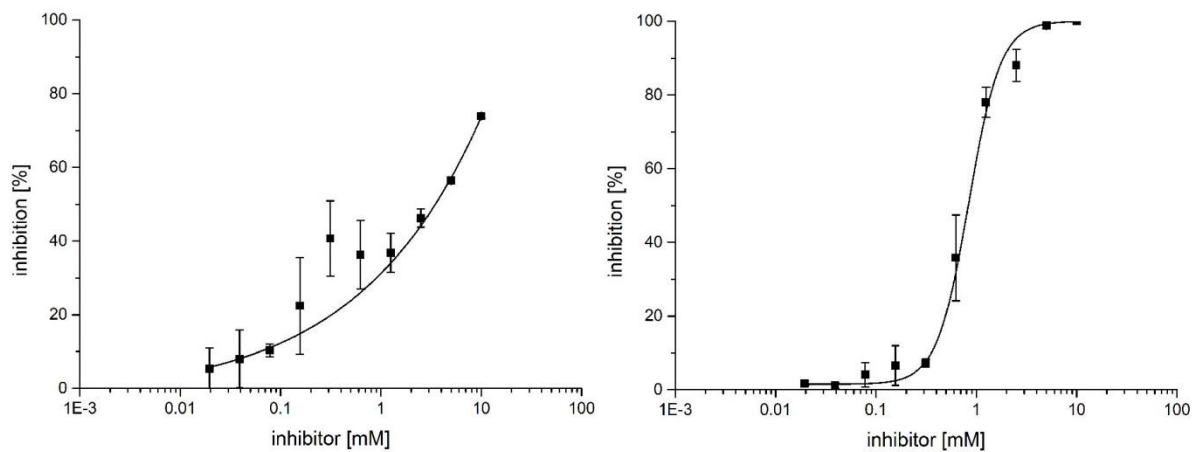


Figure S10b: Representative inhibition curves obtained in testing of **ManHPL2**. The curves result from one experiment and the depicted standard deviations from triplicate determinations on one plate, left: 20 °C, right: 40 °C.

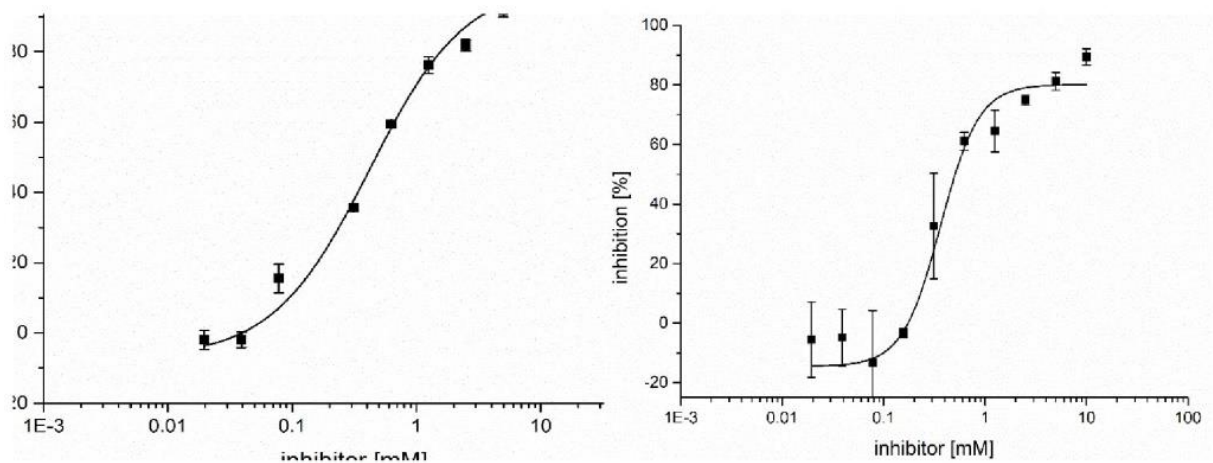


Figure S10c: Representative inhibition curves obtained in testing of **ManHPL7**. The curves result from one experiment and the depicted standard deviations from triplicate determinations on one plate, left: 20 °C, right: 40 °C.

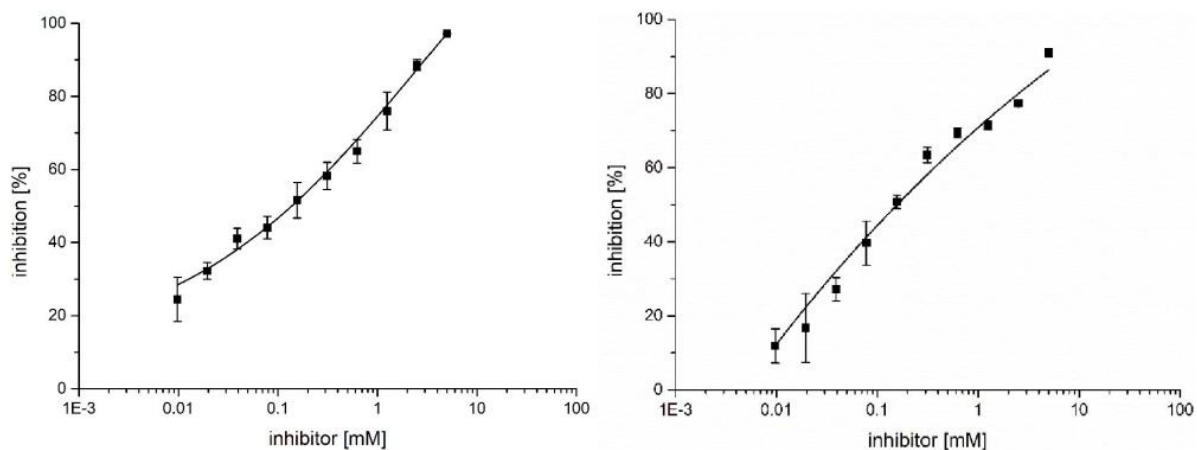


Figure S10d: Representative inhibition curves obtained in testing of **ManHPL97**. The curves result from one experiment and the depicted standard deviations from triplicate determinations on one plate, left: 20 °C, right: 40 °C.

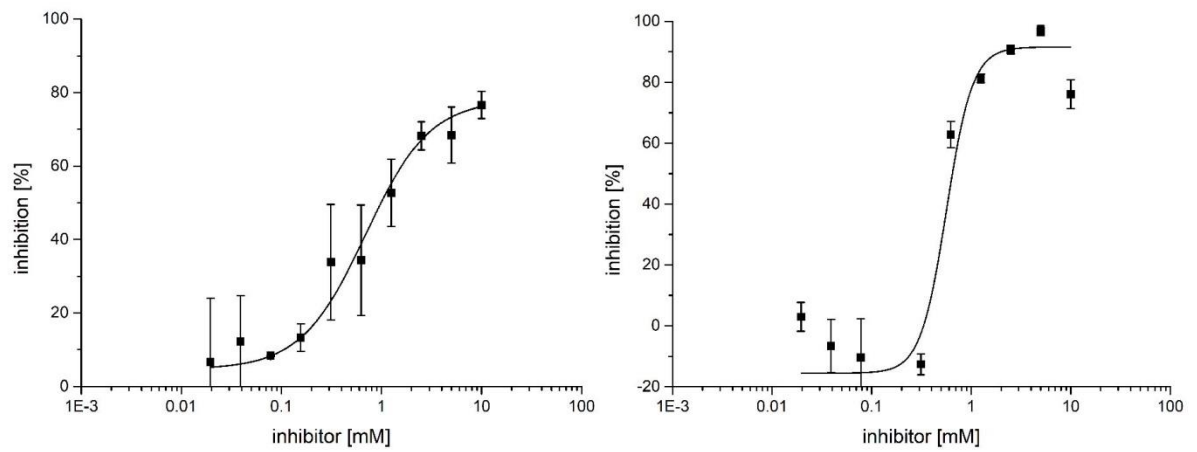


Figure S10e: Representative inhibition curves obtained in testing of **ManEL1**. The curves result from one experiment and the depicted standard deviations from triplicate determinations on one plate, left: 20 °C, right: 40 °C.

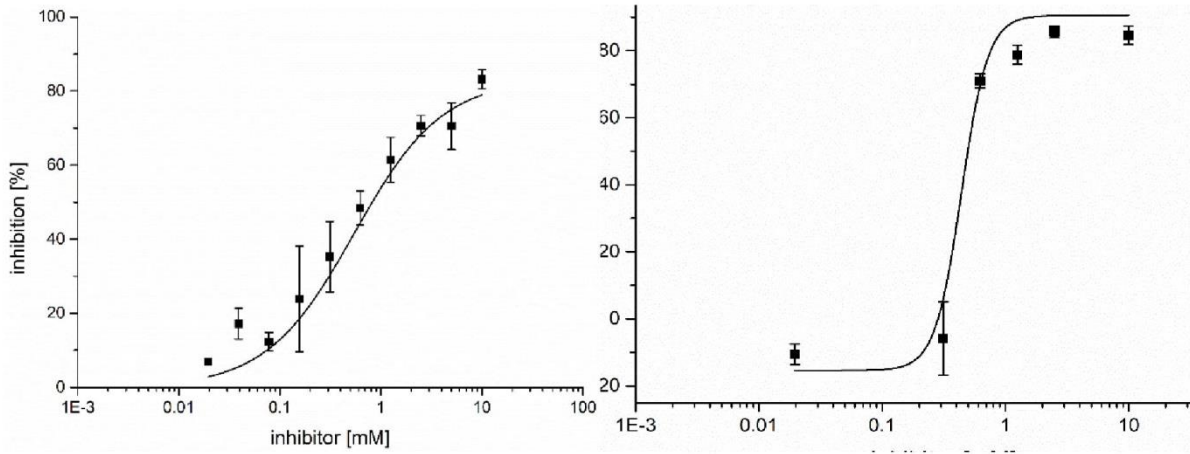


Figure S9f: Representative inhibition curves obtained in testing of **ManEL2**. The curves result from one experiment and the depicted standard deviations from triplicate determinations on one plate, left: 20 °C, right: 40 °C.

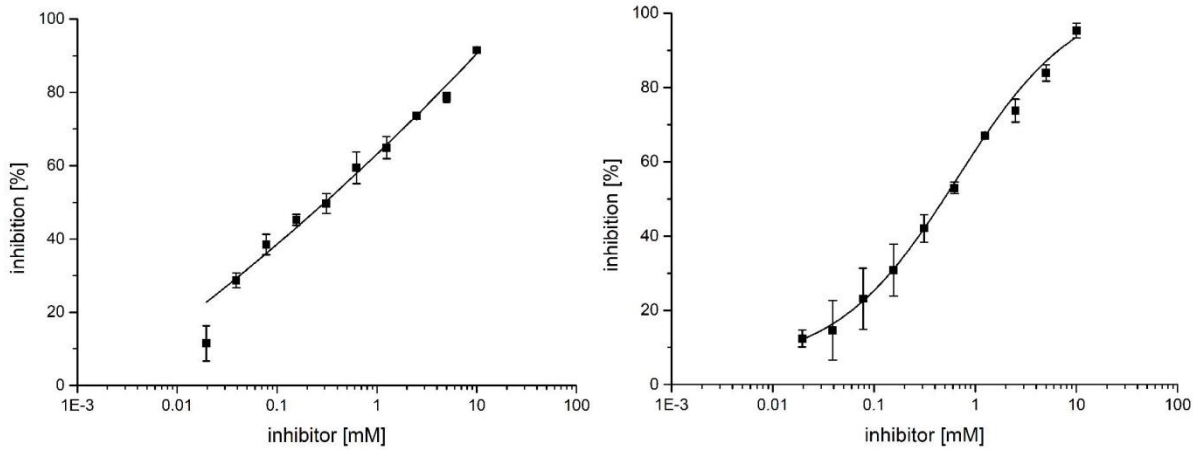


Figure S10g: Representative inhibition curves obtained in testing of **ManEL5**. The curves result from one experiment and the depicted standard deviations from triplicate determinations on one plate, left: 20 °C, right: 40 °C.

S11 Temperature dependent adhesion inhibition of ConA

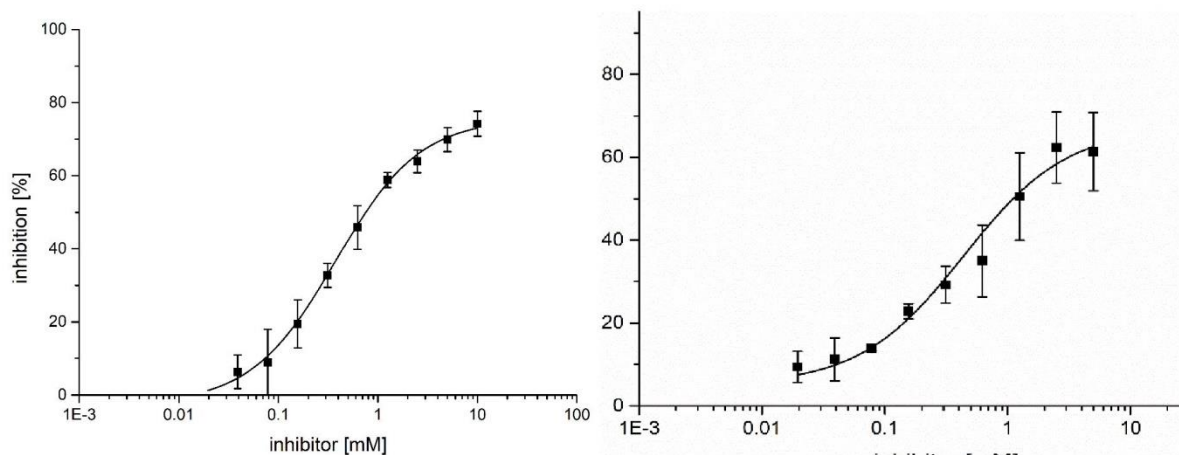


Figure S11a: Representative inhibition curves of ConA obtained in testing of **PNIPAM**. The curves result from one experiment and the depicted standard deviations from triplicate determinations on one plate, left: 20 °C, right: 40 °C.

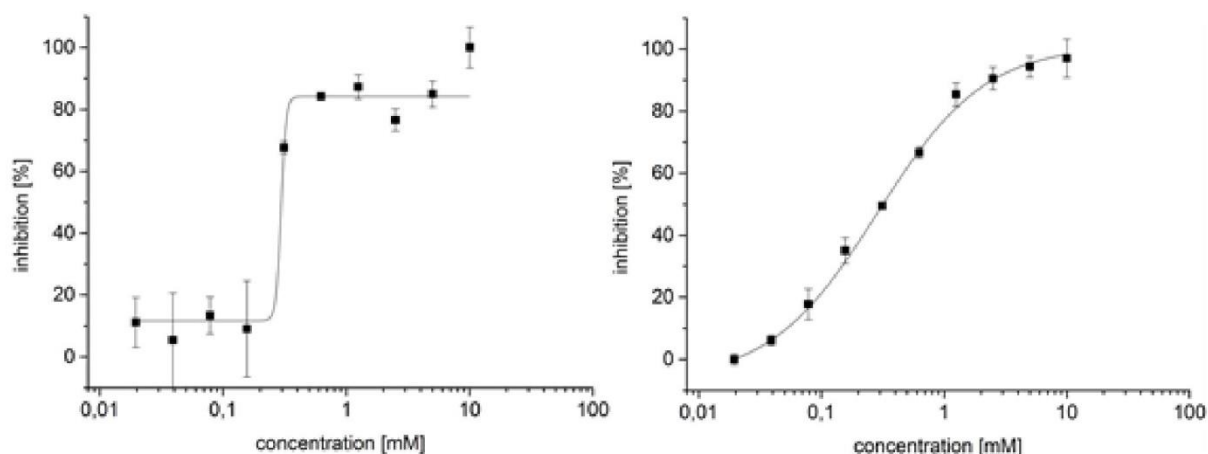


Figure S11b: Representative inhibition curves of ConA obtained in testing of **ManHPL1**. The curves result from one experiment and the depicted standard deviations from triplicate determinations on one plate, left: 20 °C, right: 40 °C.

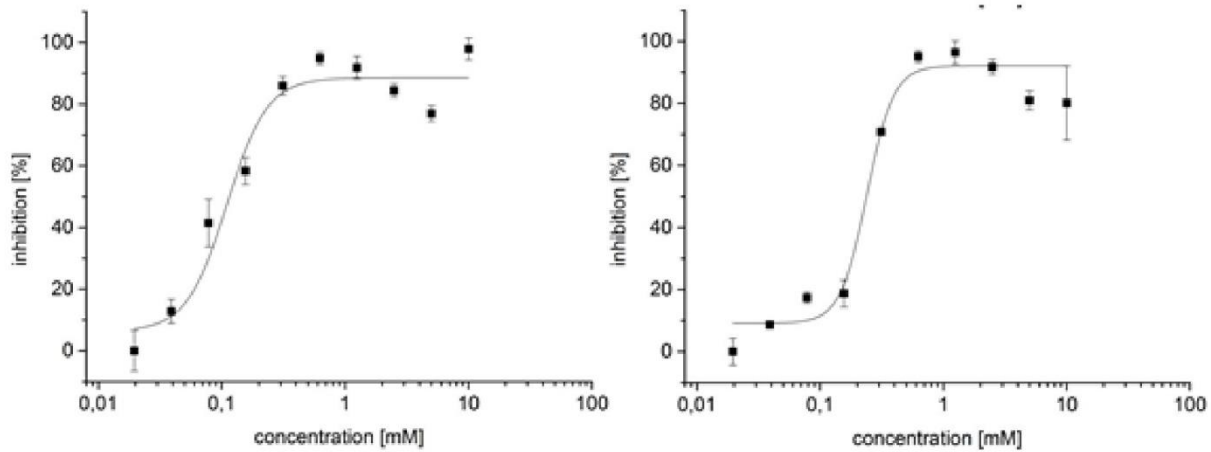


Figure S11c: Representative inhibition curves of ConA obtained in testing of **ManHPL2**. The curves result from one experiment and the depicted standard deviations from triplicate determinations on one plate, left: 20 °C, right: 40 °C.

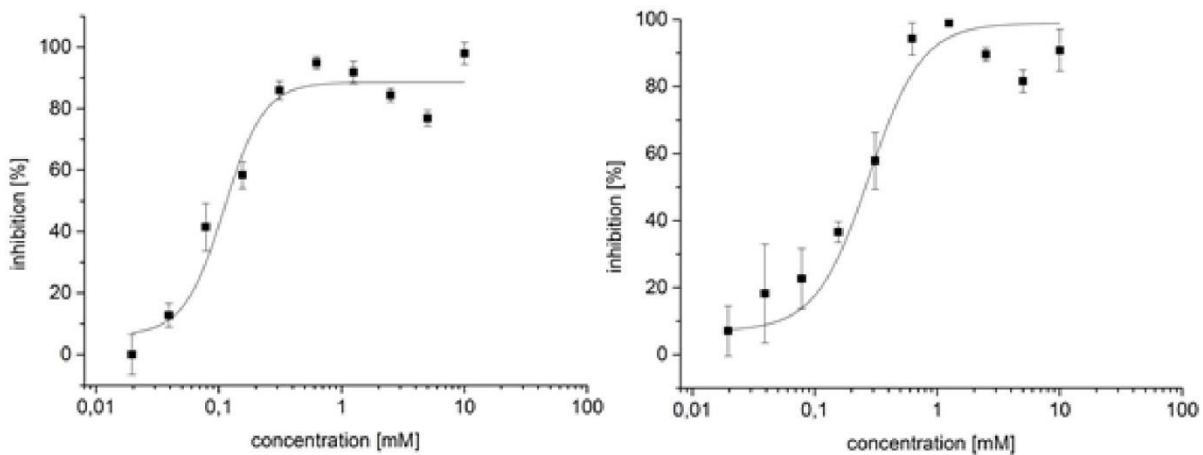


Figure S11d: Representative inhibition curves of ConA obtained in testing of **ManHPL7**. The curves result from one experiment and the depicted standard deviations from triplicate determinations on one plate, left: 20 °C, right: 40 °C.

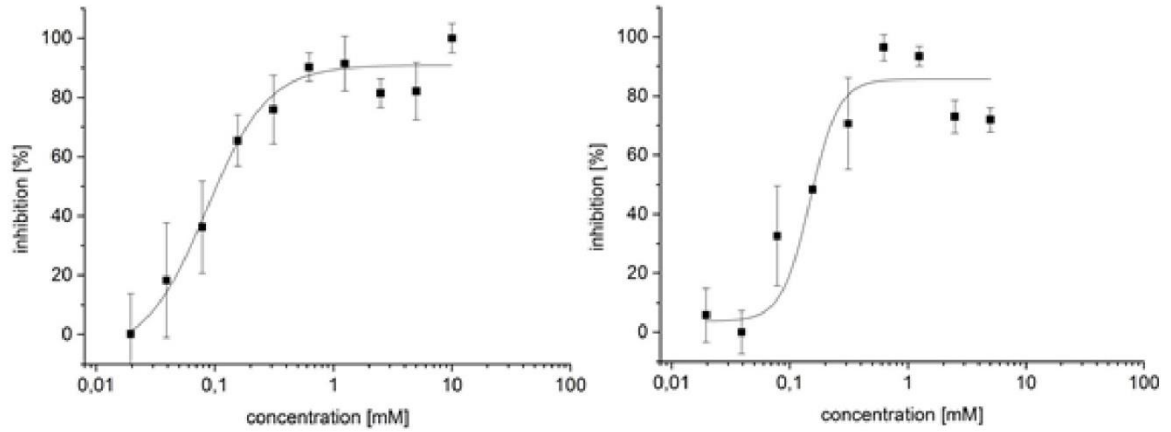


Figure S10e: Representative inhibition curves of ConA obtained in testing of **ManEL1**. The curves result from one experiment and the depicted standard deviations from triplicate determinations on one plate, left: 20 °C, right: 40 °C.

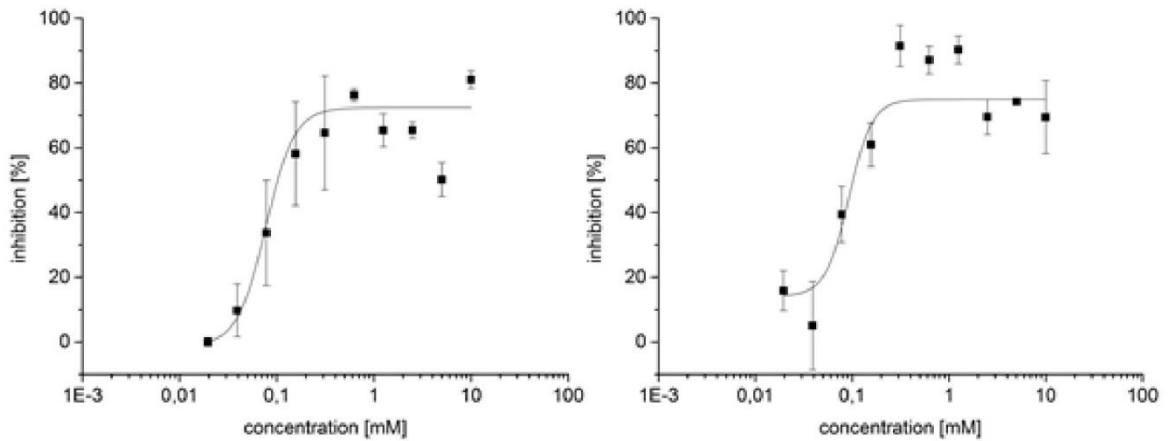


Figure S11f: Representative inhibition curves of ConA obtained in testing of **ManEL2**. The curves result from one experiment and the depicted standard deviations from triplicate determinations on one plate, left: 20 °C, right: 40 °C.

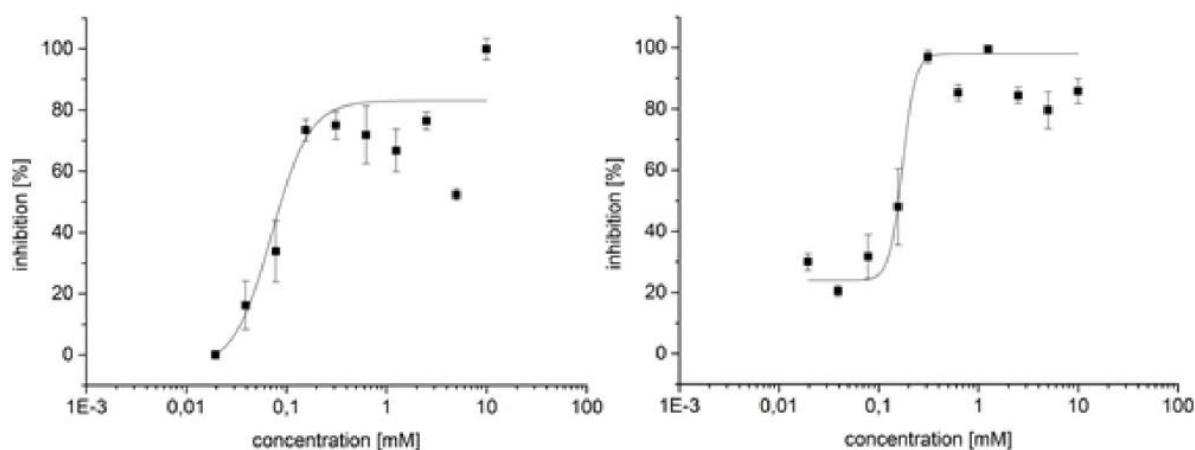


Figure S11g: Representative inhibition curves of ConA obtained in testing of **ManEL5**. The curves result from one experiment and the depicted standard deviations from triplicate determinations on one plate, left: 20 °C, right: 40 °C.

S12 Dynamic light scattering of the glycopolymers

Table S12: Hydrodynamic diameters as measured on a Malvern Nano ZS, scattering angle 173°, temperature 20°C, the dispersity was calculated from the cumulant I/μ^2 .

| polymer | hydrodynamic diameter | dispersity (DLS) |
|----------|-----------------------|------------------|
| ManHPL1 | 7.9 | 0.36 |
| ManHPL2 | 7.3 | 0.33 |
| ManEL1 | 8.3 | 0.38 |
| ManEL2 | 8.0 | 0.37 |
| ManHPL34 | 7.9 | 0.33 |
| ManHPL97 | 7.6 | 0.30 |

S13 Instrumentation

Nuclear Magnetic Resonance Spectroscopy (NMR)

^1H -NMR and ^{13}C -NMR (600 MHz) were measured on a Bruker AVANCE III 600 (Bremen, Germany). As internal standard chemical shifts were referenced to the residual non-deuterated solvents (CDCl_3 : ^1H 7.26, ^{13}C 77.16, D_2O : ^1H 4.79, $\text{DMSO-}d_6$: ^1H 2.50). All chemical shifts are reported in delta (δ) expressed in parts per million (ppm). The following abbreviations were used to indicate multiplicities: s = singlet, d = doublet, t = triplet, m = multiplet.

Size exclusion chromatography (SEC)

SEC measurements were performed using a ViscotekGPCmax VE2001 system. The System has a column set comprising one TSK HHR-H, 100 Å pore size and 10 μm particle size, 800 \times 5.0 mm [Length \times ID]pre-column and two Viskotek TSK GMHHR-M linear, 10 μm particle

size, 300 × 8.0 mm [Length × ID] columns. The columns were constantly heated to a temperature of 60 °C. N,N-Dimethylformamide (0.05 M LiBr) was used as eluent at a flow rate of 1 mL min⁻¹. For detection a Viscotek VE 3500 RI detector was used. The system was calibrated with polystyrene standards of a molecular range from 1280 g mol⁻¹ to 1373000 g mol⁻¹.

ATR-FTIR Spectroscopy

For ATR-FTIR spectroscopy measurements a NICOLET 6700 ATR-FTIR spectrometer from Thermo Scientific was used. For each measurement a background measurement was executed that was subtracted from the sample measurement.

Freeze Dryer

An Alpha 1-4 LD plus instrument from Martin Christ Freeze Dryers GmbH (Osterrode, Germany) was used for lyophilization of all polymer samples. The main drying method was set to -54 °C and 0.1 mbar.

UV-Vis Spectroscopy

On a dual-trace spectrometer Specord® 210 Plus from *Analytik Jena AG* (Jena, Germany) all UV-Vis measurements were performed at 25 °C. Using Win ASPECT PLUS software the instrument was operated. Protein concentration measurements were performed in a cuvette QX quartz cuvette (d = 1 cm, V = 3.5 mL) from Hellma Analytics (Mühlheim, Germany). For determination of sugar concentration the absorption from 350-550 nm was measured. Using the absorption and a calibration curve the concentration of carbohydrates was calculated.

Dynamic differential scanning calorimetry (DSC)

Dynamic differential scanning calorimetry (differential scanning calorimetry, DSC) was performed on a DSC 3 equipped with a FRS 5/5+ Sensor, an IntraCooler Julabo FT900 and a GC005 Gas controller of the company Mettler Toledo. Aluminum crucible with a volume of 40 µL without pin were used for the measurements. The heating and cooling rates were 15 K min⁻¹ with a total of nine segments each in a temperature range from -50 °C to 200 °C.

Microplate reader

All adhesion inhibition measurements were performed on a CLARIOstar® microplate reader from BMG LABTECH (Freiburg, Germany) at ambient temperature. Using the BMG Mars

software the measurements were evaluated. For all measurements F-bottom 96 black well plates from Greiner BIO-ONE were used.

S14 Buffer and Media

LB-Medium (PKL1162)

12.5 g of LB Broth (Miller) (powder microbial growth medium) were dissolved in 500 mL ultrapure water. The powder contains tryptone (5.0 g), sodium chloride (5.0 g) and yeast extract (2.5 g). Afterwards the solution was sterilized for 30 min at 121 °C and cooled to room temperature. 50.0 mg of ampicillin and 25.0 mg of chloramphenicol were added.

PBS buffer

Five tablets of phosphate buffered saline was dissolved in 1 L of ultrapure water. The final concentrations of the buffer were 0.01 M phosphate buffer, 0.0027 M potassium chloride and 0.137 M sodium chloride. The pH was checked with a potentiometer and set to 7.4.

LBB buffer

Lectin binding buffer (LBB) was used for all measurements with Concanavalin A. Lectin binding buffer contains 10 mM HEPES ((4-(2-hydroxyethyl)-1-piperazineethanesulfonic acid) as buffering agent, which was adjusted to a pH of 7.4 with 1 M NaOH. Thereafter, calcium chloride (1 mM) and manganese chloride (1 mM) and sodium chloride (50 mM) were dissolved in the solution. To prevent bacterial growth in the buffer sodium azide was added to a final concentration of 0.05 wt%

Carbonate-buffer solution

For the carbonate-buffer solution 1.59 g sodium carbonate and 2.52 g sodium hydrogen carbonate were dissolved in 1 of ultrapure water. Afterwards the pH was adjusted to pH 9.5.

Bacterial culture

E. coli PKL 1162 were grown in LB medium (PKL 1162) overnight in a sterilized test tube, which was covered with aluminum foil at 37 °C. The tubes were shaken with a speed of 140 rpm to guarantee a constant mixing of the solution.

1. J. A. Himanen and P. M. Pihko, *Eur. J. Org. Chem.*, 2012, DOI: 10.1002/ejoc.201200277, 3765-3780.
2. W. Hayes, H. M. I. Osborn, S. D. Osborne, R. A. Rastall and B. Romagnoli, *Tetrahedron*, 2003, **59**, 7983-7996.

4.3. Temperature-controlled adhesion to carbohydrate functionalized microgel coatings: an *E. coli* and lectin binding study

Authors: Tanja J. Paul, Alexander K. Strzelczyk, Stephan Schmidt

Issue: In preparation

Type of Paper: Full paper

Own Contribution (first author)

Collaborative design of the synthetic strategy, synthesis of glycomonomers and microgels. Characterization of the microgels via DLS and determination of the carbohydrate density via phenol sulfuric acid method. Microplate coating studies and performance of FITC-ConA and *E.coli* adhesion inhibition assay. Performance of fluorescence microscopy measurements. Interpretation of data and writing of the first manuscript draft followed by collaborative finalization of the manuscript.

Temperature-controlled adhesion to carbohydrate functionalized microgel films: an *E. coli* and lectin binding study

*Tanja J. Paul†, Alexander K. Strzelczyk and Stephan Schmidt**

†Institute of Organic and Macromolecular Chemistry, Heinrich-Heine-University Düsseldorf,
Universitätsstraße 1, 40225 Düsseldorf, Germany

Email: Stephan Schmidt – stephan.schmidt@hhu.de

* Corresponding author

KEYWORDS: responsive material, concanavalin A, microgel surface, temperature stimulus,
LCST, NIPAM, glycocalyx, biomimetic, multivalent

Abstract

The straightforward preparation of thermoresponsive mannose-functionalized monolayers of poly(*N*-isopropylacrylamide) microgels and the analysis of the specific binding of concanavalin A (ConA) and *Escherichia coli* (*E. coli*) above and below the lower critical solution temperature (LCST) are shown. Using an inhibition and direct binding assay, it was found that ConA binding is time-dependent, where at short incubation times binding is preferred below the LCST. Given sufficient time for binding to the microgel network above the LCST, the interaction of ConA to the microgel network was increased, possibly due to the flexibility of the mannose-functionalized network. For *E. coli* which is too large to diffuse into the network and presents only a monovalent lectin (FimH), binding is enhanced above the LCST. This is due to the increased mannose density of the microgel layer above the LCST, increasing the interaction to *E. coli* due to statistical binding. Importantly, once bound to the microgel layer above the LCST, neither ConA or *E. coli* could be released by a significant degree by cooling down below the LCST. Overall, this suggests that the microgel layers enable the controllable specific adhesion of carbohydrate binding species at low reversibility and that multivalent binding of small receptors in polymer networks can be enhanced by an increased network porosity and flexibility.

1. Introduction

Carbohydrates as a major component of cell surfaces mediate countless processes at the cell surface like adhesion, cell-cell communication, signal transduction and fertilization.¹⁻² Also pathogenic bacteria can harness surface-anchored carbohydrates, e.g. at the glycocalyx of the cell, to attach to cells, to colonize and to start infections.³⁻⁴ On the bacteria side these interactions are mediated by lectins, i.e. receptors at the tip of long hair-like protein complex called fimbriae.⁵⁻⁶ A prominent example of pathogens adhering to glycosylated cell surfaces is *Escherichia coli* (*E. coli*) via the mannose-specific binding site FimH at the tip of the fimbriae. *E. coli* can cause numerous infectious diseases including neonatal meningitis leading to high fatality rates of new-born children in developing countries.⁷⁻⁹ Due to the ongoing antimicrobial resistance crisis¹⁰ making it increasingly harder to fight such infections, the inhibition of bacterial lectins has been proposed as a new treatment strategy.¹¹ Such inhibitors are based on multivalent natural carbohydrates or glycoconjugates that bind to lectins with high avidity, thereby blocking them, resulting in reduced pathogen adhesion and invasion.¹²⁻¹⁷

On the other hand, surface coatings of such glycoconjugates are quite auspicious for capturing specific bacteria, e.g. in water purification, for the detection of biological contaminants or for quantifying carbohydrate-cell interactions.¹⁸⁻²⁰ For practical considerations and to improve the viability of such surfaces, it is desirable to be able to remotely control the binding of bacteria to such surfaces. For example, to capture the bacteria in a first stage to remove the contaminant and to release the bacteria in a second stage for diagnostics or simply reusing the coating. As of yet, several groups reported on the synthesis of remotely switchable thermoresponsive carbohydrate presenting LCST-polymer brushes and tested their binding to bacteria and other lectins.²¹⁻²⁶ Upon temperature increase, these polymer brushes collapse and thereby increasing the density of the

carbohydrates residues and decreasing the steric repulsion by reducing the excluded volume of the polymer chains, which leads to an increase of carbohydrate receptor binding.²⁷ Although the capture of lectins and bacteria could be readily switched “on” by raising the temperature above the phase transition temperature of the polymer, the release of bacteria or protein by lowering the temperature was not yet reported perhaps due to the strong hysteresis of the switchable glycopolymers brushes in the bound and collapsed state.²⁸

In comparison to polymer brushes, microgels allow quite simple coating procedures, and a special surface functionalization step is not needed.²⁹ Furthermore, when compared to thin polymer brushes microgel monolayers in water exhibit thicknesses of several hundred nanometers, and mimic the mechanical properties of the cell environment.³⁰⁻³¹ In addition, several groups presented the synthesis of carbohydrate functionalized microgels for the switchable binding of carbohydrate binding proteins.³²⁻³⁴ Typically, such thermosensitive microgels are composed of poly(*N*-isopropylacrylamide) or poly(oligo ethylene glycol acrylates).³⁵ Quite similarly to thermosensitive polymers, by increasing the temperature above the LCST carbohydrate functionalized microgels form polymer-polymer contacts and collapse, thereby decreasing the steric repulsion while increasing the carbohydrate density as well as the elastic modulus,^{30-31, 36} which increases *E. coli* clustering in solution.³⁴ The temperature-dependent shifts in the microgels’ elastic modulus and surface roughness can be used to create switchable cell culture surfaces that enable the controlled attachment and detachment of cells even without addressing specific cell adhesion receptors.^{31, 36-37} However, microgel coatings specifically targeting selected cells, e.g. bacteria via lectin, have not been studied so far. Therefore, in this work we aim at coatings of mannose-functionalized poly(*N*-isopropylacrylamide) microgels to test their specific temperature-dependent binding of *E. coli* in comparison to a mannose-specific model lectin (concanavalin A, ConA). We target at

the underlying mechanisms of lectin and bacterial adhesion at the soft, fuzzy microgel networks as a function of the temperature and mannose ligand density. The carbohydrate interactions of these coatings are studied via a direct binding assay and an inhibition assay at different incubation times. Finally, the requirements to again release bound bacteria and lectin from the microgel coatings are tested as well.

2. Experimental Section

2.1 Materials

N-isopropylacrylamide (NIPAM) (99%), *N,N'*-Methylenebisacrylamide (MBA) (99%), ethanol ($\geq 99.8\%$), acetic acid (99.8-100%), *p*-toluic acid (98%), phosphate buffered saline tablets (PBS), sodium methoxide ($\geq 97.5\%$), Amberlite IR 120 (hydrogen form), acetic anhydride (99.5%), manganese chloride (99%), sulfuric acid (95-98%), ammonium persulfate (APS) (98%), LB Broth (Miller, powder microbial growth medium), ethanolamine ($\geq 98\%$), dichloromethane ($\geq 99.9\%$), triethylamine ($\geq 99.5\%$), *N*-hydroxyethyl acrylamide (97%), Concanavalin A from *Canavalia ensiformis* (Jack bean) (FITC conjugate, Type IV, lyophilized powder), HEPES ($\geq 99.5\%$), methyl α -D-mannopyranoside ($\geq 99.0\%$), mannan from *Saccharomyces cerevisiae* (prepared by alkaline extraction), TWEEN® 20 (for molecular biology), chloramphenicol ($\geq 98\%$) and ampicillin sodium salt (BioReagent) were all purchased from Sigma Aldrich. Sodium dodecyl sulfate (SDS) ($\geq 99\%$), tetrahydrofuran (99.8%), ethyl acetate (99.5%), dimethyl sulfoxide ($\geq 99.9\%$), methacryloyl chloride (97%) and α -D-mannose were purchased from Acros Organics. Sodium chloride (99.98%), phenol (99%), acetonitrile (HPLC gradient grade) ($\geq 99.9\%$), magnesium sulfate (laboratory reagent grade), chloroform (99.9%), methanol (99.99%) were purchased from Fischer Scientific. n-hexane (99.9%) was purchased from VWR chemicals. Sodium hydrogen

carbonate (99%) was purchased from Appli Chem. Boron trifluoride diethyl etherate (98%) was purchased from Alfa Aesar.

2.2 Microgel synthesis

The polymerization was carried out as described previously.³⁴ In a 100 mL three-necked flask fitted with a condenser 75 mL ultrapure water, 0.7 g *N*-Isopropylacrylamide (NIPAM, 6.19 mmol), 0.05 g *N,N'*-Methylenebisacrylamide (MBA, 0.324 mmol), 0.025 g (0.087 mmol) sodium dodecyl sulfate (SDS) and the deprotected glycomonomer were added (supporting information S2). The used amount of deprotected glycomonomers differ for each polymerization batch (supporting information S2). The solution was stirred at 350 rpm with a magnetic stir bar and heated to 70 °C under a nitrogen purge for at least 40 min to remove dissolved oxygen. Next, the initiator ammonium persulfate (0.2 g, 0.9 mmol) was dissolved in 5 mL ultrapure water and added to the reaction solution to start the polymerization. During the reaction the solution was continuously purged with nitrogen and stirred at 350 rpm. The reaction was stopped after 55 min by cooling with an ice bath. After filtration by glass wool, the reactants were removed by repeated centrifugation at 10000 g and washing with water.

2.3 Phenol-sulfuric acid method (PSA)

The phenol-sulfuric acid method was used to quantify the number of glycomonomers that were included into the microgel network. First, a calibration curve was established using previously reported procedures.³⁸⁻³⁹ Using a stock solution of 320 μM methyl α-D-mannopyranoside (MeMan) a dilution series of 20 ,40 ,80 160 μM was prepared in water. To 125 μL of each solution, 125 μL 5 wt% phenol solution in ultrapure water were given, thoroughly mixed, followed by the rapid addition of 625 μL concentrated sulfuric acid and incubation for 30 min at ambient temperature. The absorbance was measured at 490 nm via UV-Vis-spectroscopy. For the

measurements of the microgel samples mixtures of 125 μL of a 0.5 wt% microgel dispersion and 125 μL of a 5 wt% phenol solution in ultrapure water were prepared. Afterward 625 μL concentrated sulfuric acid were added rapidly and incubated for 30 min at ambient temperature. After cooling, the solutions were centrifuged at 10000 g for 20 min, followed by analyzing the supernatant.

2.4 Dynamic light scattering

Measurements were performed on a Malvern NanoZS (Malvern Panalytical, Kassel, Germany) equipped with a 633 nm He/Ne-laser in backscattering configuration (171°). Microgel samples (0.05 wt%) in 1 cm polystyrene cuvettes were analyzed in a temperature range of 20 $^\circ\text{C}$ to 40 $^\circ\text{C}$ with a temperature increment of 2 $^\circ\text{C}$ and a 10-minute equilibration time between the temperature steps. For evaluating the autocorrelation functions, the decay constant and first cumulant were determined by exponential fits and the hydrodynamic radii were calculated by the Stokes-Einstein relation. For comparison, selected microgel samples were analyzed on a Nicomp 3000 setup (Particle Sizing Systems, FL, USA) at a scattering angle of 90° showing good agreement with hydrodynamic radii determined in the backscattering setup.

2.5 Atomic Force Microscopy (AFM)

AFM of dried microgel films was conducted on a JPK NanoWizard 2 (JPK Instruments AG, Berlin, Germany) using cantilevers with a nominal spring constant of 300 N/m (HQ:XSC11, MikroMash, Bulgaria) in tapping mode.

2.6 Microplate microgel coating

For coating of the 96-well plates 120 μL of a 0.1 mg/mL solution of microgel in ultrapure water were filled in each well. The plates were dried at 37 $^{\circ}\text{C}$ and shaken at 120 rpm overnight. On the next day, the plates were washed with PBST (PBS with 0.5 wt% Tween 20, 3 x 120 μL per well).

2.7 FITC-ConA adhesion inhibition assay

In the microgel coated microplate a dilution series of MeMan was prepared. 50 μL of FITC-ConA solution in LBB ($c = 0.1$ mg/mL) was added to the wells and the plates were incubated for 30 min or 24 h at 100 rpm at either 20 $^{\circ}\text{C}$ or 40 $^{\circ}\text{C}$. Afterward, the plates were washed three times with 120 μL of LBB and then filled with 100 μL of LBB per well. The LBB washing buffer was tempered either at 20 $^{\circ}\text{C}$ or 40 $^{\circ}\text{C}$. Finally, the fluorescence intensity was detected at 485 nm/535 nm and plotted as a function of the MeMan concentration to construct the inhibition curves (supporting information S4).

2.8 *E. coli* adhesion inhibition assay

The *E. coli* adhesion assay was carried out according to a recent protocol.⁴⁰ In the microgel coated microplate a dilution series of MeMan was prepared. A suspension of the GFP-expressing *E. coli* (50 μL , 2 mg/mL, OD = 0.4) was added to the wells (supporting information S5), followed by incubation for 30 min or, respectively, 24 h on a shaker (100 rpm) at either 20 $^{\circ}\text{C}$ or 40 $^{\circ}\text{C}$. Afterward, the plates were washed three times with 120 μL of PBS and then filled with 100 μL of PBS per well. The PBS washing buffer was tempered at either 20 $^{\circ}\text{C}$ or 40 $^{\circ}\text{C}$. Finally, the fluorescence intensity of the adhered *E. coli* was detected at 485 nm/535 nm, see supporting information S6 for the inhibition curves.

2.9 Fluorescence microscopy

The green fluorescent protein (GFP)-expressing *E. coli* (PKL1162) and FITC-ConA were imaged on an inverted microscope (Olympus IX73, Japan) equipped with an Olympus 60x NA 1.35 oil-immersion objective (Olympus, Japan), and a CMOS camera (DMK 33UXI174L, The Imaging Source, Germany) was used for imaging. Pictures were taken immediately after the washing cycles of the microplates.

2.10 Washing experiments

The beforehand measured microplates were again washed with cold (20 °C) or warm (40 °C) buffer solution. Therefore, in each washing cycle the microwells were filled with 120 μ L buffer, which was removed afterward, and then the wells were filled again with 120 μ L and the fluorescence intensity was readout.

3. Results and discussion

3.1. Synthesis of Carbohydrate-Functionalized Microgels

By copolymerizing different amounts of the mannose comonomers (ManEAm or ManEMAm) with NIPAM and a bifunctional crosslinker, we obtained microgels with varying mannose densities in a single synthesis step.³⁴ The mannose functionalization degree in the microgel, i.e. the amount of mannose monomer as compared to NIPAM repeat units, was 0.4 to 0.8 mol%. The samples are termed by the type and of the mannose functionalization degree, e.g. Man0.5 signifies microgels with a functionalization degree of 0.5% ManEAm. ManM0.4 and ManM0.8 describes microgels with a functionalization degree of 0.4% and, respectively, 0.8% ManEMAm. To characterize the hydrodynamic radii and swelling ratio between 20 °C and 40 °C, dynamic light

scattering (DLS) was used (see **Table 1**). DLS measurements show that both microgels with ManEMAm as comonomer have nearly the same hydrodynamic radii and the same swelling ratio although the amount of carbohydrate within the microgels is doubled. It appears that ManEMAm was incorporated into the microgel network at a higher rate as compared to ManEAm, since for Man0.5 and ManM0.8 the same molar ratios of comonomer were used, but a significantly larger amount of comonomer was incorporated for ManM0.8. From the polymerization kinetics the opposite behavior could be expected, i.e. acrylamides (ManEAm) polymerize and integrate into the microgel network faster than methacrylamides (ManEMAm). However, the polymerization was conducted above the LCST of PNIPAM where small surfactant-stabilized hydrophobic microgel precursors are formed first.³⁵ It is likely that the more hydrophobic ManEMAm is incorporated better to these growing microgel precursors as compared to the more hydrophilic monomer ManEAm. Such differences in microgel growth may explain varying microgel compositions and differences in hydrodynamic radius and swelling ratio.⁴¹ Here, Man0.5 with ManEAm as comonomer was smaller but exhibited a higher swelling ratio as compared to the ManM0.4 and ManM0.8 microgels.

Table 1. Hydrodynamic radii (R_h) and PDI of microgel samples determined via DLS, and their swelling degree additional to their carbohydrate density.

| sample name | R_h at 20 °C [nm] | PDI (DLS) | swelling ratio R_{h20}/R_{h40} | mannose functionalization degree [$\mu\text{mol g}^{-1}$] | mannose functionalization degree [%monomer] |
|-------------|---------------------|-----------|----------------------------------|---|---|
| Man0.5 | 268 ± 28 | 0.07 | 3.2 | 43 ± 4 | 0.5 |
| ManM0.4 | 365 ± 16 | 0.16 | 2.5 | 32 ± 3 | 0.4 |
| ManM0.8 | 361 ± 27 | 0.33 | 2.3 | 67 ± 5 | 0.8 |

With the three different microgels, the functionalization of microwell plate surfaces was tested to find the optimum microgel density. For consistent results in ConA and *E. coli* binding assays, it is important that the microgel films in the microwells were reproducible. Therefore, microplate surfaces were coated by straightforward drop-casting method, which included drying a microgel suspension on the multiwells followed by annealing and washing with the measurement buffer. To find out the optimal microgel surface density, different microgel concentrations (120 μL , 1 mg/mL to 0.002 mg/mL) of ManM0.4 were drop-casted in a microwell plate, and the fluorescence intensity was read out after incubation/washing with *E. coli* or FITC labeled ConA (**Figure 1**). The results showed a plateau of bound ConA and *E. coli* at around 0.1 mg/mL of microgels. AFM measurements showed that at this microgel concentration closed monolayers are formed. Therefore, all following binding assays were conducted with microgel coatings prepared from this microgel concentration and the same drop-casting procedure to assure reproducible microgel monolayers.

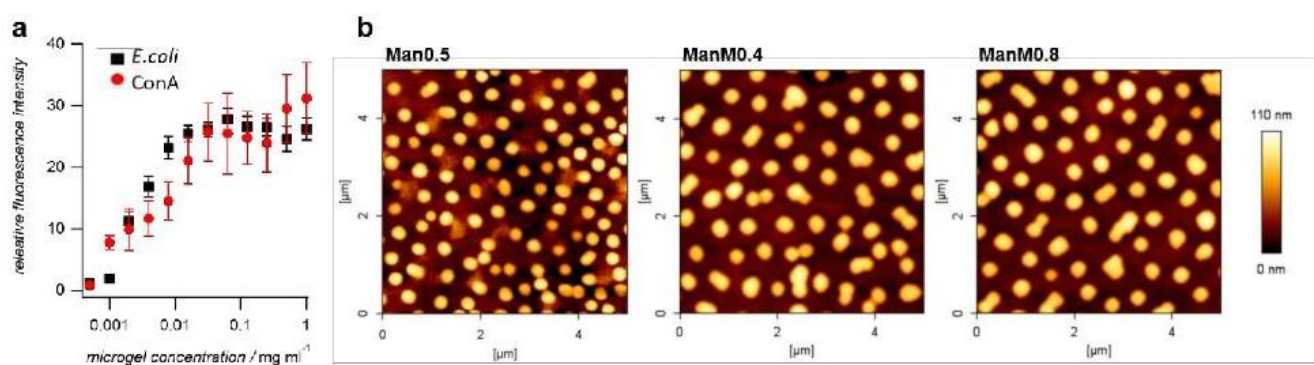


Figure 1. ManM0.4 microwell plate coatings a) *E. coli* and ConA binding as measured by fluorescence readout depended on the microgel dispersion concentration used to coat the microplate surface. Reproducible results are obtained in the plateau region around 0.1 mg/mL. b) AFM images prepared at this concentration showed monolayers. The average spacing between microgels centers coincides with the microgels' hydrodynamic diameters indicating close packed monolayers in solution.

3.2. ConA binding to microgel surfaces

Having identified the conditions for surface microgel coating, microwell plates were prepared for adhesion studies using ConA as receptor. ConA is a well-known homotetrameric model lectin that binds α -D-mannopyranoside.⁴² In the inhibition assay different amounts of the inhibitor α -D-methyl mannopyranoside (MeMan) were added to determine the inhibitory concentration (IC₅₀-values, **Figure 2**, left). IC₅₀-values show the amount of inhibitor necessary to reduce the amount of bound receptor by 50%. This means that at higher IC₅₀-values a larger amount of inhibitor was necessary to inhibit the binding between ConA and the microgel surface, thus the interaction was stronger. Comparing the IC₅₀-values at different temperatures show how the microgel phase transition affects the binding between protein receptor and the microgel surface. To directly measure the amount of bound ConA, microscope-based fluorescence measurements were carried

out on microgel layers adsorbed to the same polystyrene microwell plates used for the inhibition assay (**Figure 2**, right). The inhibition assay shows how strong ConA is bound to the microgel surfaces whereas the direct binding assay shows how much ConA binds to the microgel surfaces.

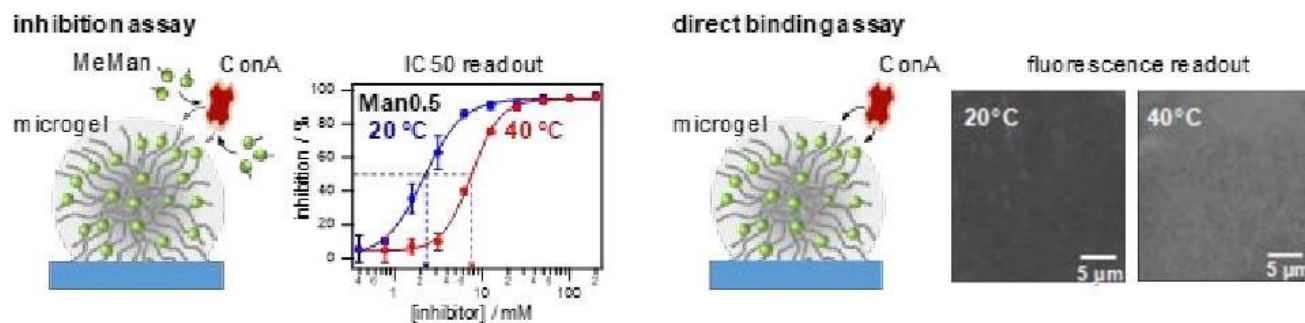


Figure 2. Schematic presentation of the ConA inhibition assay (left) and direct binding assay (right).

3.2.1. Inhibition assay

The thermoresponsive specific binding between mannose bearing microgel surfaces and ConA was analyzed with the inhibition assay by incubation with FITC-ConA and a MeMan solution series at 20 °C and 40 °C for either 30 min or 24 h. The surfaces were washed and the amount of bound FITC-ConA was determined by reading the fluorescence signal with a plate reader. The resulting inhibition curves yield the IC_{50} -values and the Hill coefficient, the slope of the curve, which is a measure for the degree of binding cooperativity (**Figure 3**).⁴³⁻⁴⁴ In this experimental setup higher IC_{50} -values would indicate that more MeMan was required to inhibit the ConA-microgel adhesion. This could be the case for a higher mannose ligand density on the surface.⁴⁵⁻⁴⁶ For an incubation time of 30 min with ConA, the IC_{50} -values were larger above the LCST (see **Figure 3**) indicating stronger binding due to a larger mannose density in the collapsed state. However, at incubation times of 24 h, the IC_{50} -values show the opposite behavior, where stronger

ConA-microgel binding is observed below the LCST. Furthermore, at 24 h of incubation, the slopes of the inhibition curves as signified by the Hill coefficients were clearly smaller below the LCST, which suggests that the degree of cooperative ConA binding to the microgel layer was larger below the LCST. A clear mannose functionalization degree dependence is observed only at short incubation times where large IC_{50} -values and stronger binding is observed for increased functionalization degrees. Such concentration dependence on ligand units is expected due to statistical effects, i.e. rapid binding and rebinding of ConA due to the short lifetime of single carbohydrate-lectin complexes.⁴⁷⁻⁴⁹ The fact that this mannose concentration dependence is not seen at long incubation times hints at a larger degree of multivalent binding where statistical effects do not dominate. Therefore, the inhibition assay suggests that binding of ConA to the microgel layer requires long incubation times to reach an equilibrium. Initially, ConA binding to collapsed microgels above the LCST is stronger compared to swollen microgels below the LCST. Given longer incubation times below the LCST, it seems that ConA is able to bind additional mannose units via multivalent binding in the more flexible microgel network. This is different above the LCST, where the microgels are collapsed and rigid the degree of multivalent cooperative binding was lower.

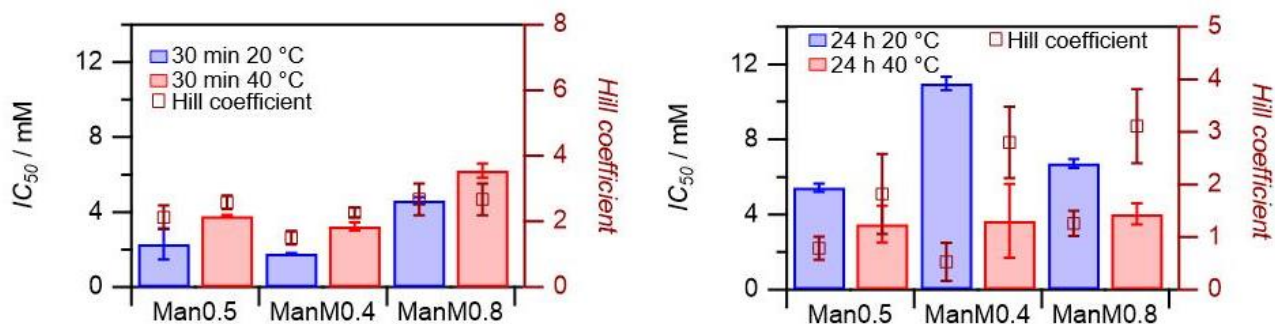


Figure 3. IC₅₀-values and Hill coefficients measured for microgel coated surfaces using Man0.5, ManM0.4 and ManM0.8 after 30 min incubation (left) and after 24 h incubation (right) using ConA as receptor. Blue bars represent measurements at 20 °C and red bars at 40 °C.

3.2.2. Direct binding assay

To directly compare the amount of bound ConA to the microgel surfaces the fluorescence intensity of ConA-FITC at the microgel surface was determined by optical microscopy above and below the LCST and at different incubation times (**Figure 4**). Microscope-based fluorescence analysis showed that more ConA was bound to microgels with larger functionalization degrees. Significantly more ConA binds after 24 h incubation, which again hints at long equilibration times. Notably, raising the temperature above the LCST resulted in an increase of bound ConA. However, when compared to the large changes in IC₅₀ upon temperature increase, these effects were small.

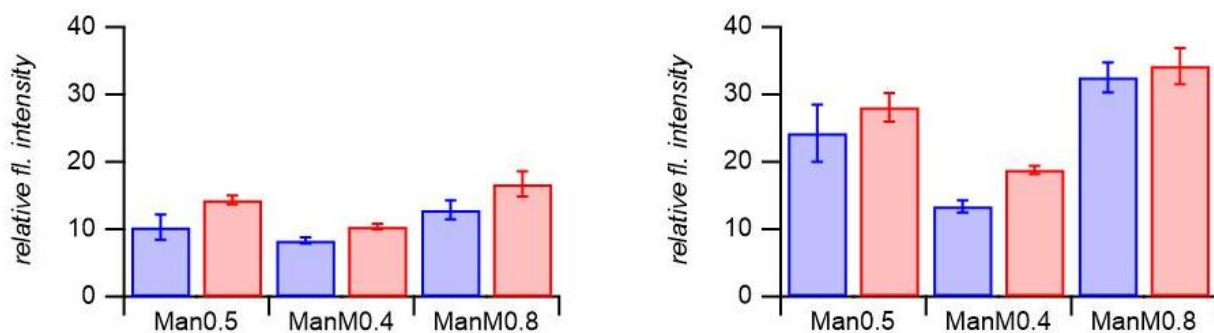


Figure 4. Fluorescence intensities measured of FITC-ConA bound to microgel surface at 20 °C (blue bars) and 40 °C (red bars) after 30 min (left) and 24 h (right) of incubation.

We interpret these findings with a delayed diffusion of the ConA molecules into the “fuzzy”, less crosslinked corona of the microgel particles. Such radial crosslinking density gradients are due to the larger polymerization rate of the bifunctional crosslinker when compared to the NIPAM and the mannose comonomers. For short incubation times, the ConA binding to microgels below the LCST was small, and the binding can easily be inhibited by the addition of MeMan since the ConA molecules could only bind the surface-exposed mannose ligands (**Figure 5**, left). For collapsed microgels it is likely that the accessibility of mannose units is increased due to the reduced steric repulsion of the network and the potential enrichment of the hydrophilic mannose units at the surface of the hydrophobic layer. Thus, for short incubation times, the amount of bound ConA and IC_{50} -values are larger above the LCST. When increasing the incubation time, the ConA molecules are allowed to diffuse into the microgel corona below the LCST enabling multivalent binding due to the flexible network as signified by increased IC_{50} -values (**Figure 5**, right). However, in the collapsed state above the LCST such diffusion into the gel is not possible, and the network is more rigid, reducing multivalent binding and lower IC_{50} -values.

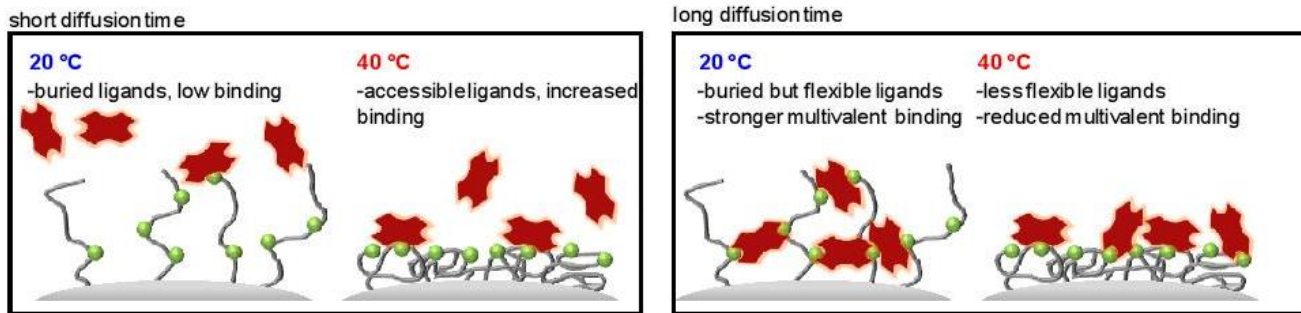


Figure 5. Schematic presentation of the surface of the microgel layer where binding and diffusion of ConA molecules is controlled by a loosely crosslinked network (microgel corona). For short diffusion times binding is overall lower below the LCST due to steric repulsion and low mannose accessibility (left). For long incubation times ConA can diffuse in the swollen network and bind multiple mannose units due to the flexibility of the network. Such multivalent binding is reduced in the collapsed state due to the more rigid network.

3.3. *E. coli* binding to microgel surfaces

To show the ability to capture carbohydrate-binding bacteria by temperature stimulus on microgel coatings, we investigated the adhesion of *E. coli*, a well-known mannose-binding bacterium. The *E. coli* adhesion was again quantified by fluorescence-based microplate readout, using the green fluorescence protein expressing type 1-fimbriated strain pKL1162.⁴⁰ The inhibition assays were conducted like the ConA binding assays. For the direct binding assay, the amount of adhered bacteria was determined using a plate reader instead of an optical microscope to increase the size of the sampled area.

3.3.1. Inhibition assay

For an incubation time of 30 min, the comparison of IC_{50} -values at 20 °C and 40 °C showed only small effects when crossing the LCST and the Hill coefficients were close to unity as expected for the monovalent FimH receptor (**Figure 6**). It is likely that an incubation time of 30 min was too small to observe clear effects given the small diffusion constants of the large *E. coli* bacteria compared to the molecular ConA. After an incubation time of 24 h, the changes in IC_{50} -values were similar for all microgel surfaces, and a clear temperature response was observed. All microgel surfaces showed an increase in IC_{50} -values at elevated temperature, i.e. more inhibitor was required to remove the bacteria from the surfaces at 40 °C. This was caused by an increase in mannose density above the LCST compared to the microgel film below the LCST. An increase in the surface density of binding motifs often correlates with increasing IC_{50} -values.⁴⁵ In case of weak carbohydrate-binding, higher rates of rebinding events for higher densities of ligands may explain this effect.⁴⁶ For collapsed microgels above the LCST, the accessibility of mannose units might be improved at the surface, which would also lead to increased binding.²⁷

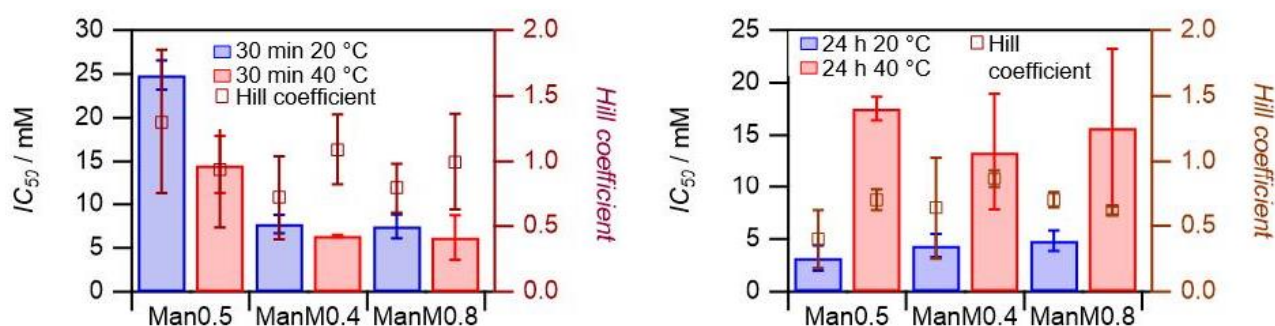


Figure 6. IC_{50} -values and Hill coefficients measured for microgel coated surfaces using Man0.5, ManM0.4 and ManM0.8 after 30 min incubation (left) and after 24 h incubation (right) using *E. coli* as receptor. Blue bars represent measurements at 20 °C and red bars at 40 °C.

3.3.2. Direct binding assay

A microscope-based readout for *E. coli* adhesion towards the microgel surface was unsuitable due to the small areas that were covered with the images. Therefore, the maximum fluorescence value measured during the microplate-based adhesion assay were analyzed. Microscope images also showed that for short incubation times of 30 min, the adhesion of *E. coli* varied strong, perhaps due to the slow diffusion of the bacteria compared to ConA. Therefore, here only the results for long adhesion times (24 h) are shown in **Figure 7**. The results show that for small microgels with low mannose density ManM0.4 and Man0.5 more *E. coli* were bound above the LCST. This might again indicate an increase in the mannose density and improved accessibility of mannose above the LCST, due to the collapse of the microgels. For ManM0.8 there was no difference in the number of adhered bacteria when changing the temperature. This suggests that the density of mannose units was sufficiently large below the LCST to bind a large number of bacteria.

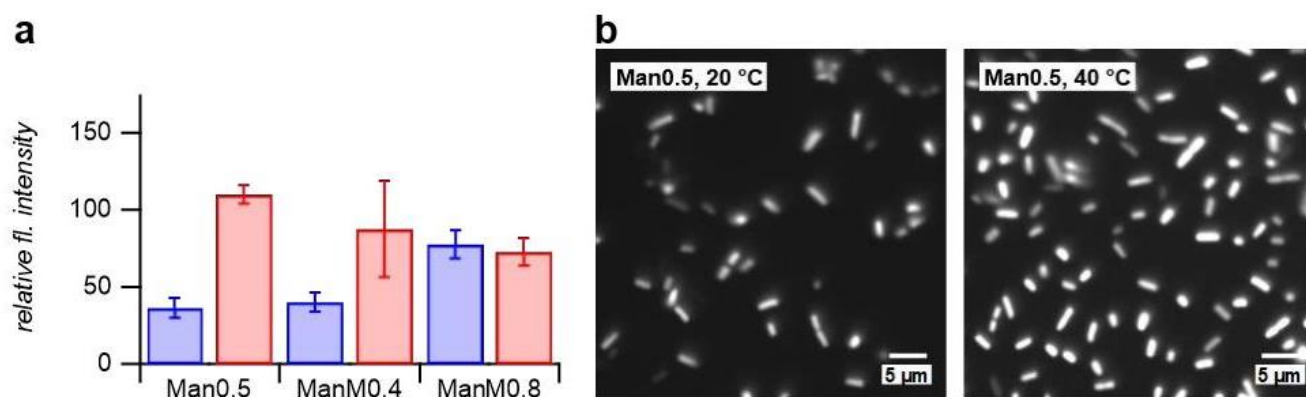


Figure 7. Direct *E. coli* binding adhesion assay. a) Fluorescence intensities measured for the direct *E. coli* adhesion on microgel surfaces after 24 h incubation. Blue bars represent measurements at 20 °C and red bars at 40 °C. b) Typical microgel surfaces after *E. coli* incubation for 24 h.

3.4. Releasing/Washing experiments

Since we have shown that the binding of microgel surfaces and the tested receptors is specific, we now wanted to see, whether the bound bacteria and lectins can be released from the surfaces. This is especially interesting for the surfaces that were incubated with *E. coli* at 40 °C for 24 h as it was seen that in this case, the collapse of the microgel leads to increased adhesion of the bacteria. In **Figure 8** it can be seen that only by washing with cold buffer (left) there is no significant decrease of the relative fluorescence intensity in comparison to the surfaces that were washed with warm buffer (**Figure 8**, right). Summarized the reswelling of the microgels upon cooling was not sufficient to release bound receptors by a substantial degree owing to a strong swelling hysteresis or persistent specific binding

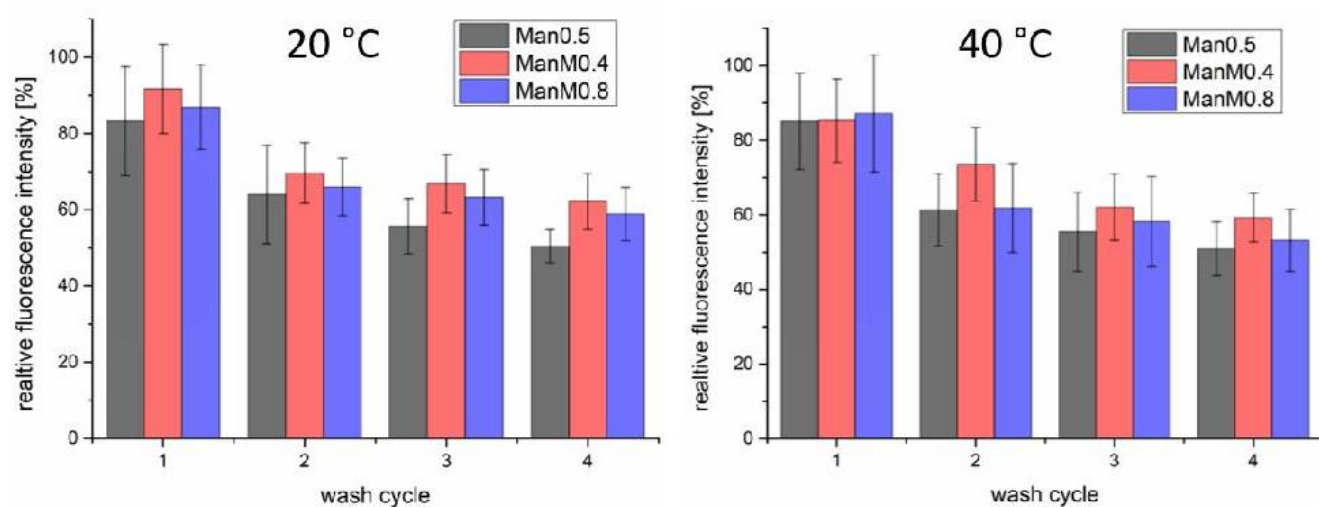


Figure 8. Relative fluorescence intensity after washing the *E. coli* incubated surfaces (24 h, 40 °C) with cold (20 °C, left) and warm buffer (40 °C, right).

o

Conclusion

PNIPAM microgel monolayer films decorated with mannose units were prepared on polystyrene microwell surfaces to study the binding of ConA and *E. coli* below (20 °C) and above (40 °C) the LCST of PNIPAM for short (30 min) and long incubation times (24 h). For long incubation times, it was shown that when increasing the temperature above the LCST, the interaction of *E. coli* with the microgel layer as measured by IC₅₀-values was increased. Also, the number of bound *E. coli* was increased. This is explained by a higher mannose density and reduced steric repulsion in the collapsed state of the microgel layer above the LCST. In contrast to strong *E. coli* binding above the LCST, for ConA the interaction to the microgel layer after 24 h incubation was stronger below the LCST. This might be explained by multivalent binding of the tetrameric receptor to the flexible swollen polymer network, which is not possible for *E. coli* since its receptor (FimH) is monovalent, and the bacteria are too large to diffuse into the microgel network. For short incubation times, the ConA binding was weaker below the LCST perhaps due to delayed diffusion of ConA in the soft swollen microgel corona. Reswelling of the microgels upon cooling was not sufficient to release bound receptors by a substantial degree owing to a strong swelling hysteresis or persistent specific binding. Overall, these results show that the capture of *E. coli* via ligand decorated microgel layers can be significantly increased above the LCST, whereas this was not possible for small multivalent receptors. Furthermore, the temperature-dependent swelling of the microgel layer could be combined with other stimuli-responsive residues, e.g. light or chemical stimuli to enable coatings with more controlled capture and release capabilities.

Author Information

Corresponding Author

* E-mail: Stephan.schmidt@hhu.de

ORCID

Stephan Schmidt: 0000-0002-4357-304X

Acknowledgments

The authors thank Maria Breuer for performing the NMR measurements and Stephanie Scheelen for performing the SEC measurements. The authors acknowledge funding by the German Research foundation (DFG) in the project SCHM 2748/5-1.

TOC

References

1. Varki, A., *Essentials of Glycobiology*. Cold Spring Harbor Laboratory Press: 2017.
2. Dwek, R. A., Glycobiology: Toward Understanding the Function of Sugars. *Chemical Reviews* **1996**, *96* (2), 683-720.
3. Ofek, I.; Mirelman, D.; Sharon, N., Adherence of *Escherichia coli* to human mucosal cells mediated by mannose receptors. *Nature* **1977**, *265* (5595), 623-625.
4. Imberty, A.; Varrot, A., Microbial recognition of human cell surface glycoconjugates. *Curr Opin Struct Biol* **2008**, *18* (5), 567-76.
5. Knight, S. D.; Bouckaert, J., Structure, Function, and Assembly of Type 1 Fimbriae. In *Glycoscience and Microbial Adhesion*, Lindhorst, T. K.; Oscarson, S., Eds. Springer Berlin Heidelberg: Berlin, Heidelberg, 2009; pp 67-107.
6. Sharon, N.; Lis, H., *Lectins: Second edition*. 2007; p 1-454.

7. Pratt, L. A.; Kolter, R., Genetic analysis of *Escherichia coli* biofilm formation: roles of flagella, motility, chemotaxis and type I pili. *Molecular microbiology* **1998**, *30* (2), 285-93.
8. Scott, J. A. G.; Brooks, W. A.; Peiris, J. S. M.; Holtzman, D.; Mulholland, E. K., Pneumonia research to reduce childhood mortality in the developing world. *The Journal of Clinical Investigation* **2008**, *118* (4), 1291-1300.
9. Osrin, D.; Vergnano, S.; Costello, A., Serious bacterial infections in newborn infants in developing countries. *Current opinion in infectious diseases* **2004**, *17* (3), 217-24.
10. Organization, W. H., *Antimicrobial resistance: global report on surveillance 2014*. 2014.
11. Bavington, C.; Page, C., Stopping bacterial adhesion: a novel approach to treating infections. *Respiration; international review of thoracic diseases* **2005**, *72* (4), 335-44.
12. Fasting, C.; Schalley, C. A.; Weber, M.; Seitz, O.; Hecht, S.; Kokschi, B.; Dervedde, J.; Graf, C.; Knapp, E. W.; Haag, R., Multivalency as a chemical organization and action principle. *Angew Chem Int Ed Engl* **2012**, *51* (42), 10472-98.
13. Ofek, I.; Hasy, D. L.; Sharon, N., Anti-adhesion therapy of bacterial diseases: prospects and problems. *Fems Immunology and Medical Microbiology* **2003**, *38* (3), 181-191.
14. Bernardi, A.; Jimenez-Barbero, J.; Casnati, A.; De Castro, C.; Darbre, T.; Fieschi, F.; Finne, J.; Funken, H.; Jaeger, K. E.; Lahmann, M.; Lindhorst, T. K.; Marradi, M.; Messner, P.; Molinaro, A.; Murphy, P. V.; Nativi, C.; Oscarson, S.; Penades, S.; Peri, F.; Pieters, R. J.; Renaudet, O.; Reymond, J. L.; Richichi, B.; Rojo, J.; Sansone, F.; Schaffer, C.; Turnbull, W. B.; Velasco-Torrijos, T.; Vidal, S.; Vincent, S.; Wennekes, T.; Zuilhof, H.; Imberty, A., Multivalent glycoconjugates as anti-pathogenic agents. *Chem. Soc. Rev.* **2013**, *42* (11), 4709-4727.
15. Bhatia, S.; Camacho, L. C.; Haag, R., Pathogen Inhibition by Multivalent Ligand Architectures. *J. Am. Chem. Soc.* **2016**, *138* (28), 8654-8666.

16. Muller, C.; Despras, G.; Lindhorst, T. K., Organizing multivalency in carbohydrate recognition. *Chem. Soc. Rev.* **2016**, *45* (11), 3275-3302.
17. Hudak, J. E.; Bertozzi, C. R., Glycotherapy: new advances inspire a reemergence of glycans in medicine. *Chem Biol* **2014**, *21* (1), 16-37.
18. Li, Z.; Feizi, T., The neoglycolipid (NGL) technology-based microarrays and future prospects. *FEBS Letters* **2018**, *592* (23), 3976-3991.
19. von der Ehe, C.; Buś, T.; Weber, C.; Stumpf, S.; Bellstedt, P.; Hartlieb, M.; Schubert, U. S.; Gottschaldt, M., Glycopolymer-Functionalized Cryogels as Catch and Release Devices for the Pre-Enrichment of Pathogens. *ACS Macro Letters* **2016**, *5* (3), 326-331.
20. Kveton, F.; Blsakova, A.; Kasak, P.; Tkac, J., Glycan Nanobiosensors. *Nanomaterials* **2020**, *10* (7), 29.
21. Wang, Y.; Kotsuchibashi, Y.; Liu, Y.; Narain, R., Study of bacterial adhesion on biomimetic temperature responsive glycopolymer surfaces. *ACS Appl Mater Interfaces* **2015**, *7* (3), 1652-61.
22. Dalier, F.; Eghiaian, F.; Scheuring, S.; Marie, E.; Tribet, C., Temperature-Switchable Control of Ligand Display on Adlayers of Mixed Poly(lysine)-g-(PEO) and Poly(lysine)-g-(ligand-modified poly-N-isopropylacrylamide). *Biomacromolecules* **2016**, *17* (5), 1727-36.
23. Vasani, R. B.; Janardanan, N.; Prieto-Simon, B.; Cifuentes-Rius, A.; Bradley, S. J.; Moore, E.; Kraus, T.; Voelcker, N. H., Microwave Heating of Poly(N-isopropylacrylamide)-Conjugated Gold Nanoparticles for Temperature-Controlled Display of Concanavalin A. *ACS Appl Mater Interfaces* **2015**, *7* (50), 27755-64.

24. Won, S.; Richards, S. J.; Walker, M.; Gibson, M. I., Externally controllable glycan presentation on nanoparticle surfaces to modulate lectin recognition. *Nanoscale Horiz.* **2017**, *2* (2), 106-109.
25. Won, S.; Hindmarsh, S.; Gibson, M. I., Triggerable Multivalent Glyconanoparticles for Probing Carbohydrate-Carbohydrate Interactions. *ACS Macro Lett.* **2018**, *7* (2), 178-183.
26. Anaya, L. M. B.; Petitdemange, R.; Rosselin, M.; Ibarboure, E.; Garbay, B.; Garanger, E.; Deming, T. J.; Lecommandoux, S., Design of Thermoresponsive Elastin-Like Glycopolypeptides for Selective Lectin Binding and Sorting. *Biomacromolecules* **2020**.
27. Paul, T. J.; Strzelczyk, A. K.; Feldhof, M. I.; Schmidt, S., Temperature-Switchable Glycopolymers and Their Conformation-Dependent Binding to Receptor Targets. *Biomacromolecules* **2020**, *21* (7), 2913-2921.
28. Strzelczyk, A. K.; Paul, T. J.; Schmidt, S., Quantifying Thermoswitchable Carbohydrate-Mediated Interactions via Soft Colloidal Probe Adhesion Studies. *Macromolecular Bioscience* **2020**, *n/a* (n/a), 2000186.
29. Schmidt, S.; Hellweg, T.; Klitzing, R., Packing Density Control in P(NIPAM-co-AAc) Microgel Monolayers: Effect of Surface Charge, pH, and Preparation Technique. *Langmuir* **2008**, *24*, 12595-12602.
30. Burmistrova, A.; Richter, M.; Uzun, C.; von Klitzing, R., Effect of cross-linker density of P(NIPAM-co-AAc) microgels at solid surfaces on the swelling/shrinking behaviour and the Young's modulus. *Colloid Polym Sci* **2011**, *289* (5-6), 613-624.
31. Schmidt, S.; Zeiser, M.; Hellweg, T.; Duschl, C.; Fery, A.; Mohwald, H., Adhesion and Mechanical Properties of PNIPAM Microgel Films and Their Potential Use as Switchable Cell Culture Substrates. *Advanced Functional Materials* **2010**, *20* (19), 3235-3243.

32. Tang, J. S. J.; Rosencrantz, S.; Tepper, L.; Chea, S.; Kloepzig, S.; Krueger-Genge, A.; Storsberg, J.; Rosencrantz, R. R., Functional Glyco-Nanogels for Multivalent Interaction with Lectins. *Molecules* **2019**, *24* (10).
33. Siirilä, J.; Hietala, S.; Ekholm, F. S.; Tenhu, H., Glucose and Maltose Surface-Functionalized Thermoresponsive Poly(N-Vinylcaprolactam) Nanogels. *Biomacromolecules* **2020**, *21* (2), 955-965.
34. Paul, T. J.; Rübél, S.; Hildebrandt, M.; Strzelczyk, A. K.; Spormann, C.; Lindhorst, T. K.; Schmidt, S., Thermosensitive Display of Carbohydrate Ligands on Microgels for Switchable Binding of Proteins and Bacteria. *ACS Applied Materials & Interfaces* **2019**, *11* (30), 26674-26683.
35. Pich, A.; Richtering, W., Microgels by Precipitation Polymerization: Synthesis, Characterization, and Functionalization. In *Chemical Design of Responsive Microgels*, Pich, A.; Richtering, W., Eds. Springer Berlin Heidelberg: Berlin, Heidelberg, 2011; pp 1-37.
36. Bergmann, S.; Wrede, O.; Huser, T.; Hellweg, T., Super-resolution optical microscopy resolves network morphology of smart colloidal microgels. *Phys. Chem. Chem. Phys.* **2018**, *20* (7), 5074-5083.
37. Uhlig, K.; Wegener, T.; Hertle, Y.; Bookhold, J.; Jaeger, M.; Hellweg, T.; Fery, A.; Duschl, C., Thermoresponsive Microgel Coatings as Versatile Functional Compounds for Novel Cell Manipulation Tools. *Polymers* **2018**, *10* (6), 12.
38. Gerchako, S.M.; Hatcher, P. G., Improved Technique for Analysis of Carbohydrates in Sediments. *Limnol. Oceanogr.* **1972**, *17* (6), 938-943.

39. Boden, S.; Wagner, K. G.; Karg, M.; Hartmann, L., Presenting Precision Glycomacromolecules on Gold Nanoparticles for Increased Lectin Binding. *Polymers (Basel)* **2017**, *9* (12), 716.
40. Hartmann, M.; Horst, A. K.; Klemm, P.; Lindhorst, T. K., A kit for the investigation of live Escherichia coli cell adhesion to glycosylated surfaces. *Chemical Communications* **2010**, *46* (2), 330-332.
41. Hoare, T.; Pelton, R., Functional group distributions in carboxylic acid containing poly(N-isopropylacrylamide) microgels. *Langmuir* **2004**, *20* (6), 2123-33.
42. Wittmann, V.; Pieters, R. J., Bridging lectin binding sites by multivalent carbohydrates. *Chemical Society Reviews* **2013**, *42* (10), 4492-4503.
43. Mammen, M.; Choi, S. K.; Whitesides, G. M., *Angew. Chem., Int. Ed.* **1998**, *37*, 2755.
44. Iannone, M. A.; Consler, T. G., Effect of microsphere binding site density on the apparent affinity of an interaction partner. *Cytometry Part A* **2006**, *69* (5), 374-383.
45. Dupin, L.; Zuttion, F.; Géhin, T.; Meyer, A.; Phaner-Goutorbe, M.; Vasseur, J.-J.; Souteyrand, E.; Morvan, F.; Chevolut, Y., Effects of the Surface Densities of Glycoclusters on the Determination of Their IC50 and Kd Value Determination by Using a Microarray. *ChemBioChem* **2015**, *16* (16), 2329-2336.
46. Jacobi, F.; Camaleno de la Calle, A.; Boden, S.; Grafmuller, A.; Hartmann, L.; Schmidt, S., Multivalent Binding of Precision Glycooligomers on Soft Glycocalyx Mimicking Hydrogels. *Biomacromolecules* **2018**, *19* (8), 3479-3488.
47. Alon, R.; Hammer, D. A.; Springer, T. A., Lifetime of the P-selectin-carbohydrate bond and its response to tensile force in hydrodynamic flow. *Nature* **1995**, *374* (6522), 539-42.

48. Chen, A.; Moy, V. T., Cross-linking of cell surface receptors enhances cooperativity of molecular adhesion. *Biophysical Journal* **2000**, *78* (6), 2814-2820.
49. Jacobi, F.; Camaleño de la Calle, A.; Boden, S.; Grafmüller, A.; Hartmann, L.; Schmidt, S., Multivalent Binding of Precision Glycooligomers on Soft Glycocalyx Mimicking Hydrogels. *Biomacromolecules* **2018**, *19* (8), 3479-3488.

Supporting Information

Temperature-controlled adhesion to carbohydrate functionalized microgel films: an *E. coli* and lectin binding study

Tanja J. Paul†, Alexander K. Strzelczyk and Stephan Schmidt*

†Institute of Organic and Macromolecular Chemistry, Heinrich-Heine-University Düsseldorf,

Email: Stephan Schmidt – stephan.schmidt@hhu.de

* Corresponding author

Contents

| | |
|--|----|
| S1 Materials..... | 3 |
| S2 Glycomonomer synthesis..... | 4 |
| Synthesis of N-(2-hydroxyethyl)-2-methacrylamide (HEMAm)..... | 4 |
| Synthesis of 1,2,3,4,6-penta-O-acetyl- α -D-mannopyranoside..... | 6 |
| Synthesis of 2'-methacrylamidoethyl-2,3,4,6-tetra-O-acetyl- α -D-mannopyranoside (AcManEMAm) | 8 |
| Synthesis of 2'-acrylamidoethyl-2,3,4,6-tetra-O-acetyl- α -D-mannopyranoside (AcManEAm)..... | 11 |
| Deprotection of the glycomonomers..... | 14 |
| Microgel Synthesis..... | 15 |
| S3 Instrumentation..... | 17 |
| Nuclear Magnetic Resonance spectroscopy (NMR)..... | 17 |
| Reversed phase high pressure liquid chromatography – mass spectrometry (RP-HPLC-MS)..... | 17 |
| UV-Vis spectroscopy..... | 17 |
| Zeta potential measurements..... | 17 |
| Microplate reader..... | 18 |
| Freeze Dryer..... | 18 |
| Dynamic light scattering..... | 18 |
| Atomic Force Microscopy (AFM)..... | 18 |

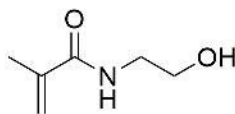
| | |
|---|----|
| S4 Temperature dependent adhesion of ConA to microgelsurfaces..... | 19 |
| S5 Bacteria cultivation, buffer and media | 22 |
| LB-Medium (PKL1162)..... | 22 |
| PB S buffer | 22 |
| LBB buffer | 22 |
| Bacterial culture | 22 |
| S6 Temperature dependent adhesion of <i>E. coli</i> to microgel surfaces..... | 23 |
| General methods..... | 26 |
| Phenol-sulfuric acid method (PSA)..... | 26 |
| Microplate surface preparation..... | 26 |
| FITC-ConA Adhesion Inhibition Assay..... | 26 |
| GFP-Based Bacterial Adhesion Inhibition Assay | 26 |
| Fluorescence Microscopy..... | 27 |
| References | 27 |

S1 Materials

N-isopropylacrylamide (NIPAM) (99%), *N,N'*-Methylenebisacrylamide (MBA) (99%), ethanol ($\geq 99.8\%$), acetic acid (99.8-100%), *p*-toluic acid (98%), phosphate buffered saline tablets (PBS), sodium methoxide ($\geq 97.5\%$), Amberlite IR 120 (hydrogen form), acetic anhydride (99.5%), manganese chloride (99%), sulfuric acid (95-98%), ammonium persulfate (APS) (98%), LB Broth (Miller, powder microbial growth medium), ethanolamine ($\geq 98\%$), dichloromethane ($\geq 99.9\%$), triethylamine ($\geq 99.5\%$), *N*-hydroxyethyl acrylamide (97%), Concanavalin A from *Canavalia ensiformis* (Jack bean) (FITC conjugate, Type IV, lyophilized powder), HEPES ($\geq 99.5\%$), methyl α -D-mannopyranoside ($\geq 99.0\%$), mannan from *Saccharomyces cerevisiae* (prepared by alkaline extraction), TWEEN® 20 (for molecular biology), chloramphenicol ($\geq 98\%$) and ampicillin sodium salt (BioReagent) were all purchased from Sigma Aldrich. Sodium dodecyl sulfate (SDS) ($\geq 99\%$), tetrahydrofuran (99.8%), ethyl acetate (99.5%), dimethyl sulfoxide ($\geq 99.9\%$), methacryloyl chloride (97%) and α -D-mannose were purchased from Acros Organics. Sodium chloride (99.98%), phenol (99%), acetonitrile (HPLC gradient grade) ($\geq 99.9\%$), magnesium sulfate (laboratory reagent grade), chloroform (99.9%), methanol (99.99%) were purchased from Fischer Scientific. *n*-hexane (99.9%) was purchased from VWR chemicals. Sodium hydrogen carbonate (99%) was purchased from Appli Chem. Boron trifluoride diethyl etherate (98%) was purchased from Alfa Aesar.

S2 Glycomonomer synthesis

Synthesis of N-(2-hydroxyethyl)-2-methacrylamide (HEMAm)



Structure of *N*-(2-hydroxyethyl)-2-methacrylamide (HEMAm).

N-(2-hydroxyethyl)-2-methacrylamide was synthesized according to a protocol published by Parry et al.¹ Briefly, ethanolamine (8 mL, 132 mmol) was dissolved in anhydrous dry chloroform (100 mL) and cooled with an ice bath to 0 °C. Then a solution of methacroyl chloride (6.4 mL, 67 mmol) and chloroform (75 mL) were slowly added, followed by stirring for 2 h at 0 °C. The formed solid was filtered off and the remaining chloroform was removed in vacuo. Next, the crude product was again dissolved in 250 mL chloroform and stirred over basic alumina for 15 h. On the next day the basic alumina was filtered off and the remaining solvent was removed under reduced pressure to give a pale-yellow oil. The product was purified by column chromatography (ethyl acetate/*n*-hexane 1:1). The overall yield of the synthesis was 80% (6.92 g).

¹H-NMR (600 MHz, CDCl₃): δ 6.41 (s, 1H, -NH), 5.73 (t, ³*J*_{HH} = 1.0 Hz, 1H, -C=CH₂ E to -CH₃), 5.37 – 5.33 (m, 1H, -C=CH₂ Z to -CH₃), 3.75 (dd, ³*J*_{HH} = 5.5, 4.5 Hz, 2H, -NHCH₂CH₂), 3.50 – 3.46 (m, 2H, -NH-CH₂-CH₂), 2.57 (s, 1H, -OH), 1.97 – 1.95 (m, 3H, -CH₃).

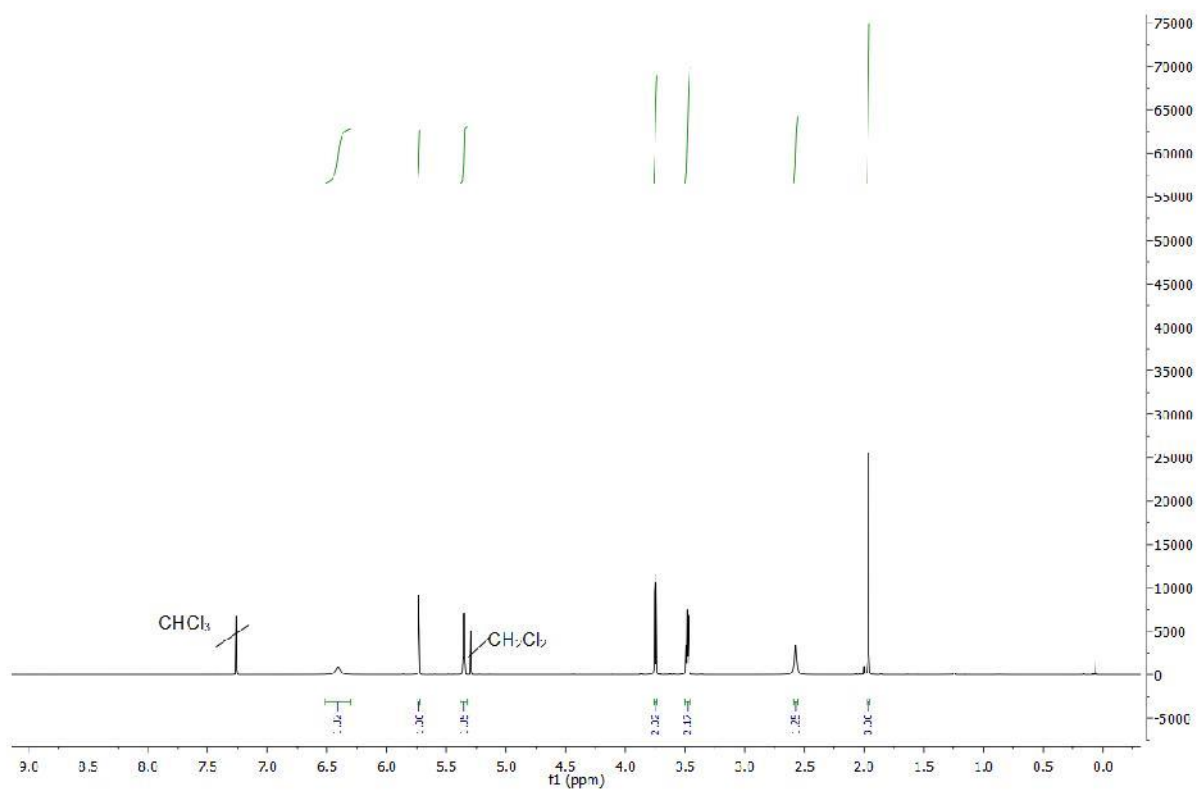
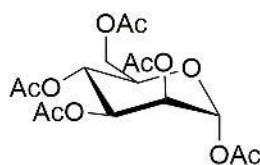


Figure 1: $^1\text{H-NMR}$ (600 MHz, CDCl_3) HEMAm.

Synthesis of 1,2,3,4,6-penta-*O*-acetyl- α -D-mannopyranoside



Structure of 1,2,3,4,6-penta-*O*-acetyl- α -D-mannopyranoside.

α -D-mannose (30.0 g, 166.6 mmol) was dissolved in 500 mL acetonitrile at 0 °C. Then *p*-toluenesulfonic acid (3.18 g, 18.5 mmol) was added and the solution was flushed with nitrogen for 20 min and over the next 20 min acetic anhydride (100 mL, 1.1 mol) was added and the solution was stirred at room temperature for 48 h. Afterwards the solvent was removed and the residue was dissolved in 600 mL ethyl acetate and washed with saturated sodium bicarbonate solution, water and dried over magnesium sulfate. Solvent was removed under reduced pressure and the product was dried under vacuum (yield: 64.2 g, 99%).

$^1\text{H-NMR}$ (600 MHz, CDCl_3) δ 6.11 - 5.83 (dd, $^3J_{\text{HH}} = 67.2, 1.8$ Hz 1H, *H1*), δ 5.50 - 5.09 (m, 3H, *H2-4*), δ 4.34 - 4.24 (m, 1H, *H5*), δ 4.18 - 3.75 (m, 2H, *H21+22*), δ 2.23 - 2.20 (s, 3H, *H6-20*), δ 2.18 - 2.15 (d, $^3J_{\text{HH}} = 2.4$ Hz, 3H, *H6-20*), δ 2.09 - 2.07 (s, 3H, *H6-20*), δ 2.06 - 2.02 (s, 3H, *H6-20*), δ 2.02 - 1.96 (s, 3H, *H6-20*).

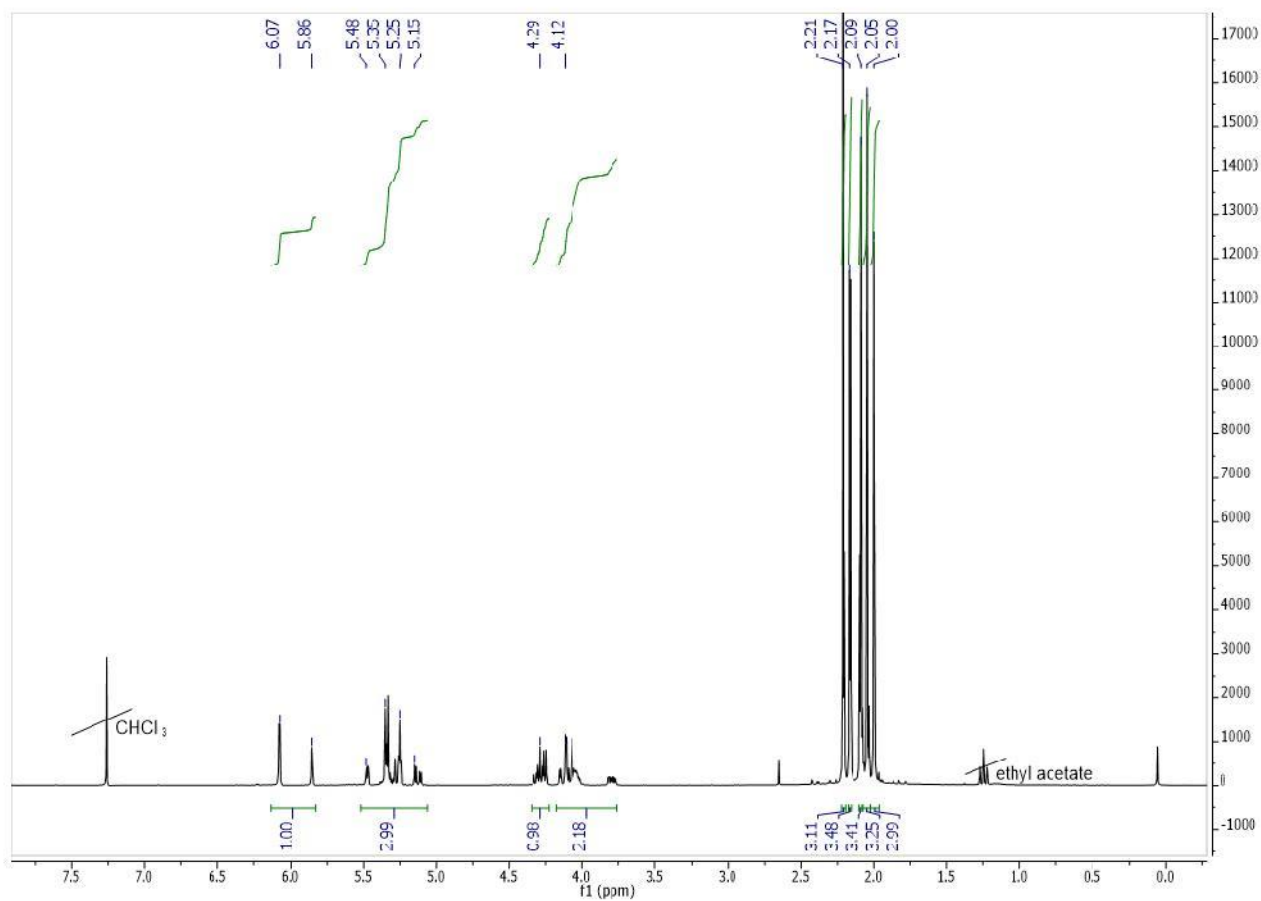
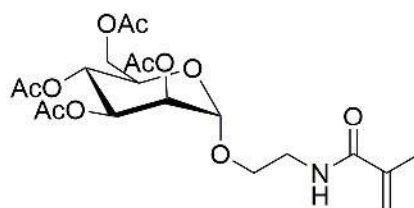


Figure 2: $^1\text{H-NMR}$ (600 MHz, CDCl_3) 1,2,3,4,6-penta-*O*-acetyl- α -D-mannopyranoside.

Synthesis of 2'-methacrylamidoethyl-2,3,4,6-tetra-O-acetyl- α -D-mannopyranoside (AcManEMAm)



Structure of 2'-methacrylamidoethyl-2,3,4,6-tetra-O-acetyl- α -D-mannopyranoside (AcManEMAm).

The synthesis was adapted from Gibson et al.² In a 1000 mL round bottom flask 1,2,3,4,6-Penta-O-acetyl- α -D-mannopyranoside (20.6 g, 52.8 mmol) and *N*-(2-hydroxyethyl)-2-methacrylamide (6.2 g, 48.2 mmol) were dissolved in dichloromethane (500 mL). Followed the solution was cooled to 0 °C and additionally purged with nitrogen for at least 15 min. After that slowly boron trifluoride diethyl etherate (35 mL, 276.2 mmol) was added to the solution. After the addition of boron trifluoride diethyl etherate was completed the reaction solution was allowed to reach room temperature. After 48 h stirring at ambient temperature organic layer was washed with ice water, two times with saturated sodium hydrogen carbonate solution, distilled water and brine. The solution was dried with MgSO₄, filtered and the remaining dichloromethane was removed under reduced pressure. The crude colorless gum was additionally purified by column chromatography (ethyl acetate/*n*-hexane 1:1). The overall yield of the colorless gum was 21% (4.65 g).

¹H NMR (600 MHz, CDCl₃) δ 6.29 (s, 1H, NH), 5.69 – 5.67 (m, 1H, -C=CH₂) 5.38 – 5.35(m, 1H, -C=CH₂), 5.34 – 5.31 (m, 1H, H2), 5.29 (dd, ³*J*_{HH} = 10.1, 3.4 Hz, 1H, H3), 5.25 – 5.20 (m, 2H, H4), 4.80 (d, ³*J*_{HH} = 1.8 Hz, 1H, H1), 4.21 (dd, ³*J*_{HH} = 12.2, 5.7 Hz, 1H, H6), 4.08 – 4.05 (m, 2H, 1H, H6'), 3.95 – 3.90 (m, 1H, H5), 3.82 – 3.77 (m, 1H, -OCH₂CH₂), 3.63 – 3.52 (m, 2H, -OCH₂CH₂, -OCH₂CH₂NH), 3.51 – 3.44 (m, 1H, -OCH₂CH₂NH), 2.12 (s, 3H, -COCH₃), 2.06 (s, 3H, -COCH₃), 2.01(s, 3H, -COCH₃), 1.96 (s, 3H, -COCH₃), 1.94 (s, 3H, -CH₃).

¹³C NMR (600 MHz, CDCl₃) δ 170.66(1C, -COCH₃), 170.11 (1C, -COCH₃), 170.05 (1C, -COCH₃), 169.70 (1C, -COCH₃), 168.51 (1C, -CONH), 139.84 (1C, COC(CH₃)CH₂), 119.93 (1C, COC(CH₃)CH₂), 97.69 (1C, C1), 69.42 (1C, C2), 69.06 (1C, C3), 68.87 (1C, C4), 67.32 (1C, C5), 66.15 (1C, -OCH₂CH₂), 62.52 (1C, C6), 39.29 (1C, NHCH₂CH₂), 21.10 (1C, -COCH₃), 20.92 (1C, -COCH₃), 20.76 (1C, -COCH₃), 18.68 (1C, -COCH₃), 14.25 (1C, -CH₃).

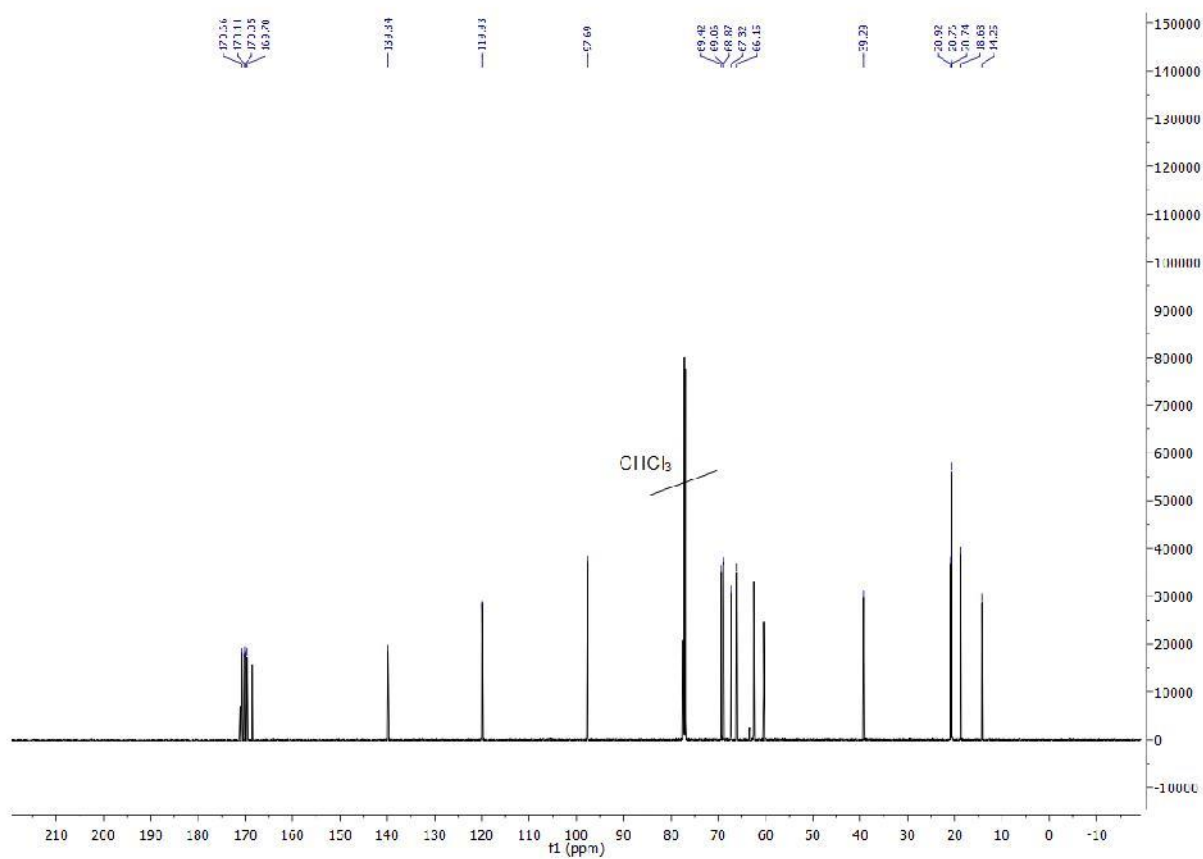
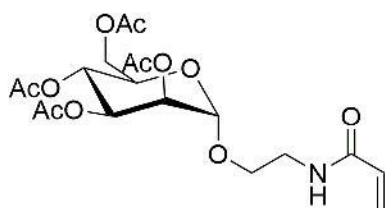


Figure 4: ^{13}C -NMR (600 MHz, CDCl_3) AcManEMAm.

Synthesis of 2'-acrylamidoethyl-2,3,4,6-tetra-*O*-acetyl- α -D-mannopyranoside (AcManEAm)



Structure of 2'-acrylamidoethyl-2,3,4,6-tetra-*O*-acetyl- α -D-mannopyranoside (AcManEAm).

The synthesis was adapted from Gibson et al.² In a 1000 mL round bottom flask 1,2,3,4,6-Penta-*O*-acetyl- α -D-mannopyranoside (20.6 g, 52.8 mmol) and *N*-(2-hydroxyethyl)-2-acrylamide (5.5 g, 48.2 mmol) were dissolved in dichloromethane (500 mL). Followed the solution was cooled to 0 °C and additionally purged with nitrogen for at least 15 min. After that slowly boron trifluoride diethyl etherate (35 mL, 276.2 mmol) was added to the solution. After the addition of boron trifluoride diethyl etherate was completed the reaction solution was allowed to reach room temperature. After 48 h stirring at ambient temperature organic layer was washed with ice water, two times with saturated sodium hydrogen carbonate solution, distilled water and brine. The solution was dried with MgSO₄, filtered and the remaining dichloromethane was removed under reduced pressure. The crude colorless gum was additionally purified by column chromatography (ethyl acetate/*n*-hexane 1:1). The overall yield of the colorless gum was 31% (6.65 g).

¹H NMR (600 MHz, CDCl₃) δ 6.28 (dd, ³*J*_{HH} = 17.0, 1.5 Hz, 1H, -HC=CH₂), 6.25 (s, 1H, NH), 6.14 (dd, ³*J*_{HH} = 17.0, 10.3 Hz, 1H, -HC=CH₂), 5.65 (dd, ³*J*_{HH} = 10.3, 1.5 Hz, 1H, -HC=CH₂), 5.29 (dd, ³*J*_{HH} = 10.0, 3.5 Hz, 1H, H3), 5.25 – 5.19 (m, 1H, H2), 4.80 (d, ³*J*_{HH} = 1.7 Hz, 1H, H1), 4.22 (dd, ³*J*_{HH} = 12.2, 5.7 Hz, 1H, H6), 4.07 (dd, ³*J*_{HH} = 4.8, 2.5 Hz, 1H, H6'), 3.95 (ddd, ³*J*_{HH} = 10.1, 5.7, 2.5 Hz, 1H, H5), 3.82 – 3.77 (m, 1H, -OCH₂CH₂), 3.62 – 3.55 (m, 2H, -OCH₂CH₂, -OCH₂CH₂NH), 3.53 – 3.45 (m, 1H, -OCH₂CH₂NH), 2.13 (s, 3H, -COCH₃), 2.06 (s, 3H, -COCH₃), 2.02 (s, 3H, -COCH₃), 1.97 (s, 3H, -COCH₃).

¹³C NMR (600 MHz, CDCl₃) δ 171.23 (1C, -COCH₃), 170.71 (1C, -COCH₃), 170.14 (1C, -COCH₃), 169.75 (1C, -COCH₃), 165.72 (1C, -CONH), 130.66 (1C, COC(CH₃)CH₂), 126.95 (1C, COC(CH₃)CH₂), 97.83 (1C, C1), 69.42 (1C, C2), 69.07 (1C, C3), 68.83 (1C, C4), 67.42 (1C, C5), 66.22 (1C, -OCH₂CH₂), 62.57 (1C, C6), 39.20 (1C, NHCH₂CH₂), 21.12 (1C, -COCH₃), 20.94 (1C, -COCH₃), 20.80 (1C, -COCH₃), 20.77 (1C, -COCH₃).

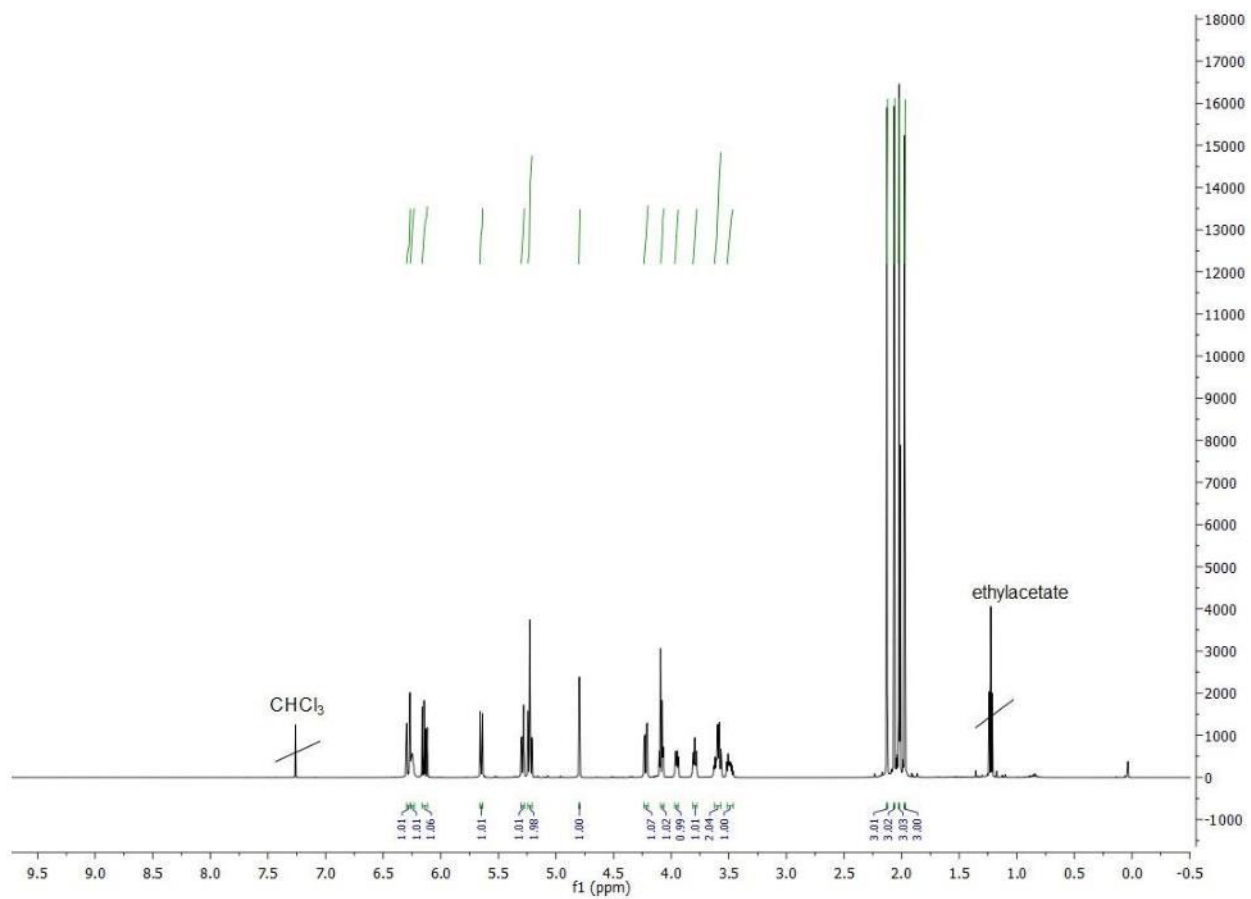


Figure 5: $^1\text{H-NMR}$ (600 MHz, CDCl_3) AcManEAm.

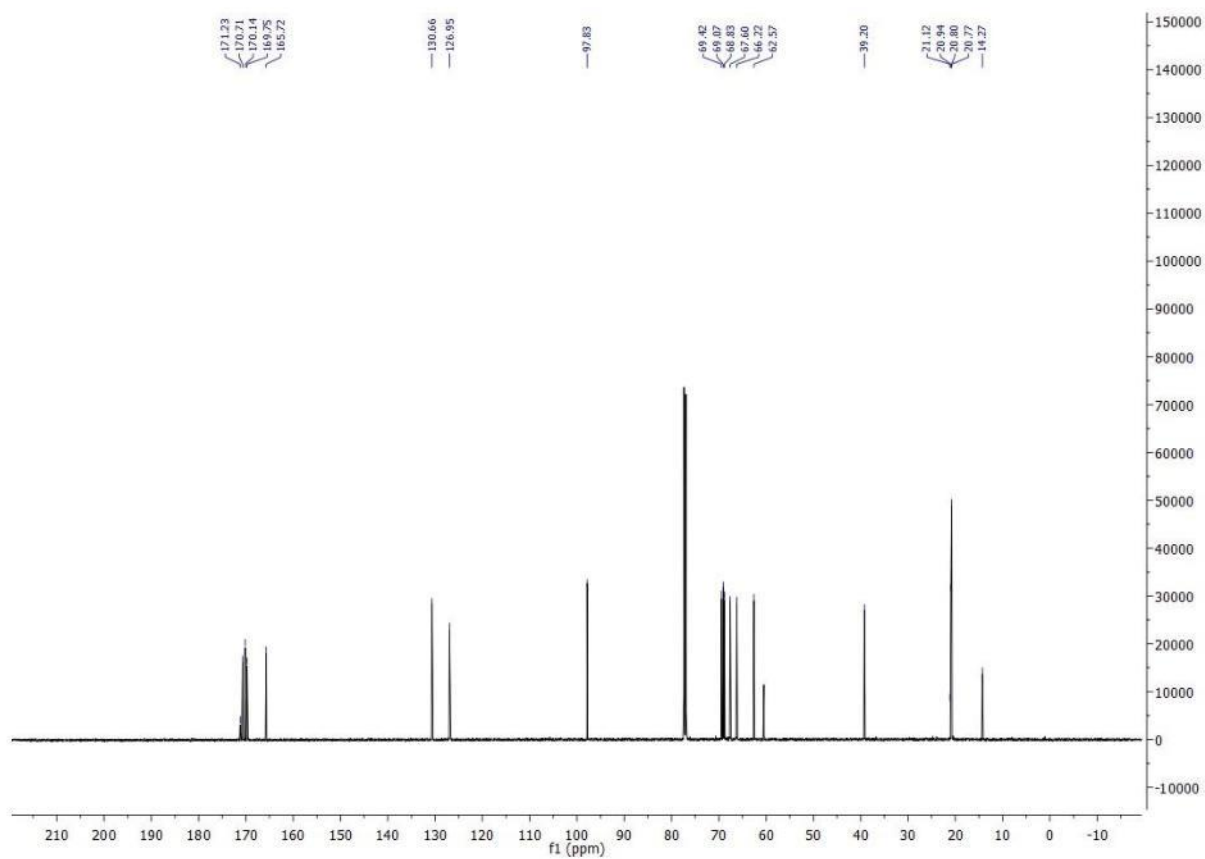
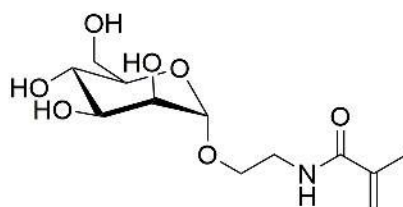


Figure 6: ^{13}C -NMR (600 MHz, CDCl_3) AcManEAm.

Deprotection of the glycomonomers

For polymerizations in water the glycomonomers had to be deprotected. Therefore, 0.5 g of the glycomonomer was given into 6.5 mL of a 0.3 M sodium methanolate solution in methanol and shaken for at least 2 h. Afterward the solution was neutralized with Amberlite IR120 and the remaining solvent was removed.



Structure of 2'-methacrylamidoethyl- α -D-mannopyranoside (ManEMAm)

^1H NMR (600 MHz, D_2O): δ 5.73 – 5.66 (m, 1H, $-\text{C}=\text{CH}_2$), 5.47 – 5.45 (m, 1H, $-\text{C}=\text{CH}_2$), 4.87 (d, $^3J_{\text{HH}} = 1.7$ Hz, 1H, H1), 3.93 (dd, $^3J_{\text{HH}} = 3.5, 1.7$ Hz, 1H, H2), 3.85 (dd, $^3J_{\text{HH}} = 12.2, 2.2$ Hz, 1H, H6), 3.83 – 3.80 (m, 1H, H3), 3.78 (dd, $^3J_{\text{HH}} = 9.5, 3.4$ Hz, 1H, H4), 3.74 (dd, $^3J_{\text{HH}} = 12.2, 5.9$ Hz, 1H, H6'), 3.71 – 3.62 (m, 2H, $-\text{OCH}_2\text{CH}_2\text{NH}$), 3.61 – 3.57 (m, 1H, H5), 3.56 – 3.51 (m, 1H, $-\text{OCH}_2\text{CH}_2\text{NH}$), 3.49 – 3.44 (m, 1H, $-\text{OCH}_2\text{CH}_2\text{NH}$), 1.93 (s, 3H, $-\text{CH}_3$).

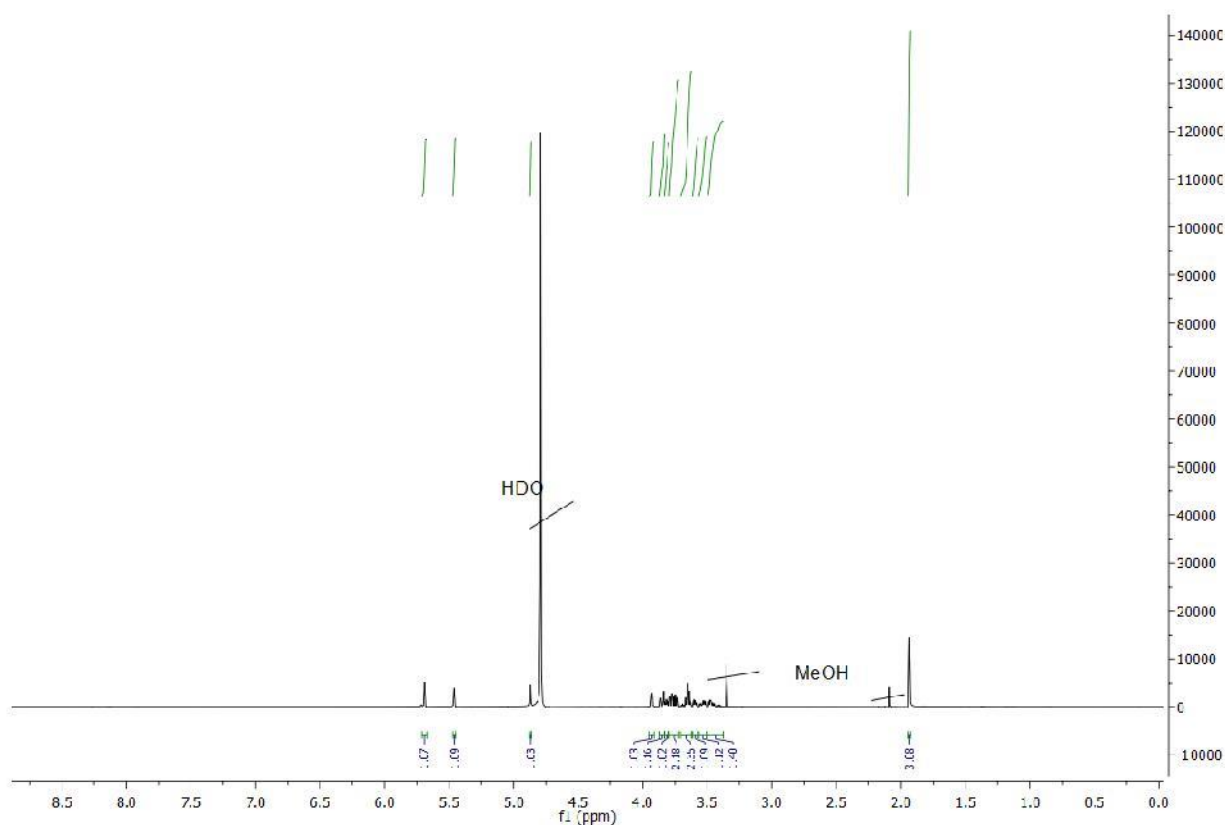


Figure 7. $^1\text{H-NMR}$ (600 MHz, D_2O) ManEMAm.

Microgel Synthesis

The polymerization was carried out in a 100 mL three-necked flask fitted with a condenser. In 75 mL ultrapure water 0.7 g *N*-Isopropylacrylamide (NIPAM, 6.19 mmol), 0.05 g *N,N'*-Methylenebisacrylamide (MBA, 0.324 mmol) and 0.025 g (0.087 mmol) sodium dodecyl sulfate (SDS) were added. Additionally, the deprotected glycomonomer was added. The used amount of deprotected glycomonomers differ for each polymerization batch (see **Table 1**). The solution was stirred at 350 rpm with a magnetic stir bar and heated to 70 °C under a nitrogen purge for at least 40 min to remove dissolved oxygen. Next, the initiator ammonium persulfate (0.2 g, 0.9 mmol) was dissolved in 5 mL ultrapure water and added to the reaction solution afterwards to start the polymerization. During the reaction the solution was continuously purged with nitrogen and stirred with 350 rpm. The reaction was stopped after 55 min by cooling with an ice bath. After filtration by glass wool, the reactants were removed by repeated centrifugation at 10000 g and washing with water.

Table 1. Used chemicals for the synthesis of the different microgel samples.

| Microgel sample | NIPAM | MBA | Mannose monomer | SDS | APS |
|-----------------|-----------------|-----------------|-------------------------------|------------------|----------------------|
| ManM0.8 | 0.7 g, 6.2 mmol | 50 mg, 324 nmol | 180 mg ,0.618 mmol ManEMAm | 25 mg 87 nmol | 200 mg 0.876 mmol |
| ManM0.4 | 0.7 g, 6.2 mmol | 50 mg, 324 nmol | 85 mg, 0.309 mmol ManEMAm | 25 mg 87 nmol | 200 mg 0.876 mmol |
| Man0.5 | 0.7 g, 6.2 mmol | 50 mg, 324 nmol | 180 mg ,0.62 mmol ManEAm | 25 mg 87 nmol | 200 mg 0.876 mmol |

S3 Instrumentation

Nuclear Magnetic Resonance spectroscopy (NMR)

¹H-NMR and ¹³C-NMR (600 MHz) were measured on a Bruker AVANCE III 600 (Bremen, Germany). As internal standard chemical shifts were referenced to the residual non-deuterated solvents (CDCl₃: ¹H 7.26, ¹³C 77.16, D₂O: ¹H 4.79). All chemical shifts are reported in delta (δ) expressed in parts per million (ppm). The following abbreviations were used to indicate multiplicities: s = singlet, d = doublet, t = triplet, m = multiplet.

Reversed phase high pressure liquid chromatography – mass spectrometry (RP-HPLC-MS)

All RP-HPLC-MS measurements were performed on an Agilent 1260 infinity instrument (Agilent Technologies, Waldbrom, Germany). The instrument is coupled to a variable wavelength detector (VWD) and was set to 214 nm and a 6120 Quadrupole LC/MS containing an Electrospray Ionization source (operating in positive ionization mode in a m/z range of 200 to 2000). A Poroshell 120 EC-C18 1.8 μm (3.0 × 50 mm, 2.5 μm) RP column was used as HPLC column. The mobile phase A was 95/5 H₂O/MeCN and B 5/95 H₂O/MeCN, both containing 0.1% formic acid. Samples were analyzed with a flow rate of 0.4 mL/min using a linear gradient from 100% A to 50% B in a time range of 17 min at 25 °C. Using OpenLab ChemStation software for LC/MS from Agilent Technologies (Waldbrom, Germany) spectral analysis of UV and MS data was performed.

UV-Vis spectroscopy

On a dual-trace spectrometer Specord® 210 Plus from Analytik Jena AG (Jena, Germany) all UV-Vis measurements were performed at 25 °C. Using Win ASPECT PLUS software the instrument was operated. Protein concentration measurements were performed in a cuvette QX quartz cuvette (d = 1 cm, V = 3.5 mL) from Hellma Analytics (Mühlheim, Germany).

Zeta potential measurements

All Zeta potential measurements were performed on a Zetasizer Nano-Z instrument (Malvern) using a DTS1070 folded capillary cell. To operate the instrument, the Zetasizer software version 7.11 (Malvern) was used. For all measurements a 0.05 wt% microgel dispersion in 5 mM Na₂HPO₄ buffer (pH 7.4) was used. All measurements were carried out at 20 °C. For all microgel samples a zeta potential of -1.0 mV to 0.3 mV was measured. The slightly negative charge can be attributed to the negative charges of the used initiator.

Microplate reader

All adhesion inhibition measurements were performed on a CLARIOstar® microplate reader from BMG LABTECH (Freiburg, Germany) at ambient temperature. Using the BMG Mars software the measurements were evaluated. For all measurements F-bottom 96 black well plates from Greiner BIO-ONE were used.

Freeze Dryer

An Alpha 1-4 LD plus instrument from Martin Christ Freeze Dryers GmbH (Osterode, Germany) was used for lyophilization of all polymer samples. The main drying method was set to -54 °C and 0.1 mbar.

Dynamic light scattering

Measurements were performed at a Malvern HPPS 3.3 instrument (Malvern Panalytical, Kassel, Germany) equipped with a 633 nm He/Ne-laser with the detector set in backscattering configuration (171°). Microgel samples (0.05 wt%) in 1 cm polystyrene cuvettes were analyzed in a temperature range of 20 °C to 40 °C with a temperature increment of 2 °C and a 10-minute equilibration time lag between the temperature steps. For evaluating the autocorrelation functions, the decay constant and first cumulant were determined by exponential fits and the hydrodynamic radii were calculated by the Stokes-Einstein relation. For comparison, selected microgel samples were analyzed on a Nicomp 3000 setup (Particle Sizing Systems, FL, USA) at a scattering angle of 90° showing good agreement with hydrodynamic radii determined in the backscattering setup.

Atomic Force Microscopy (AFM)

AFM of dried microgel films was conducted on a JPK NanoWizard 2 (JPK Instruments AG, Berlin, Germany) using cantilevers with a nominal spring constant of 300 N/m (HQ:XSC11, MikroMash, Bulgaria) in tapping mode.

S4 Temperature dependent adhesion of ConA to microgelsurfaces

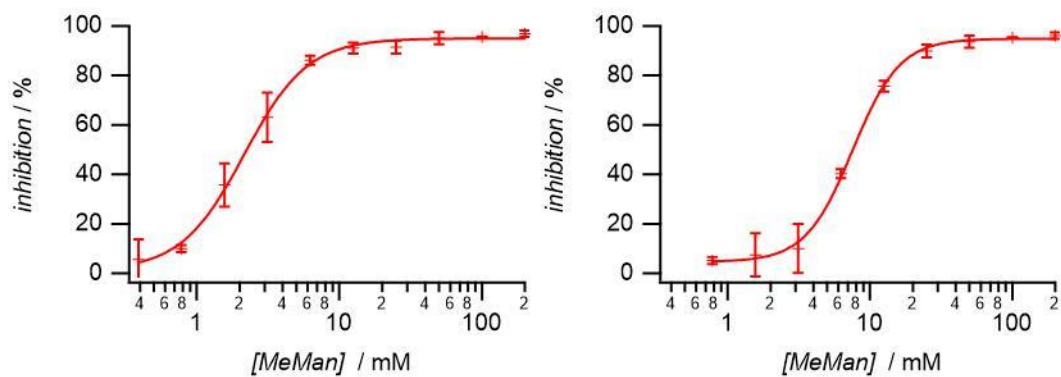


Figure 8: Inhibition measurements for Man0.5 with receptor ConA after 30 min of incubation at 20 °C (left) and 40 °C (right).

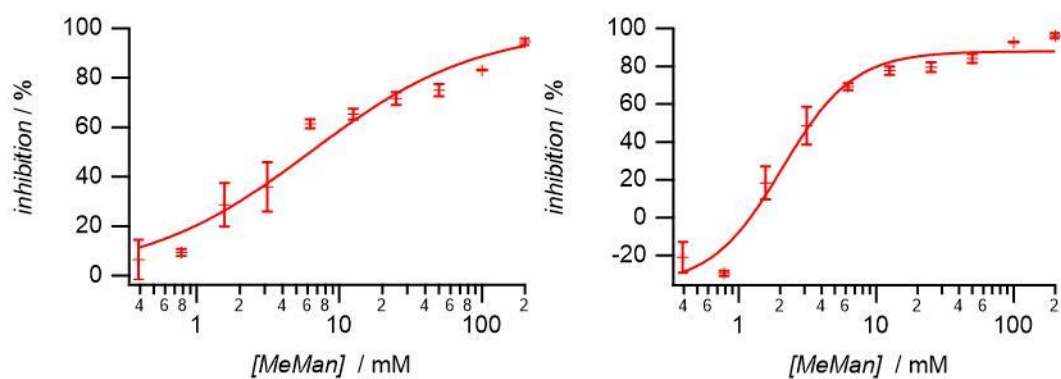


Figure 9: Inhibition measurements for Man0.5 with receptor ConA after 24 h of incubation at 20 °C (left) and 40 °C (right).

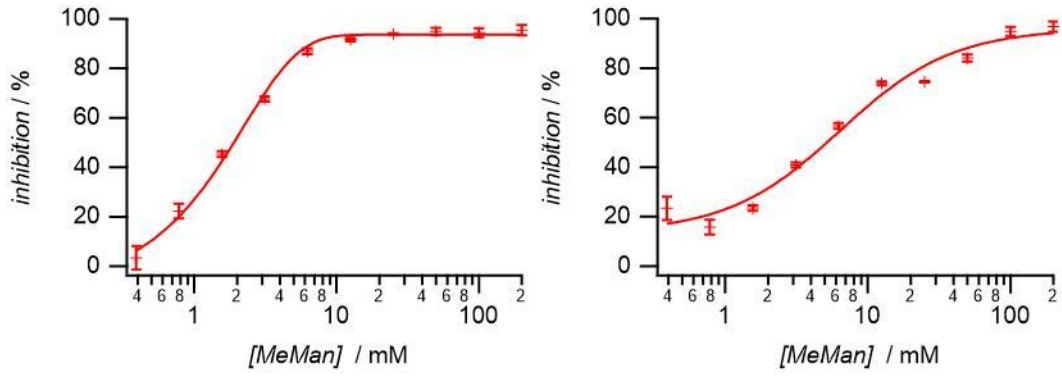


Figure 10: Inhibition measurements for ManM0.4 with receptor ConA after 30 min of incubation at 20 °C (left) and 40 °C (right).

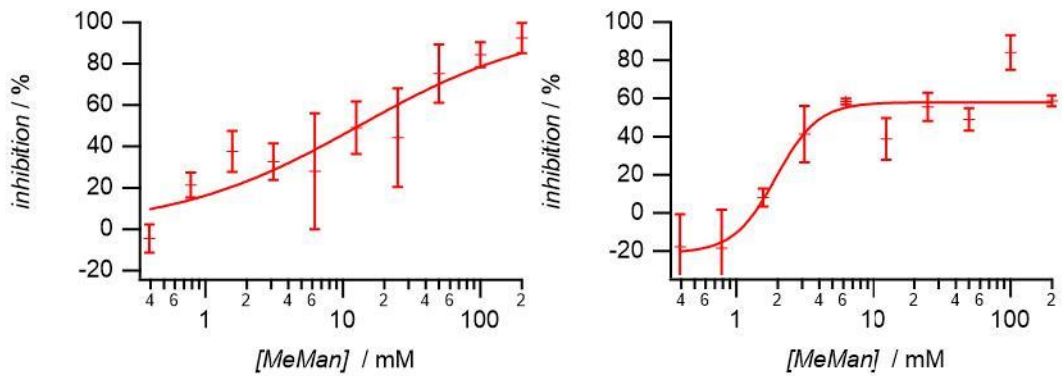


Figure 11: Inhibition measurements for ManM0.4 with receptor ConA after 24 h of incubation at 20 °C (left) and 40 °C (right).

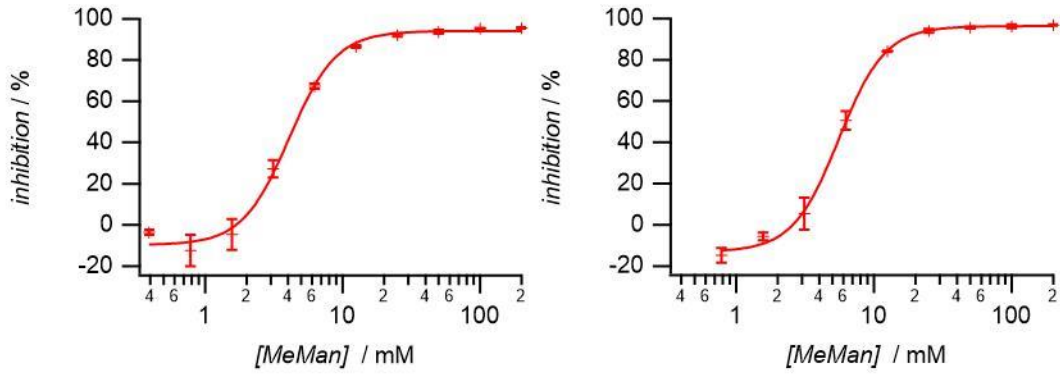


Figure 12: Inhibition measurements for ManM0.8 with receptor ConA after 30 min of incubation at 20 °C (left) and 40 °C (right).

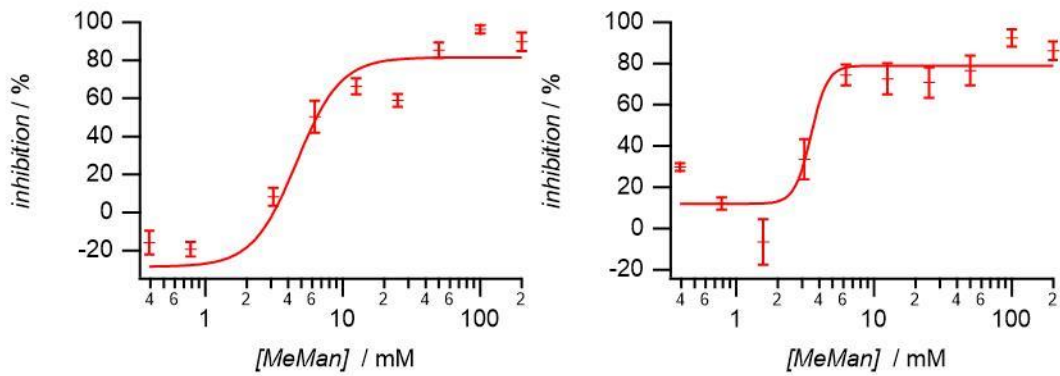


Figure 13: Inhibition measurements for ManM0.8 with receptor ConA after 24 h of incubation at 20 °C (left) and 40 °C (right).

S5 Bacteria cultivation, buffer and media

LB-Medium (PKL1162)

12.5 g of LB Broth (Miller) (powder microbial growth medium) were dissolved in 500 mL ultrapure water. The powder contains tryptone (5.0 g), sodium chloride (5.0 g) and yeast extract (2.5 g). Afterwards the solution was sterilized for 30 min at 121 °C and cooled to room temperature. 50.0 mg of ampicillin and 25.0 mg of chloramphenicol were added.

PBS buffer

Five tablets of phosphate buffered saline was dissolved in 1 L of ultrapure water. The final concentrations of the buffer were 0.01 M phosphate buffer, 0.0027 M potassium chloride and 0.137 M sodium chloride. The pH was checked with a potentiometer and set to 7.4.

LBB buffer

Lectin binding buffer (LBB) was used for all measurements with Concanavalin A. Lectin binding buffer contains 10 mM HEPES ((4-(2-hydroxyethyl)-1-piperazineethanesulfonic acid) as buffering agent, which was adjusted to a pH of 7.4 with 1 M NaOH. Thereafter, calcium chloride (1 mM) and manganese chloride (1 mM) and sodium chloride (50 mM) were dissolved in the solution. To prevent bacterial growth in the buffer sodium azide was added to a final concentration of 0.05 wt%

Bacterial culture

E. coli PKL 1162 were grown in LB medium (PKL 1162) overnight in a sterilized test tube, which was covered with aluminum foil at 37 °C. The tubes were shaken with a speed of 140 rpm to guarantee a constant mixing of the solution.

S6 Temperature dependent adhesion of *E. coli* to microgel surfaces

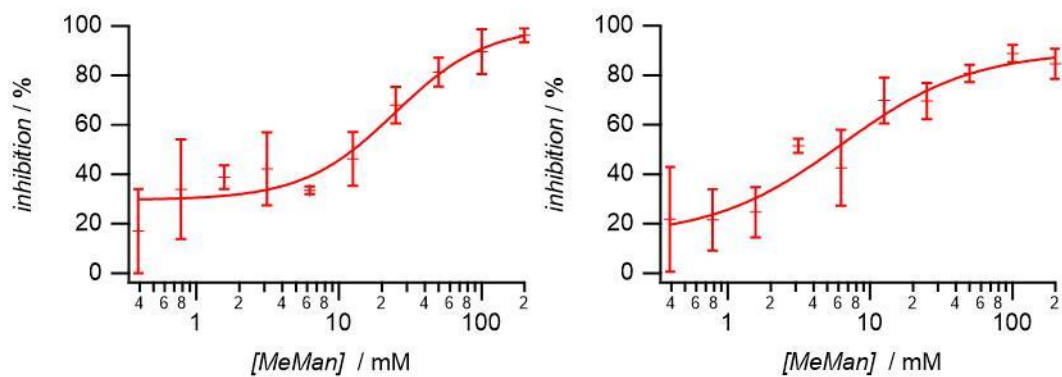


Figure 14: Inhibition measurements for Man0.5 with receptor *E. coli* after 30 min of incubation at 20 °C (left) and 40 °C (right).

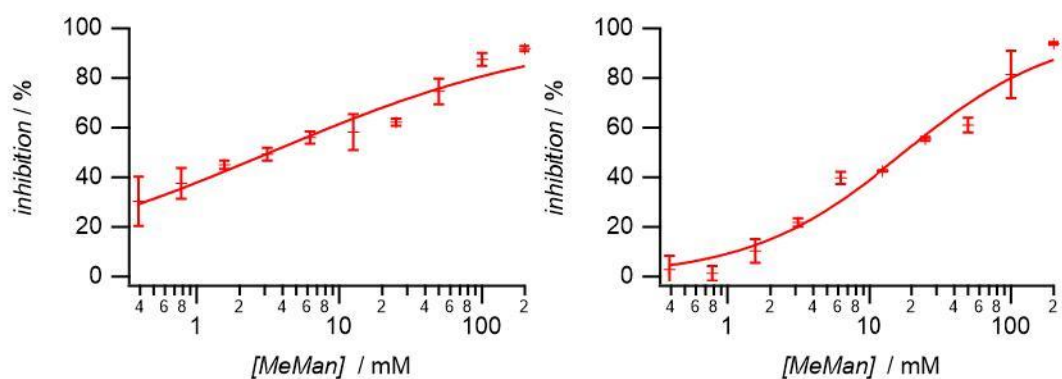


Figure 15: Inhibition measurements for Man0.5 with receptor *E. coli* after 24 h of incubation at 20 °C (left) and 40 °C (right).

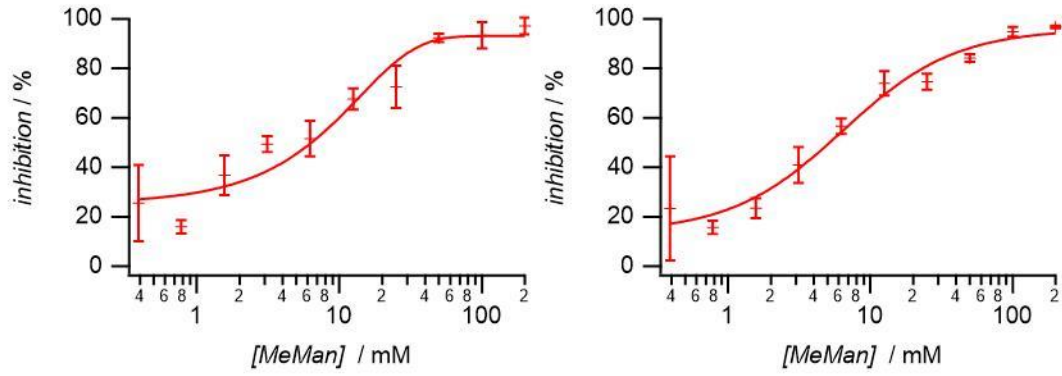


Figure 16: Inhibition measurements for ManM0.4 with receptor *E. coli* after 30 min of incubation at 20 °C (left) and 40 °C (right).

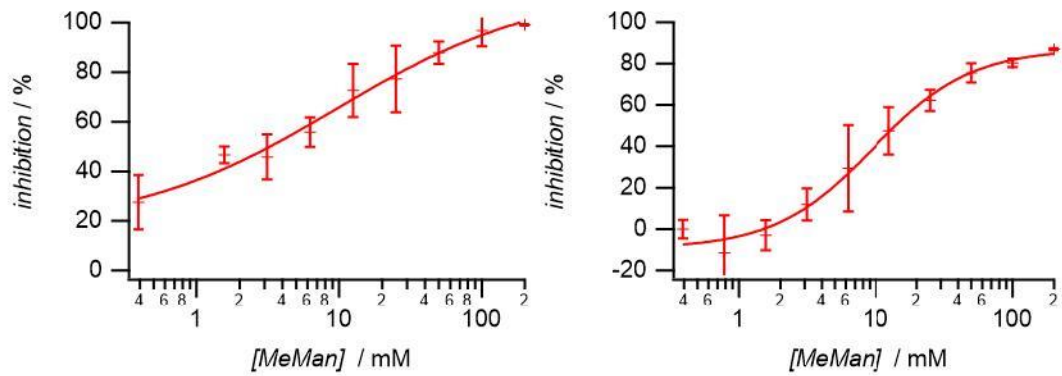


Figure 17: Inhibition measurements for ManM0.4 with receptor *E. coli* after 24 h of incubation at 20 °C (left) and 40 °C (right).

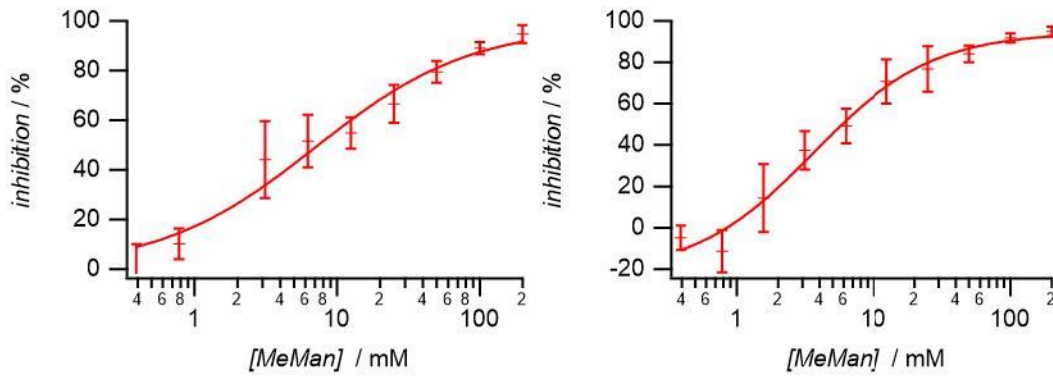


Figure 18: Inhibition measurements for ManM0.8 with receptor *E. coli* after 30 min of incubation at 20 °C (left) and 40 °C (right).

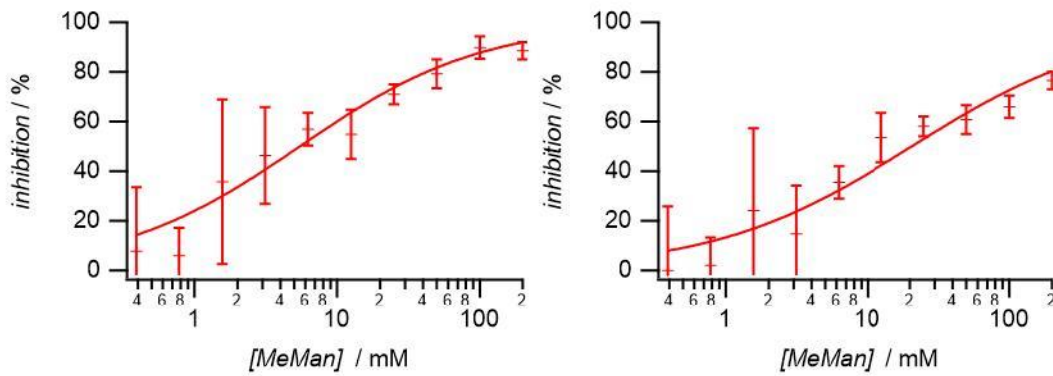


Figure 19: Inhibition measurements for ManM0.8 with receptor *E. coli* after 24 h of incubation at 20 °C (left) and 40 °C (right).

General methods

Phenol-sulfuric acid method (PSA)

The phenol-sulphuric acid method was used to quantify the number of glycomonomers that were included into the polymeric network. Firstly, a calibration curve was established using previously reported procedures.³⁻⁵ A stock solution of 320 μM methyl α -D-mannopyranoside (MeMan) and dilution series of 20, 40, 80, 160 μM in water was prepared. To 125 μL of each solution 125 μL 5 wt% phenol solution in ultrapure water were given and thoroughly mixed, followed by the rapid addition of 625 μL concentrated sulfuric acid and incubating for 30 min at ambient temperature. The absorbance intensity was measured at 490 nm via UV-Vis-spectroscopy. For the measurements of the microgel samples mixtures of 125 μL of a 0.5 wt% microgel dispersion and 125 μL of a 5 wt% phenol solution in ultrapure water were prepared. Afterward 625 μL concentrated sulfuric acid were added rapidly and incubated for 30 min at ambient temperature. Cooled solutions were centrifuged at 10000 g for 20 min, followed by analyzing the supernatant.

Microplate surface preparation

For coating of the 96-well plates 120 μL of a 0.1 mg/mL of microgel in ultrapure water were filled in each well. The plates were dried at 37 °C and shaken at 120 rpm overnight. On the next day the plates were washed with PBST (PBS with 0.5wt% Tween 20, 3 x 120 μL per well).

FITC-ConA Adhesion Inhibition Assay

In the washed and microgel coated microplate a dilution series of MeMan was prepared. Afterwards 50 μL of FITC-ConA solution in LBB ($c = 0.1$ mg/mL) was added to the wells and the plates were incubated for 30 min or 24 h at 100 rpm at either 20 or 40 °C. Afterward, the plates were washed three times with 120 μL of LBB and then filled with 100 μL of LBB per well. Finally, the fluorescence intensity was detected at 485 nm/535 nm.

GFP-Based Bacterial Adhesion Inhibition Assay

The adhesion assay was carried out according to a previous published protocol.⁶ In the washed and microgel coated microplate a dilution series of MeMan was prepared. The bacteria suspension (50 μL) at a concentration of 2 mg/mL ($\text{OD} = 0.4$) was added to the wells, and the plates were incubated for 30 min or 24 h at 100 rpm at either 20 or 40 °C. Afterward, the plates were washed three times with 120 μL of PBS and then filled with 100 μL of PBS per well. Finally, the fluorescence intensity of the adhered *E. coli* was detected at 485 nm/535 nm.

Fluorescence Microscopy

The green fluorescent protein (GFP)-expressing *E. coli* (PKL1162) and FITC-ConA were imaged on an inverted microscope (Olympus IX73, Japan) equipped with an Olympus 60x NA 1.35 oil-immersion objective (Olympus, Japan), and a CMOS camera (DMK 33UX1174L, The Imaging Source, Germany) was used for imaging. Pictures were taken immediately after the washing cycles of the microplates.

References

1. Parry, A. L.; Clemson, N. A.; Ellis, J.; Bernhard, S. S. R.; Davis, B. G.; Cameron, N. R., 'Multicopy Multivalent' Glycopolymer-Stabilized Gold Nanoparticles as Potential Synthetic Cancer Vaccines. *Journal of the American Chemical Society* **2013**, *135* (25), 9362-9365.
2. Wilkins, L. E.; Phillips, D. J.; Deller, R. C.; Davies, G.-L.; Gibson, M. I., Synthesis and characterisation of glucose-functional glycopolymers and gold nanoparticles: study of their potential interactions with ovine red blood cells. *Carbohydrate Research* **2015**, *405*, 47-54.
3. DuBois, M.; Gilles, K. A.; Hamilton, J. K.; Rebers, P. A.; Smith, F., Colorimetric Method for Determination of Sugars and Related Substances. *Analytical Chemistry* **1956**, *28* (3), 350-356.
4. GERCHAKOV, S. M.; HATCHER, P. G., IMPROVED TECHNIQUE FOR ANALYSIS OF CARBOHYDRATES IN SEDIMENTS1. *Limnology and Oceanography* **1972**, *17* (6), 938-943.
5. Boden, S.; Wagner, K. G.; Karg, M.; Hartmann, L., Presenting Precision Glycomacromolecules on Gold Nanoparticles for Increased Lectin Binding. *Polymers* **2017**, *9* (12), 716.
6. Hartmann, M.; Horst, A. K.; Klemm, P.; Lindhorst, T. K., A kit for the investigation of live *Escherichia coli* cell adhesion to glycosylated surfaces. *Chemical Communications* **2010**, *46* (2), 330-332.

5. References

- [1] Krishnaswamy, N. R., Carbohydrate chemistry from Fischer to now. *Resonance* **2011**, *16* (7), 620-639.
- [2] Khadem, H. S. E., *Carbohydrate Chemistry: monosaccharides and their oligomers*. Academic Press, LDT, New York: 1988.
- [3] Boltje, T. J.; Buskas, T.; Boons, G.-J., Opportunities and challenges in synthetic oligosaccharide and glycoconjugate research. *Nature Chemistry* **2009**, *1* (8), 611-622.
- [4] Dwek, R. A., Glycobiology: Toward Understanding the Function of Sugars. *Chemical Reviews* **1996**, *96* (2), 683-720.
- [5] Varki, A., *Essentials of Glycobiology*. Cold Spring Harbor Laboratory Press: 2017.
- [6] Werz, D. B.; Seeberger, P. H., Carbohydrates as the Next Frontier in Pharmaceutical Research. *Chemistry – A European Journal* **2005**, *11* (11), 3194-3206.
- [7] Cecioni, S.; Imberty, A.; Vidal, S., Glycomimetics versus Multivalent Glycoconjugates for the Design of High Affinity Lectin Ligands. *Chemical Reviews* **2015**, *115* (1), 525-561.
- [8] Ernst, B.; Magnani, J. L., From carbohydrate leads to glycomimetic drugs. *Nature Reviews Drug Discovery* **2009**, *8* (8), 661-677.
- [9] Imberty, A.; Varrot, A., Microbial recognition of human cell surface glycoconjugates. *Current Opinion in Structural Biology* **2008**, *18* (5), 567-576.
- [10] Opdenakker, G.; Rudd, P. M.; Ponting, C. P.; Dwek, R. A., Concepts and principles of glycobiology. *The FASEB Journal* **1993**, *7* (14), 1330-1337.
- [11] Werz, D. B.; Seeberger, P. H., Carbohydrates as the next frontier in pharmaceutical research. *Chemistry–A European Journal* **2005**, *11* (11), 3194-3206.
- [12] Werz, D. B.; Ranzinger, R.; Herget, S.; Adibekian, A.; von der Lieth, C.-W.; Seeberger, P. H., Exploring the Structural Diversity of Mammalian Carbohydrates (“Glycospace”) by Statistical Databank Analysis. *ACS Chemical Biology* **2007**, *2* (10), 685-691.
- [13] Weis, W. I.; Drickamer, K., Structural basis of lectin-carbohydrate recognition. *Annual review of biochemistry* **1996**, *65*, 441-73.
- [14] Chemani, C.; Imberty, A.; de Bentzmann, S.; Pierre, M.; Wimmerová, M.; Guery, B. P.; Faure, K., Role of LecA and LecB lectins in *Pseudomonas aeruginosa*-induced lung injury and effect of carbohydrate ligands. *Infect Immun* **2009**, *77* (5), 2065-2075.
- [15] Kimble, B.; Nieto, G. R.; Perez, D. R., Characterization of influenza virus sialic acid receptors in minor poultry species. *Virology* **2010**, *7*, 365-365.

- [16] Leonidas, D. D.; Elbert, B. L.; Zhou, Z.; Leffler, H.; Ackerman, S. J.; Acharya, K. R., Crystal structure of human Charcot-Leyden crystal protein, an eosinophil lysophospholipase, identifies it as a new member of the carbohydrate-binding family of galectins. *Structure (London, England : 1993)* **1995**, 3 (12), 1379-93.
- [17] Köttgen, E.; Reutter, W.; Tauber, R., Endogene Lectine des Menschen und ihre Zuckerliganden. *Medizinische Klinik* **2003**, 98 (12), 717-738.
- [18] Alberts, B.; Johnson, A. D.; Lewis, J.; Morgan, D.; Raff, M.; Roberts, K.; Walter, P., *Molekularbiologie der Zelle*. John Wiley & Sons: 2017.
- [19] Voet, D.; Voet, J. G.; Pratt, C. W., *Fundamentals of biochemistry: life at the molecular level*. John Wiley & Sons: 2016.
- [20] Boyd, W. C.; Shapleigh, E., Specific Precipitating Activity of Plant Agglutinins (Lectins). *Science (New York, N.Y.)* **1954**, 119 (3091), 419.
- [21] Berg, J. M.; Stryer, L.; Tymoczko, J. L., *Stryer Biochemie*. Springer-Verlag: 2015.
- [22] Nowell, P. C., Phytohemagglutinin: an initiator of mitosis in cultures of normal human leukocytes. *Cancer research* **1960**, 20, 462-6.
- [23] Sumner, J. B.; Howell, S. F., Identification of Hemagglutinin of Jack Bean with Concanavalin A. *J Bacteriol* **1936**, 32 (2), 227-237.
- [24] Edelman, G. M.; Cunningham, B. A.; Reeke, G. N.; Becker, J. W.; Waxdal, M. J.; Wang, J. L., The Covalent and Three-Dimensional Structure of Concanavalin A. *Proc Natl Acad Sci U S A* **1972**, 69 (9), 2580-2584.
- [25] Hardman, K. D.; Ainsworth, C. F., Structure of concanavalin A at 2.4-Å resolution. *Biochemistry* **1972**, 11 (26), 4910-4919.
- [26] De Schutter, K.; Van Damme, E. J., Protein-carbohydrate interactions as part of plant defense and animal immunity. *Molecules (Basel, Switzerland)* **2015**, 20 (5), 9029-53.
- [27] Blango, M. G.; Mulvey, M. A., Persistence of uropathogenic Escherichia coli in the face of multiple antibiotics. *Antimicrobial agents and chemotherapy* **2010**, 54 (5), 1855-1863.
- [28] Sharon, N., Carbohydrates as future anti-adhesion drugs for infectious diseases. *Biochimica et Biophysica Acta (BBA)-General Subjects* **2006**, 1760 (4), 527-537.
- [29] Powell, L. D.; Varki, A., I-type lectins. *Journal of Biological Chemistry* **1995**, 270 (24), 14243-14246.
- [30] Cummings, R. D.; McEver, R. P., C-Type Lectins. In *Essentials of Glycobiology*, Varki, A.; Cummings, R. D.; Esko, J. D.; Stanley, P.; Hart, G. W.; Aebi, M.; Darvill, A. G.; Kinoshita, T.; Packer, N. H.; Prestegard, J. H.; Schnaar, R. L.; Seeberger, P. H., Eds. Cold Spring Harbor Laboratory Press Copyright 2015-2017 by The

Consortium of Glycobiology Editors, La Jolla, California. All rights reserved.: Cold Spring Harbor (NY), 2015; pp 435-52.

- [31] Isberg, R. R.; Barnes, P., Dancing with the host: flow-dependent bacterial adhesion. *Cell* **2002**, *110* (1), 1-4.
- [32] Sumner, J. B., The globulins of the jack bean, *Canavalia ensiformis* preliminary paper. *Journal of Biological Chemistry* **1919**, *37* (1), 137-142.
- [33] Ambrosi, M.; Cameron, N. R.; Davis, B. G., Lectins: tools for the molecular understanding of the glycode. *Organic & biomolecular chemistry* **2005**, *3* (9), 1593-608.
- [34] Wittmann, V.; Pieters, R. J., Bridging lectin binding sites by multivalent carbohydrates. *Chemical Society Reviews* **2013**, *42* (10), 4492-4503.
- [35] Smith, E. A.; Thomas, W. D.; Kiessling, L. L.; Corn, R. M., Surface plasmon resonance imaging studies of protein-carbohydrate interactions. *Journal of the American Chemical Society* **2003**, *125* (20), 6140-6148.
- [36] Gou, Y.; Geng, J.; Richards, S. J.; Burns, J.; Remzi Becer, C.; Haddleton, D., A detailed study on understanding glycopolymer library and Con A interactions. *Journal of Polymer Science Part A: Polymer Chemistry* **2013**, *51* (12), 2588-2597.
- [37] Lis, H.; Sharon, N., Lectins: Carbohydrate-specific proteins that mediate cellular recognition. *Chemical Reviews* **1998**, *98* (2), 637-674.
- [38] Kline, K. A.; Fälker, S.; Dahlberg, S.; Normark, S.; Henriques-Normark, B., Bacterial adhesins in host-microbe interactions. *Cell host & microbe* **2009**, *5* (6), 580-92.
- [39] Sperling, O.; Fuchs, A.; Lindhorst, T. K., Evaluation of the carbohydrate recognition domain of the bacterial adhesin FimH: design, synthesis and binding properties of mannoside ligands. *Organic & biomolecular chemistry* **2006**, *4* (21), 3913-3922.
- [40] Hori, K.; Matsumoto, S., Bacterial adhesion: From mechanism to control. *Biochemical Engineering Journal* **2010**, *48* (3), 424-434.
- [41] Mulvey, M. A.; Lopez-Boado, Y. S.; Wilson, C. L.; Roth, R.; Parks, W. C.; Heuser, J.; Hultgren, S. J., Induction and Evasion of Host Defenses by Type 1-Piliated Uropathogenic *Escherichia coli*. *Science (New York, N.Y.)* **1998**, *282* (5393), 1494-1497.
- [42] Brumbaugh, A. R.; Mobley, H. L. T., Preventing urinary tract infection: progress toward an effective *Escherichia coli* vaccine. *Expert Rev Vaccines* **2012**, *11* (6), 663-676.
- [43] Barber, A. E.; Norton, J. P.; Spivak, A. M.; Mulvey, M. A., Urinary tract infections: current and emerging management strategies. *Clin Infect Dis* **2013**, *57* (5), 719-724.

References

- [44] Langermann, S.; Palaszynski, S.; Barnhart, M.; Auguste, G.; Pinkner, J. S.; Burlein, J.; Barren, P.; Koenig, S.; Leath, S.; Jones, C. H.; Hultgren, S. J., Prevention of Mucosal *Escherichia coli* Infection by FimH-Adhesin-Based Systemic Vaccination. *Science (New York, N.Y.)* **1997**, *276* (5312), 607-611.
- [45] Langermann, S.; Möllby, R.; Burlein, J. E.; Palaszynski, S. R.; Auguste, C. G.; DeFusco, A.; Strouse, R.; Schenerman, M. A.; Hultgren, S. J.; Pinkner, J. S.; Winberg, J.; Guldevall, L.; Söderhäll, M.; Ishikawa, K.; Normark, S.; Koenig, S., Vaccination with FimH adhesin protects cynomolgus monkeys from colonization and infection by uropathogenic *Escherichia coli*. *The Journal of infectious diseases* **2000**, *181* (2), 774-8.
- [46] Klemm, P.; Schembri, M. A., Bacterial adhesins: function and structure. *International Journal of Medical Microbiology* **2000**, *290* (1), 27-35.
- [47] Touaibia, M.; Roy, R., Glycodendrimers as anti-adhesion drugs against type 1 fimbriated *E. coli* uropathogenic infections. *Mini reviews in medicinal chemistry* **2007**, *7* (12), 1270-83.
- [48] Bouckaert, J.; Berglund, J.; Schembri, M.; De Genst, E.; Cools, L.; Wuhrer, M.; Hung, C. S.; Pinkner, J.; Slättegård, R.; Zavialov, A.; Choudhury, D.; Langermann, S.; Hultgren, S. J.; Wyns, L.; Klemm, P.; Oscarson, S.; Knight, S. D.; De Greve, H., Receptor binding studies disclose a novel class of high-affinity inhibitors of the *Escherichia coli* FimH adhesin. *Molecular microbiology* **2005**, *55* (2), 441-55.
- [49] Choudhury, D.; Thompson, A.; Stojanoff, V.; Langermann, S.; Pinkner, J.; Hultgren, S. J.; Knight, S. D., X-ray structure of the FimC-FimH chaperone-adhesin complex from uropathogenic *Escherichia coli*. *Science (New York, N.Y.)* **1999**, *285* (5430), 1061-6.
- [50] Wellens, A.; Garofalo, C.; Nguyen, H.; Gerven, N.; Slättegård, R.; Hernalsteens, J.-P.; Wyns, L.; Oscarson, S.; De Greve, H.; Hultgren, S.; Bouckaert, J., Intervening with Urinary Tract Infections Using Anti-Adhesives Based on the Crystal Structure of the FimH–Oligomannose-3 Complex. *PloS one* **2008**, *3*, e2040.
- [51] Lis, H.; Sharon, N., Lectins: Carbohydrate-Specific Proteins That Mediate Cellular Recognition. *Chem Rev* **1998**, *98* (2), 637-674.
- [52] Hung, C. S.; Bouckaert, J.; Hung, D.; Pinkner, J.; Widberg, C.; DeFusco, A.; Auguste, C. G.; Strouse, R.; Langermann, S.; Waksman, G., Structural basis of tropism of *Escherichia coli* to the bladder during urinary tract infection. *Molecular microbiology* **2002**, *44* (4), 903-915.
- [53] Lee, Y. C.; Lee, R. T., Carbohydrate-Protein Interactions: Basis of Glycobiology. *Accounts of Chemical Research* **1995**, *28* (8), 321-327.

- [54] Dam, T. K.; Roy, R.; Das, S. K.; Oscarson, S.; Brewer, C. F., Binding of Multivalent Carbohydrates to Concanavalin A and Dioclea grandiflora Lectin THERMODYNAMIC ANALYSIS OF THE "MULTIVALENCY EFFECT". *Journal of Biological Chemistry* **2000**, 275 (19), 14223-14230.
- [55] Barnard, A.; Smith, D. K., Self-Assembled Multivalency: Dynamic Ligand Arrays for High-Affinity Binding. *Angewandte Chemie International Edition* **2012**, 51 (27), 6572-6581.
- [56] Vrasidas, I.; de Mol, N. J.; Liskamp, R. M.; Pieters, R. J., Synthesis of lactose dendrimers and multivalency effects in binding to the cholera toxin B subunit. *European journal of organic chemistry* **2001**, 2001 (24), 4685-4692.
- [57] Mann, D. A.; Kanai, M.; Maly, D. J.; Kiessling, L. L., Probing Low Affinity and Multivalent Interactions with Surface Plasmon Resonance: Ligands for Concanavalin A. *Journal of the American Chemical Society* **1998**, 120 (41), 10575-10582.
- [58] Fasting, C.; Schalley, C. A.; Weber, M.; Seitz, O.; Hecht, S.; Kocsch, B.; Dervedde, J.; Graf, C.; Knapp, E.-W.; Haag, R., Multivalency as a Chemical Organization and Action Principle. *Angewandte Chemie International Edition* **2012**, 51 (42), 10472-10498.
- [59] Fasting, C.; Schalley, C. A.; Weber, M.; Seitz, O.; Hecht, S.; Kocsch, B.; Dervedde, J.; Graf, C.; Knapp, E. W.; Haag, R., Multivalency as a chemical organization and action principle. *Angewandte Chemie International Edition* **2012**, 51 (42), 10472-10498.
- [60] Pieters, R. J., Maximising multivalency effects in protein-carbohydrate interactions. *Organic & biomolecular chemistry* **2009**, 7 (10), 2013-2025.
- [61] Kitov, P. I.; Bundle, D. R., On the nature of the multivalency effect: a thermodynamic model. *Journal of the American Chemical Society* **2003**, 125 (52), 16271-16284.
- [62] Mack, E. T.; Snyder, P. W.; Perez-Castillejos, R.; Bilgi er, B. a.; Moustakas, D. T.; Butte, M. J.; Whitesides, G. M., Dependence of avidity on linker length for a bivalent ligand-bivalent receptor model system. *Journal of the American Chemical Society* **2012**, 134 (1), 333-345.
- [63] Deniaud, D.; Julienne, K.; Gouin, S. G., Insights in the rational design of synthetic multivalent glycoconjugates as lectin ligands. *Organic & biomolecular chemistry* **2011**, 9 (4), 966-979.
- [64] Kitov, P. I.; Sadowska, J. M.; Mulvey, G.; Armstrong, G. D.; Ling, H.; Pannu, N. S.; Read, R. J.; Bundle, D. R., Shiga-like toxins are neutralized by tailored multivalent carbohydrate ligands. *Nature* **2000**, 403 (6770), 669-672.

- [65] Kiessling, L. L.; Gestwicki, J. E.; Strong, L. E., Synthetic multivalent ligands in the exploration of cell-surface interactions. *Current Opinion in Chemical Biology* **2000**, 4 (6), 696-703.
- [66] Gestwicki, J. E.; Cairo, C. W.; Strong, L. E.; Oetjen, K. A.; Kiessling, L. L., Influencing Receptor–Ligand Binding Mechanisms with Multivalent Ligand Architecture. *Journal of the American Chemical Society* **2002**, 124 (50), 14922-14933.
- [67] Ernst, B.; Magnani, J. L., From carbohydrate leads to glycomimetic drugs. *Nature reviews. Drug discovery* **2009**, 8 (8), 661-77.
- [68] Li, X.; Chen, G., Glycopolymer-based nanoparticles: synthesis and application. *Polymer Chemistry* **2015**, 6 (9), 1417-1430.
- [69] Kiessling, L. L.; Splain, R. A., Chemical approaches to glycobiology. *Annual review of biochemistry* **2010**, 79, 619-53.
- [70] Freichel, T.; Eierhoff, S.; Snyder, N. L.; Hartmann, L., Toward Orthogonal Preparation of Sequence-Defined Monodisperse Heteromultivalent Glycomacromolecules on Solid Support Using Staudinger Ligation and Copper-Catalyzed Click Reactions. *The Journal of Organic Chemistry* **2017**, 82 (18), 9400-9409.
- [71] Gómez-García, M.; Benito, J. M.; Rodríguez-Lucena, D.; Yu, J.-X.; Chmurski, K.; Ortiz Mellet, C.; Gutiérrez Gallego, R.; Maestre, A.; Defaye, J.; García Fernández, J. M., Probing Secondary Carbohydrate–Protein Interactions with Highly Dense Cyclodextrin-Centered Heteroglycoclusters: The Heterocluster Effect. *Journal of the American Chemical Society* **2005**, 127 (22), 7970-7971.
- [72] Ladmiral, V.; Mantovani, G.; Clarkson, G. J.; Cauet, S.; Irwin, J. L.; Haddleton, D. M., Synthesis of Neoglycopolymers by a Combination of “Click Chemistry” and Living Radical Polymerization. *Journal of the American Chemical Society* **2006**, 128 (14), 4823-4830.
- [73] Soria-Martinez, L.; Bauer, S.; Giesler, M.; Schelhaas, S.; Materlik, J.; Janus, K.; Pierzyna, P.; Becker, M.; Snyder, N. L.; Hartmann, L.; Schelhaas, M., Prophylactic Antiviral Activity of Sulfated Glycomimetic Oligomers and Polymers. *Journal of the American Chemical Society* **2020**, 142 (11), 5252-5265.
- [74] Ladmiral, V.; Melia, E.; Haddleton, D. M., Synthetic glycopolymers: an overview. *European Polymer Journal* **2004**, 40 (3), 431-449.
- [75] Chabre, Y. M.; Roy, R., Recent trends in glycodendrimer syntheses and applications. *Current topics in medicinal chemistry* **2008**, 8 (14), 1237-85.
- [76] El-Boubbou, K.; Gruden, C.; Huang, X., Magnetic Glyco-nanoparticles: A Unique Tool for Rapid Pathogen Detection, Decontamination, and Strain Differentiation. *Journal of the American Chemical Society* **2007**, 129 (44), 13392-13393.

- [77] Ting, S. R. S.; Chen, G.; Stenzel, M. H., Synthesis of glycopolymers and their multivalent recognitions with lectins. *Polymer Chemistry* **2010**, *1* (9), 1392-1412.
- [78] Baier, M.; Rustmeier, N. H.; Harr, J.; Cyrus, N.; Reiss, G. J.; Grafmüller, A.; Blaum, B. S.; Stehle, T.; Hartmann, L., Divalent Sialylated Precision Glycooligomers Binding to Polyomaviruses and the Effect of Different Linkers. *Macromolecular bioscience* **2019**, *19* (5), e1800426.
- [79] van Kasteren, S. I.; Campbell, S. J.; Serres, S.; Anthony, D. C.; Sibson, N. R.; Davis, B. G., Glyconanoparticles allow pre-symptomatic in vivo imaging of brain disease. *Proc Natl Acad Sci U S A* **2009**, *106* (1), 18-23.
- [80] Dalziel, M.; Crispin, M.; Scanlan, C. N.; Zitzmann, N.; Dwek, R. A., Emerging principles for the therapeutic exploitation of glycosylation. *Science (New York, N.Y.)* **2014**, *343* (6166), 1235681.
- [81] Hudak, Jason E.; Bertozzi, Carolyn R., Glycotherapy: New Advances Inspire a Reemergence of Glycans in Medicine. *Chemistry & Biology* **2014**, *21* (1), 16-37.
- [82] Fernández-Tejada, A.; Cañada, F. J.; Jiménez-Barbero, J., Recent Developments in Synthetic Carbohydrate-Based Diagnostics, Vaccines, and Therapeutics. *Chemistry – A European Journal* **2015**, *21* (30), 10616-10628.
- [83] Garnier, P.; Wang, X.-T.; Robinson, M. A.; van Kasteren, S.; Perkins, A. C.; Frier, M.; Fairbanks, A. J.; Davis, B. G., Lectin-directed enzyme activated prodrug therapy (LEAPT): Synthesis and evaluation of rhamnose-capped prodrugs. *Journal of Drug Targeting* **2010**, *18* (10), 794-802.
- [84] Alarcón, C. d. I. H.; Pennadam, S.; Alexander, C., Stimuli responsive polymers for biomedical applications. *Chemical Society Reviews* **2005**, *34* (3), 276-285.
- [85] Kiessling, L. L.; Grim, J. C., Glycopolymer probes of signal transduction. *Chemical Society Reviews* **2013**, *42* (10), 4476-4491.
- [86] Zhang, Y.; Chan, J. W.; Moretti, A.; Uhrich, K. E., Designing polymers with sugar-based advantages for bioactive delivery applications. *Journal of Controlled Release* **2015**, *219*, 355-368.
- [87] Ghadban, A.; Albertin, L., Synthesis of glycopolymer architectures by reversible-deactivation radical polymerization. *Polymers* **2013**, *5* (2), 431-526.
- [88] Jelinek, R.; Kolusheva, S., Carbohydrate biosensors. *Chemical reviews* **2004**, *104* (12), 5987-6016.
- [89] Ahmes, M., The effect of polymer architecture, composition and molecular weight on the properties of glycopolymer-based non-viral gene delivery systems. *Biomaterials* **2011**, *32*, 5276-5290.
- [90] Becer, C. R.; Gibson, M. I.; Geng, J.; Ilyas, R.; Wallis, R.; Mitchell, D. A.; Haddleton, D. M., High-affinity glycopolymer binding to human DC-SIGN and disruption of DC-

- SIGN interactions with HIV envelope glycoprotein. *Journal of the American Chemical Society* **2010**, *132* (43), 15130-15132.
- [91] David, A.; Kopecková, P.; Kopecek, J.; Rubinstein, A., The role of galactose, lactose, and galactose valency in the biorecognition of N-(2-hydroxypropyl) methacrylamide copolymers by human colon adenocarcinoma cells. *Pharmaceutical research* **2002**, *19* (8), 1114-1122.
- [92] Gambaryan, A.; Boravleva, E.; Matrosovich, T.; Matrosovich, M.; Klenk, H.-D.; Moiseeva, E.; Tuzikov, A.; Chinarev, A.; Pazynina, G.; Bovin, N., Polymer-bound 6' sialyl-N-acetyllactosamine protects mice infected by influenza virus. *Antiviral research* **2005**, *68* (3), 116-123.
- [93] Armes, R.; Steven, P., Synthesis and aqueous solution properties of novel sugar methacrylate-based homopolymers and block polymers. *Biomacromolecules* **2003**, *4*, 1746-1758.
- [94] Bernard, J.; Hao, X.; Davis, T. P.; Barner-Kowollik, C.; Stenzel, M. H., Synthesis of various glycopolymer architectures via RAFT polymerization: from block copolymers to stars. *Biomacromolecules* **2006**, *7* (1), 232-238.
- [95] Ambrosi, M.; Cameron, N. R.; Davis, B. G.; Stolnik, S., Investigation of the interaction between peanut agglutinin and synthetic glycopolymeric multivalent ligands. *Organic & biomolecular chemistry* **2005**, *3* (8), 1476-1480.
- [96] Ting, S. S.; Gregory, A. M.; Stenzel, M. H., Polygalactose containing nanocages: the RAFT process for the synthesis of hollow sugar balls. *Biomacromolecules* **2009**, *10* (2), 342-352.
- [97] Miura, Y., Design and synthesis of well-defined glycopolymers for the control of biological functionalities. *Polymer journal* **2012**, *44* (7), 679-689.
- [98] Gauthier, M. A.; Gibson, M. I.; Klok, H. A., Synthesis of functional polymers by post-polymerization modification. *Angewandte Chemie International Edition* **2009**, *48* (1), 48-58.
- [99] Bahulekar, R.; Tokiwa, T.; Kano, J.; Matsumura, T.; Kojima, I.; Kodama, M., Polyacrylamide containing sugar residues: synthesis, characterization and cell compatibility studies. *Carbohydrate polymers* **1998**, *37* (1), 71-78.
- [100] Davies, M. C.; Dawkins, J. V.; Hourston, D. J., Radical copolymerization of maleic anhydride and substituted styrenes by reversible addition-fragmentation chain transfer (RAFT) polymerization. *Polymer* **2005**, *46* (6), 1739-1753.
- [101] Strong, L. E.; Kiessling, L. L., A general synthetic route to defined, biologically active multivalent arrays. *Journal of the American Chemical Society* **1999**, *121* (26), 6193-6196.

- [102] Meng, H.; Li, G., A Review of Stimuli-responsive Shape Memory Polymer Composites. *Polymer* **2013**, *54*, 2199-2221.
- [103] Wei, M.; Gao, Y.; Li, X.; Serpe, M. J., Stimuli-responsive polymers and their applications. *Polymer Chemistry* **2017**, *8* (1), 127-143.
- [104] Dai, S.; Ravi, P.; Tam, K. C., pH-Responsive polymers: synthesis, properties and applications. *Soft Matter* **2008**, *4* (3), 435-449.
- [105] Jochum, F. D.; Theato, P., Temperature- and light-responsive smart polymer materials. *Chemical Society Reviews* **2013**, *42* (17), 7468-7483.
- [106] Jeong, B.; Gutowska, A., Lessons from nature: stimuli-responsive polymers and their biomedical applications. *Trends in Biotechnology* **2002**, *20* (7), 305-311.
- [107] Galaev, I. Y.; Mattiasson, B., 'Smart' polymers and what they could do in biotechnology and medicine. *Trends in Biotechnology* **1999**, *17* (8), 335-340.
- [108] Mura, S.; Nicolas, J.; Couvreur, P., Stimuli-responsive nanocarriers for drug delivery. *Nat Mater* **2013**, *12* (11), 991-1003.
- [109] Huang, X.; Li, M.; Green, D. C.; Williams, D. S.; Patil, A. J.; Mann, S., Interfacial assembly of protein-polymer nano-conjugates into stimulus-responsive biomimetic protocells. *Nature Communications* **2013**, *4* (1), 2239.
- [110] Gil, E. S.; Hudson, S. M., Stimuli-responsive polymers and their bioconjugates. *Progress in Polymer Science* **2004**, *29* (12), 1173-1222.
- [111] Zhang, Q.; Weber, C.; Schubert, U. S.; Hoogenboom, R., Thermoresponsive polymers with lower critical solution temperature: from fundamental aspects and measuring techniques to recommended turbidimetry conditions. *Materials Horizons* **2017**, *4* (2), 109-116.
- [112] Fujishige, S.; Kubota, K.; Ando, I., Phase transition of aqueous solutions of poly (N-isopropylacrylamide) and poly (N-isopropylmethacrylamide). *The Journal of Physical Chemistry* **1989**, *93* (8), 3311-3313.
- [113] Burmistrova, A.; Richter, M.; Uzum, C.; von Klitzing, R., Effect of cross-linker density of P(NIPAM-co-AAc) microgels at solid surfaces on the swelling/shrinking behaviour and the Young's modulus. *Colloid and Polymer Science* **2011**, *289* (5-6), 613-624.
- [114] Solomon, O.; Corciovei, M.; Ciută, I.; Boghină, C., Properties of solutions of poly-N-vinylcaprolactam. *Journal of Applied Polymer Science* **1968**, *12* (8), 1835-1842.
- [115] Han, S.; Hagiwara, M.; Ishizone, T., Synthesis of thermally sensitive water-soluble polymethacrylates by living anionic polymerizations of oligo (ethylene glycol) methyl ether methacrylates. *Macromolecules* **2003**, *36* (22), 8312-8319.
- [116] Halperin, A.; Kröger, M.; Winnik, F. M., Poly(N-isopropylacrylamide) Phase Diagrams: Fifty Years of Research. *Angewandte Chemie International Edition* **2015**, *54* (51), 15342-15367.

- [117] Schild, H. G., Poly(N-isopropylacrylamide): experiment, theory and application. *Progress in Polymer Science* **1992**, 17 (2), 163-249.
- [118] Liu, R.; Fraylich, M.; Saunders, B. R., Thermoresponsive copolymers: from fundamental studies to applications. *Colloid and Polymer Science* **2009**, 287 (6), 627-643.
- [119] Paul, T. J.; Strzelczyk, A. K.; Feldhof, M. I.; Schmidt, S., Temperature-Switchable Glycopolymers and Their Conformation-Dependent Binding to Receptor Targets. *Biomacromolecules* **2020**, 21 (7), 2913-2921.
- [120] Crespy, D.; Rossi, R. M., Temperature-responsive polymers with LCST in the physiological range and their applications in textiles. *Polymer International* **2007**, 56 (12), 1461-1468.
- [121] Serpe, M. J.; Kim, J.; Lyon, L. A., Colloidal Hydrogel Microlenses. *Advanced Materials* **2004**, 16 (2), 184-187.
- [122] Chilkoti, A.; Chen, G.; Stayton, P. S.; Hoffman, A. S., Site-Specific Conjugation of a Temperature-Sensitive Polymer to a Genetically Engineered Protein. *Bioconjugate Chemistry* **1994**, 5 (6), 504-507.
- [123] Stayton, P. S.; Shimoboji, T.; Long, C.; Chilkoti, A.; Chen, G.; Harris, J. M.; Hoffman, A. S., Control of protein-ligand recognition using a stimuli-responsive polymer. *Nature* **1995**, 378 (6556), 472-4.
- [124] You, Y.-Z.; Kalebaila, K. K.; Brock, S. L.; Oupický, D., Temperature-Controlled Uptake and Release in PNIPAM-Modified Porous Silica Nanoparticles. *Chemistry of Materials* **2008**, 20 (10), 3354-3359.
- [125] Zhang, J.; Srivastava, R.; Misra, R. D. K., Core-Shell Magnetite Nanoparticles Surface Encapsulated with Smart Stimuli-Responsive Polymer: Synthesis, Characterization, and LCST of Viable Drug-Targeting Delivery System. *Langmuir : the ACS journal of surfaces and colloids* **2007**, 23, 6342-51.
- [126] Morones-Ramirez, J.; Frey, W., Room temperature synthesis of an optically and thermally responsive hybrid PNIPAM-gold nanoparticle. *Journal of Nanoparticle Research* **2009**, 12, 1401-1414.
- [127] Fraser, C.; Grubbs, R. H., Synthesis of Glycopolymers of Controlled Molecular Weight by Ring-Opening Metathesis Polymerization Using Well-Defined Functional Group Tolerant Ruthenium Carbene Catalysts. *Macromolecules* **1995**, 28 (21), 7248-7255.
- [128] Miura, Y.; Kato, K.; Takegawa, Y.; Kuroguchi, M.; Furukawa, J.; Shinohara, Y.; Nagahori, N.; Amano, M.; Hinou, H.; Nishimura, S., Glycoblotting-assisted O-glycomics: ammonium carbamate allows for highly efficient o-glycan release from glycoproteins. *Analytical chemistry* **2010**, 82 (24), 10021-9.

- [129] Godula, K.; Rabuka, D.; Nam, K. T.; Bertozzi, C. R., Synthesis and microcontact printing of dual end-functionalized mucin-like glycopolymers for microarray applications. *Angew Chem Int Ed Engl* **2009**, *48* (27), 4973-4976.
- [130] van Dongen, S. F. M.; de Hoog, H.-P. M.; Peters, R. J. R. W.; Nallani, M.; Nolte, R. J. M.; van Hest, J. C. M., Biohybrid Polymer Capsules. *Chemical Reviews* **2009**, *109* (11), 6212-6274.
- [131] Barbey, R.; Lavanant, L.; Paripovic, D.; Schuwer, N.; Sugnaux, C.; Tugulu, S.; Klok, H.-A., Polymer brushes via surface-initiated controlled radical polymerization: synthesis, characterization, properties, and applications. *Chemical reviews* **2009**, *109* (11), 5437-5527.
- [132] Tiwari, R.; H nders, D.; Schipmann, S.; Schulte, B. r.; Das, P.; Pester, C. W.; Klemradt, U.; Walther, A., A versatile synthesis platform to prepare uniform, highly functional microgels via click-type functionalization of latex particles. *Macromolecules* **2014**, *47* (7), 2257-2267.
- [133] Shewan, H. M.; Stokes, J. R., Review of techniques to manufacture micro-hydrogel particles for the food industry and their applications. *Journal of Food Engineering* **2013**, *119* (4), 781-792.
- [134] Saunders, B. R.; Vincent, B., Microgel particles as model colloids: theory, properties and applications. *Advances in Colloid and Interface Science* **1999**, *80* (1), 1-25.
- [135] Thorne, J. B.; Vine, G. J.; Snowden, M. J., Microgel applications and commercial considerations. *Colloid and Polymer Science* **2011**, *289* (5), 625.
- [136] Peppas, N. A.; Bures, P.; Leobandung, W.; Ichikawa, H., Hydrogels in pharmaceutical formulations. *European Journal of Pharmaceutics and Biopharmaceutics* **2000**, *50* (1), 27-46.
- [137] Peppas, N. A.; Stauffer, S. R., Reinforced uncrosslinked poly (vinyl alcohol) gels produced by cyclic freezing-thawing processes: a short review. *Journal of Controlled Release* **1991**, *16* (3), 305-310.
- [138] Schexnailder, P.; Schmidt, G., Nanocomposite polymer hydrogels. *Colloid and Polymer Science* **2009**, *287* (1), 1-11.
- [139] Rowley, J. A.; Madlambayan, G.; Mooney, D. J., Alginate hydrogels as synthetic extracellular matrix materials. *Biomaterials* **1999**, *20* (1), 45-53.
- [140] Jen, A. C.; Wake, M. C.; Mikos, A. G., Review: Hydrogels for cell immobilization. *Biotechnology and Bioengineering* **1996**, *50* (4), 357-364.
- [141] Jana, S.; Banerjee, A.; Gandhi, A., Preparation and characterization of chitosan based polyelectrolyte complex as a carrier of aceclofenac. *J PharmaSciTech* **2014**, *3* (2), 1-4.

- [142] Matsuda, T., Device-directed therapeutic drug delivery systems. *Journal of Controlled Release* **2002**, *78* (1), 125-131.
- [143] Lee, K. Y.; Mooney, D. J., Hydrogels for Tissue Engineering. *Chemical Reviews* **2001**, *101* (7), 1869-1880.
- [144] Nayak, S.; Lyon, L. A., Soft Nanotechnology with Soft Nanoparticles. *Angewandte Chemie International Edition* **2005**, *44* (47), 7686-7708.
- [145] Zhai, D.; Liu, B.; Shi, Y.; Pan, L.; Wang, Y.; Li, W.; Zhang, R.; Yu, G., Highly Sensitive Glucose Sensor Based on Pt Nanoparticle/Polyaniline Hydrogel Heterostructures. *ACS Nano* **2013**, *7* (4), 3540-3546.
- [146] Zhu, J., Bioactive modification of poly(ethylene glycol) hydrogels for tissue engineering. *Biomaterials* **2010**, *31* (17), 4639-4656.
- [147] Himmelein, S.; Lewe, V.; Stuart, M. C. A.; Ravoo, B. J., A carbohydrate-based hydrogel containing vesicles as responsive non-covalent cross-linkers. *Chemical Science* **2014**, *5* (3), 1054-1058.
- [148] Nguyen, H. H.; Payré, B.; Fitremann, J.; Lauth-de Viguerie, N.; Marty, J.-D., Thermoresponsive Properties of PNIPAM-Based Hydrogels: Effect of Molecular Architecture and Embedded Gold Nanoparticles. *Langmuir* **2015**, *31* (16), 4761-4768.
- [149] Pelton, R., Temperature-sensitive aqueous microgels. *Advances in Colloid and Interface Science* **2000**, *85* (1), 1-33.
- [150] Zhou, S.; Chu, B., Synthesis and Volume Phase Transition of Poly(methacrylic acid-co-N-isopropylacrylamide) Microgel Particles in Water. *The Journal of Physical Chemistry B* **1998**, *102* (8), 1364-1371.
- [151] Hoare, T.; Pelton, R., Functional Group Distributions in Carboxylic Acid Containing Poly(N-isopropylacrylamide) Microgels. *Langmuir* **2004**, *20* (6), 2123-2133.
- [152] Wong, J. E.; Gaharwar, A. K.; Müller-Schulte, D.; Bahadur, D.; Richtering, W., Dual-stimuli responsive PNiPAM microgel achieved via layer-by-layer assembly: Magnetic and thermoresponsive. *Journal of Colloid and Interface Science* **2008**, *324* (1), 47-54.
- [153] Yao, Z. L.; Grishkewich, N.; Tam, K. C., Swelling and shear viscosity of stimuli-responsive colloidal systems. *Soft Matter* **2013**, *9* (22), 5319-5335.
- [154] Wu, X.; Pelton, R. H.; Hamielec, A. E.; Woods, D. R.; McPhee, W., The kinetics of poly(N-isopropylacrylamide) microgel latex formation. *Colloid and Polymer Science* **1994**, *272* (4), 467-477.
- [155] Gao, J.; Frisken, B. J., Influence of Reaction Conditions on the Synthesis of Self-Cross-Linked N-Isopropylacrylamide Microgels. *Langmuir* **2003**, *19* (13), 5217-5222.

- [156] Hashmi, S. M.; Dufresne, E. R., Mechanical properties of individual microgel particles through the deswelling transition. *Soft Matter* **2009**, *5* (19), 3682-3688.
- [157] Yunker, P. J.; Chen, K.; Gratale, M. D.; Lohr, M. A.; Still, T.; Yodh, A. G., Physics in ordered and disordered colloidal matter composed of poly(N-isopropylacrylamide) microgel particles. *Rep Prog Phys* **2014**, *77* (5), 056601.
- [158] Ballauff, M.; Lu, Y., "Smart" nanoparticles: Preparation, characterization and applications. *Polymer* **2007**, *48* (7), 1815-1823.
- [159] Jacobi, F.; Camaleño de la Calle, A.; Boden, S.; Grafmüller, A.; Hartmann, L.; Schmidt, S., Multivalent Binding of Precision Glycooligomers on Soft Glycocalyx Mimicking Hydrogels. *Biomacromolecules* **2018**, *19* (8), 3479-3488.
- [160] Zhang, Z.; Chen, N.; Li, S.; Battig, M. R.; Wang, Y., Programmable Hydrogels for Controlled Cell Catch and Release Using Hybridized Aptamers and Complementary Sequences. *Journal of the American Chemical Society* **2012**, *134* (38), 15716-15719.
- [161] Schmidt, S.; Zeiser, M.; Hellweg, T.; Duschl, C.; Fery, A.; Mohwald, H., Adhesion and Mechanical Properties of PNIPAM Microgel Films and Their Potential Use as Switchable Cell Culture Substrates. *Advanced Functional Materials* **2010**, *20* (19), 3235-3243.
- [162] Burmistrova, A.; von Klitzing, R., Control of number density and swelling/shrinking behavior of P(NIPAM-AAc) particles at solid surfaces. *Journal of Materials Chemistry* **2010**, *20* (17), 3502-3507.
- [163] Wu, C., A comparison between the 'coil-to-globule' transition of linear chains and the "volume phase transition" of spherical microgels1Dedicated to the 80th birthday of Professor Renyuan Qian.1. *Polymer* **1998**, *39* (19), 4609-4619.
- [164] Burmistrova, A.; Richter, M.; Üzüüm, C.; Klitzing, R., Effect of cross-linker density of P(NIPAM-co-AAc) microgels at solid surfaces on the swelling/shrinking behaviour and the Young's modulus. *Colloid and Polymer Science* **2011**, *289*, 613-624.
- [165] Wiedemair, J.; Serpe, M. J.; Kim, J.; Masson, J.-F.; Lyon, L. A.; Mizaikoff, B.; Kranz, C., In-Situ AFM Studies of the Phase-Transition Behavior of Single Thermoresponsive Hydrogel Particles. *Langmuir* **2007**, *23* (1), 130-137.
- [166] Schmidt, S.; Motschmann, H.; Hellweg, T.; von Klitzing, R., Thermoresponsive surfaces by spin-coating of PNIPAM-co-PAA microgels: A combined AFM and ellipsometry study. *Polymer* **2008**, *49* (3), 749-756.
- [167] Lim, J.; Yeap, S. P.; Che, H. X.; Low, S. C., Characterization of magnetic nanoparticle by dynamic light scattering. *Nanoscale Research Letters* **2013**, *8* (1), 381.

- [168] Einstein, A., Über die von der molekularkinetischen Theorie der Wärme geforderte Bewegung von in ruhenden Flüssigkeiten suspendierten Teilchen. *Annalen der Physik* **1905**, 322 (8), 549-560.
- [169] Clara-Rahola, J.; Fernandez-Nieves, A.; Sierra-Martin, B.; South, A.; Lyon, L. A.; Kohlbrecher, J.; Fernandez Barbero, A., Structural properties of thermoresponsive poly (N-isopropylacrylamide)-poly (ethyleneglycol) microgels. *The Journal of Chemical Physics* **2012**, 136 (21), 214903.
- [170] Binnig, G.; Quate, C. F.; Gerber, C., Atomic force microscope. *Physical review letters* **1986**, 56 (9), 930.
- [171] Sorrell, C. D.; Lyon, L. A., Bimodal swelling responses in microgel thin films. *The Journal of Physical Chemistry B* **2007**, 111 (16), 4060-4066.
- [172] Burmistrova, A.; von Klitzing, R., Control of number density and swelling/shrinking behavior of P (NIPAM-AAc) particles at solid surfaces. *Journal of Materials Chemistry* **2010**, 20 (17), 3502-3507.
- [173] Lekka, M.; Sainz-Serp, D.; Kulik, A. J.; Wandrey, C., Hydrogel microspheres: influence of chemical composition on surface morphology, local elastic properties, and bulk mechanical characteristics. *Langmuir* **2004**, 20 (23), 9968-9977.
- [174] Glaubitz, M.; Medvedev, N.; Pussak, D.; Hartmann, L.; Schmidt, S.; Helm, C. A.; Delcea, M., A novel contact model for AFM indentation experiments on soft spherical cell-like particles. *Soft Matter* **2014**, 10 (35), 6732-6741.
- [175] Becer, C. R., The Glycopolymer Code: Synthesis of Glycopolymers and Multivalent Carbohydrate-Lectin Interactions. *Macromolecular Rapid Communications* **2012**, 33 (9), 742-752.
- [176] Vinson, N.; Gou, Y.; Becer, C. R.; Haddleton, D. M.; Gibson, M. I., Optimised 'click' synthesis of glycopolymers with mono/di-and trisaccharides. *Polymer Chemistry* **2011**, 2 (1), 107-113.
- [177] Chen, Y.; Chen, G.; Stenzel, M. H., Synthesis and lectin recognition of glyco star polymers prepared by "Clicking" thiocarbohydrates onto a reactive scaffold. *Macromolecules* **2010**, 43 (19), 8109-8114.
- [178] Geng, J.; Biedermann, F.; Zayed, J. M.; Tian, F.; Scherman, O. A., Supramolecular glycopolymers in water: a reversible route toward multivalent carbohydrate-lectin conjugates using cucurbit [8] uril. *Macromolecules* **2011**, 44 (11), 4276-4281.
- [179] Watkins, W. M.; Morgan, W., Neutralization of the anti-H agglutinin in eel serum by simple sugars. *Nature* **1952**, 169 (4307), 825-826.
- [180] Paul, T. J.; Rübél, S.; Hildebrandt, M.; Strzelczyk, A. K.; Spormann, C.; Lindhorst, T. K.; Schmidt, S., Thermosensitive Display of Carbohydrate Ligands on Microgels

- for Switchable Binding of Proteins and Bacteria. *ACS Applied Materials & Interfaces* **2019**, *11* (30), 26674-26683.
- [181] Jahangiri, A.; Owlia, P.; Rasooli, I.; Salimian, J.; Derakhshanifar, E.; Naghipour Erami, A.; Darzi Eslam, E.; Darvish Alipour Astaneh, S., Specific egg yolk antibodies (IgY) confer protection against *Acinetobacter baumannii* in a murine pneumonia model. *Journal of applied microbiology* **2019**, *126* (2), 624-632.
- [182] Engvall, E.; Perlmann, P., Enzyme-linked immunosorbent assay (ELISA) quantitative assay of immunoglobulin G. *Immunochemistry* **1971**, *8* (9), 871-874.
- [183] Cheng, C. M.; Martinez, A. W.; Gong, J.; Mace, C. R.; Phillips, S. T.; Carrilho, E.; Mirica, K. A.; Whitesides, G. M., Paper-based ELISA. *Angewandte Chemie International Edition* **2010**, *49* (28), 4771-4774.
- [184] Fruhmann, P.; Sanchis, A.; Mayerhuber, L.; Vanka, T.; Kleber, C.; Salvador, J.-P.; Marco, M.-P., Immunoassay and amperometric biosensor approaches for the detection of deltamethrin in seawater. *Analytical and bioanalytical chemistry* **2018**, *410* (23), 5923-5930.
- [185] Freichel, T.; Laaf, D.; Hoffmann, M.; Konietzny, P. B.; Heine, V.; Wawrzinek, R.; Rademacher, C.; Snyder, N. L.; Elling, L.; Hartmann, L., Effects of linker and liposome anchoring on lactose-functionalized glycomacromolecules as multivalent ligands for binding galectin-3. *RSC advances* **2019**, *9* (41), 23484-23497.
- [186] Hartmann, M.; Betz, P.; Sun, Y.; Gorb, S. N.; Lindhorst, T. K.; Krueger, A., Saccharide-modified nanodiamond conjugates for the efficient detection and removal of pathogenic bacteria. *Chemistry—A European Journal* **2012**, *18* (21), 6485-6492.
- [187] Möckl, L.; Fessele, C.; Despras, G.; Bräuchle, C.; Lindhorst, T. K., En route from artificial to natural: Evaluation of inhibitors of mannose-specific adhesion of *E. coli* under flow. *Biochimica et Biophysica Acta (BBA)-General Subjects* **2016**, *1860* (9), 2031-2036.
- [188] Scheller, H. V.; Ulvskov, P., Hemicelluloses. *Annual review of plant biology* **2010**, *61*.
- [189] Boden, S.; Reise, F.; Kania, J.; Lindhorst, T. K.; Hartmann, L., Sequence-Defined Introduction of Hydrophobic Motifs and Effects in Lectin Binding of Precision Glycomacromolecules. *Macromolecular bioscience* **2019**, *19* (4), 1800425.
- [190] Igde, S.; Röblitz, S.; Müller, A.; Kolbe, K.; Boden, S.; Fessele, C.; Lindhorst, T. K.; Weber, M.; Hartmann, L., Linear Precision Glycomacromolecules with Varying Interligand Spacing and Linker Functionalities Binding to Concanavalin A and the Bacterial Lectin FimH. *Macromolecular bioscience* **2017**, *17* (12), 1700198.

References

- [191] Mortensen, S.; Brimijoin, S.; Hooper, M.; Padilla, S., Comparison of the In Vitro Sensitivity of Rat Acetylcholinesterase to Chlorpyrifos-oxon: What Do Tissue IC₅₀ Values Represent? *Toxicology and applied pharmacology* **1998**, *148* (1), 46-49.

6 Appendix

6.1 List of abbreviations

6.1.1 General abbreviations

| | |
|----------------|--|
| e.g. | exempli gratia (for example) |
| et al. | et alii (and others) |
| <i>E. coli</i> | <i>Escherichia coli</i> |
| UTI | urinary tract infection |
| CRD | carbohydrate recognition domain |
| UCST | upper critical solution temperature |
| LCST | lower critical solution temperature |
| ATRP | atom transfer radical polymerization |
| RAFT | reversible addition-fragmentation polymerization |
| FRP | free radical polymerization |
| DLS | dynamic light scattering |
| AFM | atomic force microscopy |
| 3D | three dimensional |
| 2D | two dimensional |
| PDI | polydispersity index |
| GFP | green fluorescent protein |
| MS | mass spectrometry |
| ESI | Electrospray Ionization |
| calc. | calculated |
| NMR | nuclear magnetic resonance spectroscopy |
| RP-HPLC-MS | reversed phase high pressure liquid chromatography-mass spectrometry |
| VWD | Variable wavelength detector |
| PSA | Phenol Sulfuric Acid |
| OD | optical density |

| | |
|-----|-----------------------------------|
| SEC | size exclusion chromatography |
| IR | infrared |
| DSC | differential scanning calorimetry |
| GFP | green fluorescent protein |

6.1.2 Carbohydrate abbreviations

| | |
|-----------|--|
| Man | α -D-mannopyranoside |
| Gal | β -D-galactopyranoside |
| MeMan | methyl α -D-mannopyranoside |
| ManEMAm | <i>N</i> -(2-(α -D-mannopyranosyloxi)ethyl)methacrylamide |
| GalEMAm | <i>N</i> -(2-(β -D-galactopyranosyloxi)ethyl)methacrylamide |
| AcGalEMAm | 2'-acrylamidoethyl-2,3,4,6-tetra- <i>O</i> -acetyl- β -D-galactopyranoside |
| AcManEMAm | 2'-acrylamidoethyl-2,3,4,6-tetra- <i>O</i> -acetyl- α -D-mannopyranoside |
| ManEL | 2-aminoethyl- α -D-mannopyranoside |
| ManHPL | 3-amino-2-hydroxypropyl- α -D-mannopyranoside |
| GalHPL | 3-amino-2-hydroxypropyl- β -D-galactopyranoside |
| ManEAm | <i>N</i> -(2-(β -D-galactopyranosyloxi)ethyl)acrylamide |

6.1.3 Chemical abbreviations

| | |
|--------------------------------|--------------------------------------|
| N | nitrogen |
| O | oxygen |
| ConA | Concanavalin A |
| PNIPAM | poly(<i>N</i> -isopropylacrylamide) |
| Fe ₃ O ₄ | magnetite |
| Ca ²⁺ | calcium ions |
| MBA | methylene bisacrylamide |

| | |
|-------------------|---------------------------------------|
| MAA | methacrylic acid |
| NIPAM | <i>N</i> -isopropylacrylamide |
| AMEA | 2-aminoethylmethacrylatehydrochloride |
| APS | ammonium persulfate |
| PBS | phosphate buffered saline |
| RBITC | rhodamine B isothiocyanate |
| SDS | sodium dodecyl sulfate |
| LBB | lectin binding buffer |
| He | helium |
| Ne | neon |
| Mn ²⁺ | manganese ions |
| H | hydrogen |
| CDCl ₃ | deuteriochloroform |
| HEMAm | hydroxyethylmethacrylate |
| Ac | acetyl |
| C | carbon |
| NAS | <i>N</i> -acryloxysuccinimide |
| PNAS | poly(<i>N</i> -acryloxysuccinimide) |
| DMF | <i>N,N</i> -dimethylformamide |
| DMSO | dimethyl sulfoxide |
| BSA | bovine serum albumine |
| HPL | Hydroxypropyl |
| EL | ethyl |
| LiBr | Lithium bromide |
| FITC | fluorescein isothiocyanate |

6.1.4 Units, parameters and symbols

| | |
|---------------|-------------------------|
| nm | nanometer |
| M | mole per liter |
| °C | degree Celcius |
| D | diffusion coefficient |
| R_h | hydrodynamic radius |
| k_B | Boltzmann constant |
| T | temperature |
| η | viscosity |
| mol % | percentage of substance |
| mL | milliliter |
| g | gram |
| mmol | millimole |
| mg | milligram |
| rpm | rounds per minute |
| min | minute |
| μM | micromole per liter |
| μL | microliter |
| wt % | weight percentage |
| nm | nanometer |
| % | percent |
| vol % | volume percentage |
| μg | microgram |
| cm | centimeter |
| N | Newton |
| m | meter |
| mW | milliwatt |
| mM | millimole per liter |

| | |
|------------------|--|
| μm | micrometer |
| CFU | colony forming units |
| K | degree Kelvin |
| nmol | nanomole |
| h | hour |
| MHz | megahertz |
| Hz | Hertz |
| pmol | picomole |
| ppm | parts per million |
| mV | millivolt |
| \overline{M}_n | number average molecular weight |
| kDa | kilodalton |
| T_g | glass transition temperature |
| IC ₅₀ | Inhibitory concentration at half maximum intensity |

6.2 List of Figures

Figure 1. Schematic presentation of the different assays conducted in this thesis. In the first part (a.) the temperature-dependent binding of carbohydrate bearing microgels towards *E. coli* is shown. By raising the temperature above the LCST (40 °C), the binding of bacteria is enhanced, and more aggregates are formed. In the second part (b.) a schematic representation of the temperature-dependent adhesion inhibition assays is given. Green fluorescent protein (GFP) expressing *E. coli* or fluorescein isothiocyanate-ConA (FITC-ConA) adhere to a mannan coated surface. By the addition of glycopolymers the adhesion of the receptor towards the surface is inhibited. In the third part (c.) glyco-functionalized microgels are coated onto surfaces, and the adhesion of GFP-expressing *E. coli* and FITC-ConA is readout at temperatures below and above the LCST..... XIII

Figure 2. Schematic representation of the cell surface. The lipid double layer with membrane proteins is shown. On top of some lipids and membrane proteins, oligosaccharides are attached and, therefore, form glycolipids or glycoproteins. This dense layer of carbohydrates is called glycocalyx, and it is shown how different receptors interact with these carbohydrates. Examples for receptors that interact with the glycocalyx are bacteria, viruses, and lectins. Glycans adapted from [5]. 1

Figure 3. Chemical structures of the terminal monosaccharides found at the glycocalyx. Their appearance frequency was determined by Seeberger et al.^[12] Also shown is the schematic representation of the carbohydrates by the colored symbols. 2

Figure 4. Schematic presentation of the quaternary structure of ConA with a marker on the proteins CRD (left) (Protein Database code: 1jbc). Additionally, the amino acids and metal ions (Mn^{2+} and Ca^{2+}) are shown with their spatial arrangement during a binding event with α -D-mannopyranoside terminally bound on a scaffold R (right). Adapted from [37]. 5

Figure 5. Schematic presentation of the CRD of FimH. Amino acids responsible for the development of hydrogen bonds (grey lines) to Man are shown, as well as hydrophobic interactions between the CRD and Man (red waves). Adapted from [50] 6

Figure 6. Schematic presentation of increasing binding by multivalent presentation of ligands and receptors. A linear increase in the number in binding partners starting at a single pair (left) going to two (middle) and up to three (right) and their non-linear increase in bound states from one to seven are shown. 7

Figure 7. Schematic presentation of the effects occurring by a multivalent presentation of ligands and receptors. Statistical rebinding is shown (top, left), where the bound ligand 2 is replaced by ligand 1 due to their proximity. The chelate effect (top, right) shows the binding of two ligands, presented on the same scaffold, towards the same receptor. Clustering (bottom, left) is the binding of more than one receptor to the ligands presented on a scaffold. Sterical shielding (bottom, right) is the repulsion between the backbones and unbound ligands of two glyco-molecules preventing the displacement of the bound ligands by an unbound one from the other glyco-molecule..... 9

Figure 8. Schematic presentation of the glycocalyx (left) and scaffolds used as a glycomimetic (right). The glycomimetics vary from glycopolymers and -dendrimers, to glycomicrogels and glycofunctionalized surfaces as well as nanoparticles (top to bottom). Glycans adapted from [5]. 10

Figure 9. Scheme of different approaches for the synthesis of glycopolymers. The homopolymerization of glycomonomers can be used to synthesize glycopolymers with high carbohydrate densities (top, left). Using a second monomer during the synthesis gives copolymers with variable carbohydrate densities and switchable polymer properties (top, right). For the post-functionalization approach, a homopolymer with a reactive side group (e.g. active ester, anhydride or acid) is synthesized. In a second step, it is functionalized with carbohydrates and a nucleophile to synthesize a glycopolymer with different properties and carbohydrate densities (bottom)..... 12

Figure 10. Schematic presentation of different types of crosslinking. Physically crosslinked microgels, here exemplary based on alginate, have crosslinks via non-covalent electrostatic interactions between Ca^{2+} ions and the carboxylate groups of the alginate (left). Chemical crosslinked microgels, here exemplary based on PNIPAM, have PNIPAM chains connected via covalent bonds formed with the crosslinker MBA (right). 16

Figure 11. Schematic presentation of atomic force microscopy used for scanning a microgel coated surface. The cantilever moves upon interacting with the microgel surface leading to a laser movement on the photodiode. Those movements are transferred into a height profile of the line scanned. By using height profiles of multiple scanned lines, an image of the microgel coated surface can be calculated. 20

Figure 12. Schematic presentation of an ELISA with and without inhibitor added. The binding of the antibody-enzyme conjugate towards protein/antigen, coated onto the surface, can catalyze a reaction with a substrate giving a dye that can be read out via UV-vis (1). By

adding an inhibitor for the binding of the antibody towards the functionalized surface, the enzyme-catalyzed reaction is reduced, and an inhibition potential can be determined (2).
..... 22

Figure 13. Schemes of adhesion inhibition assays. On the left, GFP-tagged *E. coli* binds to mannan functionalized surfaces, and the number of bound bacteria can be determined via fluorescence readout (1). When an inhibitor is added, the inhibited *E. coli* can be washed off, and the fluorescence intensity during the readout decreases (2). On the right, fluorescence labelled ConA binds to mannan coated microtiter surface. The binding is determined via fluorescence readout (3). Adding an inhibitor that binds to ConA hinders the lectin from binding to the mannan surface and is washed off. Only small amounts of ConA can bind to mannan and, therefore, leads to lower fluorescence intensities (4). 23

7. Acknowledgements

Mein besonderer Dank gilt Herrn Jun. Prof. Dr. Stephan Schmidt für die stets motivierende Betreuung der vorliegenden Promotionsarbeit und der Bereitstellung des interessanten Forschungsthemas. Seine stete Unterstützung, Geduld und Hilfsbereitschaft haben mir wissenschaftlich und persönlich geholfen mich weiterzuentwickeln. Ich möchte mich zudem für die Möglichkeit bedanken auf internationalen Konferenzen meine Ergebnisse präsentieren zu können.

Außerdem möchte ich Prof. Dr. Christoph Janiak für die Übernahme des Korreferates dieser Arbeit meinen Dank aussprechen.

Frau Prof. Dr. Laura Hartmann möchte ich für die Möglichkeit danken mit Ihrer Gruppe kooperieren zu können und die damit verbundenen interessanten Gespräche.

Frau Dr. Monir Tabatabai möchte ich dafür danken, dass Sie all die Jahre ein offenes Ohr hatte. Sie hat uns stets motiviert und ich bin dankbar, dass ich zusammen mit Ihr ein Teil des Makropraktikums sein durfte. Weitergehend möchte ich mich für die Organisation und Lösung der alltäglichen Probleme und die Gespräche, sowohl bei fachlichen Fragestellungen als auch bei persönlichen Problemen, bedanken.

Des Weiteren möchte ich mich bei Stephanie Scheelen, Sonja Coors, Birgit Ohler, Maria Breuer, Michaela Kitza und Viola Schürmanns für die Organisation des Alltags und die stete Hilfsbereitschaft bedanken. Ein besonderer Dank soll jedoch an Stephanie Scheelen gehen, welche mich nicht nur andauernd mit Labormaterial ausgerüstet hat, sondern auch für die Gespräche und den Spaß, den wir zusammen hatten.

Ich möchte zudem meinen Kooperationspartnern Frau Prof. Dr. Thisbe Lindhorst und Carina Spormann bedanken. Besonders bei Carina möchte ich mich für die ausführliche „Bakterienschule“ und auch die schönen Abende in Kiel bedanken.

Ein besonderer Dank geht an Pauline Watermann, Marco Hildebrandt, Melanie Schmidt und Sophie Rübel, welche durch ihre Bachelor- und Masterarbeiten, nicht nur fachlich, sondern auch auf persönlicher Ebene zum Gelingen dieser Arbeit beigetragen haben.

Vielen Dank an alle Kollegen und Freunde, die ich während meiner Zeit am Institut gewonnen habe und die diese Zeit unvergesslich gemacht haben. Die unterstützende Arbeitsatmosphäre während der gesamten Zeit und den Spaß auf den besonderen Events,

Acknowledgments

wie den „Einstandsfeiern“, den Weihnachtsfeiern und Klassenfahrten, werden mir immer in Erinnerung bleiben. Ich möchte mich bei den Doktoranden der ersten Stunde Tanja Freichel, Kira Neuhaus, Markus Giesler, Mischa Baier, Christoph Gerke, Katharina Bücher, Hanqing Wang, Alberto Camaleño de la Calle, Sebastian Bauer und Fawad Jacobi für die herzliche Aufnahme in die Gruppe und die unvergesslichen ersten Jahre bedanken. Besonders möchte ich Mischa und Christoph für die Unterstützung und Freundschaft danken und die lustigen Stunden im Büro mit dem ein oder anderen Feierabendbier.

Weiterer Dank geht an die weiteren Mitglieder der Gruppe, die diese Zeit unvergesslich gemacht haben. Danke an Peter Pasch, Patrick Konietzny, Philipp Reuther, Miriam Hoffmann, Michelle Illmann, Serap Üclü, Luca-Cesare Blawitzki, Robert Steinfurt, Lennart Hofer, Nina Jahnke, Dana Itskalov, Lorand Bonda, Josip Stipanovic, Melina Feldhof, Alexander Banger, Lukas Fischer und Dr. Stephen Hill.

Außerdem möchte mich nochmal besonders bei meinen AK Schmidt Kollegen Fabian Schröer und Dimitri Wils bedanken. Ihr habt diese Zeit zu etwas besonderem gemacht und ich freue mich schon auf die zukünftigen Treffen mit euch.

Ich bedanke mich bei Sebastian Glomb, Dennis Dietrich und Martin Wickenheisser, die während der Bachelorarbeit, aber auch danach, mit Rat und Tat beiseite standen und für jeden Spaß zu haben waren.

Sophia Boden danke ich für die großartige gemeinsame Zeit im Büro und auf unserer Reise nach Boston und New York. Was wir zusammen erlebt haben wird mir immer in Erinnerung bleiben.

Noch einmal besonders bedanken möchte ich mich bei Theresa Seiler, Markus Giesler, Michele Illmann und Philipp Reuther. Ihr hattet immer ein offenes Ohr für mich und meine Probleme und seid mir während dieser Zeit sehr ans Herz gewachsen. Markus möchte ich für jede lustige Diskussion und jedes gemeinsame Aufregen danken. Theresa danke ich für jedes beratende Gespräch im Büro, jeden lustigen Abend und vor allem für Ihre Freundschaft. Michele, welche vom ersten Tag an ein Teil meiner Reise war, möchte ich für Ihre liebe Art danken und dafür, dass Sie einen immer mit Ihrer guten Laune ansteckt. Philipp danke ich für seine loyale Art und den ganzen Spaß im letzten Jahr. Ich hätte niemals gedacht, dass du mir nach unserem Kaffeefiasco so ans Herz wachsen würdest. Ich hoffe, dass Ihr alle weiterhin ein Teil von meinem Leben bleibt, denn ohne euch wäre es nur halb so schön gewesen.

Ich möchte meiner Familie für die stete Unterstützung während des Studiums und der Promotion danken. Danke, dass ihr mir in schweren Situationen immer beigestanden habt und mich, nicht nur finanziell, sondern auch emotional, unterstützt habt. Ich danke meinem Großvater Wilhelm Schneider dafür, dass er schon in meiner frühen Kindheit die Neugier zur Wissenschaft geweckt hat, meinem Onkel Markus Schneider für seine stete Hilfsbereitschaft und meiner Mutter Regina Paul für die Unterstützung, Liebe und verständnisvolle Art.

Mein letzter Dank geht an Alexander Strzelczyk, der durch das Studium in mein Leben getreten ist und mit mir alle Höhen und Tiefen dieser Zeit durchgestanden hat. Deine Unterstützung, deine ruhige Art und dein stetes Vertrauen in mich haben mich stets motiviert. Du warst und bist immer mein Fels in der Brandung und die Schulter an dich ich mich lehnen konnte. Ohne dich hätte ich es nicht geschafft und dafür kann ich dir nicht genug danken.

